

Computational Structural Aspects of the Phosphorus Containing Clusters and Phosphodiesterases

A Thesis

**Submitted for the Degree of
DOCTOR OF PHILOSOPHY**

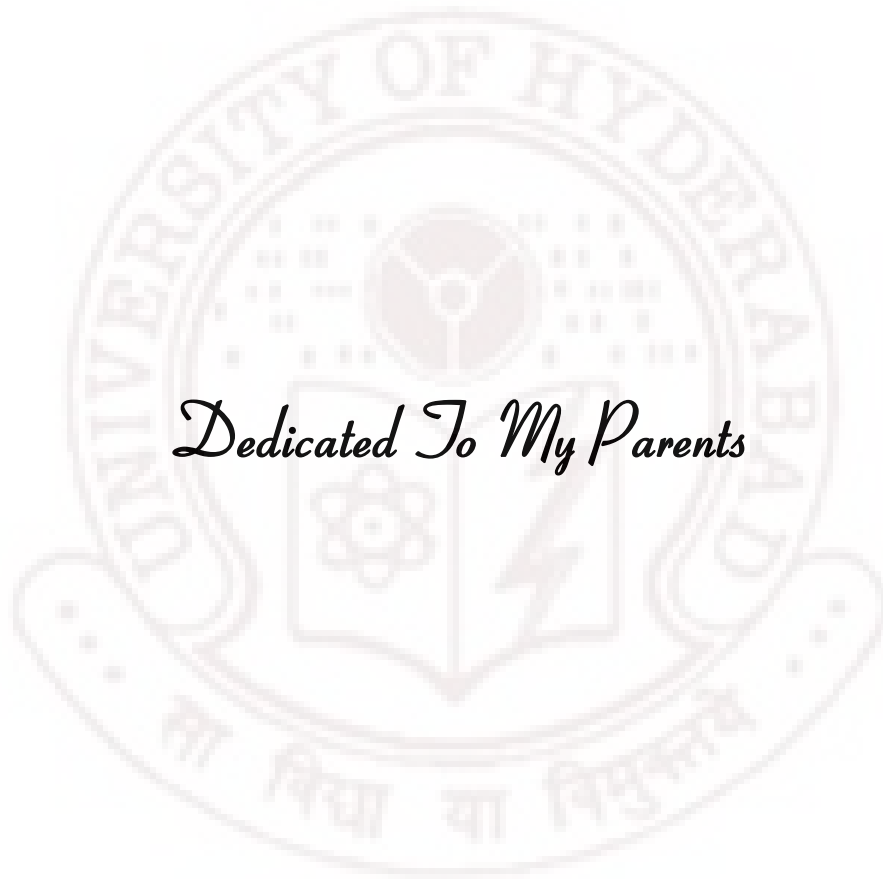
By

Dandamudi Usharani



**School of Chemistry
University of Hyderabad
Hyderabad – 500 046
INDIA**

February 2009



Dedicated To My Parents

Table of Contents

STATEMENT	xi
CERTIFICATE	xiii
ACKNOWLEDGEMENTS	xv

Chapter 1: Background of the Theoretical Methods and Abstract of the Thesis

1.1	General Introduction	3
1.2	Overview of Theoretical Methods	4
1.3	Quantum Mechanical Methods	4
1.3.1	The Born-Oppenheimer Approximation	5
1.3.2	Hartree-Fock Method	6
	1.3.2.1 Basis Sets	10
	1.3.2.2 Semi Empirical Methods	13
1.3.3	Post Hartree-Fock Methods	15
	1.3.3.1 Many Body Perturbation Theory	16
	1.3.3.2 Configuration Interaction	16
	1.3.3.3 Coupled Cluster Theory	17
1.3.4	Density Functional Theory	18
	1.3.4.1 Local Density Approximation	21
	1.3.4.2 Generalized Gradient Approximation	21
	1.3.4.3 Hybrid Functionals	22
1.3.5	Composite Methods	22

1.4	Molecular Mechanical Methods	23
1.4.1	Force Fields	24
1.4.2	Molecular Dynamics	26
1.4.3	Docking	29
1.5	Quantum Mechanical/Molecular Mechanical Methods	32
1.6	A Brief Outline of the Chapters	34
1.7	References	41

Chapter 2: Electronic Structure and Bonding in Neutral and Dianionic Boradiphospholes: $R'BC_2P_2R_2$ ($R = H, tBu, R' = H, Ph$)

2.1	Abstract	51
2.2	Introduction	52
2.3	Details of Computational Methods	57
2.4	Results and Discussions	58
2.4.1	Electron-Counting Considerations and Optimized Skeletons	58
2.4.2	Global Minima of <i>neutral</i> and <i>dianionic</i> $R'BC_2P_2R_2$	62
2.4.3	Isomers Containing 5-Membered Rings	66
2.4.4	Isomers Containing 4-Membered Rings	71
2.4.5	Isomers Containing 3-Membered Rings	78
2.4.6	Acyclic Isomers	84
2.5	Conclusions	86
2.6	References	88
2.7	Appendix	96

Chapter 3: Electronic Structure and Bonding Studies on Triple-Decker Sandwich Complexes with a P₆ as Middle Ring

3.1	Abstract	103
3.2	Introduction	104
3.3	Details of Computational Methods	106
3.4	Results and Discussions	106
3.4.1	The <i>mno</i> Rule and the Valence Electron Count	106
3.4.2	28 Valence Electron Count Complexes	109
3.4.3	26 Valence Electron Count Complexes	115
3.4.4	24 Valence Electron Count Complexes	119
3.4.5	22 Valence Electron Count Complexes	121
3.4.6	20 and 18 Valence Electron Count Complexes	125
3.5	Conclusions	128
3.6	References	129

Chapter 4: A pH Dependence of 3₁₀-Helix versus Turn in M-loop Region of PDE4: Observations on PDB Entries and an Electronic Structure Study

4.1	Abstract	137
4.2	Introduction	138
4.3	Details of Computational Methods	142
4.4	Results and Discussions	145
4.4.1	Crystal Structure Analysis	145
4.4.2	Root Mean Square Deviation	148
4.4.3	Importance of Secondary Structural Change and its Cause	150

4.4.4 Influence of pH on M-loop Region	153
4.4.5 Influence of M-loop Region on Subtype Selectivity	162
4.5 Conclusions	163
4.6 References	163

Chapter 5: Molecular Insights for the Inhibitor Selectivity between PDE4 and PDE7: Docking Study

5.1 Abstract	173
5.2 Introduction	174
5.3 Details of Computational Methods	178
5.4 Results and Discussions	179
5.4.1 Structural Comparison of PDE4 and PDE7	179
5.4.2 Docking	182
5.4.2.1 Substrate (cAMP)	182
5.4.2.2 Nonselective Inhibitor (IBMX)	183
5.4.2.3 PDE4 Inhibitors	184
5.4.2.4 PDE7 Inhibitors	188
5.4.2.5 Dual-Selective PDE4 and PDE7 Inhibitors	189
5.5 Conclusions	192
5.6 References	193

STATEMENT

I do hereby declare that the work embodied in this thesis is the result of investigations carried out by me in the **School of Chemistry, University of Hyderabad, Hyderabad, India**, and **Department of Inorganic and Physical Chemistry, Indian Institute of Science, India**, under the supervision of **Prof. Eluvathingal D. Jemmis**.

In keeping with the general practice of reporting scientific observations, due acknowledgements have been made whenever the work described is based on the findings of other investigators.

Dandamudi Usharani

CERTIFICATE

Certified that the work embodied in the thesis entitled “**Computational Structural Aspects of the Phosphorus Containing Clusters and Phosphodiesterases**” has been carried out by **Ms. Dandamudi Usharani** under my supervision and the same has not been submitted elsewhere for any degree.

Prof. Eluvathingal D. Jemmis

Thesis supervisor

Dr. Lalitha Guruprasad

Thesis co-supervisor

Dean

School of Chemistry

ACKNOWLEDGEMENTS

మాతృ దేవోభవః పితృ దేవోభవః ఆచార్య దేవోభవః అతిది దేవోభవః

I would like to recall all those people who have encouraged me to achieve goals. First I would like to thank my supervisor Prof. E. D. Jemmis, whose guidance taught me the art of doing research. I extend my deep sense of gratitude for his immense patience, kindness, constant encouragement in learning things, and due support in times of need. I especially like to thank his family for their hospitality and intimacy.

I also thank my co-supervisor Prof. Lalitha Guruprasad and for her valuable support. I am grateful to the Director of IISc, Prof. P. Balram whose kindness helped me to stay inside the IISc campus in peace. I express my sincere thanks to past and present Deans and all the faculty members of the School of Chemistry, UoH and to the past and present Chairmen and all the faculty members of IPC, IISc. Special thanks are due to Prof. K. L. Sebastian, Dr. Prabal Maiti of IISc and Prof. M. V Rajashekar, Prof. K. D. Sen of UoH for their valuable course work. I would like to thank Prof. Umapathy for his support. I wish to thank all the faculty of JNCASR, Prof. Prasad V. Bharatam of NIPER for organizing workshops, summer schools and symposia which has given an opportunity to learn basics of many new areas. I am also gratefully to Dr. G. Madhavi Sastry, Dr. G. Narahari Sastry, Dr. Soujanya, Dr. Nagasuma Chandra for their intimacy.

I greatly acknowledge Prof. John. F. Nixon, Dr. G. Narahari Sastry, Dr. Nagasuma Chandra and Prof. Santhanu Bhattacharya for their effective collaboration that led to understand wider range of problems.

I thank CSIR for the Junior and the Senior research fellowship. I am also thankful to the Centre for Modeling Simulation and Design (CMSD) at UoH and the Supercomputer Education and Research Centre (SERC) at IISc for

computational facilities. Special thanks to Mr. Vinod Kumar and Mr. Kiran for their technical support. I like to thank all the non-teaching staff of the School of Chemistry, IPC and the hostel office of IISc for their timely help.

I am very delightful to have highly co-operative colleagues of past and present in the lab. I thank Anoop and Param who helped me in learning computers and Molecular orbital concepts. The healthy group discussions of lab mates, especially clarifying the conceptual doubts of Quantum chemistry from Shameema and Prasad has immensely helped me in writing the thesis. I would like to thank others Bishu, Susmita, Jorly, Hari, Dibyendu, Subhendu and Anne for their friendliness. I thank all of them once again for love, attention and affection toward my son. I thank the summer students Shanthi, Rajesh, Umayal, Clàire, Deepthi and Renuka.

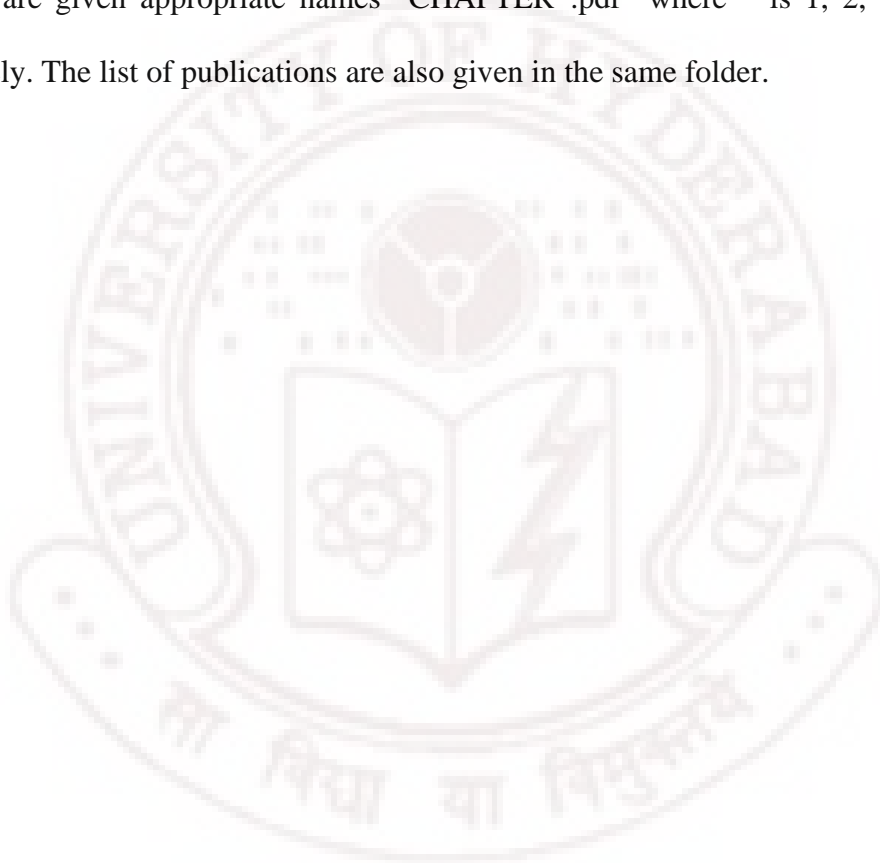
I thank my friends at School of Chemistry, JayaPrakash, Rajesh, Saritha, Narahari, Jayachandra, RajaGopal, Bhaswathi and Kishore babu for their help. I would like to thank all my friends at IICT, Srivani, Gayathri, Nagaraju, Satish, Dolly, Srinivas Reddy, Srinivas, Punagai and Mukesh and at IISc, RamKumar, Swathi, Ondrilla, Sinda, Kalidas, Santosh, Srinu, Jyothi, Neenu, Nicky, Raima, Linta, Nima, Sanjukta, Rogers, Mathew, Sandya for their best wishes.

I am indebted to my elder and younger sisters Madhavi and Roja, for their moral support, courage, taking care of my son, assurance and excellent advice to overcome problems. I am grateful even to my both brothers-in law and my sister's mothers-in laws for their best wishes. I thank my brother Pasi for his encouragement. It is incomplete to thank my father Manilal, my mother late Rajeshwari and son Chandrasekhar who are the strength of my life. I also like to thank care takers of IISc who have taught good manners to my son in my absence. Lastly I thank almighty God for having grace on me.

Dandamudi Usharani

CONTENTS OF THE CD

The main folder “Thesis” in the CD consists of CHAPTER_0.pdf that includes contents of the thesis having pages i-xvi (see the table of contents). The sub-folder “Chapters” contains five files corresponding to the five chapters comprised in the thesis. The files are given appropriate names “CHAPTER*.pdf” where * is 1, 2, 3, 4 and 5 respectively. The list of publications are also given in the same folder.





Chapter 1

Background of the Theoretical Methods and Abstract of the Thesis

Contents

1.1	General Introduction	3
1.2	Overview of Theoretical Methods	4
1.3	Quantum Mechanical Methods	4
1.3.1	The Born-Oppenheimer Approximation	5
1.3.2	Hartree-Fock Method	6
1.3.2.1	Basis Sets	10
1.3.2.2	Semi Empirical Methods	13
1.3.3	Post Hartree-Fock Methods	15
1.3.3.1	Many Body Perturbation Theory	16
1.3.3.2	Configuration Interaction	16
1.3.3.3	Coupled Cluster Theory	17
1.3.4	Density Functional Theory	18
1.3.4.1	Local Density Approximation	21
1.3.4.2	Generalized Gradient Approximation	21
1.3.4.3	Hybrid Functionals	22
1.3.5	Composite Methods	22
1.4	Molecular Mechanical Methods	23
1.4.1	Force Fields	24
1.4.2	Molecular Dynamics	26
1.4.3	Docking	29
1.5	Quantum Mechanical/Molecular Mechanical Methods	32
1.6	A Brief Outline of the Chapters	34
1.7	References	41

1.1 General Introduction

Computational chemistry is an emerging field, where computer is used as an ‘experimental’ tool to generate data, by which one may gain insight and rationalize the behavior of a large class of chemical systems. The increase in the threshold of this subfield of theoretical chemistry is due to the advancements in computer technology, availability of practical algorithms for theoretical methods and success in explaining the problems.¹ It is developed into an important tool in almost all areas of chemistry. It is an eminent tool for both theoreticians and experimentalists in analyzing the chemistry related problems. The three key steps involved in solving chemistry related problems through computational methods are (a) building an appropriate chemical model for the real system, (b) calculation of total energies and its derived properties of the system and (c) analyzing the properties obtained from calculation. Accuracy of these calculations depends on the factors such as (a) closeness of the model system to the real one, (b) type of theoretical method and (c) evaluating the quality of the obtained results in comparison to experiments. Thus the inclusion of theoretical and experimental results, knowing the limitation of theory and why the numbers are produced the way they are helps to give a better understanding on the problems.^{1,2}

There are many properties which can be studied using computational methods. Those include the structure, bonding, stability, reactivity, rates of reactions, interactions, excitation, thermal, mechanical and magnetic properties, phase transitions etc for various classes of systems (clusters, solids and biomolecules). The structure and bonding interactions of the molecules, clusters and biomolecules are the interest of this thesis work. Structure can be determined experimentally from various spectroscopic techniques

such as X-ray, electron and neutron diffraction, mass, microwave and NMR etc.^{2b} The structures are available in Cambridge Crystallographic Data Centre or Cambridge Structural Database^{3a} for small inorganic and organic molecules where as biomolecules are present in Protein and Nucleic acid Data Banks.^{3b} On the other hand theoretically one can probe the structure by calculating the potential energy surface of the small molecules using the computational quantum mechanical methods and for biomolecules using molecular mechanical methods such as homology modeling and molecular dynamics. The theoretical methods that are used in the thesis are briefly discussed in the following sub sections. The outline of the problems discussed in the next four chapters is also presented.

1.2 Overview of Theoretical Methods

There are various levels of theoretical methods and can be broadly classified as quantum mechanical (QM), molecular mechanical (MM) and hybrid quantum and molecular mechanical (QM/MM).^{1,4} The choice of these methods depends on the size of the system, accuracy and property that need to be calculated. Quantum mechanics can further be wave function and density functional based methods.⁴

1.3 Quantum Mechanical Methods⁴

The phenomenon such as black body radiation, Compton and photoelectric effect and specific heats of microscopic objects were unable to explain by Newtonian or classical mechanics. The quantum mechanics explains the motion of microscopic particles and their properties.⁴ The fundamental equation of quantum mechanics that explains the state of the physical system is Schrödinger equation.

$$H \Psi(r,t) = i\hbar \frac{\partial}{\partial t} \Psi(r,t) \quad (1.1)$$

$$H = T + V = -\frac{\hbar^2}{2m} \nabla^2 + V \quad (1.2)$$

where H is Hamiltonian operator that includes both kinetic (T) and potential energy (V) operators, $\Psi(r,t)$ is the wave function which represents the state of system, $i = \sqrt{-1}$ and \hbar is $h/2\pi$ where h is Planck's constant. The equation 1.1 is the non-relativistic time dependent Schrödinger equation.⁵ The equation which gives the stationary state of the particle is time independent Schrödinger equation (1.3). In this thesis only time independent form was used.

$$H\Psi(r) = E\Psi(r) \quad (1.3)$$

In principle, Schrödinger equation can be written for any problem but it can be exactly solvable only for particles in a box, hydrogen and hydrogen like atoms etc. In order to solve for many body systems various approximations are needed and are illustrated here.

1.3.1 The Born-Oppenheimer Approximation

This is the first approximation⁶ that simplifies the solution of Schrödinger equation for many body systems. This considers electronic and nuclear motion are separable. As the motion of nucleus is negligible compared to electron motion ($M_{\text{nuceli}} = 1837 m_e$) electron readjusts its position before the nucleus change its position. This leads to electronic Schrödinger equation (1.4) that describes the motion of electron in the field of fixed nuclei.

$$H_{el} \Psi_{el}(r, R) = E_{el}(R) \Psi_{el}(r, R) \quad (1.4)$$

$$\text{where } H_{el} = -\frac{\hbar^2}{2m_e} \sum_i^n \nabla_i^2 - \sum_A^N \sum_i^n \frac{Z_A e^2}{r_{iA}} + \sum_j^n \sum_{i>j}^n \frac{e^2}{r_{ij}} + \sum_A^N \sum_{B>A}^N \frac{Z_A Z_B e^2}{R_{AB}} \quad (1.5)$$

$$H_{el} = -\frac{1}{2} \sum_i^n \nabla_i^2 - \sum_A^N \sum_i^n \frac{1}{r_{iA}} + \sum_j^n \sum_{i>j}^n \frac{1}{r_{ij}} + \sum_A^N \sum_{B>A}^N \frac{1}{R_{AB}} \text{ in atomic units} \quad (1.6)$$

The first term in the Hamiltonian corresponds to kinetic energy of the electron and the next three terms represent the potential energy due to electron-nuclei, electron-electron and nuclei-nuclei interactions. Solving the equation 1.4 at different nuclear coordinates describe the potential energy surface for the system. The Born-Oppenheimer approximation is supported from spectral studies. Limitation of this approximation is that it cannot explain whenever electronic motion is coupled to nuclear motion such as Jahn Teller, Renner and Peierl's structural distortions, excited states, highly charged systems, as well as occurrences of charge- and spin-density waves and superconductivity.^{3g} The methods that solve the equation 1.4 using only the fundamental constants (electronic mass m_e , charge e , Planck's constant h etc) and do not include any experimental data are called *ab initio* or first principle electronic structure methods. However, solving the electronic Schrödinger equation (1.4) exactly for many body systems is difficult due to the electron-electron interactions.

1.3.2 Hartree-Fock Method

Hartree-Fock (HF) method^{4,7} is an iterative variational self consistent procedure to calculate the single Slater determinant. This is the foundation for much of modern molecular orbital theory and starting point for many other electron correlation methods. In HF method each electron's motion is described by a single-particle function (orbital) which does not depend explicitly on the instantaneous motions of the other electrons.

Thus many electron Schrödinger equation is simplified as many one electron equations (1.7).

$$(H_i^{core} + V_i^{eff})\phi_i = \varepsilon_i\phi_i \quad (1.7)$$

where $H_i^{core} = -\frac{1}{2}\nabla_i^2 - \frac{Z}{r_i}$ in a.u is the average kinetic energy and nuclear electron

attraction, V_i^{eff} is the effective potential of electron-electron interaction,

$$V_i^{eff} = \sum_{j \neq i}^N \int \frac{\phi_j^*(j)\phi_j(j)}{r_{ij}} d\tau \quad (1.8)$$

ϕ_i is the spatial one electron wave function called molecular orbital and ε_i is the one electron energy. The total Hamiltonian of equation 1.7 by expanding V_i^{eff} in terms of coulomb J_{ij} and exchange operator K_{ij} gives the Fock operator^{7b} (1.9).

$$F_i = -\frac{1}{2}\nabla_i^2 - \sum_i^N \frac{Z_\alpha}{r_{i\alpha}} + \sum_{i=1}^{N/2} \sum_{j=1}^{N/2} 2J_{ij} - K_{ij} \quad (1.9)$$

$$\text{where } J_{ij} = \int \phi_i(1)\phi_j(2) \left(\frac{1}{r_{12}} \right) \phi_i^*(1)\phi_j^*(2) d\tau \quad (1.10)$$

$$K_{ij} = \int \phi_i(1)\phi_j(2) \left(\frac{1}{r_{12}} \right) \phi_i^*(2)\phi_j^*(1) d\tau \quad (1.11)$$

J_{ij} represents the classical repulsion between electrons and K_{ij} represents the exchange interaction that is coming out from the anti symmetric nature of the wave function. These equations are called as Hartree-Fock equations. The total electronic energy by HF method for a closed shell system is obtained by summing up these one electron energies.

$$E_{HF} = \sum_{i=1}^{N/2} \left[2\varepsilon_i + \sum_{j=1}^{N/2} 2J_{ij} - K_{ij} \right] + V_{NN} \quad (1.12)$$

HF equations are mathematically complicated nonlinear equations which can be solved directly only for simple systems through numerical integration. For a molecular system, the equations can be derived by expanding the unknown molecular orbital ϕ_i in

$$\text{terms of given basis set } \chi \text{ is } \phi_i = \sum_{u=1}^n c_{ui} \chi_u \quad (1.13)$$

where c_{ui} is the orbital coefficient. This is called linear combination of atomic orbital (LCAO)- molecular orbital (MO) method.⁸ The initial set of orbital coefficients is solved by using the principles of variational theorem. It states that expectation value of energy E_ϕ calculated using any trial function of electron coordinates will be greater than the energy for exact wave function.

$$E_\phi = \frac{\int \phi^* H \phi d\tau}{\int \phi^* \phi d\tau} \geq E_0 \quad (1.14)$$

Substitution of ϕ (1.13) in above equation and introducing the resonance integral H_{uv} and overlap integral S_{uv} gives

$$\sum_{u=1}^N c_u \sum_{v=1}^N c_v S_{uv} E = \sum_{u=1}^N c_u \sum_{v=1}^N c_v H_{uv} \quad (1.15)$$

where $H_{uv} = \int \phi_u^* H \phi_v d\tau$ and $S_{uv} = \int \phi_u^* \phi_v d\tau$

The best wave function is obtained by minimizing the energy with respect to orbital coefficients c_{ui}

$$\frac{\partial E}{\partial c_{ui}} = 0 \quad (1.16)$$

This gives N simultaneous linear and homogenous equations which can be written in determinantal form called as secular determinant (1.17).

$$\begin{vmatrix} H_{11} - ES_{11} & H_{12} - ES_{12} & \dots & H_{1n} - ES_{1n} \\ H_{21} - ES_{21} & H_{22} - ES_{22} & \dots & H_{2n} - ES_{2n} \\ \dots & \dots & \dots & \dots \\ H_{n1} - ES_{n1} & H_{n2} - ES_{n2} & \dots & H_{nn} - ES_{nn} \end{vmatrix} = 0 \quad (1.17)$$

The solution of this n^{th} order determinant will give n roots i.e., a set of n energy values, $E_1, E_2, E_3, \dots, E_n$ and a set of n wave functions, $\phi_1, \phi_2, \dots, \phi_n$ for the system. Antisymmetric nature of complete wave function Ψ_{el} leads to the following Slater determinantal form of the wave function,

$$\Psi_{el} = \frac{1}{\sqrt{n!}} \begin{vmatrix} \phi_1(1) & \phi_2(1) & \dots & \phi_n(1) \\ \phi_1(2) & \phi_2(2) & \dots & \phi_n(2) \\ \dots & \dots & \dots & \dots \\ \phi_1(n) & \phi_2(n) & \dots & \phi_n(n) \end{vmatrix} \quad (1.18)$$

where, ϕ_i is the spin orbital of i^{th} particle.

Variation of the total energy (1.15) when carried out with respect to the coefficients c_{ui} leads to a set of algebraic equations and can be written in matrix form as Roothan equations⁹ (1.19).

$$FC = SCE \quad (1.19)$$

where F is Fock matrix, C is matrix representing molecular orbital coefficients, S is the overlap matrix for overlap between orbitals and $E = \epsilon_i \delta_{ij}$ where ϵ_i are one electron Fock energies.

$$F = H_{uv}^{core} + \sum_{u=1}^N \sum_{v=1}^N P_{\lambda\sigma} \left[(uv | \lambda\sigma) - \frac{1}{2} (u\lambda | v\sigma) \right] \quad (1.20)$$

where H_{uv}^{core} is the matrix representing energy of the single electron in the field of nuclei

and $P_{\lambda\sigma} = 2 \sum_{i=1}^{occ} C_{\lambda i}^* C_{\sigma i}$ is the density matrix.

A rigorous solution of HF-Roothan equations without any empirical parameters is known as *ab initio* molecular orbital theory. Since F depends on the coefficients of C , the HF-Roothan equations are solved by choosing an initial set of C and calculating matrix F . Then a new set of C is obtained from equations 1.19. This process is repeated until they are consistent. Hence this method is referred to as self consistent field (SCF) method. Basis set employed plays a crucial role in this method. Thus a better expectation value of energy can be obtained with larger basis set. The limit at which there is no change in the HF energy further by increasing the basis set is known as HF limit.^{9d} HF methods predict the ground state and related properties of most molecules. This method also gives 99% of total energy of the system. The bond breaking and making process are poorly determined by this method due to poor estimation of the correlation of electron pairs of opposite spin.

1.3.2.1 Basis Sets⁴

It is a set of mathematical functions used to represent the molecular orbitals for a system. Basis set assign a group of basis function to each atom within a molecule to approximate its orbitals.⁴ Depending upon the functional form basis set can be (a) Slater type^{10a} (b) Gaussian type^{10b} (c) Effective core potential^{10c} (d) Plane wave^{10d} etc.

(a) Slater type orbitals (STO): Atomic orbitals are best represented by STO's. The functional form of STO resembles the hydrogen like orbitals.

$$\lambda_{\zeta,n,l,m}(r, \theta, \varphi) = N r^{(n-1)} e^{-\zeta r} Y_l^m(\theta, \varphi) \quad (1.21)$$

where ζ orbital exponent is $\frac{Z-S}{a_o} = \frac{Z_{eff}}{a_o}$, S is screening constant, N is the normalization constant, $Y_{lm}(\theta, \varphi)$ contains all the angular information needed to describe the wave function (spherical harmonics) and r, θ, φ represent the polar coordinates. STO's

gives accurate solutions for atomic, diatomic and simpler linear molecules. For other molecules evaluation of many centre two electron integrals is very difficult and is time consuming computations.

(b) Gaussian type orbitals (GTO): This is introduced by Boys^{10b} and its functional form

$$\text{in Cartesian coordinates is } g_{\zeta, l_x, l_y, l_z}(x, y, z) = N x^{l_x} y^{l_y} z^{l_z} e^{-\zeta r^2} \quad (1.22)$$

where ζ represents the orbital exponent and these are primitive gaussians. Actual basis functions or contracted Gaussian functions χ_u are linear combinations of such primitive

$$\text{Gaussians } \chi_u = \sum_p d_{up} g_p \quad (1.23)$$

where d_{up} are contraction functions and g_p are primitive gaussians.

Unlike STO's there is r^2 dependence in the exponential for GTO (1.22). Thus at nucleus it leads to zero slope and fails to represent the region near the nucleus. In practice, the functional behavior of an STO is reproduced by using number of GTO's with different orbital exponents. GTO's are the popular basis functions used in electronic structure calculations. These are called STO-KG basis sets where K is the number of primitive Gaussian functions to fit an STO. They are more popular and developed by John A. Pople. STO-3G is a minimal basis set that contains minimum number of basis functions needed for each atom (3 Gaussians to fit an STO). Since the valence orbitals are involved in chemical bonding, each valence atomic orbital can be better described by increasing the basis functions. This type of separate treatment for core and valence atomic orbitals is referred as split valence basis set. Depending on the number of basis functions used for valence atomic orbital they can be double zeta (DZ), triple zeta (TZ) etc. To describe the expansion or contraction of orbitals that is caused due to environment

or for polarization related properties, a high angular momentum functions like p-functions for H and d- functions for heavy atoms are added. This type changes the shape of orbital and is termed as polarized basis set. Diffused basis set is also adding the functions to heavy and H atoms to give large region of space orbital. This is needed especially for describing the systems where electrons are far away from nucleus such as in anions, molecules with lone pairs, systems with excited states and low ionization potential etc. General representation of Pople type basis set is

$$k\text{-nlm}++G(d,p) \text{ or } k\text{-nlm}++G^{**} \quad (1.24)$$

The basis sets developed for dealing correlated systems are correlation consistent basis sets. They are developed by Dunning and represented generally as cc-PVXZ type (X= D, T, Q).

A 6-311++G (d,p) basis set was used for Boradiphosphole ($BC_2P_2H_3$) in chapter 2. It includes six Gaussians for core orbitals, valence orbital splits into three shells composed of three, one and one Gaussians and each heavy and hydrogen atom consists of diffuse and polarization functions. While for triple-decker sandwich complexes ($CpMP_6MCp$) in chapter 3 double zeta (DZ), triple zeta valence (TZV) and triple zeta valence polarization (TZVP) basis sets and chapter 4 for pentapeptide calculation 6-31+G(d) basis set were used.

(c) Effective core potential (ECP): In the case of atoms with high atomic number the number of orbitals increases with increase in electrons. This leads to more computational cost. Since the core orbital energy levels do not change significantly due to chemical bonding they are represented by average potential. Effective core potential is one of the pseudo potential whose functional form is

$$\text{ECP}(r) = \sum_{i=1}^M d_i r^{n_i} e^{-\xi_i r^2} \quad (1.25)$$

where d_i is the coefficient for each term, r is the distance from the nucleus with a power of n_i for the i^{th} term and ξ_i is an exponent of the i^{th} term. ECP's takes very less computational time as basis functions are drastically reduced due to core potential and involves only calculation for valence electrons. This basis sets are widely used for transition metals. Los Alamos National Laboratory double-zeta (LANL2DZ) basis set is one such basis set developed by Hay and Wadt.^{10e} This basis set is used in chapter 3 for transition metals in triple-decker sandwich complexes.

(d) Plane wave: Unlike other functions they are completely delocalized and therefore not to be ascribed for atoms. The functional form is

$$\chi_i(r) = e^{ikr} \quad (1.26)$$

where k is the momentum vector and r run through the Bravais lattice.

The right choice of basis set is important for quantum mechanical methods. One should be aware of Basis set superposition error (BSSE)^{10f} especially in calculating interaction (dimerization) energies which are overestimated. This is due to the expanded larger basis functions description for the wave function of the complex than the component. One of the methods to rectify this problem is counterpoise.^{10g}

1.3.2.2 Semi Empirical Methods

Semi empirical approaches⁴ start from HF equations, where the core electrons are not included for the calculation. They use a minimal basis set (STO-3G) and replace the atomic nuclei plus core electron by ion cores of charges Z_v . There are a range of such methods which differ basically on the treatment of matrix elements of Fock operator

(1.20).¹¹ The methods can be broadly classified as two types (a) Involves only one electron terms of Hamiltonian and (b) Involves both one and two electron Hamiltonian terms. Hückel and extended Hückel methods involve only one electron Hamiltonians

(1.27).¹² The former method involves only π electrons and latter includes all valence electrons. They are non SCF methods. The results obtained from these methods are useful for quick qualitative determination of wave function and predicting the geometric and energy trends.

$$H = \sum_{i=1}^N h_{eff}(i) \quad (1.27)$$

On the other hand Pariser-Parr-Pople (PPP),^{13a,b} Intermediate Neglect of Differential Overlap INDO, MNDO^{13c} methods, Austin model 1 (AM1)^{13d} and Parametric model 3 (PM3)^{13e} involve Hamiltonian that has both one and two electron terms which are replaced by parameters. These methods differ in the extent to which zero differential overlap approximation (ZDO) is invoked in evaluating electron repulsions integrals and the way parameters are specified.^{12d} ZDO is an approach to the systematic neglect of the small-in-value electron repulsion integrals. It assumes that all the products of atomic orbitals $\chi_\mu \chi_\nu$ are set to zero and the overlap integral $S_{\mu\nu} = \delta_{\mu\nu}$ (where $\delta_{\mu\nu}$ is the Kronecker delta). The ZDO approximation greatly simplifies the computation of wave functions by eliminating many of two-electron integrals. Thus neglecting of integrals and parameterization makes these calculations applied for larger systems at low cost of CPU time. AM1 and PM3 are popularized semi empirical methods used for larger systems and in hybrid QM/MM methods.

1.3.3 Post Hartree-Fock Methods

The major drawback of HF method is neglecting the electron correlation between the motions of electrons of anti-parallel spin. Hence it results severe underestimation of bond dissociation energies and deficiency in describing the compounds exhibiting Jahn-Teller distortions. Even the single determinant HF wave function may not always describe the full symmetry of the wave function. Therefore, Hartree-Fock method (single determinant approach) is unsuccessful in predicting the properties where many body correlation effects contribute significantly. The difference in the HF energy (E_{HF}) and the exact non-relativistic energy (E_{exact}) is called correlation energy (E_{corr}).

$$E_{cor} = E_{exact} - E_{HF} \quad (1.28)$$

The methods that are developed after HF explicitly treat the correlation effects and are known as Post Hartree-Fock or electron correlation methods.^{4,14} These methods should have size extensivity and size consistent properties especially when calculating, ionization potential, electron affinity, dissociation energies and oligomer gaps.

- (a) Size extensivity: when a method scales correctly with the number of particles in the system as the exact energy does, then it is said to be size-extensive.
- (b) Size consistent: when there are two non-interacting systems A and B. If a given method calculates the energy of the complex system A-B as equal to the sum of the energy of A plus the energy of B taken by themselves ($E(A + B) = E(A) + E(B)$) then it is size consistent.

Most common electron correlation methods are Møller-Plesset Perturbation Theory,¹⁵ Configuration Interaction¹⁶ and Coupled Cluster Theory.¹⁷

1.3.3.1 Many Body Perturbation Theory

Here the correlation is added as perturbation to HF wave function. Hamiltonian for perturbation theory is expressed as

$$H = H^{(0)} + \lambda H^{(1)} + \lambda^2 H^{(2)} + \dots \quad (1.29)$$

The wave function and energy are also expanded in power series of perturbation.

$$\psi = \psi^{(0)} + \lambda \psi^{(1)} + \lambda^2 \psi^{(2)} + \dots \quad (1.30)$$

$$E = E^{(0)} + \lambda E^{(1)} + \lambda^2 E^{(2)} + \dots \quad (1.31)$$

This leads Schrödinger equation to

$$H^{(0)}\psi^{(0)} = E^{(0)}\psi^{(0)} \quad (1.32)$$

$$(H^{(0)} - E^{(0)})\psi^{(1)} = (H^{(1)} - E^{(1)})\psi^{(0)} \quad (1.33)$$

These solutions give different order of correction to energy. Depending on the truncation of the series, it is Møller-Plesset 2 (MP2), MP3 and MP4 etc. These methods are size consistent even though they are non-variational.¹⁵ Among MP_n levels, MP₄ is considered to attain 90-95% of correlation effect. The limitation of these methods is that they are computationally demanding for larger systems.

1.3.3.2 Configuration Interaction (CI)

This method solves variationally a multi determinant wave function, which includes the excited states for the description of an electronic state.¹⁶

$$\Psi = c_o \psi_o + \sum_{ic} c_i^c \psi_i^c + \dots \quad (1.34)$$

where Ψ is usually an electronic ground state of the system, ψ_i 's are called Configuration state functions (CSF's) which are Slater determinants containing products

of spin orbitals with ψ_0 being the Hartree-Fock wave function (1.18) and c_0 and c_1 are the coefficients of determinants.

The method is constructed by starting with HF equations and new determinants are made by promoting the electrons from occupied to unoccupied orbitals. Based on the number of excitations used to make each determinant, CI calculations can be (a) CIS involves single excitations, (b) CISD involves single and double excitations and (c) Full CI includes all possible excitations. This method calculates energy very accurately at each level. The difference between the E_{HF} and the full CI energy is the basis set correlation energy. The drawbacks of this method are (a) truncated CI are size inconsistent and (b) limited to small molecules as cost of CPU time is very high (N^8). Multi configuration self consistent field (MCSCF) is also a multi determinant approach where both coefficients of basis functions and determinants are varied. This method is desirable whenever HF wave function gives a poor qualitative description for the system. While Complete Active Space Self Consistent Field (CASSCF) is an MCSCF method where all combinations of active space orbitals are included.

1.3.3.3 Coupled Cluster Theory

This method uses exponential form of wave function as linear combinations of many determinants.¹⁷

$$\Psi = e^T \Psi_{HF} \quad (1.35)$$

where Ψ is the exact non-relativistic ground state molecular electronic wave function,

Ψ_{HF} is the normalized ground state Hartree-Fock equation, the operator e^T is defined by Taylor series expansion and the cluster or excitation operator $T = T_1 + T_2 \dots T_n$.

$$e^T = 1 + T + \frac{T^2}{2!} + \frac{T^3}{3!} + \dots \quad (1.36)$$

$$T_1 \Psi_0 = \sum_{a=n+1}^{\infty} \sum_{i=1}^n t_i^a \Psi_i^a \quad (1.37)$$

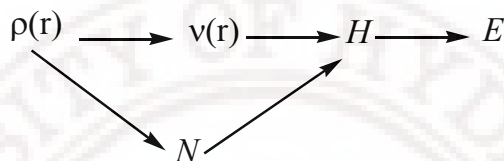
where T_1 is a one particle excitation operator, Ψ_i^a is a singly excited Slater determinant with occupied spin orbital χ_i replaced by the virtual spin orbital χ_a and t_i^a is a numerical coefficient whose value depend on i and a that are determined from equation 1.35. Even in this method based on the excitations involved in T form of operator they can be CCD, CCSD etc. Unlike CI, CC calculation of singles, doubles refer to all interactions associated with that quantity of particles (one and two body interactions).

This is one of the best method for estimating the electron correlation and predicting the molecular properties. This method is size extensive but size consistency depends on reference HF wave function. The drawback of this method is the determination of the cluster amplitudes t for all of the operators included in the particular approximation. This method is also limited to small molecules only. QCISD is an intermediate method of CC and CI developed by Pople and co-workers.¹⁸ It is widely used for small molecules and gives good results for calculating correlation energies. All the post Hartree-Fock methods are computationally very expensive and can be handled in solving only for small size systems.

1.3.4 Density Functional Theory

In HF and Post HF methods the energy and its derived properties are obtained from wave function. For a many body system, wave function is complex due to the increase in number of variables (3 spatial and a spin coordinates for each electron). Hence they cannot be applied for larger systems. While density functional theory derives

energies and related properties from the electron probability density $\rho(x, y, z)$, which depends only on 3 variables. This was proposed by Thomas-Fermi¹⁹ for non-interacting uniform electron gas, which was later proved by Hohenberg-Kohn theorems.^{20a,b} The theorems states that the ground state energy of an N electron system is functional of the electron density $\rho(r)$, and energy is minimum when evaluated with the exact ground state density.



Consequently energy is functional of density $E = E_v[\rho]$ (1.38)

where $E_v[\rho] = T[\rho] + V_{ee}[\rho] + V_{ext}[\rho]$ (1.39)

and $T[\rho]$ is the electronic kinetic energy functional, V_{ee} is the electron-electron interaction potential functional and V_{ext} is the electron nuclei potential energy interaction called as external potential given as

$$V_{ext} = \int v(r)\rho(r)dr = \sum_{A=1}^N \frac{Z_A}{r_{iA}} \quad (1.40)$$

The first two terms of equation 1.39 are unknown as they are independent of external potential and can be determined by minimizing the energy with respect to variations in $\rho(r)$ (second Hohenberg-Kohn theorem, 1.41).

$$E_v[\rho] \geq E_v[\rho_o] \quad (1.41)$$

The real application of these theorems in solving chemical problems came into light only after Kohn-Sham formalism.^{20c} This formalism has given an idea for (a)

determining the density without finding the wave function and (b) determining the properties from the electron density.

$$\left[-\frac{1}{2}\nabla_i^2 + v_{eff}(r) \right] \psi_i = \epsilon_i \psi_i \quad (1.42)$$

where first two terms represent the one electron Hamiltonian, ψ_i is Kohn-Sham orbital, ϵ_i is the Kohn-Sham orbital energy and v_{eff} is the effective potential given as

$$v_{eff}(r) = v_{ext}(r) + v_{coul} + v_{xc} \quad (1.43)$$

where v_{ext} is external potential (nuclei-electron attraction), v_{coul} is the columbic

repulsion of electron- electron, $v_{xc} = \frac{\delta E_{xc}[\rho(r)]}{\delta \rho}$ is exchange correlation potential and

E_{xc} is the exchange correlation energy. These equations are also solved iteratively as HF equations and the total energy is given as

$$E_{DFT} = \sum_{i=1}^N \epsilon_i + V_{NN} \quad (1.44)$$

The advantages of DFT over HF method are (a) includes correlation effects (as the Hamiltonian of the Kohn-Sham equation 1.42 considers both exchange and correlation part in the form of functional v_{xc} where as Fock operator of Hartree-Fock equation 1.9 has only exchange part (K_{ij})) and (b) for large system also density depends only on three variables. Although DFT has advantages the crucial quantities E_{xc} and v_{xc} decide the liability of the results. The E_{xc} is an unknown term and is approximated. E_{xc} is usually divided into separate parts, referred to as the exchange and correlation parts given

$$\begin{aligned} E_{xc} &= (T[\rho] - T_s[\rho]) + (V_{ee}[\rho] - V_{coul}[\rho]) \\ \text{as } E_{xc} &= E_x + E_c \end{aligned} \quad (1.45)$$

Various approximations are used to obtain the E_{xc} . These include local density, gradient density and hybrid methods.

1.3.4.1 Local Density Approximation (LDA)

This is the simplest approximation proposed by Hohenberg and Kohn.^{19a} LDA assumes that density can be treated locally as a uniform electron gas where the density is a slowly varying function with position. The E_{xc} in LDA is given as

$$E_{xc}^{LDA} = \int \rho(r) \varepsilon_{xc}(\rho) dr \quad (1.46)$$

$$v_{xc} = \varepsilon_{xc}[\rho(r)] + \rho(r) \frac{\partial \varepsilon_{xc}[\rho]}{\partial \rho} \quad (1.47)$$

where $\varepsilon_{xc}[\rho]$ is the exchange correlation energy per electron in a homogenous electron gas with electron density ρ . In more general case where α and β densities are not equal then LDA is replaced by local spin density approximation (LSDA). This method is not very successful in calculating systems involving weak intermolecular interactions and van der Waals attractions.

1.3.4.2 Generalized Gradient Approximation (GGA)

In this method exchange and correlation energy are dependent both on electron density $\rho(r)$ and its gradient $\nabla \rho$.^{19a,b} They are useful when electron density varies with the position. General form of the GGA is

$$E_x^{GGA}[\rho^\alpha, \rho^\beta] = \int f[\rho^\alpha(r), \rho^\beta(r), \nabla_{\rho^\alpha(r)}, \nabla_{\rho^\beta(r)}] dr \quad (1.48)$$

These functionals tend to improve the total and atomic energies in comparison to LDA. The GGA functional used in this thesis is Becke- Perdew functional.^{21a,b}

1.3.4.3 Hybrid Functionals

These functionals include the mixture of HF and DFT exchange along with DFT correlation. As the exchange part can be completely evaluated by HF method. The general form is

$$E_{xc}^{Hybrid} = c_{HF} E_x^{HF} + c_{DFT} E_{xc}^{DFT} \quad (1.49)$$

The most common hybrid functional used in the thesis (chapter1 and 2) is B3LYP which uses a combination of the three-parameter Becke exchange functional^{21c} along with the Lee-Yang-Parr non local correlation functionals.^{21d} Its functional form is

$$E_{xc}^{B3LYP} = (1 - c_0 - c_x) E_x^{LSDA} + c_0 E_x^{HF} + c_x E_x^{B88} + (1 - c_c) E_c^{VWN} + c_c E_c^{LYP} \quad (1.50)$$

where c 's are constants ($c_0 = 0.20$, $c_x = 0.72$ and $c_c = 0.81$) to give best fit experimental atomization energies.

1.3.5 Composite Methods

This method uses a series of *ab initio* calculations with added empirical corrections. The Gaussian (Gn)^{22a} and complete basis set (CBS)^{22b} are two such composite methods. These methods are used to accurately determine the thermodynamic data such as enthalpy of formation, molecular atomization energies etc. These methods are also limited for smaller size systems. In this thesis G3B3 composite method was used.^{22c} The total energy at 0 K is

$$E_{G3B3} = E_{MP4/6-31G(d)} + E_{QCI} + E_{Plus} + E_{2df,p} + E_{G3large} + E_{SO} + E_{Hlc} + E_{ZPE} \quad (1.51)$$

$$\text{where } E_{QCI} = E_{QCISD(T)/6-31G(d)} - E_{MP4/6-31G(d)} \quad (1.52)$$

$$E_{plus} = E_{MP4/6-31+G(d)} - E_{MP4/6-31G(d)} \quad (1.53)$$

$$E_{2df,p} = E_{MP4/6-31G(2df,p)} - E_{MP4/6-31G(d)} \quad (1.54)$$

$$E_{G3Large} = E_{MP4(Full)/G3Large} - E_{MP4/6-31G(2df,p)} - E_{MP4/6-31G(d)} \quad (1.55)$$

$$\text{For molecules } E_{Hlc} = -An_{\beta} - B(n_{\alpha} - n_{\beta}) \text{ and atoms } E_{Hlc} = -Cn_{\beta} - D(n_{\alpha} - n_{\beta}) \quad (1.56)$$

where n_{α} and n_{β} represent the number of α and β electrons, A and C represent the corrections for paired valence electrons and B and D is for unpaired valence electrons.

E_{SO} = spin orbit correction for atomic species, E_{ZPE} = zero point energy correction.

The steps involved for calculating E_{G3B3} energy are (a) Equilibrium structure is initially obtained from hybrid B3LYP level with 6-31G(d) basis, and the zero point energy correction (E_{zpe}) is obtained from the frequency calculation at same level of theory. (b) Equilibrium geometry is refined further at higher level such as MP4(full)/6-31G(d) to obtain all the electron correlation energies. (c) A series of single point energy calculations are carried out at higher levels and energy is modified by series of corrections as E_{QCI} (for correlation effects beyond fourth order of perturbation theory), E_{plus} (for the correction of diffuse functions of basis set), $E_{2df,p}$ (for the correction of polarization functions), $E_{G3large}$ (for some core polarizations as well as multiple set of valence polarizations). (d) High level corrections are added to account for the remaining deficiencies in energy calculations. All electronic structure calculations are done using Gaussian²³ and ADF²⁴ program packages.

1.4 Molecular Mechanical Methods

Molecular mechanical methods use classical mechanics to model and predict the properties of molecular systems. In this method electrons are not explicitly examined, but are assumed to find an optimal distribution about the nuclei. The energy of the system is calculated as a function of the nuclear positions only. It considers atoms as spheres or balls those have net charges and bonds as springs. The interactions that held together this

collection of particles in molecule are simple harmonic forces. The sum of energies arising from various types of the forces that are described in terms of individual potential functions gives the molecular potential energy (V) or steric energy of molecule. Another fundamental assumption in this method is transferability of the functional form and parameters, since molecules tend to be composed of units which are structurally similar in different molecules. The method is invariably used to carry out calculations on systems containing large number of atoms such as biomolecules, polymers etc in predicting structural properties.^{2,25}

1.4.1 Force Fields

A force field is used to describe the potential energy of a system of particles (typically but not necessarily atoms). The functional form of a force field² is

$$\begin{aligned}
 V(R^N) = & \sum_{bonds}^N \frac{k_i}{2} (l_i - l_{i,0})^2 + \sum_{angles}^N \frac{k_i}{2} (\theta_i - \theta_{i,0})^2 + \sum_{torsions}^N \frac{V_n}{2} (1 + \cos(n\omega - \gamma)) \\
 & + \sum_{cross}^N \frac{k_i}{2} (\theta_i - \theta_{i,0}) [(l_1 - l_{1,0}) + (l_2 - l_{2,0})] + \\
 & + \sum_{i=1}^N \sum_{j=i+1}^N \left(4\epsilon_{ij} \left[\left(\frac{\sigma_{ij}}{r_{ij}} \right)^{12} - \left(\frac{\sigma_{ij}}{r_{ij}} \right)^6 \right] + \frac{q_i q_j}{4\pi\epsilon_0 r_{ij}} \right)
 \end{aligned} \tag{1.57}$$

where V denotes the potential energy which is a function of the positions (R) of N particles. The first term in equation 1.57 is bond stretching energy, which represents the interaction between pairs of bonded atoms modeled by a harmonic potential where bond length l_i deviates from the reference (equilibrium) value $l_{i,0}$. The second term is the bond bending energy which is the summation of valence angles in the molecule modeled using a harmonic potential. The third term is a torsional potential that models how the energy changes when bond rotates. These three terms describe a single aspect of molecular shape

and are called as valence terms. The fourth term is the bond-stretch cross term that describes how the equilibrium bond lengths tend to shift as bond angles change. The last term in equation 1.57 represents the non bonded valence term. This is calculated between all pairs of atoms (i and j) in different molecules or in the same molecule separate by at least three bonds. This term is modeled using a Lennard-Jones potential for van der Waals interactions and Coulombic potential term for electrostatic interactions. Since the constants (k_b , V_n and σ_{ij}) of equation 1.57 are parameterized using the spectroscopic data or quantum mechanical calculations they are also called as empirical force field methods. MM calculations needs initial atomic coordinates and atom types. Atom type gives the information of atom's atomic number and molecular environment of each atom in a molecule.

In general force fields are of two types (a) Class I or harmonic and (b) Class II. Class I force fields are usually applicable for larger systems such as DNA and proteins (AMBER, CHARMM, GROMOS, OPLS). It includes the harmonic potential for the stretch and bending energy (valence terms), Lennard-Jones potential for van der Waals energy. It has no cross terms. On the other hand Class II force fields (MM2, MM3, CFF etc) are applicable for small or medium sized organic systems. It includes a number of cross terms, at least as cubic expansions of stretch and bending energy and exponential potential for van der Waals energy. Force fields can be united-atom or all-atom type. In united atom hydrogens are not treated explicitly and thus save computational time.

Various force fields that are in use are MM2, MM3, CHARMM, AMBER, ESFF, CFF, GROMOS, CVFF, Tripos, OPLS, MMFF, UFF etc. They basically differ in (a) functional form of each term, (b) number of cross terms used and (c) the data used to

parameterize the constants. The performance of force field is more sensitive to non-bonded and torsional terms. The parameters of one type of force field are not usually transferable to another type. AMBER and UFF force fields are used in chapter 4 and Tripos force field is used in chapter 5. Assisted Model Building with Energy Refinement (AMBER)^{26a} is specifically parameterized for proteins and nucleic acids. It is name of a force field and molecular mechanics program also. It uses only five bonding (valence) and non-bonding terms with sophisticated electrostatic treatment and excludes cross terms. Universal Force Field (UFF)^{26b} is applicable for all elements in the periodic table but most widely used for systems containing inorganic elements. It uses four valence terms and excludes electrostatic term. The number of parameters are relatively small in UFF hence cannot achieve accuracy compared to other highly parameterized force fields as MMFF94. The Tripos force field (SYBYL)^{26c} is applicable to small organic molecules and proteins and is used for drug design. It uses four valence terms and an electrostatic term.

The least computational cost of molecular mechanics allows its use in procedures such as molecular dynamics, conformational energy searching, and docking that require large numbers of energy evaluations. The following sections discusses about molecular dynamics and docking aspects that were used in chapter 4 and 5.

1.4.2 Molecular Dynamics

It is a simulation of the time-dependent behavior of atomic and molecular system such as vibrational or Brownian motion. It provides details of system changes from one configuration or conformation to another. This method is generally used to investigate structure, dynamics and thermodynamics of the systems with a feasible time of

computation. To compute the time evolution of the system, we need to solve the time dependent Schrödinger equation for the N-particle wave function (1.1) or approximate the system as classical particles and use classical mechanics. Finding the wave function for the system more than 4 or 5 atoms is extremely difficult using time dependent Schrödinger equation and hence is not applicable for larger systems. On the other hand molecular mechanical methods are efficiently used to understand the complex and dynamic phenomenon that occur in biological process such as protein stability, conformational changes, protein folding, ion transport in membranes etc.

The molecular dynamic (MD) simulations²⁷ are based on Newton's second law, $F=ma$ where F is the force exerted on the particle, 'm' is the mass and 'a' is the acceleration of the particle. Integration of the equations of motion then yields a trajectory that describes the positions, velocities and acceleration of particles that vary with time. The macroscopic observables such as pressure, energy, heat capacities, diffusion coefficients, radial distribution functions etc are determined from this trajectory using statistical mechanics. Unlike Monte Carlo method (another simulation technique), MD is deterministic method and once the positions and velocities of each atom are known, the state of the system can be predicted at any time in the past or the future. For the calculation of trajectory one only needs initial positions of the atoms and initial distribution of velocities. The initial velocities are often chosen randomly from a Maxwell-Boltzmann or Gaussian distribution. For a given temperature the probability that an atom i has a velocity v_x in the x direction at a temperature T is

$$p(v_{ix}) = \left(\frac{M_i}{2\pi k_B T} \right)^{\frac{1}{2}} e^{-\left[\frac{M_i v_{ix}^2}{2k_B T} \right]} \quad (1.58)$$

Further, velocities and accelerations are determined by the gradient of the potential energy (V) as

$$F = m \frac{d^2 x}{dt^2} = \nabla_i V \quad (1.59)$$

The potential energy is a function of atomic positions ($3N$) for all the atoms in the system. There is no analytical solution to the equation of motion due to complicated nature of this function and are solved numerically. The numerical algorithms that integrate the equations of motion are Verlet, Leap-Frog, Velocity-Verlet, Predictor-corrector and Beeman's.^{2a} The characteristics of the integrator are (a) time reversibility and (b) phase space volume should be preserved. All these algorithms assume that the positions, velocities and accelerations can be approximated by Taylor series expansion. Among the four, best is Velocity-Verlet algorithm as it needs less disk storage and there is no compromise in precision, CPU time. The system positions, velocities and accelerations are obtained from this algorithm as

$$r(t + \delta t) = r(t) + v(t)\delta t + \frac{1}{2}a(t)\delta t^2 \quad (1.60)$$

$$v(t + \delta t) = v(t) + \frac{1}{2}[a(t) + a(t + \delta t)]\delta t \quad (1.61)$$

Computing forces is the most time consuming process in MD. The calculation of the non-bonded interactions especially electrostatic interaction play significant role on the results. The three methods to compute long range coulomb forces are Ewald summation; Particle Mesh Ewald and Cell multipole.^{2a} Depending on the evaluation of observables or property there are different types of ensembles used in MD calculations. An ensemble is a collection of all possible systems which have different microscopic states but have an

identical macroscopic or thermodynamic state. The different ensembles are (a) Micro canonical ensemble (NVE) corresponds to isolate system where number of atoms, volume and energy are fixed. (b) Canonical ensemble (NVT) where number of atoms, volume and temperature are fixed. (c) Isobaric-Isothermal ensemble (NPT) where number of atoms, temperature and pressure are fixed. (d) Grand Canonical ensemble (μ VT) where chemical potential μ , temperature and volume are fixed. For maintenance of fixed pressure various types of barostat (Berendsen and Nosé-Hoover) and for fixed temperature thermostats (Anderson, Berendsen etc) are used. The molecular dynamics calculations mainly depends on force field functional form, evaluation of long range forces, time step etc. Time step should be one order of magnitude less than the time scale of the shortest motion of system. AMBER, CHARMM, GROMOS are some of the MD programs. AMBER²⁸ was used for analyzing the average number of water molecules that are surrounding the Phosphodiesterase 4 (PDE4) enzyme (chapter 4).

1.4.3 Docking

It is the process of finding the best fit of two molecules in 3 dimensional space.²⁹ This method can be applied when X-ray structure or theoretical model is known for the molecule. Hence is known as a structure based design method. It helps to discover or design molecules that can interact with biochemical targets such as proteins or DNA. Based on the type of input molecules docking is of two types. Docking of two macromolecules like proteins or DNA-protein is macromolecular docking. Because of large degrees of freedom the energetically favorable complexes are evaluated based on geometric properties such as shape complementarity. Other type is small molecule (ligand or substrate) docked to macromolecule (DNA or protein). This substantially

differs from macromolecular docking in the fact that conformational flexibility of the ligand molecule is of importance along with geometrical properties to decide the low-energy complexes. Thus, depending on the flexibility of ligand molecular docking can be rigid or flexible type. The steps involved in docking are (a) conformational search (posing) and (b) scoring the obtained conformations which finally gives a rational idea of best fit of molecule.

There are several types of conformational searching methods^{2,29} used in docking programs. They are (a) geometric search method such as descriptor matching, grid search, fragment based type and (b) energy search method such as simulation annealing or MD. They can also be divided as (a) systematic search which is deterministic, exhaustive and extensive and (b) stochastic search which is random, non deterministic (simulation annealing and evolutionary algorithms) method. Descriptor based method analyze the receptor for regions of likely complementarity (eg: DOCK). It is a very fast method and provides a reasonable sampling of particular region of receptor site. Grid search method samples six degrees of freedom of orientation space (soft docking). They find the neighborhood of the correct solution that cannot be guaranteed with discrete sampling method. The step size used in the search determines the time of search and accuracy of result. Fragment-joining method identifies regions of high complementarity by docking functional groups (as fragments) into receptors (eg: FLEX). It is an incremental construction algorithm which is deterministic and exhaustive. Thus overcomes the rigid ligand issues and also when ligand has more number of flexible or rotatable bonds.

In energy search methods the configurational and conformational aspects of docking are taken care because there are multiple minima and complex topography of molecular potential surfaces. Simulation annealing developed by Goodsell and Olson uses Metropolis algorithm to find the low energy complexes (eg: AUTODOCK).³⁰ It is a quite efficient one in considering the number of degrees of freedom. Evolutionary algorithms are genetic and Lamarckian genetic algorithms and are very much popularized in the recent times. This method mimics the evolutionary process where the individuals are considered as configurations in search space and fitness function decides which individuals survive and produce off springs. In this thesis Lamarckian genetic algorithm³¹ that is available in AUTODOCK³⁰ was used (chapter 5). It is very successful in reproducing the co crystal structures that have many rotatable bonds.

After conformational sampling, ranking them with respect to binding energy to a given protein is critical. The function that ranks the conformations and gives the binding affinity estimation is scoring. The prediction of the best fit of molecule (true positives) in the receptor pocket depends mainly on scoring function. There are three types of scoring functions used in several docking programs. They are (a) force field, (b) empirical and (c) knowledge based scoring.^{2a,29} Force Field scoring can be directly applied to protein-ligand complexes. It is very good in selecting docking modes but difficult to compare different molecules on this basis. In force field scoring function entropy and solvation effects are not considered. Empirical scoring function approximates the binding affinity as a sum of weighted interactions (hydrogen-bonding, hydrophobic, ionic interactions and binding affinity) that contribute to binding effect. These functions are calibrated with a set of experimental binding affinities obtained from the known protein-ligand complexes.

Inconsistency of this data will cause problems. While knowledge based scoring functions is based on inverse formulation of Boltzmann law. It is used to derive the sets of atom-pair potentials by favoring preferred contacts and penalizing repulsive interactions.

Even though molecular mechanical methods are applied widely to understand for the complex process in biomolecules, they are mainly limited in understanding the electronic structural changes (bond breaking, bond forming, charge transfer and electronic excitations etc) and in application to metallo-proteins due to the lack of effective parameters.

1.5 Quantum Mechanical/Molecular Mechanical Methods

The fundamental idea in this method is that to divide a large condensed phase system into two regions as QM and MM.³² The reactive chemical event is contained within the QM region, while the surrounding condensed phase is modeled by MM. The Hamiltonian and energy of the whole system are given as

$$H = H_{QM} + H_{MM} + H_{QM/MM} \quad (1.62)$$

$$E = E_{QM} + E_{MM} + E_{QM/MM} \quad (1.63)$$

There are many levels of accuracy used for the QM region such as DFT or *ab initio* HF method when there are small number of atoms and semi empirical methods such as PM3 or AMI or empirical valence bond (EVB) for considerable large number of atoms. On the other hand empirical Hamiltonian can be any typical force fields such as AMBER, GROMOS, CHARMM and UFF etc.^{32b}

The key aspects of QM/MM method is the interactions between the QM and MM regions. There are two types of interactions³² (a) In order to account the influence of surrounding solvent on the enzyme of QM region (or ligand in protein active site),

electrostatic and van der Waals interactions of QM/MM interface must be included and (b) In enzymatic reaction of the large biomolecules where QM/MM interface involves covalent bonds needs special treatment. The capable way of handling both bonding (bond stretching, bond bending and internal rotation) and non bonded interactions (electrostatic and van der Waals interactions) limits the success of this method.

The electrostatic interaction which is key element in coupling is treated in two ways. They are mechanical embedding and electrostatic embedding. In mechanical embedding QM region is calculated quantum mechanically in absence of MM region and treats the interactions of QM/MM interface at MM level. Hence it is simpler but less accurate due to the lack of accurate set of electrostatic MM parameters for atoms in QM region and ignoring potential perturbation of the electronic structure of QM region by charge distribution of MM region. In electrostatic or electronic or electric embedding the QM region is calculated quantum mechanically in presence of MM region and treats the interactions of QM/MM interface by including certain one electron Hamiltonian terms. As a result the electronic structure of the QM region adjusts to the charge distribution in the MM region. It is more accurate and computationally expensive. The limitation is constructing appropriate one electron term.³²

There are two most successful ways to treat the QM/MM interface when a covalent bond is involved. They are link atom and frozen orbital approaches.³¹ In link atom approach, the link atom is used to saturate the dangling bond of the QM/MM interface. This link atom is usually a hydrogen atoms or a parameterized atom that mimics the properties of the original bond. They are treated explicitly in QM calculation but do not interact with the MM atoms. It is widely used but introducing the artificial link

atoms increases extra degrees of freedom and also the QM/MM energy is more complicated. In frozen orbital approach, localized frozen molecular orbitals are used at QM/MM interface. The localized orbitals are determined by calculations on small model compounds and assumed to be transferable. This is more fundamental and accurate than link atom approach as the frozen orbitals provide the QM description of the charge distribution at QM/MM interface and are better parameterized.

The QM/MM methods are not only quite successful in explaining the complex enzymatic reactions in biomolecules but are also useful in understanding the substitution and solvation effects in large inorganic molecules.³³ A ONIOM³⁴ two layer QM/MM method was used to understand the solvation effect in the PDE4 enzyme (chapter 4).

1.6 A Brief Outline of the Chapters

The electronic structure and bonding aspects of clusters such as boradiphosphole and triple-decker sandwich complexes with a P_6 as middle ring are studied in chapter 2 and chapter 3. The chemical bonding was understood by applying isolobal analogy and electron counting rules. The isolobal analogy introduced by R. Hoffmann³⁵ constructs a link between inorganic (organo-metallic) and organic chemistry. Later it is extended to BH and CH fragments in carboranes, BH and Si, and P and CR fragments in phosphorus-organic compounds.³⁵⁻³⁷ The isolobal fragments have same number, symmetry, energy and occupancy of frontier orbitals which leads to existence of similar structural analogs. Application of the CH and P isolobal connection to the cyclopentadienyl anion (Cp^-) has extended the utility of Cp^- type ligands. The various *neutral* and *monoanionic* phospholes ($EtBu_2C_2P_2$ where $E = P^-, As^-, Sb^-, S, Se$ and Te) which are isostructural and isoelectronic

to cyclopentadienyl anion (Cp^-) ligand are of considerable importance because of their ability to stabilize monovalent metals.

However, *cationic* ($\text{EtBu}_2\text{C}_2\text{P}_2$ where $\text{E} = \text{P}^+, \text{As}^+, \text{Sb}^+$) and *neutral* phospholes ($\text{EtBu}_2\text{C}_2\text{P}_2$ where $\text{E} = \text{BPh}, \text{Sn}, \text{Ge}$ and Pb), analog of Cp^+ , which are synthesized in recent years have different structures. The Cp^+ which is a 4π electron system with 20 valence electrons (5C-C, 5C-H bonds) can exist in triplet D_{5h} or vinylcyclopropenyl-type structure. All heterophospholes except $\text{PhBtBu}_2\text{C}_2\text{P}_2$ which has a tricyclopentane-type structure exist in *nido*-type geometry. To understand the structural anomaly a potential energy surface of *neutral* and *dianionic* boradiphosphole ($\text{R}'\text{BC}_2\text{P}_2\text{R}_2$) were explored in the second chapter.

Optimization of classical and non-classical *neutral* and *dianionic* $\text{BC}_2\text{P}_2\text{H}_3$ isomers at the hybrid DFT (B3LYP/6-311++G (d,p)) and composite (G3B3) methods gave a variety of geometric and positional isomers as minima. Vinylcyclopropenyl-type structure was found to be lowest energy structure for $\text{BC}_2\text{P}_2\text{H}_3$ at B3LYP/6-311++G (d,p) level of theory. However, at the G3B3 method (that includes correlation and basis set effects) two more low-energy isomers are obtained for $\text{BC}_2\text{P}_2\text{H}_3$ (atricyclopentane-, a *nido*-type). This shows that *neutral* $\text{BC}_2\text{P}_2\text{H}_3$ isomers in comparison to the isolobal Cp^+ and $\text{H}_n\text{C}_n\text{P}_{5-n}^+$ isomers has a competition between 2π delocalized vinyl cyclopropenyl- and cluster-type structures (*nido* and tricyclopentane). Substitution of H on C by *t*Bu and H on B by Ph in $\text{BC}_2\text{P}_2\text{H}_3$ showed that lowest energy isomer to be experimentally known tricyclopentane structure rather than *nido*-type as observed in $\text{tBu}_2\text{C}_2\text{P}_3^+$. The lower preference for *nido* boradiphosphole was due to the poor overlap of BH capping orbital with phosphorus $3p_z$ orbitals of basal ring. This makes the bond-stretch isomer

tricyclopentane-type structure of lower energy. On the other hand $\text{BC}_2\text{P}_2\text{H}_3^{2-}$ at both levels and with similar substituents (C-*t*Bu and B-Ph) favors cyclic planar geometry as lowest energy structure. The factors that affect stability of 3- 4- 5- membered ring and acyclic geometrical and positional isomers of *neutral* and *dianionic* $\text{BC}_2\text{P}_2\text{H}_3$ isomers are (i) relative bond strengths (ii) availability of electrons for the empty 2p-boron orbital, and (iii) steric effects of the *t*Bu groups in the $\text{HBC}_2\text{P}_2\text{tBu}_2$ systems.³⁸

In the third chapter structural diversity that is present in P_6 middle ring of triple-decker sandwich (CpMP_6MCp) clusters were studied. The P_6 ring existed as (a) symmetrical and planar for $\text{M}=\text{Mo}$, W where valence electron count [VEC] is 28, (b) distorted with four long and two short P-P bonds and yet planar for $\text{M}=\text{V}$ (26 VEC), (c) distorted with two long and four short P-P bonds and yet planar for $\text{M}=\text{Nb}$ (26 VEC) and (d) nonplanar chair like conformation for $\text{M}=\text{Ti}$ (24 VEC). The traditional valence electron count (VEC) for CpMP_6MCp includes 10 π electrons from 2 Cp, 6 π electrons from P_6 and valence electrons of two oxidized metal atoms. We have applied *mno* rule, which states the number of electron pairs required for stable condensed polyhedral structure is $m + n + o$, where m is the number of polyhedra, n is the number of vertices and o is the number of single atom bridges. Although this was devised primarily for applications in condensed polyhedral boranes,^{39a,b} it is also applicable to metallocenes and multiple-decker sandwiches.^{39c} According to *mno* rule CpMP_6MCp needs 25 skeletal electron pairs or 50 electrons ($m=3$, $n=18$, $o=2$ plus two for the two nido arrangements) or 18 VEC to be stable. So the structures with 28 VEC or 60 skeletal electrons (if all VE of the metal and σ electrons that is 20 from ten C-C bonds of the two Cps, 12 from 6 P-P bonds are included) have 10 electrons more than required by *mno* rule. The nature of the

interactions exhibited by these extra electrons and how they affect the overall structure were investigated by studying structure and bonding of CpMP_6MCp triple-decker sandwich complexes, ranging from 18–28 valence electrons (VE) with $\text{M} = \text{Sc}, \text{Y}, \text{Ti}, \text{Zr}, \text{Hf}, \text{V}, \text{Nb}, \text{Ta}, \text{Cr}, \text{Mo}, \text{and W}$. To model 18 and 20 VEC triple-decker complexes a $\text{C}_3\text{B}_3\text{H}_6$ and $\text{P}_3\text{B}_3\text{H}_3$ cationic and anionic middle rings are used. A density functional theory (DFT) and hybrid HF-DFT methods were employed.

The distortion of P_6 middle ring and other finer structural details in 28, 26, 24 and 22 VEC was controlled by filling of additional electrons to varied type of molecular orbitals. In 28 VE complexes complete filling of $2a^*$ and $2b^*$ orbitals lead to planar symmetrical P_6 middle ring, while the occupancy in either $2a^*$ or $2b^*$ alone explains the in-plane distortions (asymmetric) in 26 VE complexes. In comparison to 28 VE complexes, the puckering of P_6 middle ring in 24 VE complexes was due to the greater stabilization of $5a$ and the extra stabilization of the +4 oxidation state of Ti. The quintet state of 22 VE complexes was planar as $2a^*$ and $2b^*$ is half filled. Similar geometrical and bonding patterns observed between $\text{CpScP}_6\text{ScCp}$ and $\text{C}_2\text{P}_3\text{H}_2\text{ScC}_3\text{P}_3\text{H}_3\text{ScC}_2\text{P}_3\text{H}_2$ support the carbon–phosphorus analogy further. The modeled 20 VE systems ($\text{CpScC}_3\text{B}_3\text{H}_6\text{ScCp}^-$ and $\text{CpScP}_3\text{B}_3\text{H}_3\text{ScCp}^-$) with 52 skeletal electrons (20 VE) have in plane distortion of the middle rings. The modeled 18 VE systems ($\text{CpScC}_3\text{B}_3\text{H}_6\text{ScCp}^+$ and $\text{CpScP}_3\text{B}_3\text{H}_3\text{ScCp}^+$) with 50 skeletal electrons as stipulated by the *mno* rule were planar middle P_6 ring triple-decker sandwich complexes.⁴⁰

The next two chapters discusses about molecular insights to the inhibitor selectivity of the phosphodiesterase enzyme. Designing small molecules (inhibitors) that bind specifically to a family of enzyme (target) is an important step in drug discovery

development. Phosphodiesterases (PDEs) are metalloenzymes which hydrolyze phosphodiesterase bond of cyclic adenosine 3',5'-monophosphate (cAMP) and cyclic guanosine 3',5'-monophosphate (cGMP) into the corresponding 5'-nucleotides (AMP and GMP) in various cells. They play a vital role in the regulation of various physiological functions. Among the 12 PDE isozymes, cAMP specific enzymes PDE4 and PDE7 were studied. PDE4 is a keen target for the inflammatory diseases such as asthma, chronic obstructive pulmonary disease (COPD), allergic rhinitis, type II diabetes and rheumatoid arthritis. However, development of PDE4 drugs is hampered due to the side effects such as nausea, vomiting, dyspepsia, headache and emesis. The several strategies to overcome the side effects are (a) selectivity towards low affinity form over low affinity rolipram binding site, (b) targeting broader PDE family, (c) low blood brain barrier drugs, (d) disease activated drugs and (e) subtype selectivity of PDE4. PDE4 is coded by four genes named as A, B, C and D and are called as subtypes. Chapter 4 is about how to achieve PDE4 subtype selectivity. For this 35 PDE4B and 4D X-ray crystal structures were investigated. A characteristic secondary structural difference (3_{10} -helix versus turn) was found in M-loop region which is near to the active site pocket. Twelve of PDE4B have a 3_{10} -helix and the four PDE4B and nineteen PDE4D structures have a turn in the M-loop region. An experimental variable pH seems to be controlling this structural variation rather than the sequential differences in the PDE4.

At lower pH there is a possibility of protonation, thermodynamics of protonation and deprotonation of the aspartic acid, cysteine side chains and amide bonds of M-loop (SPMCD) residues were calculated. The pentapeptide residue (SPMCD) models were investigated in the gas phase and in the explicit solvent using ONIOM method at

B3LYP/6-31+G* and B3LYP/6-31+G*:UFF levels of theory respectively. The isodesmic equations of the various protonation states show that the turn containing structure is thermodynamically more stable when proline or cysteine is protonated. The preference for the turn structure on protonation, (pH =6.5-7.5) is due to an increase in the number of the hydrogen bonding and electrostatic interactions gained by surrounding environment such as adjacent residues and solvent molecules. The average number of solvent molecules (H₂O) available in the 3₁₀-helix and turn containing structures is also analyzed by molecular dynamics (MD) simulation with explicit water for 10ns under NPT conditions.⁴¹ Further analysis of molecular properties such as hydrophobicity and MOLCAD surface for residues of the M-loop region have shown that larger hydrophobic group consisting ligands can be better accommodated in the Q2 pocket of PDE4B.⁴² Thus the variations in local (physiological) pH at the point of interaction and hydrophobic groups of Q2 pocket can be added parameters in optimizing the specificity of PDE4 inhibitors.

Chapter 5 is focused on dual selectivity of cAMP specific PDE4 and PDE7 enzymes (targeting broader family). The reason is both of them are abundant in inflammatory cells and are considered as therapeutic targets for treating various inflammatory diseases with minimal side effects. To understand the basis of inhibitor selectivity X-ray structures of PDE4 and PDE7 were analyzed systematically. We have found that some crucial residues are altered in the Q1 and Q2 pockets of active site of these proteins. Later the substrate cAMP, nonselective isobutylmethyl xanthine (IBMX), PDE4 specific rolipram and PDE7 specific BRL-50481 inhibitors were docked to the co-crystal structures of PDE4 and PDE7 using Lamarckian genetic algorithm in

AUTODOCK. The docked energies obtained were well correlated to its specificity of binding. The important interactions with substrate cAMP are conserved in both enzymes indicating its selectivity to catalyze cAMP. The small difference in docking energies of rolipram analogs and spiroquinazolinones cannot explain the selectivity as external conditions, water and peripheral residues can also influence binding. In the case of a PDE4-specific inhibitor such as rolipram, the lower affinity towards PDE7 is due to the variation of two residues in the Q2 pocket (a) Ser⁴⁴²/Ile⁴¹² residue causes steric repulsions with cyclopentoxo group of rolipram (b) Met⁴¹¹/Thr³⁸¹ residue reduces the hydrophobic interactions with the rolipram.

These alterations of residues also reduced the size of Q2 pocket in PDE7 compared to PDE4. On the other hand variation of Tyr⁴⁰³/Ser³⁷³ residue in the Q1 pocket of PDE7 affects the hydrogen bonding with Gln⁴¹³ residue and increases the size of pocket. Further the influence of Q1 and Q2 pocket residues in inhibitor selectivity was studied by docking the less hydrophobic substituents containing ligands such as modified rolipram (where cyclopentoxo group is replaced by CH₂CH₂OH) and pyrazole analogs to PDE4 and PDE7. They all indicate an improved binding towards the PDE7 and comparable lowest docked energies with respect to the PDE4. Thus size and nature of Q1 and Q2 pockets play crucial role for the inhibitor binding to PDE4 and PDE7.

1.7 References

1. (a) Jensen, F. *Introduction to Computational Chemistry*, John Wiley & Sons, Inc., New York, **1999**. (b) Foresman, J. B.; Frisch, A. *Exploring Chemistry with Electronic Structure Methods*, Gaussian Inc., Pittsburgh, USA, **1996**. (c) Young, D. *Computational Chemistry: A Practical Guide for Applying Techniques to Real*

- World Problems*, John Wiley & Sons, Inc., New York, **2001**. (d) Schaeffer III, H. F. *Electronic Structure of Atoms and Molecules*, Addison-Wesley, Massachusetts, USA, **1972**. (e) Clark, T. A *Handbook of Computational Chemistry*, John Wiley & Sons, Inc., New York, **1985**. (f) Lewars E. G. *Computational Chemistry: Introduction to the Theory and Applications of Molecular and Quantum Mechanics*, Kluwer Academic Publishers, Massachusetts, USA, **2003**.
2. (a) Leach, A. R. *Molecular modeling Principles and Applications*, Pearson Education Limited, **1996**. (b) Hinchliffe, A. *Molecular modeling for Beginners*, John Wiley & Sons, Inc., New York, **2003**.
3. (a) <http://www.ccdc.cam.ac.uk/products/csd/> (b) <http://www.rcsb.org> (c) <http://ndbserver.rutgers.edu>
4. (a) Levine, I. N. *Quantum Chemistry*, 5th Edition, Prentice Hall, NJ, **2000**. (b) Prasad, R. K. *Quantum Chemistry*, New Age International Limited, New Delhi, **2006**. (c) McQuarrie, D. A. *Quantum Chemistry*, Oxford University Press, California, USA, **1983**. (d) Chandra, A. K. *Introductory Quantum Chemistry*, Tata Mc-Graw Hill Publishing Co., New Delhi, **1988**. (e) Lowe, J. P. *Quantum Chemistry*, Academic Press, New York, **1978**. (f) Pople, J. A. (Nobel lecture) *Angew. Chem. Int. Ed.*, **1999**, 38, 1894-1902. (g) Barden, C. J.; Schaefer III, H. F. *Pure. Appl. Chem.*, **2000**, 72, 1405-1423.
5. Schrödinger, E. *Ann. Physik.*, **1926**, 79, (new384), 361-376.
6. Born, M.; Oppenheimer, J. R. *Ann. Physik.*, **1927**, 84, (new 389), 457-484.
7. (a) Hartree, D. R. *Proc. Cambridge Phil. Soc.*, **1928**, 24, 89-110. (b) Fock, V. A. *Z. Phys.*, **1930**, 61, 126-148. (c) Fock, V. A. *Z. Phys.*, **1930**, 62, 795-805.

8. Hehre, W. J.; Radom, L.; Schleyer, P. v. R.; Pople, J. A. *Ab-initio Molecular Orbital Theory*, John Wiley & Sons, Inc., New York, **1986**.
9. (a) Roothaan, C. C. J. *Rev. Mod. Phys.*, **1951**, *23*, 69-89. (b) Roothaan, C. C. J. *Rev. Mod. Phys.*, **1960**, *32*, 179-185.
10. (a) Slater, J. C. *Phys. Rev.*, **1930**, *36*, 57-64. (b) Boys, S. F. *Proc. Roy. Soc., (London)*, **1950**, *A200*, 542-554. (c) Frenking, G.; Seijo, L.; Bohme, M.; Dapprich, S.; Ehlers, A. W.; Jonas, V.; Neuhaus, A.; Otto, M.; Stegmann, R.; Veldkamp, A.; Vyboishchikov, S. F.; *Rev. Comput. Chem.*, **1996**, *8*, 63-68. (d) Ihm, J.; Zunger, A.; Cohen, M. L. *J. Phys.*, **1979**, *C12*, 4409-4422. (e) Hay P. J.; Wadt, W. R. *J. Chem. Phys.*, **1985**, *82*, 270-283. (f) Liu, B.; McLean, A. D. *J. Chem. Phys.*, **1973**, *59*, 4557-4558. (g) Boys, S. F.; Bernardi, F. *Mol. Phys.*, **1970**, *19*, 553-566.
11. (a) Sadlej, J. *Semi-empirical Methods of Quantum Chemistry*, Ellis Harwood, Chichester, **1985**. (b) Zerner, M. C. *Rev. Comput. Chem.*, **1991**, *2*, 313-320. (c) Kohanoff, J. *Electronic Structure Calculations for Solids and Molecule*, Cambridge University Press, New York, **2006**. (d) Pople, J. A.; Beveridge, D. L. *Approximate Molecular Orbital Theory*, Mc-Graw Hill Publishing Co., NewYork, **1970**.
12. (a) Hückel, E. *Z. Phys.*, **1931**, *70*, 204-286. (b) Hoffmann, R. *J. Chem. Phys.*, **1963**, *39*, 1397-1412.
13. (a) Pariser, R.; Parr, R. G. *J. Chem. Phys.*, **1953**, *21*, 466-471. (b) Pople, J. A. *Trans. Faraday Soc.*, **1953**, *49*, 1375-1385. (c) Dewar, M. J. S.; Thiel, W. *J. Am. Chem. Soc.*, **1977**, *99*, 4899-4907. (d) Dewar, M. J. S.; Zoebisch, E. G.; Healy, E.

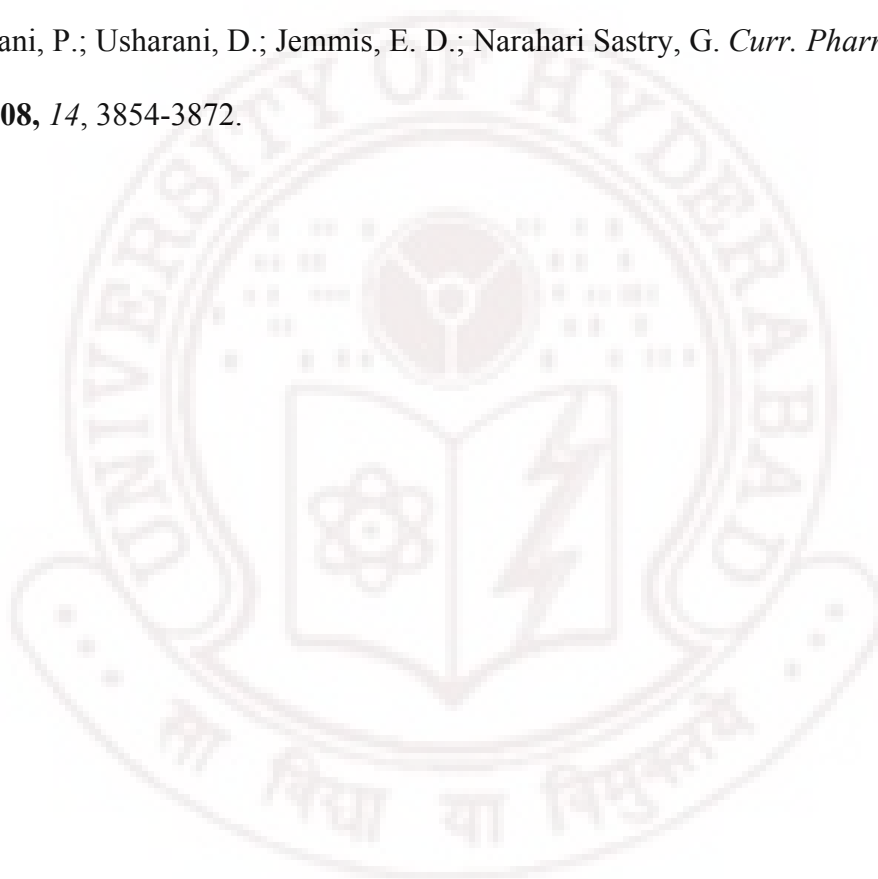
- F.; Stewart, J. J. P. *J. Am. Chem. Soc.*, **1985**, *107*, 3902-3909. (e) Stewart, J. J. P. *J. Comput. Chem.*, **1989**, *10*, 209-220.
14. (a) Hurley, A. C. *Electron Correlation in Small Molecules*, Academic Press, London, **1977**. (b) Wilson, S. *Electron Correlation in Molecules*, Clarendon Press, Oxford, **1984**. (c) Raghavachari, K.; Anderson, J. B. *J. Phys. Chem.*, **1996**, *100*, 12960-12973.
15. (a) Moller, C.; Plesset, M. S. *Phys. Rev.*, **1934**, *46*, 618-622. (b) Bartlett R. J. *Ann. Rev. Phys. Chem.*, **1981**, *32*, 359-401.
16. (a) Hylleraas, E. A. *Z. Physik.*, **1928**, *48*, 469-494. (b) Hylleraas, E. A. *Z. Physik.*, **1929**, *54*, 347-366.
17. (a) Čížek, J. *J. Chem. Phys.*, **1966**, *45*, 4256-4266. (b) Čížek, J. *Int. J. Quantum Chem.*, **1977**, *5*, 359-379. (c) Bartlett, R. J.; Musial, M. *Rev. of Modern Phys.*, **2007**, *79*, 291-352.
18. Pople, J. A.; Head-Gordan, M.; Raghavachari K. *J. Chem. Phys.*, **1987**, *87*, 5968-5975.
19. (a) Parr, R. G.; Yang, W. *Density Functional Theory of Atoms and Molecules*, Oxford University Press, Oxford, **1989**. (b) Dreisler, R. M.; Gross, E. K. V. *Density Functional Theory: An Approach to the Quantum Many-body Problem*, Springer-Verlag, Berlin, **1990**. (c) Baerends, E. J.; Gritsenko, O. V. *J. Phys. Chem. A.*, **1997**, *101*, 5383-5402. (d) Geerlings, P.; De Proft, F.; Langenaeker, W. *Chem. Rev.*, **2003**, *103*, 1793-1873. (e) Kohn, W.; Becke, A. D.; Parr, R. G. *J. Phys. Chem.*, **1996**, *100*, 12974-12980.

20. (a) Hohenberg, P.; Kohn, W.; *Phys. Rev.*, **1964**, *136*, B864-B871. (b) Hohenberg, P.; Kohn, W.; Sham, L. J. *Advances in Quantum Chemistry*, Vol. **21**, Academic Press, **1990**. (c) Kohn, W.; Sham, L. J. *Phys. Rev.*, **1965**, *140*, A1133-A1138. (d) Kohn, W. *Rev. Mod. Phys.*, **1999**, *71*, 1253-1266.
21. (a) Becke, A. D. *Phys. Rev. A*, **1988**, *38*, 3098-3100. (b) Perdew, J. P. *Phys. Rev. B*, **1986**, *33*, 8822-8824. (c) Becke, A. D. *J. Chem. Phys.*, **1993**, *98*, 5648-5652. (d) Lee, C.; Yang, W.; Parr, R. G. *Phys. Rev. B*, **1988**, *37*, 785-789.
22. (a) Pople, J. A.; Head-Gorden, H.; Fox, D. J.; Raghavachari, K.; Curtiss, L. A. *J. Chem. Phys.*, **1989**, *90*, 5622-5629. (b) Ochterski, J. W.; Petersson, G. A.; Monotgomery, J. A.; *J. Chem. Phys.*, **1996**, *104*, 2598-2619. (c) Baboul, A. G.; Curtiss, L. A.; Redfern, P. C. Raghavachari, K. *J. Chem. Phys.*, **1999**, *110*, 7650-7657.
23. Frisch, M. J. *et al.* **Gaussian 03**, Revision C.02, D.03 version, Gaussian, Inc., Wallingford CT.
24. Baerends, E. J. *et al.* **ADF2003.01**, SCM, Theoretical Chemistry, Vrije Universiteit, Amsterdam, The Netherlands.
25. (a) Burkert, U.; Allinger, N. L. *Molecular mechanics*, ACS Monograph, Washington, D. C, **1982**, *177*. (b) Allinger, N. L. *J. Am. Chem. Soc.*, **1977**, *99*, 8127-8134. (c) Schlecht, M. F. *Molecular Modeling on the PC*, John Wiley & Sons, Inc., New York, **1998**. (d) Rappè, A. K.; Casewit, C.J. *Molecular Mechanics across Chemistry*, University Science Books, Sausalito, **1997**.
26. Cornell, W. D.; Cieplak, P.; Bayly, C. I.; Gould, I. R.; Merz Jr., K. M.; Ferguson, D. M.; Spellmeyer, D. C.; Fox, T.; Caldwell, J. W.; Kollman, P. A. *J. Am. Chem.*

- Soc.*, **1995**, *117*, 5179-5197. (b) Rappé, A. K.; Casewit, C. J.; Colwell, K. S.; Goddard III, W. A.; Skiff, W. M. *J. Am. Chem. Soc.*, **1992**, *114*, 10024-10035. (c) Clark, M.; Cramer III, R. D.; Opdenbosch, N. V. *J. Comput. Chem.*, **1989**, *10*, 982-1012.
27. (a) Karplus, M.; McCammon, J. A.; *Nature Struct. Bio.*, **2002**, *9*, 646-652. (b) Gunsteren, W. F.v. *et al.*, *Angew. chem. Int. Ed.*, **2006**, *45*, 4064-4092. (c) Adcock, S. A.; McCammon, J. A. *Chem. Rev.*, **2006**, *106*, 1589-1615.
28. Case, D. A.; Darden, T. A.; Cheatham, III, T. E.; Simmerling, C.; Wang, J.; Duke, R. E.; Luo, R.; Merz, K. M.; Pearlman, D. A.; Crowley, M.; Walker, R. C.; Zhang, W.; Wang, B.; Hayik, S.; Roitberg, A.; Seabra, G.; Wong, K. F.; Paesani, F.; Wu, X.; Brozell, S.; Tsui, V.; Gohlke, H.; Yang, L.; Tan, C.; Mongan, J.; Hornak, V.; Cui, G.; Beroza, P.; Mathews, D. H.; Schafmeister, C.; Ross, W. S.; Kollman, P. A. **AMBER9**, 9th ed.; University of California: San Francisco, CA.
29. (a) Mannhold, R.; Kubinyi, H.; Timmerman, H. *Methods and Principles in Medicinal Chemistry*, John Wiley & Sons, Inc., New York, **2001**. (b) Halperin, I.; Ma, B.; Wolfson, H.; Nussinov, R. *Proteins: Structure, Function, and Genetics*, **2002**, *47*, 409-449. (c) Schneider, G.; Böhm, H.-J. *Drug Disc. Today*, **2002**, *7*, 64-70. (d) Kuntz, I. W.; Meng, E. C.; Shoichet, B. K. *Acc. Chem. Res.*, **1994**, *27*, 117-123.
30. **AUTODOCK**, 10550, North Torrey Pines Road, La Jolla, CA, 92037-1000 USA.
31. (a) Morris, G. M.; Goodsell, D. S.; Halliday, R. S.; Huey, R.; Hart, W. E.; Belew, R. K.; Olson, A. J. *J. Comput. Chem.*, **1998**, *19*, 1639-1662. (b) Hu, X.; Balaz, S.; and Shelver, W. H. *J. Mol. Graph. Model.*, **2004**, *22*, 293-307.

32. (a) Thiel, W. *Curr. Opin. in Chem. Bio.*, **2007**, *11*, 182-187. (b) Friesner, R. A.; *Drug Disc. Today: Technologies*, **2004**, *1*, 253-260. (c) Monard, G.; Merz Jr, K. M. *Acc. Chem. Res.*, **1999**, *32*, 904-911. (d) Lin, H.; Truhlar, D. G. *Theor. Chem. Acc.*, **2007**, *117*, 185-199.
33. (a) Ryde, U., *Curr. Opin. in Chem. Bio.*, **2003**, *7*, 136-142. (b) Bo, C.; Maseras, F. *J. Chem. Soc. Dalton Trans.*, **2008**, 2911-2919.
34. (a) Dapprich, S.; Komáromi, I.; Suzie Byun, K.; Morokuma K.; Frisch, M. J. *J. Mol. Struct. (THEOCHEM)*, **1999**, *462*, 1-21. (b) Vreven, T.; Morokuma, K.; Farkas, Ö.; Schlegel, H. B.; Frisch M. J. *J. Comput. Chem.*, **2003**, *24*, 760-769. (c) Vreven, T.; Byun, K. S.; Komáromi, I.; Dapprich, S.; Montgomery Jr., J. A.; Morokuma, K.; Frisch, M. J. *J. Chem. Theory Comput.*, **2006**, *2*, 815-826.
35. Hoffmann, R. (Nobel Lecture) *Angew. Chem. Int. Ed.*, **1982**, *21*, 711-724.
36. (a) Prasad, B. V.; Jemmis, E. D.; Tsuzuki, S.; Tanabe, K. *Proc. Ind. Acad. Sci (Chem. Sci)*, **1990**, *102*, 107-115. (b) Prasad, B. V.; Jemmis, E. D.; Tsuzuki, S.; Tanabe, K. *J. Phys. Chem.*, **1990**, *94*, 5530-5535. (c) Giju, K. T.; Jemmis, E. D. *The Encyclopedia of Computational Chemistry*, John Wiley & Sons, Chichester, **1998**, *2*, 1449-1455.
37. Dillon, K. B.; Mathey, F.; Nixon, J. F.; *Phosphorus: The Carbon Copy: From Organophosphorus to Phospha-organic Chemistry*, John Wiley & Sons, Chichester, **1998**.
38. Usharani, D.; Poduska, A.; Nixon, J. F.; Jemmis, E. D. *Accepted in Chem. Euro. J.*
39. (a) Jemmis, E. D.; Balakrishnarajan, M. M.; Pancharatna, P. D. *J. Am. Chem. Soc.*, **2001**, *123*, 4313-4323. (b) Jemmis, E. D.; Balakrishnarajan, M. M.; Pancharatna,

- P. D. *Chem. Rev.*, **2002**, *102*, 93-144. (c) Jemmis, E. D.; Jayasree, E. G.; Parameswaran, P. *Chem. Soc. Rev.*, **2006**, *35*, 157-168.
40. Usharani, D.; Prasad, D. L. V. K.; Nixon, J. F.; Jemmis, E. D. *J. Comput. Chem.*, **2007**, *28*, 310-319.
41. Usharani, D.; Srivani, P.; Narahari Sastry, G.; Jemmis, E. D.; *J. Chem. Theory Comput.*, **2008**, *4*, 974-984.
42. Srivani, P.; Usharani, D.; Jemmis, E. D.; Narahari Sastry, G. *Curr. Pharma. Design*, **2008**, *14*, 3854-3872.





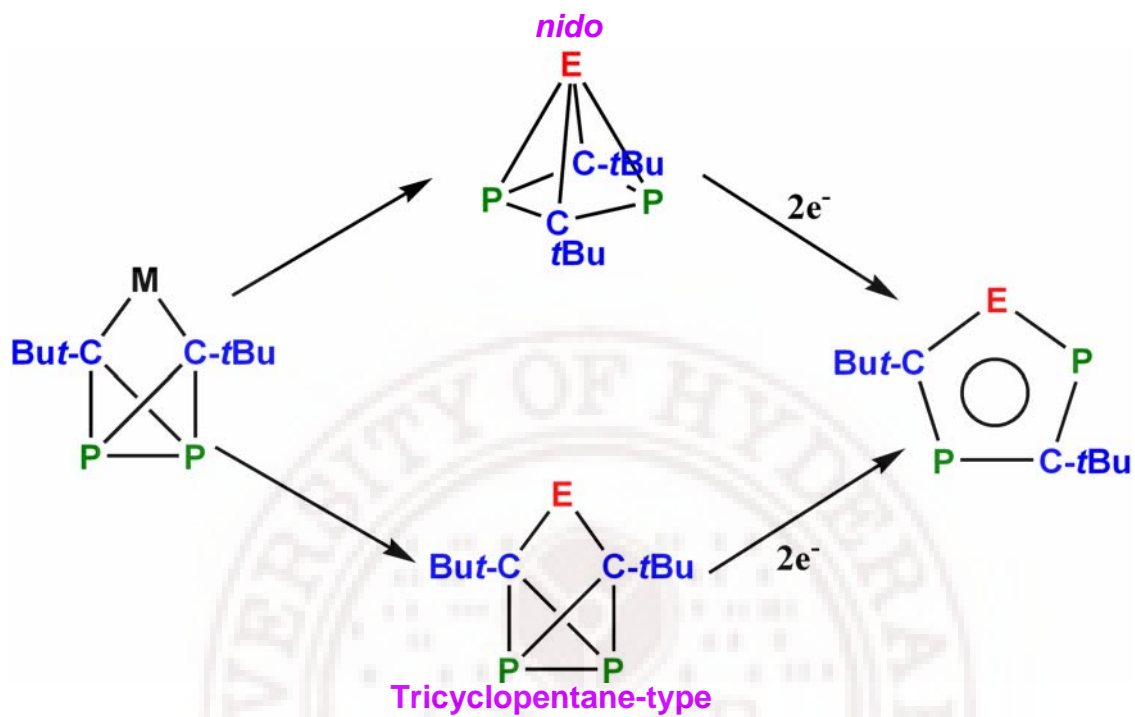
Chapter 2

Electronic Structure and Bonding in Neutral and Dianionic
Boradipospholes: $R'BC_2P_2R_2$ ($R = H, tBu, R' = H, Ph$)

Contents

2.1	Abstract	51
2.2	Introduction	52
2.3	Details of Computational Methods	57
2.4	Results and Discussions	58
2.4.1	Electron-Counting Considerations and Optimized Skeletons	58
2.4.2	Global Minima of <i>neutral</i> and <i>dianionic</i> $R'BC_2P_2R_2$	62
2.4.3	Isomers Containing 5-Membered Rings	66
2.4.4	Isomers Containing 4-Membered Rings	71
2.4.5	Isomers Containing 3-Membered Rings	78
2.4.6	Acyclic Isomers	84
2.5	Conclusions	86
2.6	References	88
2.7	Appendix	96

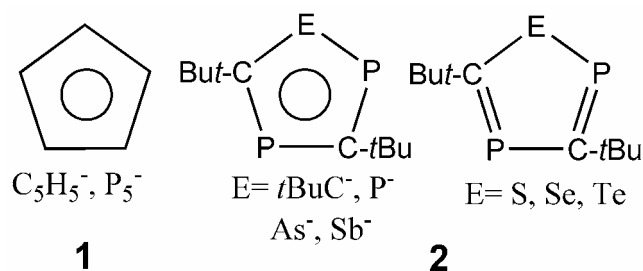
2.1 Abstract



2.2 Introduction

The isolobal analogy between P and CR fragments has become widely recognized over the past decade.^{1,2} An extensive range of unsaturated phospho-organic and phospho-organometallic compounds has been reported and many parallels drawn between both unsaturated 3-, 4-, 5- and 6- membered organic rings and acyclic compounds and their phosphorus-containing counterparts. Similar developments and parallels have been established in organo-phosphorus cage compounds that are usually formed by synthetic routes involving oxidative coupling of polyphospholyl anions $P_nC_nR_{5-n}$ ($n = 2, 3$) and thermal or metal-mediated oligomerisation of phosphalkynes, $P\equiv CR$ ($R = tBu$).^{1,3}

Application of the CH and P isolobal connection to the cyclopentadienyl anion (Cp^- , **1**) has extended the utility of Cp-type ligands. For example, complete isolobal substitution of $C_5H_5^-$ gives P_5^- , which exhibits similar ligating properties both in metallocenes and triple-decker sandwich complexes.⁴ The ring anions $tBu_2C_2P_3^-$ and $tBu_3C_3P_2^-$ have been especially useful in stabilizing metals in low oxidation states, and a wide range of sandwich and half-sandwich complexes involving p-, d- and f-block metals have been reported using such systems.⁵⁻¹² These Cp^- variants $tBu_2C_2P_3^-$ and $tBu_3C_3P_2^-$ may potentially be single-source precursors for the manufacture of semiconductors, as they form easily sublimable η^5 -complexes with Ga, In and Tl.¹³⁻¹⁴ Moreover, isoelectronic substitutions on 1,2,4-triphospholyl $tBu_2C_2P_3^-$ **2** gives the possibility of both *neutral* and *anionic* equivalents of Cp^- , typified by *anionic* arsena- and stibolyl heterodiphospholyl rings and *neutral* 1,2,4-thia-, seleno- and telluro- diphospholes, shown in **Scheme 2.1**.¹⁵⁻¹⁸

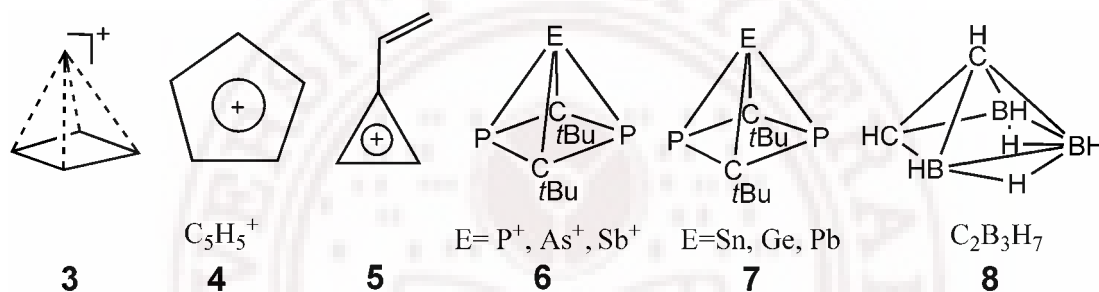


Scheme 2.1. Heterocyclic analogues of the cyclopentadienyl anion.

The cyclopentadienyl cation (Cp^+) also presents an interesting story. Initially Hofmann and Stohrer suggested a *nido* **3** structure for Cp^+ (similar to B_5H_9) which was further substantiated by Masamune *et al.*, who observed long-lived derivatives of square pyramidal Cp^+ .^{19a-c} While the structure of substituted Cp^+ has been shown earlier either to be a near planar triplet (D_{5h})^{19d} or a singlet (C_{2v}),^{19e} the structure of the parent system is debated both experimentally^{19b-i} and theoretically.^{19a,20} Early semiempirical calculations could not establish whether *nido* **3** or the nonplanar structure is the global minimum for Cp^+ .^{20a-c} Using EPR spectroscopy, it was shown that the planar triplet structure is generated for Cp^+ .^{19g} Depending upon the level of calculation, *ab initio* results show that there is a change in the relative energies of the lower-energy structures such as *nido* **3**, planar triplet **4** and vinylcyclopropenyl **5**.^{20e-i} At the G2 level of theory, it is shown that the energy difference between the triplet D_{5h} structure **4** or a vinylcyclopropenyl cation **5** is negligible, whereas *nido* **3** is high in energy (**Scheme 2.2**).^{20j}

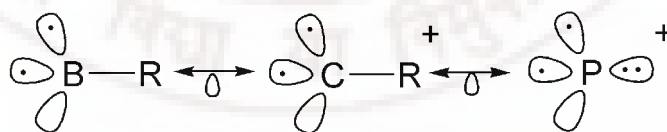
A full isolobal substitution of CH by P in Cp^+ gives P_5^+ which has been found in the gas phase by laser ablation of solid phosphorus.^{21a} It has a *nido* structure rather than the controversial planar ground state found in Cp^+ .^{21b,c} Other partially substituted compounds such as 3,5-*t*Bu₂-1,2,4- C_2P_3^+ , as well as the isoelectronic *cationic* arsena- and stibolyl heterodiphospholes **6** and *neutral* stanna-, germa- and plumba-diphospholes **7**

also exhibit a *nido* structure. All these compounds are readily obtained from a zirconocene 1,3-diphospha-bicyclo[1.1.0]butane complex, $[\text{ZrCp}_2\text{tBu}_2\text{C}_2\text{P}_2]$ upon treatment with the appropriate trihalide and the Lewis acid AlCl_3 .²²⁻²⁴ The presence of P atoms stabilizing a cluster-type ground state geometry, appears to be a common feature of the isolobal substitution of P for CH ,^{21c} as well as for other isolobal connections such as BH^- and CH in the carborane clusters **8**,²⁵ and the heavier group 14 elements Sn, Ge, and Pb **7**(Scheme 2.2).²³⁻²⁴



Scheme 2.2. Known structures of the heterocyclic analogues of the cyclopentadienyl cation.

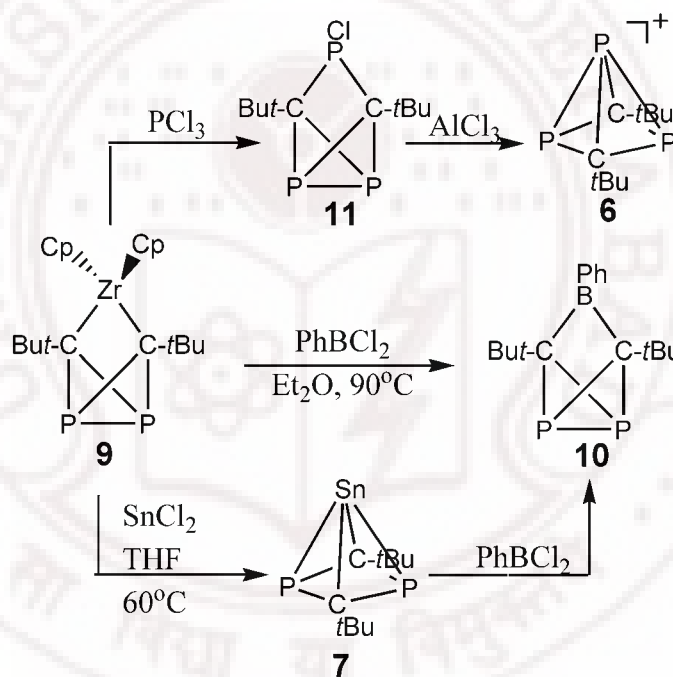
Application of isolobal (and isoelectronic) principles to both Cp^- and Cp^+ have given a variety of structural and synthetic possibilities. We are interested in exploring yet another isolobal connection namely that between BR , CR^+ and P^+ (**Scheme 2.3**).^{25b}



Scheme 2.3. The isolobal relationship among BR , CR^+ and P^+ fragments.

Isolobal substitution of a single BR for P^+ in the *nido*-3,5-*t*Bu₂-1,2,4- C_2P_3^+ **6** has been found to give not another *nido* structure, but rather a tricyclo[2.1.0.0]pentane $\text{PhBtBu}_2\text{C}_2\text{P}_2$ structure **10**. This compound can be readily made either by treatment of the zirconocene 1,3-diphospha-bicyclo[1.1.0]butane with PhBCl_2 ²⁶ or in unpublished work

more efficiently by treatment of *nido*-3,5-*t*Bu₂-1,2,4-C₂P₂Sn (**7**) with PhBCl₂^{23b} (**Scheme 2.4**). Compound **10** has been fully structurally characterized by a single crystal X-ray diffraction study.^{23b} The precursor of **6** is the tricyclic P-chloro triphosphacyclopentane **11**, which is also obtained from ZrCp₂*t*Bu₂C₂P₂ **9** by reaction with PCl₃.^{22,26} Exchange of free and coordinated Cl⁻ in **11** favors a S_N2 pathway²⁷ and has provided a multitude of synthetic possibilities such as substitution of Cl⁻ for fluoride, hydride, or tertiary phosphines, to give various phosphorus-rich cage compounds²⁸ and serves as a source of the *nido*-3,5-*t*Bu₂-1,2,4-C₂P₃⁺ **6** and planar 3,5-*t*Bu₂-1,2,4-C₂P₃⁻ **2** ions.²⁹



Scheme 2.4. Synthetic routes for heterophospholes and their cations.

It appears that cluster-type geometries are favored when BH or P⁺ groups are isolobally substituted for CH⁺ (**Scheme 2.4**). However, there appears to be a potential stabilization of alternative ground-state structures, depending on whether a BR or P⁺ group is present. With this unexpectedly stable tricyclopentane structure **10** as the isolobal equivalent of Cp⁺, a question arose as to whether a planar cyclic structure (as

with Cp^- , P_5^- , and other $\text{H}_n\text{C}_n\text{P}_{5-n}^-$ structures) is stable for the isolobal equivalent of Cp^- , $\text{PhBtBu}_2\text{C}_2\text{P}_2^{2-}$. Moreover, we were interested in exploring how the potential energy surface (PES) of $\text{BC}_2\text{P}_2\text{H}_3$ and $\text{BC}_2\text{P}_2\text{H}_3^{2-}$ compares with the $\text{H}_n\text{C}_n\text{P}_{5-n}^+$, and Cp^+ and Cp^- counterparts and whether there are additional lower-energy structures that are accessible only upon isolobal substitution of BH for P^+ .

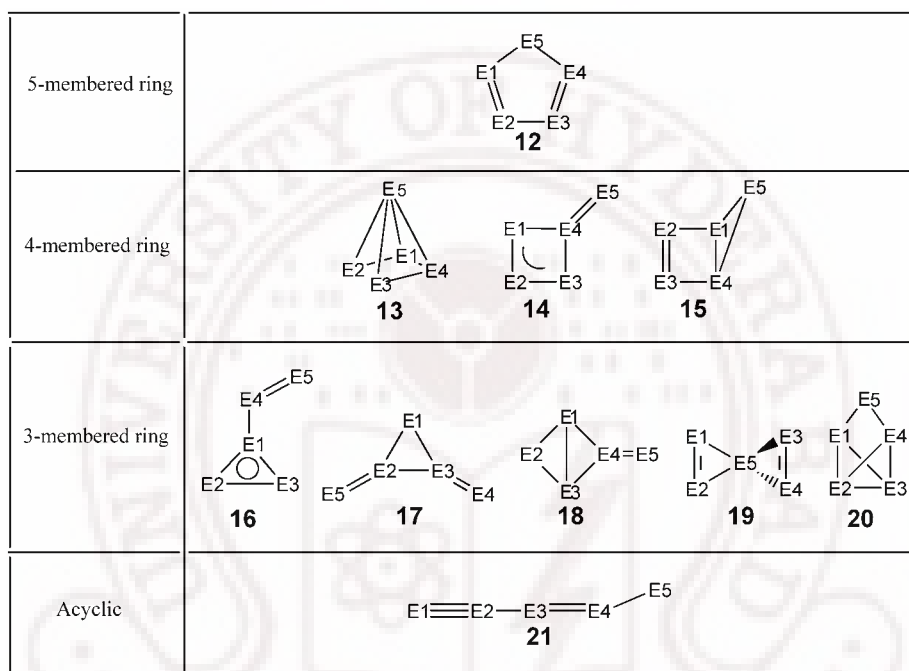


Chart 2.1. Simplified skeletons of the optimized isomers of $\text{BC}_2\text{P}_2\text{H}_3$, with the generic “E” representing a B, C, or P atom is shown. In some cases, the π bonding is delocalized over several atoms and is not shown in detail here. Owing to the large number of acyclic isomers (both linear and branched), for simplicity only one skeleton **21** is shown.

In this chapter we will discuss the global minima, geometric and positional isomers and the steric effects (substitution of *t*Bu for H, as bulky substituents are known to affect relative isomer stabilities)³⁰ on $\text{BC}_2\text{P}_2\text{H}_3$ and $\text{BC}_2\text{P}_2\text{H}_3^{2-}$. Both of the PES have been explored through optimization of all possible 3-, 4- and 5-membered rings and acyclic systems, with the most stable skeletons shown in **Chart 2.1**.

2.3 Details of Computational Methods

A total of 172 positional isomers for both the $\text{BC}_2\text{P}_2\text{H}_3$ and $\text{BC}_2\text{P}_2\text{H}_3^{2-}$ species were optimized using the hybrid Hartree-Fock/DFT (B3LYP) method, which involves a combination of the three-parameter Becke exchange functional³¹ with the Lee-Yang-Parr non-local correlation functional.³² The basis set 6-311++G (d,p) was used, which includes diffuse and polarization functions both for heavy atoms and hydrogens. The choice of this functional and basis set was guided by a previous study on the $\text{Sn}/\text{Bu}_2\text{C}_2\text{P}_2$ system.^{23c} 93 *neutral* and 80 *dianionic* $\text{BC}_2\text{P}_2\text{H}_3$ isomers were found to be minima and were studied further with the composite G3B3 method³³ that is known to closely reproduce experimental relative energies. The G3B3 method uses the optimized geometries at the B3LYP/6-31G(d) level and the single point energies of MP4(FC)/6-31G(d), MP4(FC)/6-31+G(d), MP4(FC)/6-31G(2df,p), QCISD(T,FC)/ 6-31G(d) and MP2(FU)/G3large basis set and adds high level ($\Delta\text{HLC} = -A n_\beta - B(n_\alpha - n_\beta)$ where $A=6.760$, $B=3.233$) and zero point energy corrections at B3LYP/6-31G(d).³³

In order to model the experimental structure $\text{PhBtBu}_2\text{C}_2\text{P}_2$ (**10**), all minimum energy structures were substituted with two *t*Bu groups. This substitution always occurred on carbon whenever two C-H groups were present in the structure. However, in some structures that had either zero or one C-H group the *t*Bu was substituted on either B-H or P-H. 90 *neutral* and 72 *dianionic* $\text{HBC}_2\text{P}_2\text{tBu}_2$ isomers were found to be minima at B3LYP/6-311++G (d,p) level of theory. Further substitution of H on B by Ph for the two low lying *neutral* (**13a** and **20a**) and four (**12a'**, **12b'**, **12g'** and **12k'**) *dianionic* $\text{HBtBu}_2\text{C}_2\text{P}_2$ isomers were also calculated with B3LYP/6-311++G (d,p). Throughout the chapter a prime (') indicates “*dianionic species*”. The frequencies of all isomers were

calculated in order to evaluate the nature of the stationary points and the natural bond orbital (NBO) method was used for a bonding analysis.³⁴ The Gaussian 03 program package was used for all calculations.³⁵ Due to self-interaction errors, *dianionic* calculations often have unbound eigenvalues^{36a,b} and this study on $\text{BC}_2\text{P}_2\text{H}_3^{2-}$ isomers is no exception. This error can be corrected with more sophisticated methods,^{36b-d} but, this was not attempted in this study due to the large number of isomers. The orbital energies for these *dianions* are less positive at G3B3 than at B3LYP level. This is likely due to the inclusion of added corrections for correlation effects at G3B3 level. In general, the relative energies of the geometric and positional isomers were found to be constant for both B3LYP and G3B3 levels, although structures with delocalized π bonding in vinylcyclopropenyl-type and acyclic isomers are higher in energy and others are lower in energy with the G3B3 method.^{36e,f} However, one major difference was that in $\text{BC}_2\text{P}_2\text{H}_3$, G3B3 level gives three geometric isomers as potential global minima, whereas B3LYP level gives just one. In discussion the G3B3 results refer to the ground-state structures of $\text{BC}_2\text{P}_2\text{H}_3$, and the remaining discussion will refer to the B3LYP results of structures that are within 50 kcal/mol (with respect to the *t*Bu system) for the *neutral* and *dianionic* species, The remaining structures above 50 kcal/mol are given in the **Appendix (2.7.1-2.7.3)**. A table of bond distance ranges for typical bond lengths for heterocyclic structures as given by a CSD search is also given in the **Appendix (2.7.4)**.

2.4 Results and Discussions

2.4.1 Electron-Counting Considerations and Optimized Skeletons

In Cp^- 20 electrons are involved in σ bonds (5 C-C, 5 C-H) and 6 electrons occupy the π system. In the cyclic planar $\text{BC}_2\text{P}_2\text{H}_3^{2-}$ (**12**) a similar electron counting is expected:

(5 E-E, 3 E-H) and two P lone pairs (due to the isolobal analogy between CH and P), leaving six electrons for π bonding. In Cp^+ , having the vinylcyclopropenyl structure **5**, the number of σ bonds remains the same and only 4 electrons are in the π system. However, the sterically hindered isolobal equivalent tricyclopentane $\text{PhBtBu}_2\text{C}_2\text{P}_2$ **10**, has 20 electrons in σ bonds (7 E-E and 3 E-H) and there are 4 electrons in two P lone pairs and no π electrons. Thus, in the analysis comparing the *neutral* and *dianionic* $\text{BC}_2\text{P}_2\text{H}_3$ species, a close attention is paid to how these 24 electrons (or 26, in the case of $\text{BC}_2\text{P}_2\text{H}_3^{2-}$) are arranged in the optimized structures, as this will not only help us understand if cluster-type (multi-center, two-electron) bonding is present, but also enable the limits of the isolobal analogy between P^+ and BR (or P and CR) to be determined.

Electronic structure calculations of various 3-, 4-, and 5- membered ring (cyclic) and linear (acyclic) molecules gives ten basic skeletons determined by bond distance values and NBO and MO analyses (**Chart 2.1**). Although attempts were made to optimize other geometries such as bicyclic, trigonal pyramidal, planar tetra-coordinated and tricyclic structures, they all optimized to the structures found in **Chart 2.1**. Except for the spirane-type geometry **19**, all other $\text{BC}_2\text{P}_2\text{H}_3$ structure types retain one lone pair on each phosphorus, giving 20 electrons in 10 bond pairs.

The bond pairs present in the various isomers are as follows: 10 σ bonds (**20**); 9 σ bonds and a π bond (**15** and **18**); 8 σ and 2 π bonds (**12**, **14**, **16** and **17**); 7 σ and 3 π bonds (**21**); and 7 σ and 6 “interstitial electrons” shared between the cap and ring (**13**).³⁷ Depending on the isomer, the π bonds can be localized or delocalized. When two electrons are added to give $\text{BC}_2\text{P}_2\text{H}_3^{2-}$, (apart from changes in the stability of many isomers) they lead to the following changes in bonding. (i) if there is delocalized π

bonding in the *neutral* structure, there tends to be π localization in the *dianion*; (ii) if no π bonds exist, then a σ bond is usually broken; (iii) these two electrons generally result in a -1 charge on either B or P, usually by filling of a P-P π^* orbital or by creating a tetra-coordinate B atom. A combination of these factors typically leads to distribution of the 26 electrons as 10 bonding pairs and 3 lone pairs or 11 bond pairs and 2 lone pairs, depending on the connectivity and hybridization of the atoms in the skeletons (**Chart 2.1**).

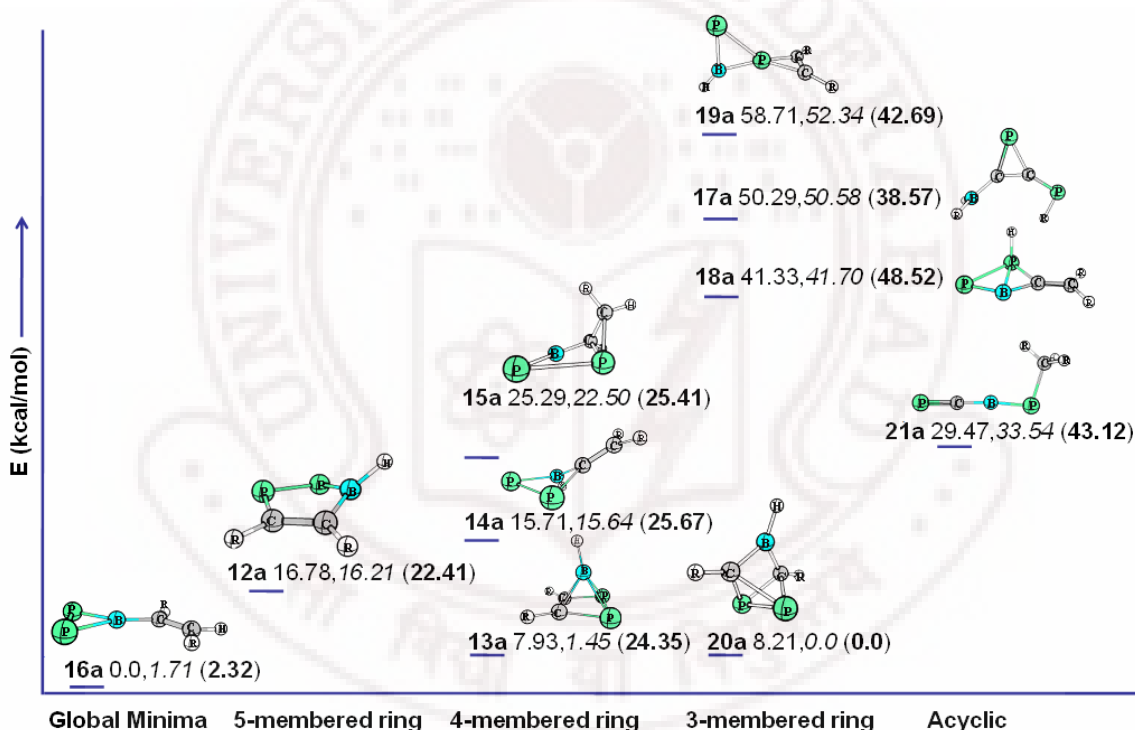


Figure 2.1. The global minima and lowest-energy geometrical structures for the $\text{BC}_2\text{P}_2\text{H}_3$ isomers. Relative energies (kcal/mol) in the normal (H-substituted) and **bold** font (*t*Bu-substitution of H on C) in parenthesis are given at B3LYP/6-311++G (d,p) and those in *italics* (H-substituted) are at G3B3 level. The isomers are arranged according to the H-substituted energies.

The lowest-energy structures for each skeleton given in **Chart 2.1** are shown in **Figures 2.1** ($\text{BC}_2\text{P}_2\text{H}_3$) and **2.2** ($\text{BC}_2\text{P}_2\text{H}_3^{2-}$), and similar structures are also observed when hydrogens are substituted by *t*Bu groups. There is a relation between steric bulk and isomeric stability which is a common feature of all skeletons, especially whenever there are *t*Bu substitutions on adjacent or the same atoms. Steric effects for the lowest-energy structures (or in a few exceptionally interesting cases) will be further discussed.

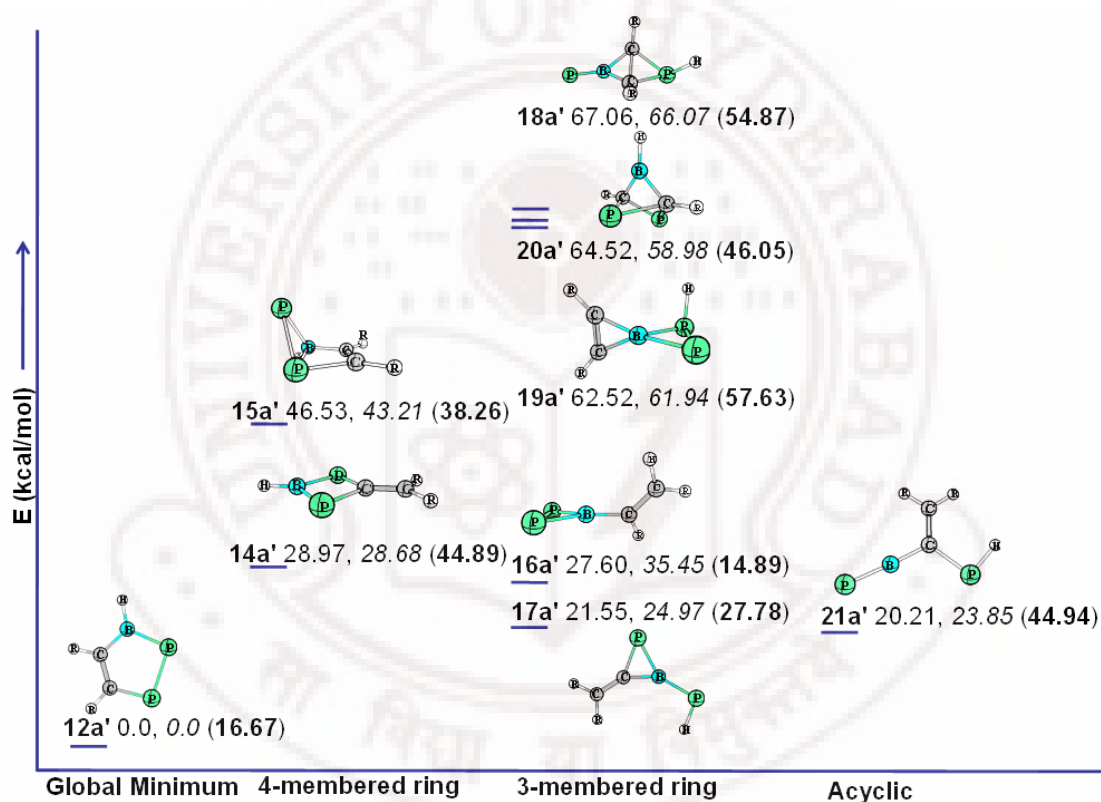


Figure 2.2. The global minimum and lowest-energy geometrical structures for the $\text{BC}_2\text{P}_2\text{H}_3^{2-}$ isomers. Relative energies (kcal/mol) in the normal (H-substituted) and **bold** font (*t*Bu-substitution of H on C) in parenthesis are given at B3LYP/6-311++G (d,p), whereas those in *italics* (H-substituted) are at the G3B3 level. The isomers are arranged according to the H-substituted energies.

2.4.2 Global Minima of *neutral* and *dianionic* $R'BC_2P_2R_2$

Depending on the method used, several possible global minima for $BC_2P_2H_3$ are obtained. At the B3LYP/6-311++G (d,p) level, the global minimum is a vinyl cyclopropenyl structure (**16a**) (**Figure 2.1**), which differs from the experimentally characterized $PhBtBu_2C_2P_2$ molecule **10** that has a tricyclopentane-type structure.^{23b} Delocalization of 2 π electrons in the P_2B ring (which could also be considered to be a 3c-2e π bond), is suggested by the P-P and B-P distances of 2.10 Å and 1.85 Å that have some degree of multiple bond character. There is a double C-C bond (1.34 Å) and some B-C π interaction as well, with a B-C distance of 1.54 Å that is shorter than the sum of their neutral radii (1.67 Å). However, at the G3B3 level, there are three potential global minima, indicating a relatively flat PES: the lowest structure is a tricyclopentane (**20a**), with *nido* (**13a**) and vinylcyclopropenyl (**16a**) structures just 1.45 and 1.71 kcal/mol higher in energy. The geometric parameters of the vinylcyclopropenyl structure are identical to that found with B3LYP (P-P=2.10, B-P, 1.85, C-C=1.34 and B-C= 1.54Å).

This vinylcyclopropenyl structure has been found to be one of two possible ground states for Cp^+ , the other being the cyclic triplet D_{5h} structure,^{20j} with energetic separations as small as 1.1 kcal/mol.^{21c} For comparison, a triplet calculation on **12a** at B3LYP reveals that the triplet lies about 10 kcal/mol higher in energy than the singlet and 27.70 kcal/mol above the global minimum (**Figure 2.1**). At the G3B3 level, the triplet and singlet energies are 32.89 and 16.21 kcal/mol respectively. A large energy gap between the cyclic D_{5h} and vinylcyclopropenyl-type structure has also been calculated upon isolobal substitution of P for CH in the $H_nC_nP_{5-n}^+$ series (using G3X method)^{21c}: when one or two CH groups are replaced by P to give $H_4C_4P^+$ and $H_3C_3P_2^+$, the cyclic

(triplet) structures are 9.0 and 20.3 kcal/mol higher than the vinylcyclopropenyl-type geometry respectively.^{21c}

The other two low-lying isomers (*nido* and tricyclopentane-type) are also energetically viable ground-state structures for $\text{BC}_2\text{P}_2\text{H}_3$ (at G3B3). The *nido* geometry is a minimum in the $\text{H}_n\text{C}_n\text{P}_{5-n}^+$ series (where $n>0$ has P in the capping position)²² and is observed in 3-hydroxyhomotetrahedrane derivatives^{19c} of Cp^+ . In the case of $\text{BC}_2\text{P}_2\text{H}_3$ the BH cap is found to be the lowest-energy isomer, with the adjacent carbons in the basal ring (thermodynamic product).²² The tricyclopentane structure (**20a**), found experimentally as **10** is unstable for the Cp^+ and carbaphosphole analogues. However, it has been characterized for compounds having a $t\text{Bu}_2\text{C}_2\text{P}_2$ base and bridging fragments that are isolobal to BR, such as ZrCp_2 , CO and GeI_2 (Scheme 2.4).^{19,25a,26,38,39}

Upon increasing the steric bulk the lowest-energy structure for $\text{HB}t\text{Bu}_2\text{C}_2\text{P}_2$ at the B3LYP level is the tricyclo[2.1.0.0]pentane (**20a**) structure, with the second lowest as the vinylcyclopropenyl-type **16a**. The *nido* isomer (**13a**) is destabilized due to steric repulsions between the adjacent carbon atoms; hence, it is higher by 24.35 kcal/mol (Figure 2.1). But further substitution of H on B by Ph gives the experimental structure **10** to be lower in energy than the *nido* structure with a BH cap (**13a** and **13c**) (by 10.14 and 7.95 kcal/mol respectively) and excludes the possible existence of **16a**. This tricyclopentane $\text{PhB}t\text{Bu}_2\text{C}_2\text{P}_2$ has a capping BPh group and a single P-P bond, similar to the experimental structure **10**.^{23b} This theoretical structure, however, has slightly different P-P and P-C bond distances (up to 0.08 Å as compared to the experimental geometry shown in Appendix 2.7.5).

The stability of this tricyclopentane-type structure seems to indicate that the isolobal substitution between BR and P^+ does not hold: the substitution of *t*Bu and phenyl groups increases the energy difference between the low-lying isomers and favours the tricyclopentane-type over the *nido* structure in $R'BR_2C_2P_2$ ($R' = H, Ph$ and $R = tBu$). This is likely due to less stabilization of the HOMO molecular orbital, where the BH capping orbital interacts with $P-\pi^*$ orbital has poor overlap, so it converts to a tricyclopentane-type structure accompanied by cross over of HOMO-LUMO levels and increase in HOMO-LUMO gap (**Figure 2.3**). In contrast, when there is a bridging P^+ fragment in $P_3(tBuC)_2^+$, the ground state is the *nido* geometry.^{29a}

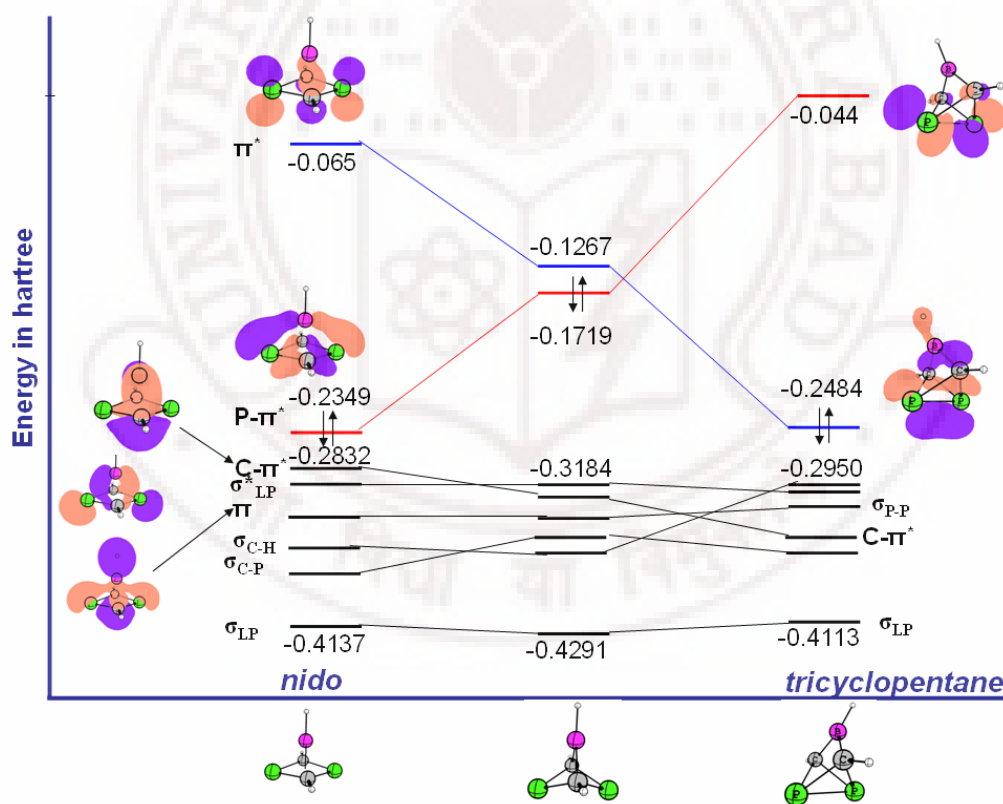


Figure 2.3. Correlation diagram from *nido* to tricyclopentane-type structure of $BH_2C_2P_2$ at B3LYP/6-311++G (d,p) level of theory.

The *nido* and tricyclopentane structures are related by bond-stretch isomerism, as noted by Hoffmann *et al.*^{19a} Mc Grady *et al.*^{21c,22} calculated that, for the less sterically crowded $\text{H}_2\text{C}_2\text{P}_3^+$, the fluxional exchange of the apical and basal P atoms in the *nido* structure goes through a tricyclopentane transition state (37 kcal/mol) and this fluxionality also appears to occur in the experimentally characterized $\text{P}_3(\text{tBuC})_2^+$. This tricyclopentane structure is obtained experimentally when there is a (*neutral*) bridging PX group (X=H, F, Cl, I).²⁸

For $\text{BC}_2\text{P}_2\text{HR}_2^{2-}$, the global minimum is a planar cyclic structure, regardless of whether B3LYP or G3B3 levels are used, or whether H or *t*Bu groups are present (**Figure 2.2**). In $\text{BC}_2\text{P}_2\text{H}_3^{2-}$ (**12a'**), filling of the three π levels occurs as in Cp^- , with E-E distances intermediate between single and double bond lengths. The P-P distance of 2.21 Å, however, is slightly long for a delocalized bond, but NBO calculations indicate that there is a significant P-P π bonding interaction. Substitution of H on carbon by *t*Bu results in another cyclic positional isomer **12b'** as a minimum, which has two C-B bonds and one P-P bond. Substitution of H on B by Ph gives one more structure, **12g'**, which has three C-P bonds similar to other *neutral* and *anionic* heterodiphospholes **2** (**Scheme 1, Table 1**). Steric effects of these isomers will be discussed in more detail in the following section.

In summary, the global minima for both *neutral* and *dianionic* $\text{BC}_2\text{P}_2\text{HR}_2$ (R=H, *t*Bu) varies, depending on the substituents. The isolobal substitution of BH for P^+ does indeed provide alternative low-energy structures, as the tricyclopentane and vinylcyclopropenyl-type (at G3B3 level). This suggests that $\text{BC}_2\text{P}_2\text{H}_3$ has a competition between 2 π delocalized vinylcyclopropenyl-type and cluster geometries (*nido* and

tricyclopentane-type). The increased steric bulk in the *neutral* species changes the ground state structure from a vinylcyclopropenyl (**16a**) to a tricyclopentane-type (**20a**) structure, however, adding two electrons gives a cyclic planar structure for both the H- and *t*Bu-substituted species (**12a'** or **12b'**) at B3LYP level. Since the relative energies of other geometrical and positional isomers of all eleven skeletons of *neutral* and *dianionic* BC₂P₂H₃ are unaltered (Tables 2.1-2.8), discussion from this point will only focus on isomers at the B3LYP level.

2.4.3 Isomers Containing 5-Membered Rings

The 5-membered ring isomers have two basic skeletons as minima: borane- (which has B-H and B-E bonds) and boryl (which has only B-E bonds)-type. The cyclic BH(CH)₂P₂ system has 5 E-E, 3 E-H σ bonds and 4 π electrons. Skeletons **12a**, **b**, **g**, **k** are analogous to Cp⁺ and are non-planar,²⁰ with BH rising above the plane by 20-30°; however, the boryl structures are both planar and non-planar, depending on whether there is a CH₂ fragment (**12c**, **e**, **f**, **i** and **j**) or a PH group (**12d**, **h**, **l**, **n**, **o**) (Table 2.1).

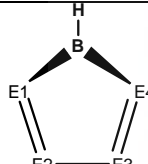
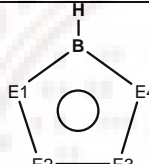
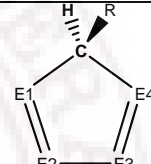
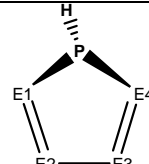
The difference in planarity for the boryl structures can be understood by considering the sp³ CH₂ group to be isolobal with the PH group with one C-H bond equivalent to a P lone pair. Since a P lone pair will occupy more space than a C-H bond, the lone pair-bond pair repulsion is likely to push the P atom out of the plane by 5-10° in the structures. The non-planarity of the borane structure, however, appears to have different origins. An NBO analysis indicates that there is back donation from the π (E1-E2 or E3-E4) bond to an empty B lone pair orbital, which could favor a non-planar structure. It is difficult to rationalize energetic trends among the positional isomers, especially when energy differences are of the order of a few kcal/mol. However, an NBO

analysis indicates that, for the borane structures, the lower-energy structures tend to have more π -back donation into the B lone pair orbital than the higher-energy structures.

For the boryl species, the structure with the largest number of B-C bonds is lowest in energy, whereas the structure without any B-C bonds is highest in energy. For the non-planar structures, those with P-P bonds are lowest in energy and boron non-adjacent to the pyramidal phosphorus is slightly more stable. Other than for **12m**, which changes to a methylenecyclobutenyl-type structure, similar geometries and bonding are maintained upon *t*Bu substitution. There is a slight reordering of the energies, with **12b** as the lowest-energy structure, likely dipping below **12a** because of reduced steric repulsions. In general, most of these structures that are lower in energy do not have a C-C bond, thus reducing the steric repulsions between the *t*Bu groups (**Table 2.1**).

In these 5-membered rings, boron has a vacant orbital, which is mainly 2p in the borane structure and a sp^2 hybridized, in-plane orbital in the boryl structures. Addition of two electrons to $HB(CH)_2P_2$ changes the non-planar borane to a cyclic planar structure, where 6 π electron delocalization results in aromatic character similar to that of Cp^- and P_5^- anions. The energetic differences among the borane structures range from 1-10 kcal/mol. As expected, substitution of H on carbon by a *t*Bu group destabilizes the isomers having adjacent carbons, thus giving **12b'** as the lowest-energy structure (**Figure 2.4**). Interestingly, however, isoelectronic Sn, P^+ and As^+ analogues of BH in **12k'** have been synthesized.⁴⁰ Calculations on phenyl-substituted boradiphospholes found to have yet another minima **12g'** that is similar to the other *neutral* and *anionic* heterodiphospholes **2** (**Scheme 2.1**).

Table 2.1. Relative energies (kcal/mol) of 5-membered ring isomers of *neutral* and *dianionic* BC₂P₂HR₂ species with skeleton (**12**); (R = H) are given in normal font at B3LYP and *italics* font for at G3B3 level. Numbers in parenthesis pertain to relative energies (kcal/mol) when R= *t*Bu at B3LYP level.

Struc ture	Arrangement of atoms in the skeleton				Relative energies of 12 skeleton				
					<i>neutral</i>	<i>dianion</i> ^a	<i>neutral</i>	<i>dianion</i> ^a	<i>neutral</i>
No	E1	E2	E3	E4					
12a	P	P	CR	CR	16.78, 16.21 (22.41)	0.0, 0.0 (16.67)			
12b	CR	P	P	CR	17.44, 16.79 (11.66)	6.06, 4.31 (0.0)			
12c	B	CR	P	P			18.73, 18.45 (14.79)	52.09, - (44.24)	
12d	P	B	CR	CR					23.50, 21.86 (23.47)
12e	CR	P	P	B			24.51, 22.81 (26.70)	55.89, - (63.40)	
12f	P	CR	B	P			26.60, 26.04 (23.70)	63.65, 64.24 (52.70)	
12g	CR	P	CR	P	27.35, 25.38 (21.97)	10.41, 7.50 (5.22)			
12h	P	CR	B	CR					27.99, 26.44 (19.58)
12i	P	CR	P	B			30.98, 29.59 (28.56)	57.92, 56.87 (51.88)	
12j	P	P	B	CR			31.05, 30.67 (35.59)	64.11, 64.99 (53.12)	
12k	P	CR	CR	P	32.80, 31.84 (50.89)	4.83, 3.80 (22.54)			
12l	P	CR	CR	B					37.29, 36.87 (42.96)
12m	P	B	P	CR			39.05, 37.57 (-)	66.33, 64.51 (-)	
12n	CR	CR	B	P					42.22, 38.51 (37.43)
12o	CR	P	CR	B					42.34, 39.54 (38.40)

^a The arrangements of atoms are similar for the *dianion*; thus all *dianionic* isomers are referred with the same structure number (No) and a “'”. A “-” indicates that the isomer converged to another isomer.

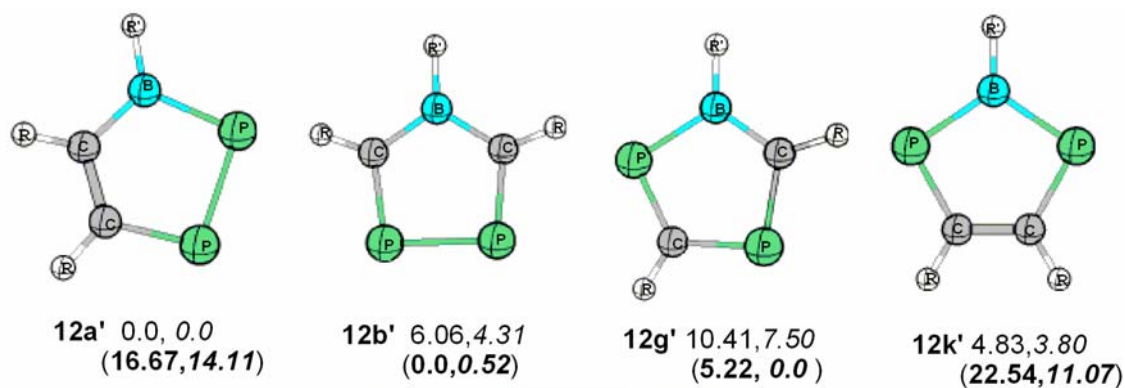
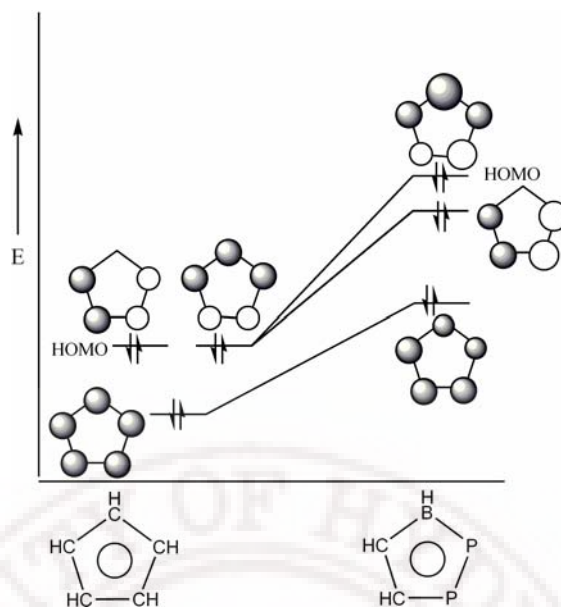


Figure 2.4. Relative energies (kcal/mol) of four planar cyclic $R'BC_2P_2R_2^{2-}$ species ($R = H, tBu, R' = H, Ph$) are shown in normal ($R=R'=H$), **bold** ($R = tBu, R'=H$) and **bold italics** ($R = tBu, R'=Ph$) fonts, at B3LYP/6-311++G (d,p) whereas those in *italics* ($R=R'=H$) are at G3B3 level.

A comparison of the π MO levels for Cp^- and $BC_2P_2H_3^{2-}$ (**12a'**), shown in **Scheme 2.5**, reveals several noticeable differences. (i) the π degeneracy of Cp^- is broken, as expected with the asymmetric substitution of a BH group and two P atoms, (ii) the presence of the more electropositive B and P atoms pushes the energy levels up by 4.07 eV, which could be due to the additional charge and substitution of hetero atoms (BH and P). However, the increase in energy level is significantly larger (positive eigen values), (iii) the π -molecular orbital (MO) that contains a zero node lies below the σ -MO's, similar to that observed⁴¹ for P_5^- . This higher-energy frontier orbital suggests that $BC_2P_2H_3^{2-}$ might bind more effectively to more electropositive elements as compared to Cp^- . Moreover, the large coefficient on B in the HOMO suggests that a Lewis acid might preferentially attack at this position (or alternatively at the P adjacent to CH, which also has a large coefficient). These differences between Cp^- and $BC_2P_2H_3^{2-}$ might offer synthetic utility in future experiments.



Scheme 2.5. The π molecular orbital comparison of Cp^- and $\text{BC}_2\text{P}_2\text{H}_3^{2-}$ (**12a'**).

The negative nucleus independent chemical shifts (NICS) values at the ring center and at 1 Å above the ring for these isomers clearly indicate the $\text{BC}_2\text{P}_2\text{H}_3^{2-}$ ion is as aromatic as Cp^- and other heterodiphospholes⁴² (**Table 2.2**). These values do not correlate with their stabilities, however, as found with the $\text{H}_n\text{C}_n\text{P}_{5-n}^+$ series,^{21c} where the more stable structures have greater aromaticity.

Table 2.2. The NICS values at ring center [NICS (C)] and at 1 Å [NICS (1 Å)] above the ring center [NICS (1 Å)] for the four planar *dianionic* **12** isomers: the **bold** and **bolditalics** font values correspond to the $\text{HBtBu}_2\text{C}_2\text{P}_2$ and $\text{PhBtBu}_2\text{C}_2\text{P}_2$ structures.

Aromaticity	Cp^-	12a'	12b'	12g'	12k'
NICS (C)	-13.41	-10.53	-10.55	-9.98	-10.81
		-8.69	-8.34	-7.16	-8.85
NICS (1 Å)	-9.71	-7.57	-9.79	-5.67	-5.68
		-9.08	-9.55	-9.44	-9.02
		-7.53	-8.13	-7.08	-7.85
		-7.69	-8.04	-6.72	-5.86

The planar and non-planar structures found for the *neutral* boryl species are also found to be minima in the corresponding *dianion*; however, they are at relatively higher

energies and the bonds are elongated by 0.03-0.10 Å. In these $\text{BC}_2\text{P}_2\text{H}_3^{2-}$ isomers, the two additional electrons enter the boron sp^2 lone pair orbital, thus resembling boryl lithium.⁴³ These structures maintain two localized π bonds as in the *neutral* structure. In the case of the non-planar boryl systems, the isomer in which boron is adjacent to the pyramidal phosphorus is slightly more stable than the others, but all are above 50 kcal/mol (**SI**). Substitution of H by *t*Bu also changes the relative energies of the isomers, but only **12e'** is destabilized.

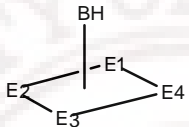
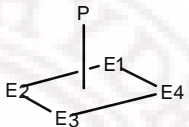
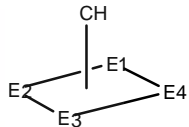
2.4.4 Isomers Containing 4-Membered Rings

Optimized 4-membered rings exhibit three main skeletons: *nido*- (**13**), methylenecyclobutenyl- (**14**) and envelope- (**15**) types (**Chart 2.1**). The *nido* structure **13** has cluster bonding (7 σ bonds) and based on the ring- and cap-phenomenon, it contains six interstitial electrons.³⁷ The energies of the six optimized isomers **13a-13e**, which involve BH, CH or P fragments in the capping position, reveal that BH is a preferred cap⁴⁴ over both P and CH at both B3LYP and G3B3 levels (**Table 2.3**).

The stability of **13a** over **13c** could be due to the greater C-C bond strength as compared to that of C-P. The adjacent carbon basal ring (**13a**) again would be the thermodynamic product as in $\text{EH}_2\text{C}_2\text{P}_3^+$ (E= P or As or Sb),²² but conversion to **13b** through **13e** intermediate could also be feasible due to its relatively low energy (34.06 kcal/mol). Only one *nido* structure with a capping P (**13b**) converged, which is in contrast to the $\text{H}_n\text{C}_n\text{P}_{5-n}^+$ series^{21c} in which the P is a favored cap for a variety of *nido*-based positional isomers. Other structures with a P cap and non-adjacent carbons optimized to a tricyclopentane structure **20**, which is 2.8 kcal/mol lower than **13b**. In comparison to $\text{H}_4\text{C}_4\text{P}^+$, $\text{H}_3\text{C}_3\text{P}_2^+$ and $\text{H}_2\text{C}_2\text{P}_3^+$ structures, $\text{BC}_2\text{P}_2\text{H}_3$ has the *nido* geometry close to

vinylcyclopropenyl-type structure at G3B3 level and is 7.93 kcal/mol high at B3LYP level (**Figure 2.1**).

Table 2.3. Relative energies (kcal/mol) of *nido* geometry (**13**) isomers of *neutral* $\text{HBC}_2\text{P}_2\text{R}_2$ species; (R = H) are given in normal font at B3LYP and *italics* font at G3B3 level. Numbers in parenthesis pertain to relative energies (kcal/mol) when R= *t*Bu at B3LYP.

Struc ture	Arrangement of atoms in the skeleton				Relative energies of <i>neutral</i> skeleton 13		
No	E1	E2	E3	E4			
13a	CR	CR	P	P	7.93, <i>1.45</i> (24.35)		
13b	CR	CR	BH	P		11.01, <i>3.81</i> (9.69)	
13c	P	CR	P	CR	15.67, 6.69 (23.83)		
13d	BH	CH	P	P			25.75, 18.63 (22.52)
13e	BH	P	CR	P			34.06, 26.13 (30.92)

Substitution of H on C by *t*Bu changes the preferred order of capping to $\text{P} > \text{CH} > \text{BH}$, because the two *t*Bu groups that are adjacent to each other tend to increase the ring size. $\text{tBu}_2\text{C}_2\text{P}_3^+$ has non-adjacent carbon atoms with P in the capping position, while in $\text{HBtBu}_2\text{C}_2\text{P}_2$ this isomer (**13b**) is higher than tricyclopentane-type structure by 23.48 kcal/mol (**Figure 2.1**). The substitution of H on B by Ph stabilizes the tricyclopentane-type structure over *nido* **13a** and **13b** by 10.14 and 7.95 kcal/mol respectively (see earlier global minimum discussion). Addition of two electrons to the *nido* structure geometry, however, breaks one of the 3c-2e bonds to give either an envelope **15** or tricyclopentane-type (**20**) structure will be discussed later.

Regarding the methylenecyclobutenyl-type structures, all are non-planar (except for **14f**) and have 5 E-E and 3 E-H σ bonds, as well as 4 π electrons distributed in a C=C double bond and an allylic resonance structure. This series has a broad range of positional

isomers as local minima. Structures **14a** and **14b**, which contain a C=CH₂ fragment, are more stable than the other isomers. The stability ordering of the remaining isomers, C=PH > P≡P > C=BH₂ > P=CH > P=BH₂, might be related to the bond strengths and the lowered stability of penta-coordinated phosphorus and tetra-coordinated sp² P and B atoms (**Table 2.4**). (Note that all tetra-coordinated sp² phosphorus structures (P=CH > P=BH₂) are above 50 kcal/mol are in **Appendix 2.7.3**). Substitution of H on C by *t*Bu reorders the isomers, with preference for a structure containing non-adjacent C atoms (**14c**) as the lowest-energy structure.

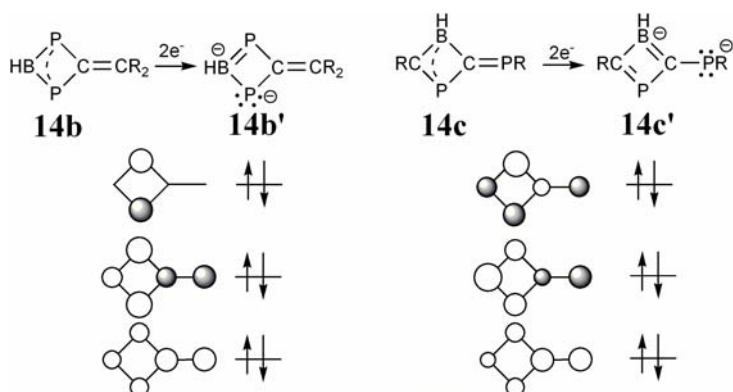
This methylenecyclobutenyl-type structure has been reported for Cp⁺ and in H_nC_nP_{5-n}⁺ (n=1-3), as the number of P atoms increases, this structure becomes more destabilized as compared to the ground-state *nido* geometry.^{20g,21c} The stability of the *nido* over the methylenecyclobutenyl-type geometry shows that for both, BC₂P₂H₃ and H_nC_nP_{5-n}⁺, the presence of B and P atoms prefer cluster-type bonding (**Figure 2.1**). However, when there are more C atoms such as in Cp⁺, cluster bonding suggested earlier^{19a} is less preferred over cyclic structure.^{20j,21c}

In comparison to the *neutral* species, a greater number of BC₂P₂H₃²⁻ structures optimize to a planar methylenecyclobutenyl-type structure, although many are higher than 50 kcal/mol and do not appear in **Table 2.4**. As with the *neutral* structures, the lowest-energy BC₂P₂H₃²⁻ species also has a C=CH₂ fragment. Adding two electrons, results in a transition from delocalized allylic resonance within the four-membered ring to localized π bonding. This change in allylic to localized π bonding can be understood by considering the π MO's of two representative structures **14b'** and **14c'** (**Scheme 2.6**).

Table 2.4. Relative energies (kcal/mol) of methylenecyclobutenyl-type (**14**) isomers of *neutral* and *dianionic* BC₂P₂HR₂ species; (R = H) are given in normal font at B3LYP and *italics* font at G3B3 level. Numbers in parenthesis pertain to relative energies (kcal/mol) when R=*t*Bu at B3LYP.

Struc ture	Arrangement of atoms in the skeleton			Relative energies for skeleton 14			
				<i>neutral</i>	<i>dianion</i> ^a	<i>neutral</i>	<i>dianion</i> ^a
No	E1	E2	E3				
14a	P	P	BH	15.71, 15.64 (25.67)	32.35, 33.86 (42.98)		
14b	P	BH	P	24.82, 23.02 (38.0)	28.97, 28.68 (44.89)		
14c	P	CR	BH			32.11, 30.75 (21.68)	57.51, 56.12 (41.01)
14d	CR	P	BH			35.38, 35.79 (26.13)	49.69, 49.72 (-)
14e	CR	BH	P			37.21, 37.09 (33.52)	42.22 (-)
No	Arrangement of atoms in the skeleton						
14f	BH	CR	CR	48.34, 47.08 (43.86)	71.48, 69.26 (60.92)		-
14g	P	P	CR			50.27, 47.93 (38.23)	
14h	P	CR	P			56.53, 49.91 (41.73)	38.97, 35.02 (23.14)
14i	CR	BH	CR	67.50, 62.28 (51.20)	57.02, 49.81 (43.56)		

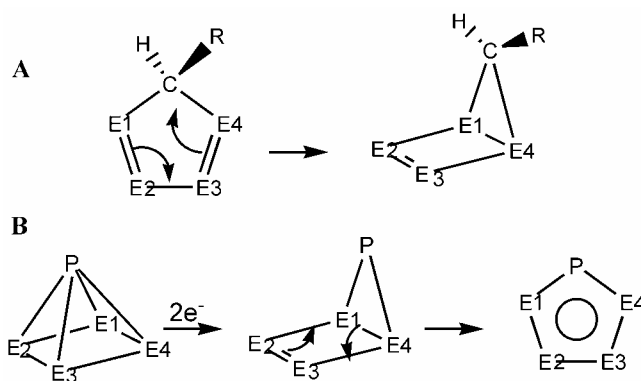
^a The arrangements of atoms are similar for the *dianion*; thus all *dianionic* isomers are referred with the same structure number (No) and a “'”. A “-” indicates non converged structures.



Scheme 2.6. A top view of the filled π molecular orbitals of the methylenecyclobutenyl-type structures $\text{BC}_2\text{P}_2\text{HR}_2^{2-}$ (**14b'** and **14c'**).

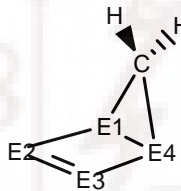
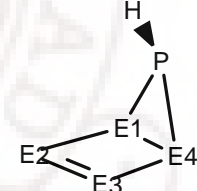
For the *neutral* structure (**14b** and **14c**), only the two lower MO's are filled, which correspond to the delocalized equivalents of the methylene and allylic π bonds (**Scheme 2.6**). Addition of two electrons fills one of two allylic π MO's, giving a π lone pair on one P atom and a localized B=P π in **14b'**, as seen in all structures except **14c-e**. In those structures, filling of the HOMO gives rise to two double bonds in the ring, as shown in **14c'** (**Scheme 2.6**). The lowest-energy structure **14a'** has filling of a π^* orbital to give two P lone pairs. *t*Bu substitution gives a similar trend in stability as the *neutral* species, with **14c'** structure being the lowest in energy.

Fusion of a 4- and a 3- membered ring results in an envelope-like structure **15**. This skeleton has 6 E-E and 3 E-H σ bonds, as well as one localized π bond in the four-membered ring. From all isomers, those with BH, CH, and P groups in the bridgehead converge to *nido* geometry, and the only local minima have a bridging CH_2 unit or the isolobal PH group (**Table 2.5**). These isomers can be recognized as rearrangements of planar and non-planar boryl skeletons (**Scheme 2.7A**).



Scheme 2.7. The rearrangement of *neutral* boryl isomers to an envelope structure (**A**) and square pyramid to envelope conversion upon addition of two electrons (**B**).

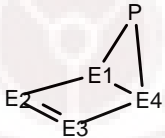
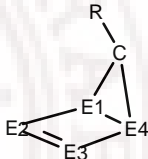
Table 2.5. Relative energies (kcal/mol) of envelope-type (**15**) isomers of $\text{BC}_2\text{P}_2\text{HR}_2$; ($\text{R} = \text{H}$) are given in normal font at B3LYP and *italics* font at G3B3 level. Numbers in parenthesis pertain to relative energies (kcal/mol) when $\text{R} = t\text{Bu}$ at B3LYP.

Structure	Arrangement of atoms in skeleton				Relative energy of <i>neutral</i> skeleton 15	
No	E1	E2	E3	E4		
15a	CR	B	P	P	25.29, 22.50 (25.41)	
15b	P	P	CR	B	30.99, 29.30 (22.39)	
15c	P	B	CR	P	37.42, 32.02 (29.92)	
15d	CR	P	P	B	41.15, 38.41 (39.19)	
15e	P	B	P	CR	41.32, 38.16 (46.31)	
15f	P	CR	CR	B		42.44, 40.28 (37.06)
15g	CR	B	CR	P		44.13, 39.01 (36.36)
15h	P	CR	P	B	45.92, 42.51 (40.51)	
15i	CR	P	CR	B		49.08, 46.07 (39.35)

Thus, rearrangement of boryl structures **12f**, **j**, or **m** could give rise to the isomers **15a**, **c**, and **e** that contain B in the four-membered ring. In a similar way to the 5-membered boryl rings, the PH- containing structures are less stable than the CH_2 -containing structures. **15a** is lower energy than **15b** because of the better availability of

the phosphorus lone pair to interact with the adjacent boron atom. It is difficult to determine why some positional isomers are more stable than others, especially given the range of P-P distances in these structures (ranging from 2.06 to 2.40 Å). Substitution of *t*Bu for H on carbon gives **15b** as the lowest-energy structure, which does not have adjacent carbon atoms (**Table 2.5**).

Table 2.6. Relative energies (kcal/mol) of envelope-type (**15**) isomers of $\text{BC}_2\text{P}_2\text{HR}_2^{2-}$ species; (R = H) are given in normal font at B3LYP and *italics* font at G3B3 level. Numbers in parenthesis pertain to relative energies (kcal/mol) when R=*t*Bu at B3LYP.

Struc ture	Arrangement of atoms in skeleton				Relative energy of <i>dianion</i> skeleton 15	
						
No	E1	E2	E3	E4		
15a'	P	CR	CR	BH	46.53, 43.21	(38.26)
15b'	P	CR	BH	CR	52.75, 46.95	(36.96)
15c'	CR	BH	P	CR	54.69, 52.59	(52.48)
15d'	P	BH	CR	CR	56.63, 52.61	(52.24)
15e'	CR	CR	P	BH	59.22, 53.36	(56.11)
15f'	CR	P	CR	BH	60.39, 55.87	(43.0)
15g'	CR	BH	P	P	61.32, 57.18 (51.07)	

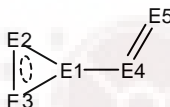
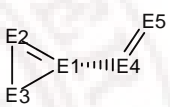
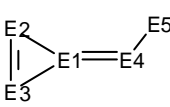
In contrast to the $\text{BC}_2\text{P}_2\text{HR}_2$ systems, envelope structures with bridging BH, CH and P fragments are only obtained as minima in $\text{BC}_2\text{P}_2\text{HR}_2^{2-}$ and all of the bridging CH_2 and PH structures converge to planar and non-planar boryl species, while BH bridges, are higher than 50 kcal/mol in energy (**Appendix 2.7.1**). The relative energies indicate that P⁻ is a more preferred bridge over CH⁻ or BH²⁻ and those structures with a P⁻ bridgehead and B in the three-membered ring are also lower in energy than those with B in the E2 or E3 position (**Table 2.6**).

These 12 isomers can be considered as being derived from the *nido* geometry (**Scheme 7B**). In these structures, P has two lone pairs and CH and BH have just one lone pair. Envelope structures have also been found as intermediates in the interconversion between a *nido* (*cationic*) and planar cyclic (*anionic*) structure, as in the synthesis of a $\text{Sb}t\text{Bu}_2\text{C}_2\text{P}_2$ species that has an envelope $\text{ClSb}t\text{Bu}_2\text{C}_2\text{P}_2$.⁴⁵ The high energies of the **15a'**-**15d'** isomers and their rearrangement to cyclic planar **12a'**, **b'**, **g'** and **k'** hints that they might also be potential intermediates in the conversion of a *neutral nido* structure to a *dianionic* cyclic geometry (**Scheme 2.7B**). Substitution of *t*Bu groups has similar optimized geometry, in which adjacent C-C bond structures are high in energy and **15b'** is the lowest-energy structure (**Table 2.6**).

2.4.5 Isomers Containing 3-Membered Rings

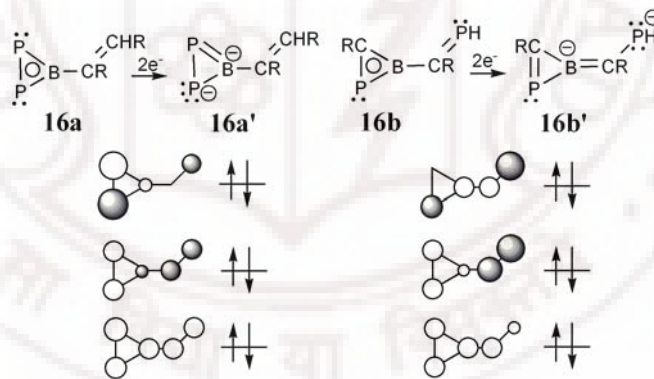
Optimized 3-membered ring isomers exhibit four basic skeletal types: vinylcyclopropenyl **16**, bismethylene-substituted cyclopropene **17**, bicyclic structures such as bicyclobutane **18** and spirane **19**, and tricyclopentane- **20** (**Chart 2.1**). The *neutral* vinyl cyclopropenyl skeleton has 5 E-E and 3 E-H σ bonds, and two of the four π electrons can be considered being delocalized in the three-membered ring, with the remaining two electrons in the C=C bond. There are 9 vinyl-type structures that have C=CH₂, CH=PH, P=CH₂, P=PH and BH=PH groups bound to the ring through a B or a C (**Table 2.7**). Interestingly, all structures with P in the “E1” position converged to a spirane-type geometry. There are also three high-energy hypervalent phosphorous structures with a formal triple P \equiv P bond as local minima (**Appendix 2.7.2**). The lowest-energy vinylcyclopropenyl-type structure is **16a**, which is also the global minimum at B3LYP level and one of three at G3B3 level (see earlier discussion).

Table 2.7. Relative energies (kcal/mol) of vinylcyclopropenyl-type (**16**) structures in *neutral* and *dianionic* BC₂P₂HR₂ species; (R = H) are given in normal font at B3LYP and *italics* font at G3B3 level. Numbers in parenthesis pertain to relative energies (kcal/mol) when R=*t*Bu at B3LYP.

Structure	Arrangement of atoms in skeleton					Relative energies of skeleton 16		
						<i>neutral</i>	<i>dianion</i> ^a	<i>dianion</i> ^a
No	E1	E2	E3	E4	E5			
16a	B	P	P	CR	CHR	0.0, 1.71 (2.32)	27.60, 35.45 (14.86)	
16b	B	CR	P	CR	PR	25.06, 25.99 (16.17)		53.22, 57.58 (-)
16c	B	CR	P	P	CHR	27.91, 28.22 (13.69)	65.66, 68.81 (42.38)	
16d	B	CR	CR	P	PH	29.04, 30.84 (14.35)	-	-
16e	C	BH	P	CR	PR	29.10, 31.16 (37.21)		37.55, 41.39 (36.87)
16f	C	BH	P	P	CR ₂	29.46, 29.37 (43.67)	-	-
16g	C	BH	CR	P	PR	32.46, 34.16 (21.98)		48.55, 51.96 (34.08)
16h	C	P	CR	BH	PR	54.59, 57.63 (39.95)	-	-
16i	C	CR	P	BH	PR	55.72, 58.63 (41.12)	49.54, 54.33 (36.80)	

^a Since the arrangements of atoms are similar for the *dianion*; so all *dianionic* isomers are referred with the structure number (No) and a “'”. A “-” indicates that the isomer converged to another isomer.

Furthermore, in some structures such as **16c** and **d**, there is a slight out-of-plane twisting of the vinyl group, which occurs when P is in the E4 position. The increase in steric bulk of $\text{BC}_2\text{P}_2\text{HtBu}_2$ species causes reordering of the energies, giving a new global minimum, a tricyclopentane-type structure (**20a**). **16a** still remains the lowest-energy vinylcyclopropenyl-type structure in series (**Figure 2.1**). The $\text{BC}_2\text{P}_2\text{H}_3^{2-}$ series also exhibits similar local minima structures (**Table 2.7**), except for **16b**. However, on reduction, it appears that a shift from delocalized to localized bonding in the three-membered ring occurs and the 2- charge is distributed on one BR^- atom and one P^- or PR^- group. This shift to localized bonding in the three-membered ring can be understood through the filling of the π MO's of two representative structures **16a'** and **16b'**, shown in **Scheme 2.8**.

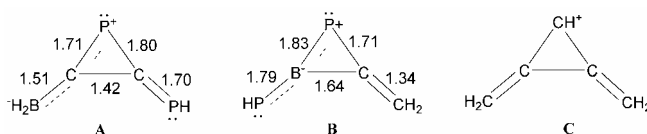


Scheme 2.8. A top view of the filled π molecular orbitals of the vinylcyclopropenyl-type structures $\text{BC}_2\text{P}_2\text{HR}_2^{2-}$ (**16a'** and **16b'**).

For the *neutral* system (**16a** and **16b**), the two lowermost MO's are filled. Depending on the position of the atoms, there are two possible MO's that can be filled on two-electron reduction to give $\text{BC}_2\text{P}_2\text{H}_3^{2-}$. Those structures with P in the E3 position, such as **16a'**, have a filled HOMO that gives a P^- and a π bond between the other two

members of the cyclopropene ring. Those structures with a PR group in the E5 position, such as **16b'**, have filling of a HOMO that instead shifts the localized π bond to the E2-E3 position and places a -1 charge on the PR group (**Scheme 2.8**). Unlike the *neutral* isomers, all B atoms bonded to the vinyl group are higher in energy as compared to those with a C atom and twisting in **16d** converges to the spirane-type geometry **19d**. The relative energies of the positional isomers appear to depend on the amount of π overlap in the bond between the vinyl-type fragment and the cyclopropene group, as given by NBO analysis. As before, upon substitution of *t*Bu, all isomers are stabilized except for **16b'** (**Table 2.7**).

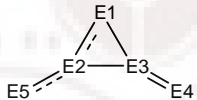
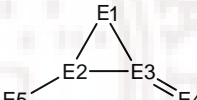
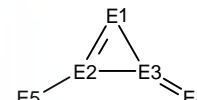
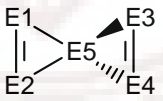
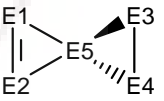
The bismethylenecyclopropene-type series **17** which can exist in the gas phase⁴⁶ represents another class of $\text{BC}_2\text{P}_2\text{H}_3$ isomers that are around 50–90 kcal/mol higher than the global minimum structure. This series has 5 E-E and 3 E-H σ bonds, and the four π electrons can be found in one ethylene and one allylic bond (such as in **17a** and **b**) or as in one ethylene and one cyclopropene bond (**17c**), as shown in **Table 2.8**. Structures **17a** and **b** are isolobal with a bismethylenecyclopropene *cation* (**Scheme 2.9**), with an isolobal connection between P^+ and CH^+ , BH_2^- with CH_2 , and PH with CH_2 . Formal charges have been placed on the B and P atoms, but these are a slight exaggeration because the two π electrons are delocalized over three atoms. The other three isomer species are very high in energy (>80 kcal/mol, **Appendix 2.7.3**). Substitution of H by *t*Bu stabilizes all the isomers due to less steric crowding (**Table 2.8**).



Scheme 2.9. Lewis structures for (A) **17a**, (B) **17b**, and (C) a bismethylenecyclopropene *cation*. Bond distances for the optimized structures are given in Å.

Only four isomers are obtained as minima in the *dianionic* species, as the other neutral isomers (except **17c**) upon addition of two electrons converge to cyclic and linear isomers **21d'**, **i'**, and **j'**. In these *dianions*, one localized π bond is present and the remaining four electrons are found either in another localized π bond or in a P lone pair orbital. *t*Bu substitution stabilizes **17b'**, making it about 15 kcal/mol higher in energy than the global minimum (**Table 2.8**).

Table 2.8. Relative energies (kcal/mol) of 3-membered ring isomers of *neutral* and *dianionic* $\text{BC}_2\text{P}_2\text{HR}_2$ species with skeleton **17** and **19**; (R = H) are given in normal font at B3LYP and *italics* font at G3B3 level. Numbers in parenthesis pertain to relative energies (kcal/mol) when R=*t*Bu at B3LYP.

Structure	Arrangement of atoms in skeleton					Relative energies of <i>neutral</i> and <i>dianion</i> ^a skeleton 17		
								
No	E1	E2	E3	E4	E5			
17a	P	C	C	PH	BHR	50.29, 50.58 (38.57)		
17a'	P	C	B	PH	CR ₂		21.55, 24.97 (27.78)	
17b	P	B	C	CR ₂	PH	52.04, 53.35 (50.11)		
17b'	CR	C	B	PH	PH			27.30, 31.03 (15.12)
17c	CH	B	C	PHR	P			62.33, 61.68 (47.18)
No	Arrangement of atoms in skeleton					<i>neutral</i>		<i>dianion</i> ^a
								
19a	P	BH	CR	CR	P	58.71, 52.34 (42.69)		
19b	P	CR	BH	PR	C	61.32, 60.57 (48.16)		> 50 kcal/mol
19c	P	CR	CR	BH	P	62.39, 55.89 (47.12)		-
19d	CR	CR	PH	P	B	-		62.52, 61.94 (43.28)

^a Since the arrangements of atoms are similar for the *dianion* so all *dianionic* isomers are referred with the structure number (No) and a "'". A "-" indicates that the isomer converged to another isomer.

Other stable isomers include the bicyclobutane-type systems **18** with 6 E-E and 3 E-H σ bonds and 2 π electrons in a localized double bond which are also structurally similar to some silicon carbide clusters.⁴⁷ Among the four optimized isomers of **18**

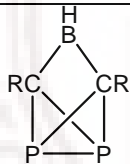
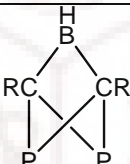
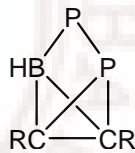
(Figure 2.1 and Appendix 2.7.2), the one containing a $C=CH_2$ fragment (**18a**) is lowest in energy, which was also present in the lowest-energy isomer of the methylenecyclobutenyl structure (Figure 2.1). Only one bicyclobutane structure is a minimum for the dianion (**18a'**), which is quite high in energy (67.06 kcal/mol), and contains a $P=B^{2-}$ group (Figure 2.2). Addition of two electrons to all other isomers results in linear structures (such as **21a'**) and other high-energy, methylenecyclobutenyl-type structures with elongated B-P and P-P bonds.

The spirane⁴⁸ skeleton **19** is another bicyclic structure having 6 E-E and 3 E-H σ bonds and four π electrons. Nine possible $BC_2P_2H_3$ isomers exist but only three are local minima: they are quite high in energy and have either P or C in the sp^3 -hybridised, tetracoordinate position (Table 2.8). All spirane structures with a central B atom optimized to a vinylcyclopropenyl series. Increased steric bulk caused by *t*Bu substitution leads to stabilization of these three isomers by about 15 kcal/mol, and **19a** is the most stable, despite having *t*Bu groups on adjacent carbons. For $BC_2P_2H_3^{2-}$, however, spirane geometries with both central B and P atoms are observed (but still at very high energies). The boron-based spirane **19d'** is more stable (62 kcal/mol) than the phosphorus counterpart **19a'** (103.04 kcal/mol, Appendix 2.7.3). *t*Bu substitution provides further stabilization of the structures (Table 2.8), as seen for the *neutral* species.

The final skeleton in the three-membered ring series is the tricyclopentane-type geometry, which has 10 σ bonds (7 E-E, 3 E-H) and two lone pairs on the phosphorus atoms. Almost every possible isomer optimizes into the *nido* structure: only one, **20a**, with a bridging BH group, is a stationary point, lying 8.2 kcal/mol higher in energy than the global minimum (Table 2.9). *t*Bu substitution gives a global minimum that is also

found experimentally with $\text{PhBtBu}_2\text{C}_2\text{P}_2$ **10**²³ (see earlier discussion). For $\text{BC}_2\text{P}_2\text{H}_3^{2-}$, five positional isomers were found to be minima, albeit at high energy (above 50 kcal/mol (**Appendix 2.7.3**). One lower-energy structure, **20a'**, appears to be related to **20a**, with the two additional electrons entering the P-P σ^* orbital, stretching the distance from 2.17 Å to 2.86 Å. All *t*Bu substituted isomers, both *neutral* and *dianionic* species are stabilized and maintain a similar energetic ordering.

Table 2.9. Relative energies (kcal/mol) of 3-membered ring isomers of *neutral* and *dianionic* $\text{BC}_2\text{P}_2\text{HR}_2$ species with skeleton **20**; (R = H) are given in normal font at B3LYP and *italics* font at G3B3 level. Numbers in parenthesis pertain to relative energies (kcal/mol) when R=*t*Bu at B3LYP.

Structure No	Relative energies for skeleton 20		
	<i>neutral</i>	<i>dianion</i>	
			
20a	8.21, 0.0 (0.0)		
20a'		64.19, 58.97 (46.05)	
20b'			65.39, 58.77 (48.81)

2.4.6 Acyclic Isomers Linear or Branched

The acyclic isomers have 8 σ bonds (5 E-E and 3 E-H) and 6 π electrons, which can be distributed in a variety of localized and delocalized combinations. These type of structures are known for C_5H_5 radicals and cations in the interstellar medium and also as precursors to soot in rich-fuel flames.^{20g,46,49} There are a large number of $\text{BC}_2\text{P}_2\text{H}_3$ minima but they are higher in energy than linear Cp^+ isomers.^{20g} The lowest-energy structure, **21a**, has a C-P triple bond and a delocalized P-B-C π bond (**Figure 2.5**). The other lower-energy structures have a triple bond between E1 and E2 or (E2 and E3) and a

double bond between E3 and E4 (or E4 and E5) (**21a-21f, 21h, Figure 2.5**) and higher have more delocalized double bonds over four atoms **21g** (**Figure 2.7.6**). Isolobal substitution of CH with P and CH₃ with PH₂ gives **21d** (**Figure 2.5**), which is 10 kcal/mol higher in energy than **21a** due to lone pair-lone pair repulsions. The availability of electrons for the boron 2p orbitals seems to be a prime factor for the relative stability of isomers.

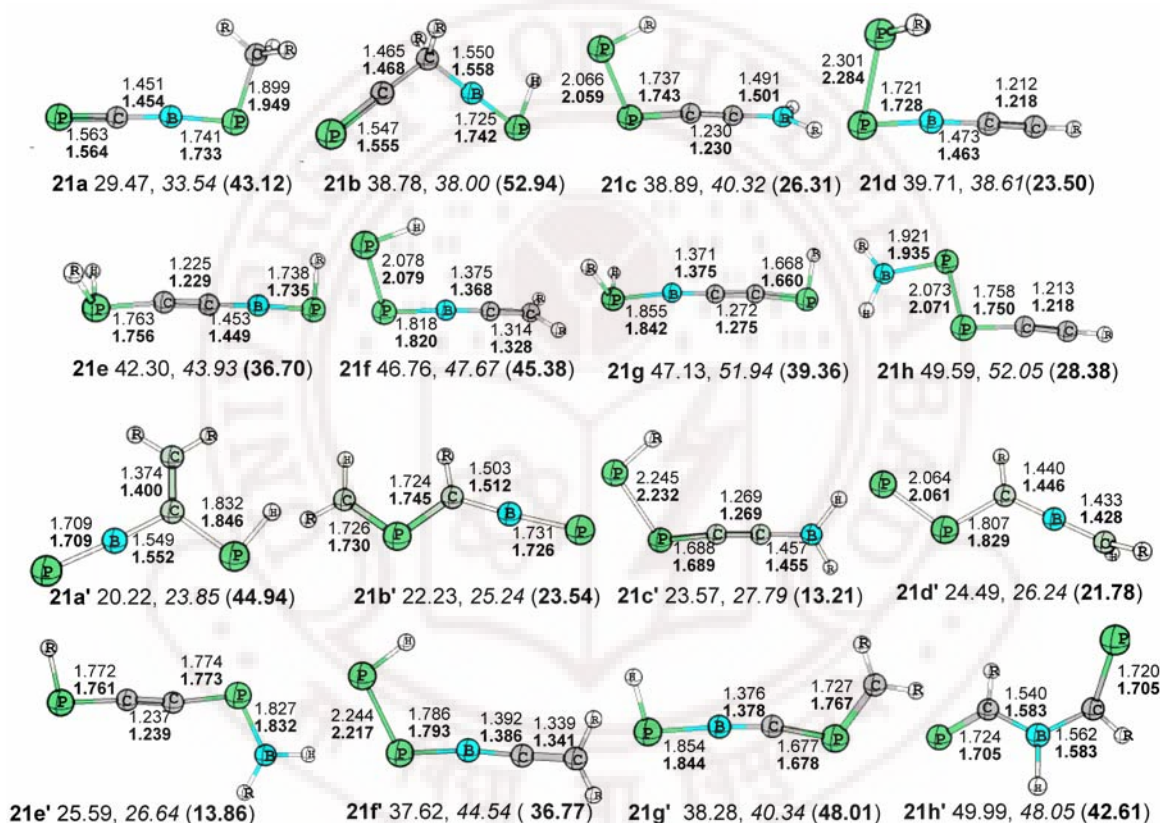


Figure 2.5. Relative energies (kcal/mol) and geometrical parameters of acyclic isomers of *neutral* and *dianionic* $\text{BC}_2\text{P}_2\text{HR}_2$ species (**21**); (R = H, *t*Bu) are shown in normal (H-substituted) and **bold** font (*t*Bu-substitution of H on C) in parenthesis respectively are at B3LYP/6-311++G (d,p) level and those in *italics* (H-substituted) are at G3B3 level.

Upon addition of two electrons and optimization of **21a**, a cyclic isomer is obtained; however, the other stable *dianionic* linear isomers usually result from optimizations starting from high-energy bicyclic or bismethylenecyclopropene-type structures (**Figure 2.5**). The lowest-energy $\text{BC}_2\text{P}_2\text{H}_3^{2-}$ isomer is a branched structure, which has localized π bonds and a B^- and PH^- group (**Figure 2.5**). Substitution of *t*Bu groups for both the *neutral* and *dianionic* species causes a reordering of the isomeric energies, giving **21d'** and **21e'** as the lowest-energy structures.

2.5 Conclusions

Optimization of classical and non-classical *neutral* and *dianionic* $\text{BC}_2\text{P}_2\text{H}_3$ isomers at the B3LYP/6-311++G (d,p) and G3B3 levels give a variety of geometric and positional isomers, which includes planar and non-planar five-membered rings, methylenecyclobutenyl-, *nido*-, envelope-, vinylcyclopropenyl-, tricyclopentane-, spirane-, bismethylenecyclopropene-type structures, and acyclic. The vinylcyclopropenyl- (**16a**) and planar cyclopentadienyl-type (**12a'**) structures are global minima for *neutral* and *dianionic* $\text{BC}_2\text{P}_2\text{H}_3$ species at the B3LYP level. On the other hand G3B3 level, gives two other structures (i) a *nido* (**13a**) and (ii) a tricyclopentane (**20a**) in addition to the vinyl cyclopropenyl-type as the global minima. In comparison to Cp^+ and $\text{H}_n\text{C}_n\text{P}_{5-n}^+$, there is a competition among a 2π delocalized structure (**16a**) and two cluster geometries (**13a** and **20a**) in $\text{BC}_2\text{P}_2\text{H}_3$ isomers; however a cyclic planar structure (**12a'**) is the unambiguous ground state $\text{BC}_2\text{P}_2\text{H}_3^{2-}$. Apart from having three low-lying minima for $\text{BC}_2\text{P}_2\text{H}_3$, the G3B3 level decreases the energies of delocalized structures, but the positional and $\text{BC}_2\text{P}_2\text{H}_3^{2-}$ isomers relative stabilities remain unaltered.

Except the in spirane- and tricyclopentane-type isomers, replacement of H by *t*Bu at B3LYP/6-311++G (d,p) changes the relative energies of the *neutral* and *dianionic* geometrical and positional $\text{HBC}_2\text{P}_2\text{R}_2$ isomers. *t*Bu groups substituted on adjacent or the same carbon in general leads to destabilization. However, for $\text{HB}(\text{tBuC})_2\text{P}_2$ the minimum is a tricyclopentane-type structure with vinyl cyclopropenyl at 2.32 kcal/mol high in energy. Here also it differs from its isoelectronic counterpart, $\text{EtBu}_2\text{C}_2\text{P}_2$ (E = Sn, Ge, Pb, P^+ , As^+ and Sb^+), which is experimentally found in a *nido* or *nido* geometry. Further substitution of B-Ph for B-H affords a tricyclopentane-type structure which is again stable over the BH capped *nido* structure by 10.14 kcal/mol. Owing to substituent effects, BR has a different experimental structure compared to its other isolobal analogue $\text{P}_3(\text{tBuC})_2^+$. The smaller stabilization of $\text{R}'\text{BC}_2\text{P}_2\text{R}_2$ in *nido*-type geometry is due to the poor overlap of BR capping orbital to $\text{P}-\pi^*$ orbital of tBuC_2P_2 base, thus it converts to a tricyclopentane-type geometry accompanied by a cross over of HOMO-LUMO levels and increase of the HOMO-LUMO gap.

The global minima of $\text{BC}_2\text{P}_2\text{H}_3^{2-}$ is a planar cyclic isomer **12a'** and, upon substituting more sterically bulky groups, other positional isomers **12b'** and **12g'** are obtained for $\text{HBtBu}_2\text{C}_2\text{P}_2$ and $\text{PhBtBu}_2\text{C}_2\text{P}_2$, respectively. These global minima, unlike the *neutral* species, resemble their isoelectronic counterparts, such as $\text{EtBu}_2\text{C}_2\text{P}_2$ (E = S, Se, Te) heterophospholyl rings $\text{EtBu}_2\text{C}_2\text{P}_2^-$ (E = P^- , As^- , Sb^-), and polyphospholyl rings $\text{R}_{5-n}\text{C}_n\text{P}_{5-n}^-$ (n = 0-5). The relative energies of geometrical and positional isomers of *neutral* and *dianionic* $\text{HBC}_2\text{P}_2\text{R}_2$ (R=H, *t*Bu) species depend upon (i) relative bond strengths (ii) availability of electrons for the empty 2p-boron orbital, and (iii) steric effects of the *t*Bu groups in the $\text{HBC}_2\text{P}_2\text{tBu}_2$ systems.

2.6 References

1. Dillon, K. B.; Mathey, F.; Nixon, J. F. *Phosphorus: The Carbon Copy: From Organophosphorus to Phospha-organic Chemistry*, John Wiley & Sons, Chichester, **1998**.
2. Mathey, F. *Angew. Chem. Int. Ed. Engl.*, **2003**, *42*, 1578-1604.
3. (a) Streubel, R. *Angew. Chem., Int. Ed.*, **1995**, *34*, 436-438 and references therein.
(b) Mack, A.; Regitz, M. in *Carbocyclic and Heterocyclic Cage Compounds and Their Building Blocks*, (Ed.: K. K. Laali), J. A. I. Press, Stamford, CT, USA, **1999**, p. 199. (c) Nixon, J. F. *ibid.*, p. 257. (d) Weber, L. *Adv. Organometal. Chem.*, **1997**, *41*, 1. (e) Regitz, M.; Hoffmann, A.; Bergsträsser, U. in *Modern Acetylene Chemistry* (Eds. P. J. Stang, F. Diederich), VCH, Weinheim, **1995**. (f) Appel, R.; in *Multiple Bonds and Low Coordination in Phosphorus Chemistry* (Eds. M. Regitz, O. Scherer), Georg Thieme Verlag, New York, **1990** p.153. (g) Bartsch, R.; Hitchcock, P. B.; Nixon, J. F. *J. Organometal. Chem.*, **1989**, *375*, C31-C34. (h) Caliman, V.; Hitchcock, P. B.; Nixon, J. F.; Hofmann, M.; Schleyer, P. von R. *Angew. Chem., Int. Ed.*, **1994**, *33*, 2202-2203. (i) Geissler, B.; Wettling, T.; Barth, S.; Binger, P.; Regitz, M. *Synthesis*, **1994**, 1337-1343. (j) Tabellion, F.; Nachbauer, A.; Leininger, S.; Peters, C.; Preuss, F.; Regitz, M. *Angew. Chem. Int. Ed.*, **1998**, *37*, 1233-1235. (k) Wettling, T.; Schneider, J.; Wagner, O.; Kreiter C. G.; Regitz, M. *Angew. Chem., Int. Ed.*, **1989**, *28*, 1013-1014. (l) Geissler, B.; Barth, S.; Bergsträsser, U.; Slany, M.; Durkin, J.; Hitchcock, P. B.; Hofmann, M.; Binger, P.; Nixon, J. F.; Schleyer, P. von R.; Regitz, M. *Angew. Chem., Int. Ed.*, **1995**, *34*, 484-487. (m) Al-Ktaifani, M. M.; Bauer, W.; Bergsträsser, U.; Breit, B.;

- Francis, M. D.; Heinemann, F. W.; Hitchcock, P. B.; Mack, A.; Nixon, J. F.; Pritzkow, H.; Regitz, M.; Zeller, M.; Zenneck, U. *Chem. Eur. J.*, **2002**, 8, 2622-2623. (n) Avent, A. G.; Cloke, F. G. N.; Francis, M. D.; Hitchcock, P. B.; Nixon, J. F. *Chem. Commun.*, **2000**, 879-880. (o) Al- Ktaifani, M. M.; Hitchcock, P. B.; Nixon, J. F. *Inorg. Chim. Acta.*, **2003**, 356, 103-108.
4. Reddy, A. C.; Jemmis, E. D. *Organometallics*, **1988**, 7, 1561-1564.
 5. Nixon, J. F. *Chem. Rev.*, **1988**, 88, 1327-1362.
 6. Nixon, J. F. *Chem. Soc. Rev.*, **1995**, 24, 319-328.
 7. Mathey, F. *Coord. Chem. Rev.*, **1994**, 137, 1-52.
 8. Regitz, M.; Binger, P. *Angew. Chem. Int. Ed. Engl.*, **1988**, 27, 1484-1508.
 9. Nixon, J. F. *Coord. Chem. Rev.*, **1995**, 145, 201-258.
 - 10 Francis, M. D.; Hitchcock, P. B.; Nixon, J. F.; Schnöckel, H.; Steiner, J. J. *Organomet. Chem.*, **2002**, 646, 191-195.
 - 11 Schnepf, A.; Stößer, G.; Carmichael, D.; Mathey, F.; Schnöckel, H. *Angew. Chem. Int. Ed. Engl.*, **1999**, 38, 1646-1649.
 - 12 Callaghan, C.; Clentsmith, G. K. B.; Cloke, F. G. N.; Hitchcock, P. B.; Nixon, J. F.; Vickers, D. M. *Organometallics*, **1999**, 18, 793-795.
 - 13 Clentsmith, G. K. B.; Cloke, F. G. N.; Francis, M. D.; Green, J. C.; Hitchcock, P. B.; Nixon, J. F.; Suter, J. L.; Vickers, D. M. *J. Chem. Soc. Dalton Trans.*, **2000**, 1715-1721.
 - 14 Wann, D. A.; Hinchley, S. L.; Robertson, H. E.; Francis, M. D.; Nixon, J. F.; Rankin, D. W. H. *J. Organomet. Chem.*, **2007**, 692, 1161-1167.

- 15 (a) Jones, C.; Ryan C. Thomas *J. Organomet. Chem.*, **2001**, 622, 61-65. (b) Helm, M. L.; Hitchcock, P. B.; Nixon, J. F.; Nyulászi, L.; Szieberth, D. *J. Organomet. Chem.*, **2002**, 659, 84-91.
- 16 Francis, M. D.; Hibbs, D. E.; Hursthouse, M. B.; Jones, C.; Malik, K. M. A. *J. Organomet. Chem.*, **1997**, 527, 291-293.
- 17 (a) d'Arbeloff-Wilson, S. E.; Hitchcock, P. B.; Krill, S.; Nixon, J. F. Nyulászi, L.; Regitz, M. *J. Am. Chem. Soc.*, **2000**, 122, 4557-4562. (b) Francis, M. D.; Jones, C.; Morley, C. P. *Tetrahedron Lett.*, **1999**, 40, 3815-3816.
- 18 (a) Francis, M. D.; Hibbs, D. E.; Hitchcock, P. B.; Hursthouse, M. B.; Jones, C.; Mackewitz, T.; Nixon, J. F.; Nyulaszi, L.; Regitz, M.; Sakarya, N. *J. Organomet. Chem.*, **1999**, 580, 156-160. (b) Caliman, V.; Hitchcock, P. B.; Nixon, J. F.; Nyulászi, L.; Sakarya, N. *Chem. Commun.*, **1997**, 1305-1306.
- 19 (a) Stohrer, W. D.; Hoffmann, R. *J. Am. Chem. Soc.*, **1972**, 94, 1661-1668. (b) Masamune, S.; Sakai, M.; Ona, H.; *J. Am. Chem. Soc.*, **1972**, 94, 8955-8956. (c) Masamune, S.; Sakai, M.; Ona, H.; Jones, A. J. *J. Am. Chem. Soc.*, **1972**, 94, 8956-8958. (d) Breslow, R.; Chang, H. W.; Yager, W. A. *J. Am. Chem. Soc.*, **1963**, 85, 2033-2034. (e) Breslow, R.; Hill, R.; Wasserman, E. *ibid.* **1964**, 86, 5349-5350. (f) Breslow, R.; Chang, H. W.; Hill, R.; Wasserman, E. *J. Am. Chem. Soc.*, **1967**, 89, 1112-1119. (g) Saunders, M.; Berger, R.; Jaffe, A.; McBride, J. M.J.; O'Neill, Breslow, R.; Hoffmann, J. M.; Jr., Perchonock, C.; Wasserman, E. ; Hutton R. S.; Kuck, V. J. *J. Am. Chem. Soc.*, **1973**, 95, 3017-3018. (h) Allen, A. D.; Sumonja M.; Tidwell, T. T. *J. Am. Chem. Soc.*, **1997**, 119, 2371-2375. (i) Wörner H. J.; F. Merkt, *Angew. Chem. Int. Ed. Engl.*, **2006**, 45, 293-296.

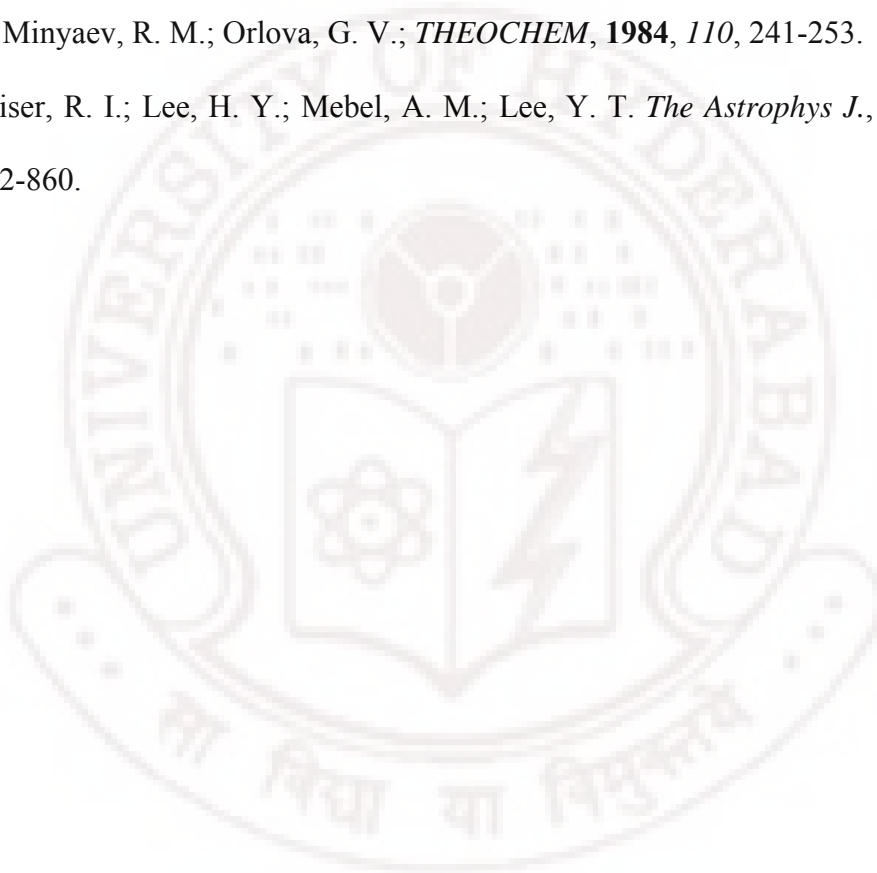
- 20 (a) Kollmar, H. J.; Smith, H. O.; Schleyer, P. von R. *J. Am. Chem. Soc.*, **1973**, *95*, 5834-5836. (b) Dewar, M. J. S.; Haddon, R. C. *J. Am. Chem. Soc.*, **1973**, *95*, 5836-5837. (c) Dewar, M. J. S.; Haddon, R. C. *J. Am. Chem. Soc.*, **1974**, *96*, 255-256. (d) Leone, R. E.; Schleyer, P. von R. *Angew. Chem. Int. Ed. Engl.*, **1970**, *9*, 860-890. (e) Hehre, W. J.; Schleyer, P. von R. *J. Am. Chem. Soc.*, **1973**, *95*, 5837-5839. (f) Kohler, H. J.; Lischka, H. *J. Am. Chem. Soc.*, **1979**, *101*, 3479-3486. (g) Feng, J.; Leszczynski, J.; Weiner B.; Zerner, M. C. *J. Am. Chem. Soc.*, **1989**, *111*, 4648-4655. (h) Glukhovtsev, M. N.; Reindl B.; Schleyer, P. von R. *Mendeleev. Commun.*, **1993**, *3*, 100-102. (i) Reindl B.; Schleyer, P. von R. *J. Comput. Chem.*, **1998**, *19*, 1402-1420. (j) Glukhovtsev, M. N.; Bach R. D.; Laiter, S. *J. Phys. Chem.*, **1996**, *100*, 10952-10955.
- 21 (a) Hearley, A. K.; Johnson, B. F. G.; McIndoe, J. S.; Tuck, D. G. *Inorg. Chim. Acta.*, **2002**, *34*, 105-112. (b) Chen, M. D.; Huang, R. B.; Zheng, L. S.; Zhang, Q. E.; Au, C. T. *Chem. Phys. Lett.*, **2000**, *325*, 22-28. (c) Pantazis, D. A.; McGrady, J. E.; Lynam, J. M.; Russell, C. A.; Green, M. J. *Chem. Soc. Dalton Trans.*, **2004**, 2080-2086.
- 22 Fish, C.; Green, M.; Jeffery, J. C.; Kilby, R. J.; Lynam, J. M.; McGrady, J. E.; Pantazis, D. A.; Russell, C. A.; Willans, C. E. *Chem. Commun.*, **2006**, 1375-1377.
- 23 (a) Francis, M. D.; Hitchcock, P. B. *Chem. Commun.*, **2002**, 86-87. (b) Francis, M. D. Hitchcock, P. B. unpublished personal communication to Nixon J. F. (c) Wann, D. A.; Hinchley, S. L.; Borisenko, K. B.; Robertson, H. E.; Francis, M. D.; Nixon, J. F.; Rankin, D. W. H. *J. Chem. Soc. Dalton Trans.*, **2005**, 1972-1978.

- 24 (a) Francis, M. D.; Hitchcock, P. B. *Organometallics*, **2003**, 22, 2891-2896. (b) Francis, M. D.; Hitchcock, P. B. *Organometallic*, **2003**, 22, 2897-2901.
- 25 (a) Canac, Y.; Bertrand G. *Angew. Chem. Int. Ed. Engl.*, **2003**, 42, 3578-3580. (b) Condick, P. N.; Fox, M. A.; Greatrex, R.; Jones, C.; Ormsby, D. L. *Chem. Commun.*, **2002**, 1448-1449.
- 26 Binger, P.; Wettling, T.; Schneider, R.; Zurmühlen, F.; Bergsträsser, U.; Hoffmann, J.; Maas, G.; Regitz, M. *Angew. Chem. Int. Ed. Engl.*, **1991**, 30, 207-210.
- 27 (a) Fish, C.; Green, M.; Jeffery, J. C.; Kilby, R. J.; Lynam, J. M.; Russell, C. A.; Willans, C. E.; McGrady, J. E.; Pantazis, D. A.; Whitwood, A. C. *Angew. Chem. Int. Ed.*, **2006**, 45, 3628-3631. (b) Slattery, J. M.; Fish, C.; Green, M.; Hooper, T. N.; Jeffery, J. C.; Kilby, R. J.; Lynam, J. M.; McGrady, J. E.; Pantazis, D. A.; Russell, C. A.; Willans, C. E. *Chem. Euro. J.*, **2007**, 13, 6967-6974.
- 28 Willans, C. E.; Fish, C.; Green, M.; Kilby, R. J.; Lynam, J. M.; Russell, C. A.; Whitwood, A. C. *J. Chem. Soc. Dalton Trans.*, **2008**, 3422-3428.
- 29 (a) Lynam, J. M.; Copsey, M. C.; Green, M.; Jeffery, J. C.; McGrady, J. E.; Russell, C. A.; Slattery, J. M.; Swain, A. C. *Angew. Chem. Int. Ed.*, **2003**, 42, 2778-2782. (b) Fish, C.; Green, M.; Jeffery, J. C.; Kilby, R. J.; Lynam, J. M.; Russell, C. A.; Willans, C. E. *Organometallics*, **2005**, 24, 5789-5791.
- 30 Nyulászi, L. *J. Organomet. Chem.*, **2005**, 690, 2597-2602.
- 31 (a) Becke, A. D. *J. Chem. Phys.*, **1993**, 98, 5648-5652. (b) Becke, A. D. *Phys. Rev. A.*, **1988**, 38, 3098-3100.
- 32 Lee, C.; Yang, W.; Parr, R. G. *Phys. Rev. B.*, **1988**, 37, 785-789.

- 33 Baboul, A. G.; Curtiss, L. A.; Redfern, P. C.; Raghavachari, K. *J. Chem. Phys.*, **1999**, *110*, 7650-7657.
- 34 Reed, A. E.; Curtiss, L. A.; Weinhold, F. *Chem Rev.*, **1988**, *88*, 899-926.
- 35 Gaussian 03, Revision B.02, Frisch, M. J.; Trucks, G. W.; Schlegel, H. B.; Scuseria, G. E.; Robb, M. A.; Cheeseman, J. R.; Montgomery, Jr., J. A.; Vreven, T.; Kudin, K. N.; Burant, J. C.; Millam, J. M.; Iyengar, S. S.; Tomasi, J.; Barone, V.; Mennucci, B.; Cossi, M.; Scalmani, G.; Rega, N.; Petersson, G. A.; Nakatsuji, H.; Hada, M.; Ehara, M.; Toyota, K.; Fukuda, R.; Hasegawa, J.; Ishida, M.; Nakajima, T.; Honda, Y.; Kitao, O.; Nakai, H.; Klene, M.; Li, X.; Knox, J. E.; Hratchian, H. P.; Cross, J. B.; Bakken, V.; Adamo, C.; Jaramillo, J.; Gomperts, R.; Stratmann, R. E.; Yazyev, O.; Austin, A. J.; Cammi, R.; Pomelli, C.; Ochterski, J. W.; Ayala, P. Y.; Morokuma, K.; Voth, G. A.; Salvador, P.; Dannenberg, J. J.; Zakrzewski, V. G.; Dapprich, S.; Daniels, A. D.; Strain, M. C.; Farkas, O.; Malick, D. K.; Rabuck, A. D.; Raghavachari, K.; Foresman, J. B.; Ortiz, J. V.; Cui, Q.; Baboul, A. G.; Clifford, S.; Cioslowski, J.; Stefanov, B. B.; Liu, G.; Liashenko, A.; Piskorz, P.; Komaromi, I.; Martin, R. L.; Fox, D. J.; Keith, T.; Al-Laham, M. A.; Peng, C. Y.; Nanayakkara, A.; Challacombe, M.; Gill, P. M. W.; Johnson, B.; Chen, W.; Wong, M. W.; Gonzalez, C.; and Pople, J. A.; Gaussian, Inc., Wallingford CT, **2004**.
- 36 (a) McKee, M. L. *J. Phys Chem.*, **1996**, *100*, 3473-3481 and references there in. (b) Stowasser, R.; Hoffmann, R. *J. Am. Chem. Soc.*, **1999**, *121*, 3414-3420. (c) Tschumper, G. S.; Schaefer, H. F. *J. Chem. Phys.*, **1997**, *107*, 2529-2541. (d) Galbraith, J. M.; Schaefer, H. F. *J. Chem. Phys.*, **1996**, *105*, 862-864 and

- references there in. (e) Priyakumar, U. D.; Sastry, G. N.; *J. Org. Chem.*, **2002**, *67*, 271-281. (f) Priyakumar, U. D.; Dinadayalane T. C.; Sastry, G. N. *New J. Chem.*, **2002**, 347-353.
- 37 Barron, A. R.; Cowley, A. H.; Hall, S. W.; Nunn, C. M.; *Angew. Chem. Int. Ed. Engl.*, **1988**, *27*, 837-839.
- 38 (a) Maier, G.; Rang, H.; Kalinowski, H-O. *Angew. Chem. Int. Ed.*, **1989**, *28*, 1232-1234. (b) Lokbani-Azzouz, N. S.; Costuas, K.; Halet, J.-F.; Saillard, J.-Y. *THEOCHEM*, **2001**, *571*, 1-6.
- 39 (a) Butts, C. P.; Green, M.; Hooper, T. N.; Kilby, R. J.; McGrady, J. E.; Pantazis, D. A.; Russell, C. A. *Chem. Commun.*, **2008**, 856-858. (b) Eisler, D. J.; Less, R. J.; Naseri, V.; Rawson, J. M.; Wright, D. S. *J. Chem. Soc. Dalton Trans.*, **2008**, 2382-2384.
- 40 Zhai, H-J.; Wang, L-S. *J. Phys. Chem. A.*, **2002**, *106*, 5600-5606 and references there in.
- 41 (a) Padma, M. E. J. *J. Org. Chem.*, **1992**, *57*, 3694-3698. (b) Nyulászi, L.; *Chem. Rev.*, **2001**, *101*, 1229-1246.
- 42 Segwa, Y.; Yamsahita, M.; Nozaki, K. *Science*, **2006**, *314*, 113-115.
- 43 Jemmis, E. D. *J. Am. Chem. Soc.*, **1982**, *104*, 7017-7020.
- 44 Fish, C.; Green, M.; Jeffery, J. C.; Kilby, R. J.; Lynam, J. M.; McGrady, J. E.; Russell, C. A.; Pantazis, D. A. Willans, C. E. *Angew. Chem. Int. Ed.*, **2006**, *45*, 6685-6689.

- 45 (a) Ding, H.; Boguslavskiy, A. E.; Maier, J. P. *Phys. Chem. Chem. Phys.*, **2005**, 7, 888-891. (b) Yang, B.; Huang, C.; Wei, L.; Wang, J.; Sheng, L.; Zhang, Y.; Qi, F.; W. Zheng, W-K. Li, *Chem Phys Lett.*, **2006**, 423, 321-326.
- 46 (a) Ritty, C. M. L. *J. Chem. Phys.*, **1994**, 100, 175-180. (b) Pardhan, P. Ray, A. K. *THEOCHEM*, **2005**, 716, 109-130.
- 47 (a) Kostler, W.; Linti, G. *Eur. J. Inorg. Chem.*, **2001**, 1841-1846. (b) Minkin, V. I.; Minyaev, R. M.; Orlova, G. V.; *THEOCHEM*, **1984**, 110, 241-253.
- 48 Kaiser, R. I.; Lee, H. Y.; Mebel, A. M.; Lee, Y. T. *The Astrophys J.*, **2001**, 548, 852-860.



2.7 Appendix

Table 2.7.1. Relative energies (kcal/mol) of *neutral* and *dianionic* $\text{BC}_2\text{P}_2\text{HR}_2$ species with skeletons (**12**) and (**15**); (R = H, *t*Bu). Numbers in parenthesis pertain to relative energies (kcal/mol) when H is substituted by *t*Bu at B3LYP level.

No	Arrangement of atoms in the skeleton				Relative energies of skeletons			
					12	15	15	
					<i>dianion</i>	<i>neutral</i>	<i>dianion</i>	
	E1	E2	E3	E4				
12d'	P	B	CR	CR	54.66 (-)			
12h'	P	CR	B	CR	69.45 (54.94)			
12l'	P	CR	CR	B	53.38 (-)			
12n'	CR	CR	B	P	75.88 (65.95)			
12o'	CR	P	CR	B	68.73 (60.74)			
12p'	CR	CR	P	B	61.74 (74.28)			
15j	CR	P	B	CR		52.06 (56.69)		
15k	B	P	CR	CR		58.94 (56.94)		
15h'	BH	P	CR	P			69.40 (60.87)	
15i'	P	BH	CR	P			72.70 (61.18)	
15j'	CR	P	BH	P			75.39 (62.94)	
15k'	P	CR	CR	P				77.07 (65.63)
15l'	CR	P	CR	P				84.96 (63.64)

Table 2.7.2. Relative energies (kcal/mol) of *neutral* and *dianionic* $\text{BC}_2\text{P}_2\text{HR}_2$ species with skeletons **14** and **18**; ($\text{R} = \text{H}, t\text{Bu}$). Numbers in parenthesis pertain to relative energies (kcal/mol) when H is substituted by $t\text{Bu}$.

No	Arrangement of atoms in the skeleton			Relative energies for skeleton 14			
				<i>neutral</i>	<i>dianion</i> ^a	<i>neutral</i>	<i>dianion</i> ^a
	E1	E2	E3				
14j	BH	CR	P			77.33 (65.87)	91.82 (84.81)
14k	P	CR	C	78.64 (59.80)	77.28 (61.21)		
14l	P	C	CR	83.39 (69.95)	-		
14m	BH	P	CR			90.69 (77.87)	78.37 (66.27)
14n	C	P	CR	90.81 (78.67)	97.19 (-)		
14p	CR	BH	P			93.25 (76.34)	69.09 (-)
	Arrangement of atoms in the skeleton			Relative energies for neutral skeleton 18			
16j						68.55 (76.62)	54.41 (35.84)
16k						73.36 (61.94)	59.36 (43.08)
18b				41.87 (66.10)			
18c	B	CR ₂	P		42.25 (51.55)		
18d	B	PR	CR		75.50 (64.94)		

Table 2.7.3. Relative energies (kcal/mol) of 3-membered ring isomers of *neutral* and *dianionic* $BC_2P_2HR_2$ species with skeleton **17**, **19** and **20**; (R = H, *t*Bu). Numbers in parenthesis pertain to relative energies (kcal/mol) when H is substituted by *t*Bu.

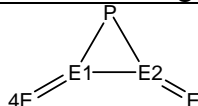
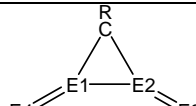
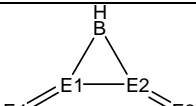
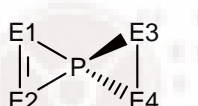
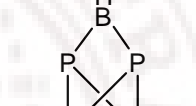
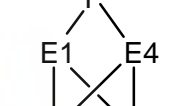
No	Arrangement of atoms in skeleton				Relative energies of skeleton. 17			
	E1	E2	E3	E4				
17d	C	P	P	BR		81.82 (88.66)		
17e	C	P	CR ₂	BH	87.47 (96.74)			
17f	B	P	P	CHR		91.55 (50.23)		
17c'	P	C	CR ₂	P			54.62 (57.63)	
17d'	P	B	PH	CR		81.27 (72.49)		
No	Arrangement of atoms in skeleton					Relative energies of dianionic skeleton. 19 and 20		
	E1	E2	E3	E4				
19a'	CR	CR	BH	P	P	116.69 (83.83)		
19b'	BH	CR	CR	P	P	103.04 (78.60)		
20c'	CR	BH	CR	P	P			67.55 (58.15)
20d'	P	BH	CR	P	CR			83.45 (63.57)
20e'	P	CR	CR	P	BH		94.43(73.32)	

Table 2.7.4. The bond distance ranges for typical bond lengths for heterocyclic structures according to CSD search and bond strength are given below

Bond Type	Covalent radii	Distance (Å)	Bond strength (kJ/mol)
C-C	1.54	1.54-1.59	346
C=C		1.34-1.42	602
C≡C		1.20- 1.24	835
P-P	2.15	2.15- 2.28	201
P=P		2.085-2.11	
B-C	1.60	1.62-1.72	356
B=C		1.58-1.60	
B-P	1.94	1.98-2.05	
B=P		1.90-1.94	
C-P	1.86	1.80-1.89	264
C=P		<1.80	

Table 2.7.5. The comparison of geometrical parameters of experimental **8** structure with **20a** (RBP₂C₂R' isomers (R= H or Ph, R'= H or *t*Bu) that are obtained at B3LYP/6-311++G (d,p) level of theory.

Geometrical parameters	Bond lengths in Å			
	Expt	BC ₂ P ₂ H ₃	HBC ₂ <i>t</i> Bu ₂ P ₂	PhBC ₂ <i>t</i> Bu ₂ P ₂
B-C(1)	1.546(2)	1.543	1.545	1.553
B- C(6)	1.568(3)	-	-	1.570
P(1)- C(1)	1.813(2)	1.870	1.883	1.890
P(1)- C(1)'	1.879(2)	1.871	1.883	1.890
P(1)- P(2)	2.106(2)	2.159	2.167	2.155
P(2)- C(1)	1.882(2)	1.954	1.972	1.964
P(2)- C(1)'	1.958(2)	1.954	1.972	1.964
C(1)- C(2)	1.510(2)	-	1.519	1.521
C(2)- C(5)	1.527(2)	-	1.546	1.541
C(2)-C(3)	1.528(3)	-	1.542	1.543
C(2)-C(4)	1.528(3)	-	1.540	1.546
C(6)-C(7)	1.389(2)	-	-	1.406
C(7)-C(8)	1.392(2)	-	-	1.394
C(8)-C(9)	1.370(2)	-	-	1.394

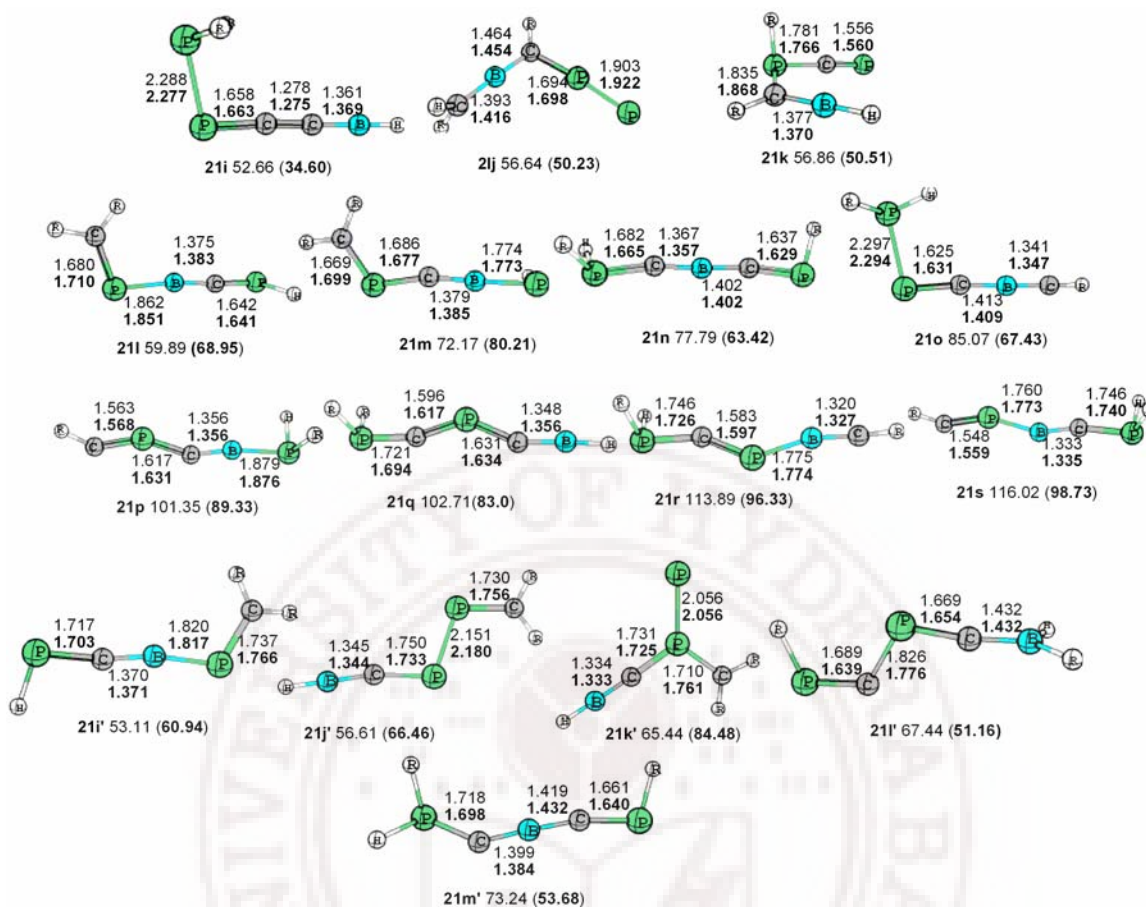


Figure 2.7.6. Relative energies (kcal/mol) and geometric parameters of acyclic (linear or branched) of *neutral* and *dianionic* $BC_2P_2HR_2$ species (**21**); (R = H, *t*Bu,) are in the normal (H-substituted) and **bold** font (*t*Bu-substitution of H on C) in parenthesis are given by B3LYP/6-311++G (d,p) level of theory.



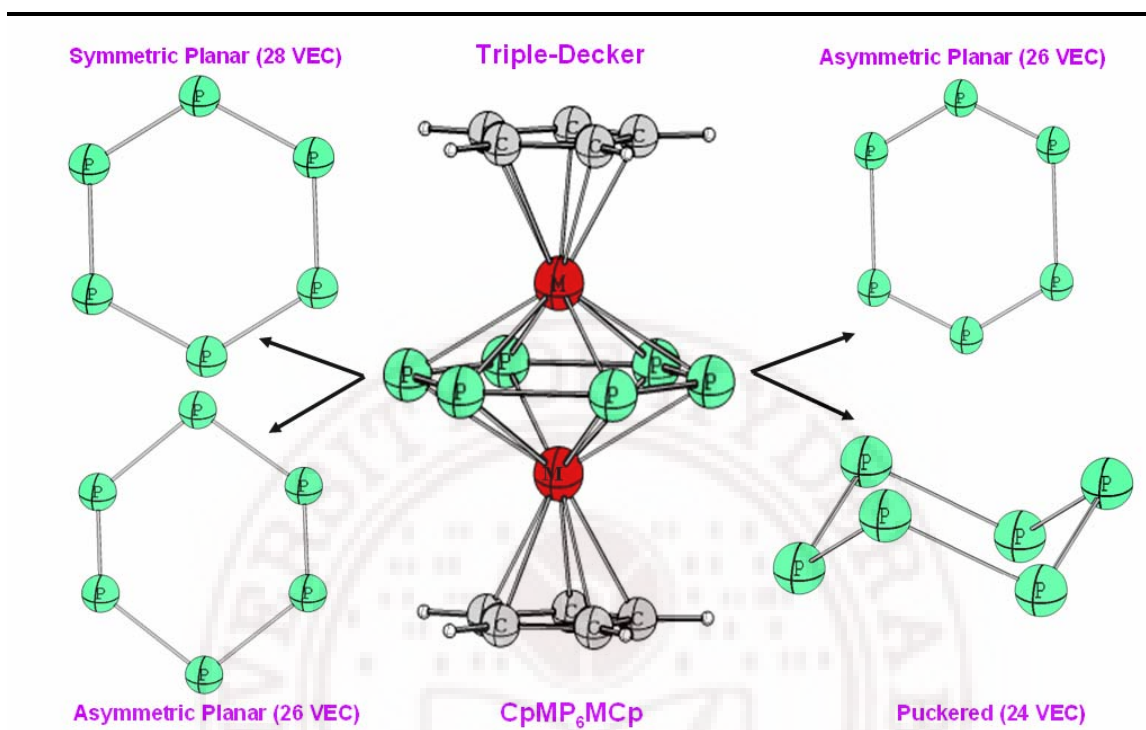
Chapter 3

Electronic Structure and Bonding Studies on Triple-Decker Sandwich Complexes with a P_6 as Middle Ring

Contents

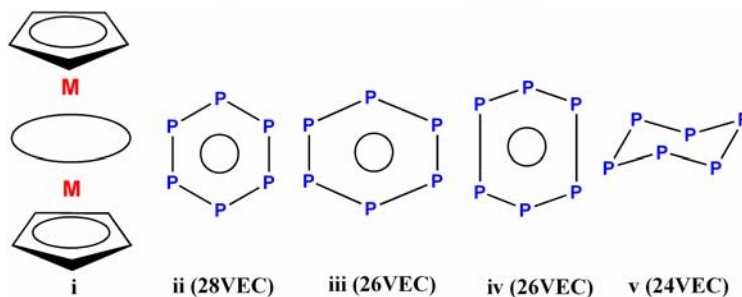
3.1	Abstract	103
3.2	Introduction	104
3.3	Details of Computational Methods	106
3.4	Results and Discussions	106
3.4.1	The <i>mno</i> Rule and the Valence Electron Count	106
3.4.2	28 Valence Electron Count Complexes	109
3.4.3	26 Valence Electron Count Complexes	115
3.4.4	24 Valence Electron Count Complexes	119
3.4.5	22 Valence Electron Count Complexes	121
3.4.6	20 and 18 Valence Electron Count Complexes	125
3.5	Conclusions	128
3.6	References	129

3.1 Abstract



3.2 Introduction

Cyclopentadienyl ligand has been a building block for various sandwich complexes. The discovery of ferrocene was a landmark in organometallic chemistry and further developments in metallocene chemistry have significantly influenced the subsequent development of the field. Syntheses of metallocenes having increasing number of rings and metals led to triple-, multiple-decker and one-dimensional sandwich complexes.¹ Triple-decker complex is a combination of two metals and three rings (**Scheme 3.1**). Werner and Slazer synthesized the first triple-decker sandwich complex $\text{Ni}(\text{Cp})_3^+$, which led to the synthesis of this class of compounds.² A variety of middle rings involving heteroatoms, such as boron, phosphorus and arsenic, have been synthesized.²⁻⁶ Further, extended one-dimensional metal-benzene complexes and sandwich molecular wires have shown characteristic electrical and magnetic properties. They are considered as promising materials in molecular electronics.⁷ In this chapter we concentrated on structural diversity that is present with P_6 as the middle ring in triple-decker sandwich (CpMP_6MCp) clusters. The ring exists as (a) symmetrical and planar for $\text{M}=\text{Mo}$, W , (b) distorted with four long and two short P-P bonds and yet planar for $\text{M}=\text{V}$, (c) distorted with two long and four short P-P bonds and yet planar for $\text{M}=\text{Nb}$, and (d) nonplanar chair like conformation for $\text{M}=\text{Ti}$ (**Scheme 3.1**).



Scheme 3.1. Geometry of the middle P_6 ring in triple-decker sandwich complexes having 28, 26, and 24 valence electron counts (VEC).

The electronic requirements of multiple decker sandwiches have traditionally been assessed using molecular orbital (MO) studies of several individual structures. Others and we had carried out detailed studies on triple-decker sandwiches to explain qualitatively the variety of structures having different number of electrons.⁸⁻¹¹ Often a qualitative MO picture leads to several possible distortions from the expected geometry. For example, a qualitative analysis suggests that both the complexes CpVP_6VCp and $\text{CpNbP}_6\text{NbCp}$ may have distorted P_6 rings,¹¹ however the preferred distortions cannot be predicted (**Scheme 3.1**). The triple-decker sandwich complexes offer a testing ground for computational approaches and we present here a DFT study of a family of triple-decker sandwiches CpMP_6MCp .

In the recent years the *mno* Rule¹² was formulated by us to predict the number of electrons that would make a condensed polyhedral structure stable. Although this was devised primarily for applications in condensed polyhedral boranes,¹³ it is also applicable to metallocenes and multiple-decker sandwiches.¹⁴ Here this rule will be applied to triple-decker sandwiches containing P_6 middle rings (**Scheme 3.1**). Since the electron counting rule is based on the structural skeleton alone, any extra electrons present on the metal atoms and the ligands beyond those stipulated will dictate the finer details of the structure. We therefore have also studied the nature of the interactions exhibited by these extra electrons and how they affect the overall structure.

As seen in chapter 1, there has been extensive data accumulated to support a close analogy between unsaturated systems containing phosphorus and carbon.¹⁵ It is therefore of considerable interest to see how far these two elements can be interchanged in the 6-membered middle ring of triple-decker complexes without affecting the structural details.

We have therefore compared triple-decker complexes having P_6 as the middle rings to those containing both C_3P_3 and B_3P_3 middle rings. A Sc complex having C_3P_3 middle ring is the only well characterized complex of a 22 VE triple-decker complex.^{6e}

3.3 Details of Computational Methods

Structures of all $CpMP_6MCp$, ranging from 18-28 valence electrons (VE) with $M = Sc, Y, Ti, Zr, Hf, V, Nb, Ta, Cr, Mo$ and W and $C_2P_3H_2ScC_3P_3H_3ScC_2P_3H_2$ triple-decker sandwich complexes were optimized at the hybrid Hartree-Fock/DFT (B3LYP) level with Gaussian 03¹⁶ program and at the Generalized Gradient approximation GGA (Becke- Perdew functional)^{17,18} method with ADF¹⁹ (Amsterdam Density Functional) program. The Basis sets, LANL2DZ,²⁰ TZV,^{21a} TZVP^{21b} were used with the B3LYP method, which uses a combination of the three-parameter Becke exchange functional²² along with the Lee-Yang-Parr non local correlation functionals.²³ A double zeta (DZ) basis set and a triple zeta plus polarization (TZP) basis set was used with frozen core for Sc, Ti, V and Cr up to 2p, for Y, Zr, Nb, Mo up to 3d, for Hf, Ta, W up to 4d, for C and O 1s, and for P up to 2p with the ADF program.¹⁹ The nature of the stationary points was determined by evaluating the second derivatives of the energy (Hessian matrix). The total and Zero Point energies and geometric parameters of the all optimized structures are given in the **Table 3.2-3.6**. The 18 and 20 VE triple-decker complexes were modeled by $CpScB_3P_3H_3ScCp^{+1}$, $CpScB_3C_3H_6ScCp^{+1}$ and their anions.

3.4 Results and Discussions

3.4.1 The *mno* Rule and the Valence Electron Count

There are six experimentally well-characterized triple-decker (TD) sandwich complexes containing P_6 as the middle ring, **Table 3.1**. The geometry of the P_6 ring

differs considerably from each other in these complexes. The four major geometrical distortions exhibited by the P_6 unit are indicated in **Scheme 3.1 (ii-v)**. According to the *mno* Rule the number of electron pairs required for stable condensed polyhedral structure is $m + n + o$, where m is the number of polyhedra, n is the number of vertices and o is the number of single atom bridges. This total has to be augmented by the extra electron pairs associated with nido systems as stipulated by the Wades Rules.²⁴ Accordingly 25 skeletal electron pairs ($m=3$, $n=18$, $o=2$ plus two for the two nido arrangements) are needed for the triple-decker sandwiches to be stable.

Table 3.1. Triple-decker sandwich complexes with P_6 middle ring characterized by X-ray crystallography, along with their spin multiplicity ($2S+1$), valence electron count (VEC), *mno* electron count (SEC) and available skeletal electrons.

Complex	Middle P_6 ring	$2S+1$	VEC	<i>mno</i> count (SEC)	Available electrons	Ref
$[(Cp^*Mo)_2(\mu-\eta^6:\eta^6-P_6)]$	ii	1	28	$m+n+o+p$ (3+18+2+2) 25 electron pairs =50	10CH+6P+2Mo =30+18+12 = 60	6a
$[(Cp^*W)_2(\mu-\eta^6:\eta^6-P_6)]$	ii	1	28	50	60	6b
$[(Cp^*V)_2(\mu-\eta^6:\eta^6-P_6)]$	iii	1	26	50	58	6b
$[(Cp^*Nb)_2(\mu-\eta^6:\eta^6-P_6)]$	iv	1	26	50	58	6c
$[(Cp''Nb)_2(\mu-\eta^6:\eta^6-P_6)]$	iv	1	26	50	58	11
$[(Cp^*Ti)_2(\mu-\eta^6:\eta^6-P_6)]$	v	1	24	50	56	6d
$[(C_2P_3Sc)_2(\mu-\eta^6:\eta^6-P_3C_3')]$	ii	5	22	50	54	6e

$Cp^* = \eta^5 - C_5Me_5$; $Cp' = \eta^5 - C_5Me_4Et$; $Cp'' = 1,3,5 - tBu_2C_5H_3$ $C_2' = C_2(tBu)_2$ and $C_3' = C_3(tBu)_3$.

Let us consider the number of electron pairs available for skeletal bonding in $CpMoP_6MoCp$: (a) 30 valence electrons from 10CH of the two Cp rings, (b) 18 electrons from the P_6 ring and (c) two electrons from the two Mo atoms. This is in accord with the anticipated oxidation state of +1 for the metal in view of the traditional formulation of -1

for the Cp ligand. This analysis leaves out ten valence electrons (5 electrons on each metal of the complex). The traditional valence electron count (VEC) for $\text{CpMoP}_6\text{MoCp}$ leads to 28 (10 π electrons from 2 Cp, 6 π electrons from P_6 and 12 electrons from two Mo atoms). The difference between the *mno* electron count and the VEC (50 vs 28) comes from two different sources. The *mno* electron count corresponding to the skeletal electron pairs includes both σ and π electrons. The number of σ electrons corresponds to 32 (20 from ten C-C bonds of the two Cps, 12 from 6 P-P bonds). If this is added to VEC the total of electrons becomes 60, ten more than the skeletal electron pair count obtained using the *mno* Rule. The further difference arises from the fact that during the skeletal electron pair count only one electron each from the metals was considered. The remaining 5 electrons each on the metals would bring the electron count to 60. The distinct advantage of the *mno* Rule is that it anticipates triple-decker sandwiches with less number of electrons by as much as ten in comparison to $\text{CpMoP}_6\text{MoCp}$. As **Table 3.1** indicates, VEC ranging from 28 to 24 are known among triple-decker sandwiches with P_6 middle ring.⁶ A 22-electron complex is also available with planar $\text{C}_3\text{P}_3\text{R}_3$ as middle ring. We show here that 18 and 20 VE complexes may also be possible. It should be noted that even though we discuss structures with VE counts up to 28, VE counts as high as 34 have been noticed among triple-decker sandwiches.⁷

The role of additional electrons beyond that stipulated by the *mno* Rule in controlling the structure is manifested in the four major geometric variations seen in these complexes, **Scheme 3.1**. Mo and W compounds with 28 VEC have symmetric planar P_6 ring (**Scheme 3.1, ii**).^{6a,b} The 26 VE complexes of V^{6b} and $\text{Nb}^{6c,11}$ retain the planarity of the ring, but with two minor and distinct in-plane distortions represented by **iii** and **iv** in

Scheme 3.1. These are reminiscent of the distortions possible for the two singlets for planar $C_6H_6^{+2}$ where one or the other π MO of the degenerate pair of an ideal D_{6h} structure is occupied. However, unlike in $C_6H_6^{+2}$, the distortions in V and Nb complexes are small. The Ti TD sandwich complex with 24 VEC has a puckered P_6 ring (**Scheme 3.1, v**).^{6d} Lastly, Sc in the 22 VEC ($C_2P_3H_2ScC_3P_3H_3ScC_2P_3H_2$) complex is in the +1 oxidation state and has in principle two additional valence electrons on each metal.^{6e} The structure retains planar C_3P_3 middle ring. We study each of these complexes using electronic structure theory. The success in reproducing experimental structures encourages to project structures having less than 22 VEC that may be attempted synthetically.

Results of studies on the 28 VEC structures are discussed first. This is followed by the 26, 24 and 22 VEC structures. Hypothetical structures involving 18 and 20 VEC are discussed at the end. A comparison of the structural parameters as a function of the number of electrons is made to see the subtle ways in which the P_6 ligand changes its shape as the number of electrons exceeds that stipulated by the *mno* counts in increments of two.

3.4.2 28 Valence Electron Count Complexes

There are two X-ray structures corresponding to the Mo and W complexes $Cp^*MP_6MCp^*$.^{6a,b} The standard P-P and M-P distances bring the two metals close to each other so that there is a strong direct Mo-Mo interaction. While these are anticipated even at relatively long distances for dz^2-dz^2 type of sigma interactions, there are substantial interactions between the δ type orbitals at these short distances. Thus the near degenerate HOMO in the 28 VE complex is an antibonding combination of M-M δ bonding orbitals

and P-P σ bonding orbitals ($2a^*$, $2b^*$, **Figure 3.1**). The corresponding bonding combinations ($2a$, $2b$) are much lower in energy. This does not lead to a distortion of the P_6 ring in the plane as both the near degenerate MOs are filled at the 28 VEC.

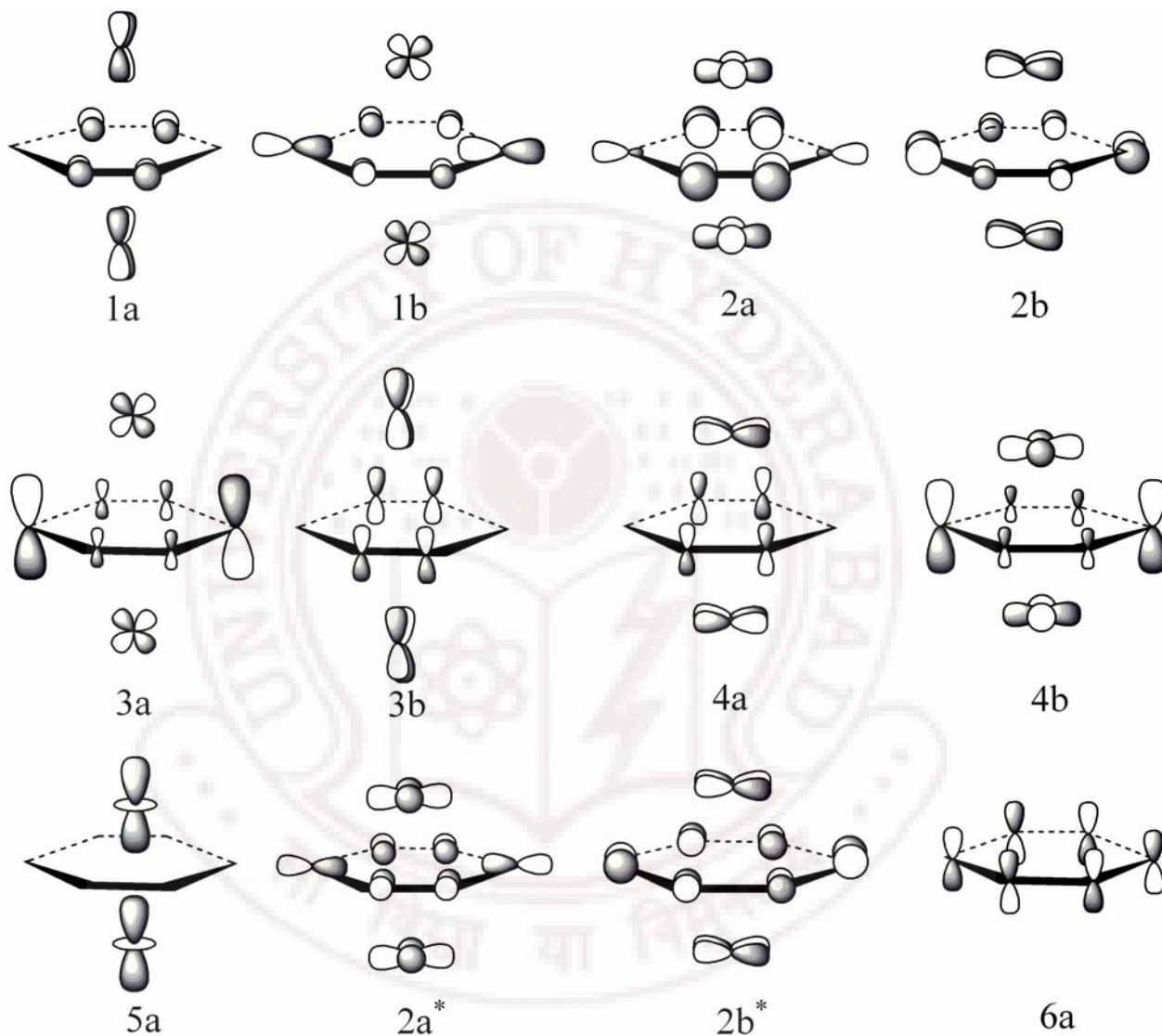


Figure 3.1. The dominant MOs responsible for ligand metal interactions in the TD sandwich complexes. The C_2 symmetry labels from $CpMoP_6MoCp$ complex is followed through out this chapter.

The M-M δ^* orbitals provide another strong interaction with the degenerate π^* level of P_6 (4a, 4b, **Figure 3.1**). The bonding combination is highly stabilized and can be considered as the equivalent of acceptance of four electrons by P_6 . The corresponding antibonding orbitals are very high in energy and are vacant. The degenerate π and π^* combination of metal orbitals interact strongly with the in-plane P_6 σ orbitals and the degenerate π levels of P_6 respectively. The bonding combinations are highly stabilized (1a, 1b, 3a, 3b, **Figure 3.1**), while the antibonding combinations are not in the bonding range. The occupancy of the near degenerate pair of orbitals in full, be it P-P σ or π , do not lead to any distortion of the P_6 ring. Structures with planar P_6 ring are shown to be minima at all levels. The bond lengths are overestimated at all levels employed; results at GGA/TZP are the closest to experiment (**Table 3.2**). Detailed influences such as these have to be taken into account in applying the *mno* electron count, indicating once again that electron counting rules only provide approximate yes or no answers. The binuclear tungsten complex also retains the same occupancy and similar structure. The bond lengths vary considerably with the method used. Best results are obtained using the GGA method and TZP basis set. (The structural parameters are comparable to that found experimentally). There is no experimental structure corresponding to $CpCrP_6CrCp$, however our study shows this complex to be a minimum. The major structural difference is the shorter M-M distance of 2.44 Å, expected for the first row transition metal element. This also brings the M-M σ bonding MO down in energy. The orbital occupancy is similar to those in the Mo and W analogs. The details of the occupied MOs of the 28 VEC system helps us to understand the distortions observed in the 26 VEC complexes (**Figure 3.2**). The calculated structural details of all 28 VEC complexes studied are given in the (**Figure 3.3A, Table 3.2**)

Table 3.2. Total energies in a.u, number of imaginary frequencies, spin multiplicity (2S+1), structure of the middle ring, and geometrical parameters of 28 VE triple-decker sandwich (CpMP₆MCp) complexes done at various levels are tabulated.

28 VEC	Method	Basis set	T.energy	Nimag	2S+1	Middle ring	M-M	P1-P2	P2-P3	P3-P4	P4-P5	P5-P6	P6-P1
(CpCr) ₂ P ₆	B3LYP	LANL2DZ	-598.22606	0	1	P ₆ (ii)	2.445	2.285	2.293	2.296	2.293	2.285	2.282
	GGA	DZ	-21.99172	2	1	P ₆ (ii)	2.460	2.287	2.293	2.296	2.293	2.287	2.284
		TZP	-6.35805	0	1	P ₆ (ii)	2.515	2.177	2.181	2.179	2.174	2.170	2.172
(CpMo) ₂ P ₆	Expt	–	–	–	1	P ₆ (ii)	2.647	2.167	2.167	2.167	2.167	2.167	2.167
	B3LYP	LANL2DZ	-561.19576	0	1	P ₆ (ii)	2.647	2.336	2.343	2.345	2.343	2.336	2.334
	GGA	DZ	-2.46352	0	1	P ₆ (ii)	2.653	2.346	2.349	2.351	2.349	2.346	2.344
		TZP	-6.45469	0	1	P ₆ (ii)	2.693	2.223	2.227	2.229	2.227	2.223	2.221
(CpW) ₂ P ₆	Expt	–	–	–	1	P ₆ (ii)	2.639	2.174	2.177	2.169	2.174	2.177	2.169
	B3LYP	LANL2DZ	-561.76325	0	1	P ₆ (ii)	2.630	2.342	2.349	2.351	2.349	2.342	2.340
	GGA	DZ	-6.22092	0	1	P ₆ (ii)	2.669	2.364	2.366	2.365	2.359	2.353	2.356
		TZP	-6.52478	1	1	P ₆ (ii)	2.744	2.235	2.238	2.236	2.232	2.233	2.232

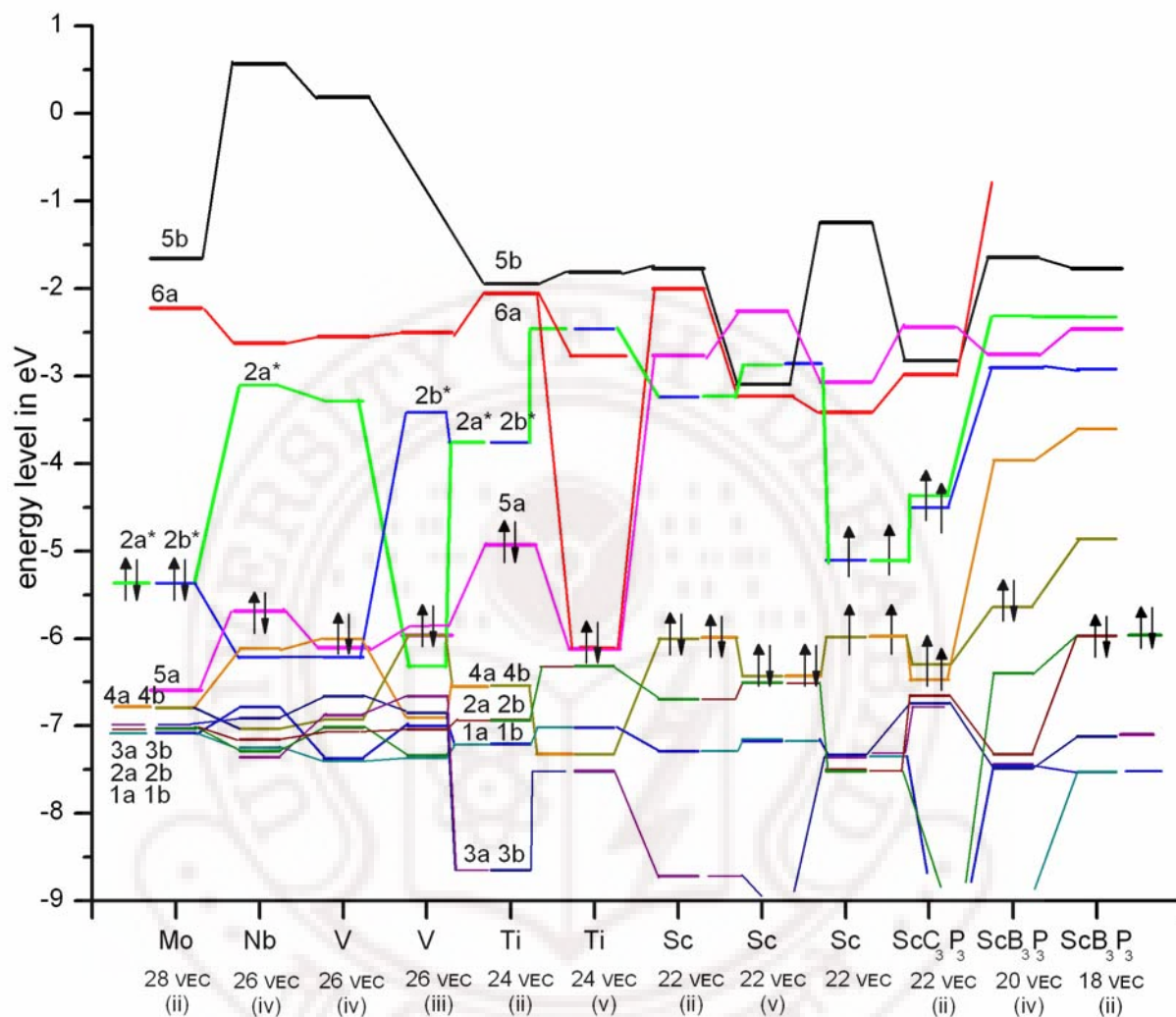


Figure 3.2. Correlation diagram of the energy levels of optimized CpMP₆MCp triple-decker sandwich complex ranging from 28 to 18 VEC, C₂P₃H₂ScC₃P₃H₃ScC₂P₃H₂ (22 VEC), and CpScB₃P₃H₃ScCp of 20 and 18 VEC at B3LYP/LANL2DZ level. The middle ring structures are labeled in the bracket using the notation of Scheme 3.1. As the anion (20 VE) and cation (18 VE) structures have very different relative energy levels in comparison to the neutral complexes, energy levels from the corresponding neutral structures are used in the diagram.

3.4.3 26 Valence Electron Count Complexes

There are two binuclear Nb structures known having a middle P_6 ring (**Table 3.1**). The terminal ligands are tetramethyl ethylcyclopentadienyl^{6c} and 2,3-di-*t*Bu-cyclopentadienyl.¹¹ In both the structures the P_6 ring is distorted, but planar. There are four relatively short P-P bonds and two long P-P bonds (**Scheme 3.1, iv**). These are averaged as 2.157 Å and 2.242 Å (C_5Me_4Et) and 2.111 Å and 2.347 Å (C_5H_3 (1,3-di-*t*Bu)). There is also a vanadium structure having the same VEC of 26, but with a different distortion for the P_6 ring. Here there are 4 long P-P bonds and two short P-P bonds.^{6b} Though the difference between them is small (0.054 Å), it is significant in comparison to the standard deviation reported experimentally.

The structure of the model complex for Nb, $CpNbP_6NbCp$, was optimized at three levels. The two-long, four-short pattern of P_6 ring is reproduced at all levels. This structural distortion can be understood from the correlation diagram involving 28 and 26 VEC structures, (**Figure 3.2**). The two highest occupied MOs of the 28 VEC compound corresponds to the antibonding combination of the M-M δ MOs and the σ MOs of P_6 ($2a^*$ and $2b^*$, **Figure 3.1**). The occupation of these two near degenerate levels keeps the P_6 ring symmetric. Removal of two electrons leads to a distortion so that the degeneracies are lifted and the observed diamagnetic structures are obtained. In the Nb complex the MO that is vacated is $2a^*$. The MO $2b^*$ has 4 P-P bonding and 2 P-P antibonding interactions, leading to the four-short and two-long P-P distances. This is the only structure corresponding to a minimum that is obtained at B3LYP/LANL2DZ and having a stationary point at all other levels studied (**Table 3.3**). Attempts were made to calculate the structure by populating the $2a^*$ in place of $2b^*$. Despite starting with a middle P_6 ring

with distortions anticipated from such an occupancy, a structure with four-short and two-long P-P bonds was obtained. The distortion is, in some ways, similar to the Jahn-Teller distortion anticipated in benzene dication or benzene dianion. For example $C_6H_6^{+2}$ has two planar structures with four-long and two-short and four-short and two-long C-C distances depending on which of the two π MOs are filled (**Figure 3.4**). Here the distances are 1.477 Å and 1.335 Å in the first case and 1.375 Å and 1.533 Å in the other. In comparison, the differences in the long and short P-P distances are often less, probably because the differences arise from σ MOs that are delocalized to the two metals, so that the influence of the MO on the structure of any part of the molecule is much less.

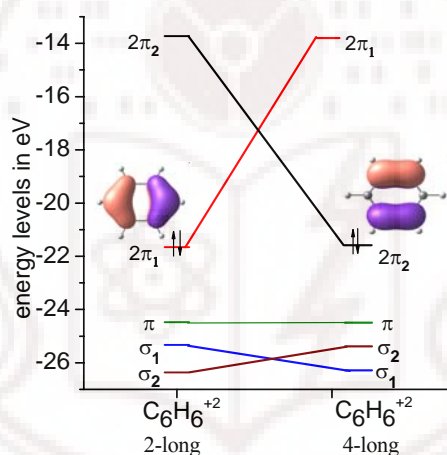


Figure 3.4. Correlation diagram connecting the MOs of the two distorted $C_6H_6^{+2}$ structures optimized at HF/6-31+G*.

Optimization of the structure of the vanadium complex $CpVP_6VCp$ at B3LYP/LANL2DZ gave a minimum energy structure corresponding to two-long and four-short P-P bonds. This is contrary to the experimental structure where two-short and four-long P-P bonds are observed.^{6b} A starting structure having distortions similar to what is found in the experimental structure led to a stationary point with two imaginary vibrational frequencies.

Table 3.3. Total energies in a.u, number of imaginary frequencies, spin multiplicity (2S+1), structure of the middle ring, and geometrical parameters of 26 VE triple-decker sandwich complexes done at various levels are tabulated.

²⁶ VEC	Method	Basis set	T.Energy	Nimag	2S+1	Middle ring	M-M	P1-P2	P2-P3	P3-P4	P4-P5	P5-P6	P6-P1
(CpV) ₂ P ₆	Expt	–	–	–	1	P ₆ (iii)	2.628	2.159	2.150	2.108	2.162	2.131	2.086
	B3LYP	LANL2DZ	-568.73356	2	1	P ₆ (iii)	2.564	2.201	2.395	2.383	2.205	2.395	2.392
		LANL2DZ	-568.73888	0	1	P ₆ (iv)	2.552	2.488	2.257	2.258	2.488	2.256	2.257
	uB3LYP	LANL2DZ	-568.73267	2	3	P ₆ (iii)	2.737	2.219	2.387	2.394	2.222	2.400	2.392
		LANL2DZ	-568.75229	2	5	P ₆ (ii)	3.304	2.332	2.318	2.316	2.336	2.316	2.318
	B3LYP	TZV	-4323.3561	1	1	P ₆ (iii)	2.593	2.185	2.364	2.363	2.189	2.363	2.364
		TZV	-4323.3597	0	1	P ₆ (iv)	2.573	2.234	2.454	2.235	2.235	2.457	2.234
		TZVP	-4323.6551	1	1	P ₆ (iii)	2.619	2.091	2.253	2.253	2.094	2.253	2.253
		TZVP	-4323.6578	0	1	P ₆ (iv)	2.602	2.137	2.338	2.133	2.139	2.339	2.132
	GGA	DZ	-6.01175	1	1	P ₆ (iv)	2.566	2.263	2.465	2.250	2.263	2.474	2.249
		TZP	-6.32171	1	1	P ₆ (iii)	2.621	2.089	2.254	2.254	2.092	2.254	2.254
		TZP	-6.32386	0	1	P ₆ (iv)	2.613	2.136	2.350	2.125	2.137	2.361	2.124
		TZP	-6.31005	3	3	P ₆ (iii)	2.701	2.203	2.203	2.158	2.201	2.202	2.162
		TZP	-6.28171		5	P ₆ (ii)	3.108	2.173	2.172	2.173	2.175	2.173	2.172
(CpNb) ₂ P	Expt(Cp')	–	–	–	1	P ₆ (iv)	2.791	2.240	2.181	2.149	2.243	2.156	2.140
	Expt(Cp'')	–	–	–	1	P ₆ (iv)	2.828	2.347	2.116	2.104	2.347	2.116	2.104
	B3LYP	LANL2DZ	-538.79735	0	1	P ₆ (iv)	2.781	2.270	2.269	2.611	2.269	2.271	2.598
	GGA	DZ	-6.13162	2	1	P ₆ (iv)	2.788	2.260	2.289	2.577	2.262	2.288	2.570
		TZP	-6.43875	1	1	P ₆ (iv)	2.821	2.141	2.151	2.485	2.141	2.151	2.483
		TZP	-6.31005	3	3	P ₆ (iii)	2.701	2.203	2.203	2.158	2.202	2.202	2.162
(CpTa) ₂ P	B3LYP	LANL2DZ	-541.81484	0	1	P ₆ (iv)	2.966	2.365	2.367	3.418	2.355	2.543	2.441
		DZ	-6.14941	1	1	P ₆ (iv)	2.811	2.304	2.266	2.589	2.304	2.264	2.582
	GGA	TZP	-6.44851	1	1	P ₆ (iv)	2.856	2.154	2.153	2.485	2.156	2.153	2.474

This structure with four-long and two-short bond is only 2.35 kcal/mol higher in energy than the structure with the two-long and four-short P_6 ring. The factors that influence the P-P distances are many. It is not possible to explain the variation easily. For example, as noted above, the differences between the long and the short P-P distances in the two Nb complexes available are 0.085 Å with ethyl, tetramethylcyclopentadienyl and 0.236 Å with 1,3-di-*t*Bu-cyclopentadienyl complex. Our attempts to follow the imaginary frequencies of the vanadium TD complex having four-long and two-short P-P bonds led to a structure having four-short and two-long bonds.

Further attempts were made to obtain a vanadium structure with four-long and two-short P-P bonds in many ways. Starting geometries with four-long and two-short P-P bonds as in the experimental structure led to minimum in energy with four-short and two-long P-P bonds at B3LYP/LANL2DZ, B3LYP/TZVP and GGA/TZP levels. A starting geometry with four-long P-P bonds which are distinctly longer (2.27 Å) at B3LYP/TZV, B3LYP/TZVP and GGA/TZP levels led to stationary points with one or two imaginary frequencies. The difference in energy between the two types of distorted structures is in the range of 1.35 - 2.35 kcal/mol. Optimization of the vanadium structure, starting with the exact X-ray coordinates with all substituents as in the experimental structure did not retain the four-long two-short P_6 ring. At all levels, a structure with four-short two-long P_6 ring is obtained. Obviously the methods used are not reliable enough to reproduce such small differences found in X-ray structures when the differences in energy are small. It should also be noted that the difference between the short and the long P-P bonds in the V complex is only 0.054 Å. The correlation diagram using the calculated MO energy

levels indicate that the occupancy of the levels are similar for the Nb and the V complexes when the distortions are similar (**Figure 3.2**).

Isoelectronic $\text{CpTaP}_6\text{TaCp}$ complex is not known experimentally so far. Optimization of geometry at the B3LYP/LANL2DZ level led to a structure with non-planar distorted P_6 ring (**Figure 3.3B**). On the other hand, optimization at GGA/DZ or GGA/TZP level led to a structure having P_6 ring with two-long and four-short P-P bonds (**Scheme 3.1, iv**). An electronic structure description similar to that of the 26 VEC Nb complex is applicable here.

3.4.4 24 Valence Electron Count Complexes

The metals Ti, Zr and Hf are candidates for 24 VEC complexes with the general formula CpMP_6MCp . An X-ray structure for $\text{Cp}^*\text{TiP}_6\text{TiCp}^*$ is available where the P_6 ligand has a puckered arrangement (**Scheme 3.1, v**).^{6d} Theoretical studies at all levels considered here reproduce the puckered structure (**Figure 3.3C**), even though the bond lengths are systematically overestimated (**Table 3.4**). The best way to understand the structure of these complexes is by relating them to the 28 VEC Mo complex. On removal of four electrons from the strongly antibonding (between M-M δ bond and the P-P σ bonds) near degenerate HOMOs ($2a^*$, $2b^*$, **Figure 3.2**), which kept the P_6 ring in-plane, other options become important. For example the M-M sigma bonding MO which has practically no interaction with the P_6 ring MOs ($5a$, **Figure 3.1**) can gain this interaction by distorting the rings and stretching the M-M bond. The stability of the +4 oxidation state of Ti also helps this process. A distortion of P_6 to a cyclohexane like chair conformation leads to the ligand which can be described as P_6^{-6} , so that there are 6 lone pairs in the equatorial directions and six electron pairs along the axial directions, (**Scheme 3.1, v**).²⁵

Table 3.4. Total energies in a.u, number of imaginary frequencies, spin multiplicity (2S+1), structure of the middle ring, and geometrical parameters of 24VE triple-decker sandwich complexes done at various levels are tabulated.

24 VEC	Method	Basis set	T.Energy	Nimag	2S+1	Middle ring	M-M	P1-P2	P2-P3	P3-P4	P4-P5	P5-P6	P6-P1
(CpTi) ₂ P ₆	Expt	–	–	–	1	P ₆ (v)	3.187	2.228	2.240	2.250	2.228	2.240	2.250
	B3LYP	LANL2DZ	-542.35405	0	1	P ₆ (v)	3.250	2.463	2.461	2.461	2.461	2.461	2.461
	GGA	DZ	-5.98643	0	1	P ₆ (v)	3.173	2.452	2.452	2.451	2.451	2.451	2.452
		TZP	-6.26087	0	1	P ₆ (v)	3.209	2.311	2.304	2.303	2.307	2.303	2.307
(CpZr) ₂ P ₆	B3LYP	LANL2DZ	-519.38473	0	1	P ₆ (v)	3.485	2.508	2.508	2.509	2.506	2.509	2.508
	GGA	DZ	-6.03469	0	1	P ₆ (v)	3.418	2.492	2.492	2.492	2.492	2.492	2.492
		TZP	-6.31276	2	1	P ₆ (v)	3.489	2.337	2.335	2.338	2.341	2.336	2.335
(CpHf) ₂ P ₆	B3LYP	LANL2DZ	-524.04545	0	1	P ₆ (v)	3.501	2.503	2.503	2.504	2.501	2.504	2.503
	GGA	DZ	-6.06466	0	1	P ₆ (v)	3.406	2.490	2.494	2.486	2.490	2.499	2.492
		TZP	-6.33103	0	1	P ₆ (v)	3.440	2.337	2.331	2.330	2.339	2.331	2.333

This is isoelectronic to cyclohexane chair conformation except that each C-H bond is now a lone pair. Three electron pairs each will be directed to a Ti atom so that the structure is best described as two $\text{Cp}^{-1}\text{Ti}^{+4}\text{P}_3^{-3}$ complexes with minimal direct Ti-Ti interactions. The extra stabilization of this MO arises from mixing the totally antibonding $\text{P}_6 \pi$ MO (6a, **Figure 3.1**) which has no interaction with the metals in the 28 VE complex, (**Figure 3.2**). Calculations at all levels lead to this distorted structure. Similar structures are obtained with Zr and Hf complexes. These are realizable synthetic targets.

3.4.5 22 Valence Electron Count Complexes

Although the complexes $\text{CpScP}_6\text{ScCp}$ and CpYP_6YCp have not been synthesized, the corresponding, fully structurally characterized, complex $\text{P}_3\text{C}_2t\text{Bu}_2\text{ScP}_3\text{C}_3t\text{Bu}_3\text{ScP}_3\text{C}_2t\text{Bu}_2$ containing two peripheral η^5 -bonded 1,2,4-triphosphacyclopentadienyl rings and an η^6 -ligated 1,3,5-triphospha-benzene middle ring, has been made by co-condensation of Sc atoms and phospho-alkyne $t\text{BuCP}$.^{6e} The close parallel between the bonding behavior of unsaturated phospho-organic compounds and their better known organic counter parts has been well documented.^{15,26} Photoelectron spectroscopic measurements and DFT calculations on the 1,3,5-triphospha-benzene, $\text{P}_3\text{C}_3t\text{Bu}_3$, and its tricarbonyl complexes^{27,28} $\text{M}(\text{CO})_3(\eta^6\text{-P}_3\text{C}_3t\text{Bu}_3)$, ($\text{M} = \text{Cr}, \text{Mo}, \text{W}$), have established that the phospho-arene complexes show a higher first Ionization Energy (IE) than their carbocyclic analogs. Furthermore an electronic structure analysis indicates stronger bonding in the former as a result of greater metal-ligand back donation to the lower lying LUMOs of the phosphorous substituted ring. In view of these we studied the complexes with P_6 as well as $\text{C}_3\text{P}_3\text{H}_3$ as middle rings (**Figure 3.5A**).

The structure of the model complex, CpScP₆ScCp was optimized by keeping the P₆ unit in-plane at the B3LYP level using the basis sets LANL2DZ, TZV and TZVP. These turn out to be higher order stationary points having 5, 3 and 3 imaginary vibrational frequencies respectively (**Table 3.5**). A minimum in energy is obtained with a non planar P₆ structure, which resembles a chair conformation of cyclohexane. In general the extend of puckering is considerably less than that found for the Ti complexes having 24 VE. This is reflected in the smaller P-P-P-P dihedral angle of 13.0° in Sc complex in comparison to 27.3° in the Ti complex at the B3LYP/LANL2DZ level. The planar structures are higher in energy by magnitudes ranging from 2.08 to 8.70 kcal/mol. Two factors suggested us to consider an open shell arrangement with four unpaired electrons, one electron in each 4a, 4b, 2a* and 2b* MOs (**Figure 3.2**). The experimental structure P₃C₂tBu₂ScP₃C₃tBu₃ScP₃C₂tBu₂ has a magnetic moment of 3.98 μB at room temperature. Additionally the MO energy levels 4a, 4b and the 2a* and 2b* were not very far apart in a semiempirical calculation on this complex.¹¹ A structure with planar P₆ ring is obtained for CpScP₆ScCp at the UB3LYP/TZVP level. The P₆ ring, though planar, appears to be distorted in the direction of 3 P₂ units. There is no experimental support for such an observation except the fact that the 3 isolated P₂ units are lower in energy than P₆.²⁹ The Yttrium complex CpYP₆YCp presents a similar picture and is not discussed in detail.

The closest experimental structure with 22 VE is that of C₂P₃H₂ScC₃P₃H₃ScC₂P₃H₂. Here the structure is characterized well. The C₃P₃ unit is planar. The compound is found to be paramagnetic corresponding to four unpaired electrons at room temperature. Depending on the method and the spin multiplicity used, structures with planar and puckered C₃P₃ unit are obtained.

Table 3.5. Total energies in a.u, number of imaginary frequencies, spin multiplicity (2S+1), structure of the middle ring, and geometrical parameters of 22 VE triple-decker sandwich complexes done at various levels are tabulated.

22 VEC Molecule	Method	Basis set	T.energy	Nimag	2S+1	Middle ring	M-M	P1-P2	P2-P3	P3-P4	P4-P5	P5-P6	P6-P1
CpScP ₆ ScCp	B3LYP	LANL2DZ	-519.10339	5	1	P ₆ (ii)	3.509	2.340	2.338	2.338	2.338	2.340	2.341
		LANL2DZ	-519.1165	0	1	P ₆ (v)	3.591	2.387	2.368	2.367	2.380	2.390	2.396
		TZV	-3956.8811	3	1	P ₆ (ii)	3.453	2.293	2.294	2.294	2.294	2.293	2.293
		TZV	-3956.895	0	1	P ₆ (v)	3.544	2.332	2.332	2.333	2.332	2.332	2.333
		TZVP	-3957.1563	3	1	P ₆ (ii)	3.501	2.191	2.192	2.192	2.192	2.191	2.191
		TZVP	-3957.1596	0	1	P ₆ (v)	3.544	2.208	2.208	2.212	2.213	2.213	2.209
	uB3LYP	LANL2DZ	-519.0187	1	5	P ₆ (ii)	3.226	2.189	2.800	2.190	2.800	2.189	2.772
	B3LYP	TZV	-3956.785	2	5	P ₆ (ii)	3.219	2.175	2.701	2.177	2.701	2.175	2.679
	B3LYP	TZVP	-3957.043	0	5	P ₆ (ii)	3.218	2.060	2.674	2.063	2.674	2.060	2.651
	GGA	DZ	-5.83803	0	1	P ₆ (v)	3.416	2.361	2.365	2.371	2.365	2.361	2.363
		TZP	-6.13489	2	1	P ₆ (ii)	3.523	2.193	2.194	2.191	2.188	2.186	2.189
CpYP ₆ YCp	B3LYP	LANL2DZ	-502.09686	0	1	P ₆ (v)	3.870	2.499	2.496	2.497	2.504	2.507	2.503
	uB3LYP	LANL2DZ	-502.01744	2	5	Planar	3.505	2.182	2.971	2.183	2.971	2.182	2.958
	GGA	DZ	-5.85392	3	1	P ₆ (v)	3.820	2.376	2.377	2.377	2.377	2.376	2.377
(C ₂ P ₃ H ₃ Sc) ₂	Expt	–	–	–	5	C ₃ P ₃ H ₃ (ii)	3.573	1.803	1.806	1.800	1.805	1.794	1.802
C ₃ P ₃ H ₃	B3LYP	LANL2DZ	-422.40348	0	1	C ₃ P ₃ H ₃ (v)	3.564	1.889	1.891	1.893	1.892	1.895	1.892
		TZV	-4864.7199	0	1	C ₃ P ₃ H ₃ (v)	3.565	1.873	1.878	1.878	1.873	1.876	1.874
		TZVP	-4865.0316	0	1	C ₃ P ₃ H ₃ (ii)	3.550	1.818	1.821	1.820	1.815	1.819	1.817
	uB3LYP	LANL2DZ	-422.2874	1	5	C ₃ P ₃ H ₃ (ii)	4.160	1.843	1.844	1.844	1.842	1.840	1.833
	GGA	TZP	-5.19507	0	1	C ₃ P ₃ H ₃ (ii)	3.546	1.821	1.826	1.824	1.818	1.820	1.819
		TZP	-5.0825	4	5	C ₃ P ₃ H ₃ (ii)	4.152	1.796	1.793	1.792	1.795	1.796	1.793

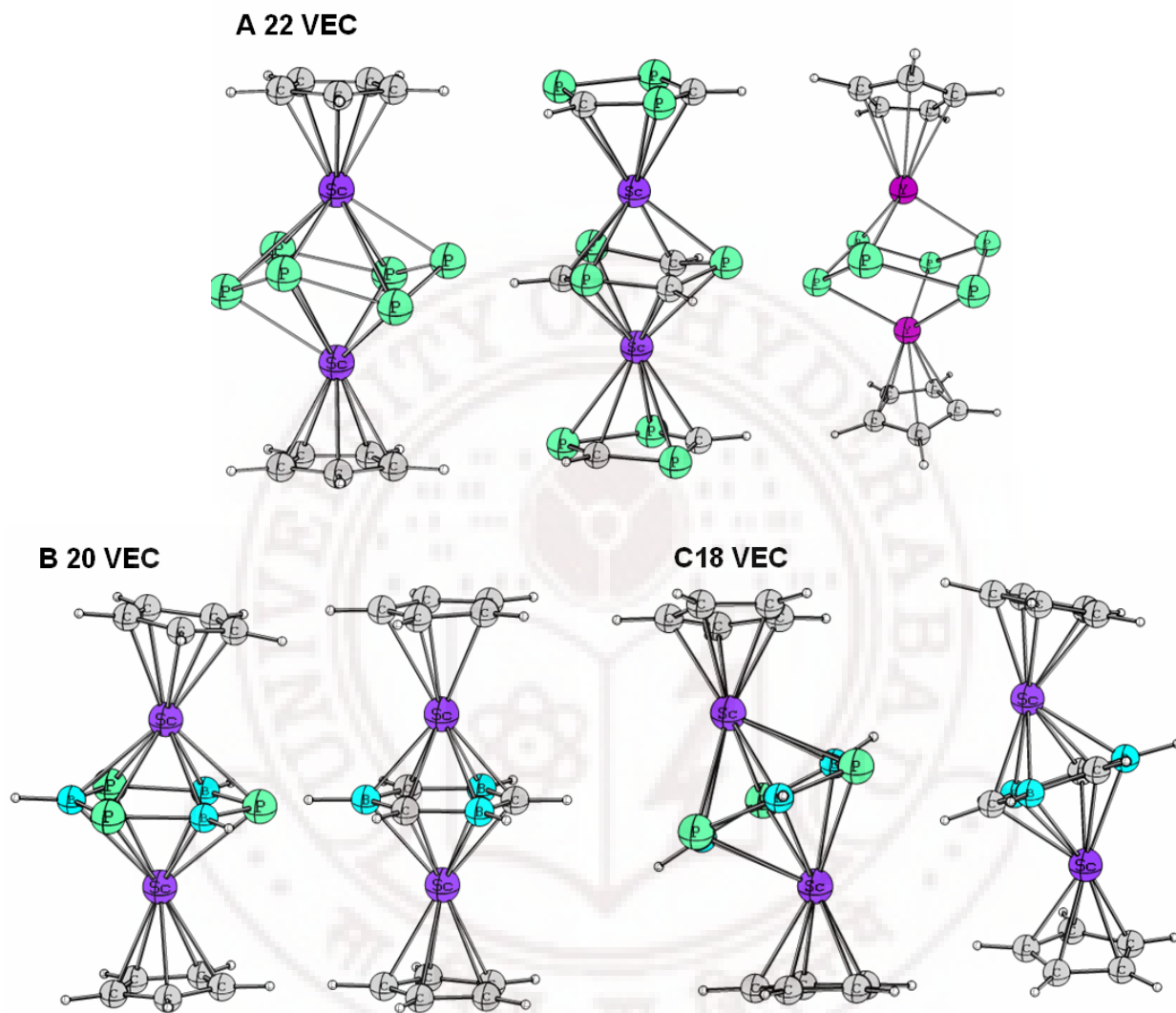


Figure 3.5. Optimized structures of CpMP6MCp complexes at B3LYP/LANL2DZ level of theory.

For example optimization at GGA/TZP and B3LYP/TZVP lead to planar C_3P_3 unit. Change of methods and basis set leads to dramatic differences. Structures with puckered C_3P_3 unit are minima at B3LYP/LANL2DZ and B3LYP/TZV levels (**Table 3.5**). A quintet structure obtained at UB3LYP/LANL2DZ has a planar C_3P_3 unit and one imaginary vibrational frequency, while the same spin multiplicity at GGA/TZP leads four imaginary frequencies with a flat C_3P_3 structure. In view of the many low lying levels accessible better methods that include electron correlation explicitly are required to describe the electronic structure of the complexes with the less number of valence electrons.

3.4.6 20 and 18 Valence Electron Count Complexes

No example of a triple-decker sandwich with 20 or 18 VE are known. In view of the bonding interactions involving d orbitals and the ligands we have decided to study 20 and 18 VE structures by replacing three P or C atoms of the C_3P_3 ring in $C_3P_3H_3(CpSc)_2$ by three BH groups and adding a positive or negative charge. Thus the model selected for 20 and 18 VE structures are anion and cation of $B_3P_3H_3(CpSc)_2$ and $C_3B_3H_6(CpSc)_2$. According to the *mno* Rule 50 skeletal electrons (18 VE) are required for stability and so it is interesting to see the resulting structures.

At the B3LYP/LANL2DZ level a minimum in energy was obtained for $CpScB_3P_3H_3ScCp^{-1}$ (**Figure 3.5B**). The structure has two-long and four-short B-P distances for the central ring. This is anticipated from the correlation diagram, **Figure 3.2**. Removal of two electrons from the 22 VE Sc complex leads to a near degenerate HOMO, corresponding to 4a and 4b. A distortion leads to the occupation of 4a, which is distinctly antibonding for two B-P bonds. These are similar to the distortions observed

Table 3.6. Total energies in a.u, number of imaginary frequencies, spin multiplicity (2S+1), structure of the middle ring, and geometrical parameters of 20 and 18 VE triple-decker sandwich complexes done at various levels are tabulated.

20 VEC Anion	Method	Basis set	T. Energy	Nimag	2S+1	Middle ring	M-M	P1-B1	B1-P2	P2-B2	B2-P3	P3-B3	B3-P1	CpMP ₃ B ₃ H ₃
(CpSc) ₂	B3LYP	LANL2DZ	-576.03237	0	1	B ₃ P ₃ H ₃ (iv)	3.634	1.95	1.959	2.057	1.933	1.945	2.056	175.6
B ₃ P ₃ H ₃		TZVP	-3009.44119	0	1	B ₃ P ₃ H ₃ (iv)	3.565	1.908	1.917	2.012	1.887	1.893	2.006	177.1
	GGA	TZP	-6.70462	0	1	B ₃ P ₃ H ₃ (iv)	3.575	1.929	1.953	1.934	1.936	1.953	1.926	179.7
(CpSc) ₂ C ₃ B ₃ H ₆	Method	Basis set	T.Energy	Nimag	1	Middle ring	M-M	B1-C2	C2-B2	B2-C3	C3-B3	B3-C1	C1-B1	CpMC ₃ B ₃ H ₆
	B3LYP	LANL2DZ	-672.61884	0	1	C ₃ B ₃ H ₆ (iv)	3.631	1.558	1.622	1.545	1.557	1.622	1.547	178.3
		TZVP	-2101.41862	0	1	C ₃ B ₃ H ₆ (iv)	3.661	1.548	1.612	1.534	1.548	1.612	1.536	178.5
	GGA	TZP	-7.50906	0	1	C ₃ B ₃ H ₆ (iv)	3.679	1.562	1.612	1.535	1.564	1.616	1.541	178.8
18 VEC Cation	Method	Basis set	T. Energy	Nimag	2S+1	Middle ring	M-M	P1-B1	B1-P2	P2-B2	B2-P3	P3-B3	B3-P1	CpMP ₃ B ₃ H ₃
(CpSc) ₂	B3LYP	LANL2DZ	-575.70557	0	1	B ₃ P ₃ H ₃ (ii)	4.008	1.968	1.953	1.961	1.965	1.958	1.956	152.4
B ₃ P ₃ H ₃		TZVP	-3009.1275	1	1	B ₃ P ₃ H ₃ (ii)	3.900	1.929	1.923	1.927	1.93	1.922	1.924	155
	GGA	TZP	-6.37561	0	1	B ₃ P ₃ H ₃ (ii)	3.886	1.935	1.935	1.935	1.935	1.935	1.935	179.5
(CpSc) ₂ C ₃ B ₃ H ₆	Method	Basis set	T.Energy	Nimag	1	Middle ring	M-M	B1-C2	C2-B2	B2-C3	C3-B3	B3-C1	C1-B1	CpMC ₃ B ₃ H ₆
	B3LYP	LANL2DZ	-672.36091	0	1	C ₃ B ₃ H ₆ (ii)	3.855	1.558	1.554	1.554	1.559	1.554	1.555	149.1
		TZVP	-2101.17281	1	1	C ₃ B ₃ H ₆ (ii)	3.915	1.549	1.544	1.545	1.549	1.544	1.546	150.3
	GGA	TZP	-7.23462	4	1	C ₃ B ₃ H ₆ (ii)	3.906	1.558	1.558	1.557	1.556	1.558	1.558	176.4

for the 26 VEC Nb and V complexes. Once again it is the structure having two-long four-short B_3P_3 middle ring that is found to be a minimum in energy. There is an interesting difference between these examples. In the 26 VE complexes it is the σ MOs of the P_6 ligands that dictated the bond length variations. In the structure with 6 VE less, it is the π^* MOs of the middle ring that are decisive in directing the distortions.

According to this analysis an 18 VE structure should have a middle ring which is planar. The cation, $CpScB_3P_3H_3ScCp^{+1}$, is optimized at the B3LYP/LANL2DZ level and is found to be a minimum in energy with planar central B_3P_3 ring (**Figure 3.5C**). In addition to the variation in the structure of the central ring, there is substantial elongation of the Sc-Sc bond length from 3.63 Å in 20 VE anion to 4.00 Å in the 18 VE cation. This also arises from vacating the MO 4a (**Figure 3.2**) which in addition to being antibonding between a pair of B-P bonds, is also bonding between the central ring and the metals. The cyclopentadienyl group in the 18 VE complex $CpScP_3B_3H_3ScCp^{+1}$, is not symmetrical with respect to the Sc-Sc axis (**Figure 3.5C**). The Cp is bent by 152° from the Sc-Sc axis (**Table 3.6**). Similar distortion of the C_5H_5 ring is also observed in the metallocene Cp_2Sc (144°) and has been studied in detail.³⁰

We have studied the isoelectronic 20 and 18 VE systems, $CpScC_3B_3H_6ScCp^{-1}$ and $CpScC_3B_3H_6ScCp^{+1}$, even though the central C_3B_3 ligand is farther removed from P_6 which is the thrust of this study. The general structural details are similar to those obtained for structures with the B_3P_3 middle ring. The 20 VE structure has a planar distorted C_3B_3 ring with two-long and four-short C-B bonds. The 18 VE system has a symmetrical C_3B_3 ring. The Sc-Sc distance is considerably longer than that in the 20 VE complex. The Cp rings here are tilted away from the Sc-Sc axis in these examples as well

(Figure 3.5C). These are encouraging results in terms of synthetic targets for less than 22 VEC complexes, the lowest known so far.

3.5 Conclusions

The electronic structure studies of a series of triple-decker sandwiches with VEC ranging from 28 to 18 with P_6 middle ring explain several observations. The 28 VEC corresponds to ten additional electrons than the 50 electrons anticipated for this skeleton by the *mno* Rule. The occupancy of electrons established for the 28 VE well-characterized complexes of Mo and W helps in explaining the geometrical variations observed for structures with decreasing number of electrons. The hypothetical $CpCrP_6CrCp$ is calculated to be stable and has a structure very similar to the 28 VE complexes of Mo and W. Reduction of two electrons lead to a distortion of the structure so that the near degeneracy that existed in the HOMO of the 28 VE complex ($2a^*$, $2b^*$) is lifted. The occupancy of one or the other of these two MOs leads to distinct differences: occupancy of $2b^*$ leads to the distortion of the P_6 ring as observed in the two Nb complexes. Occupancy of the $2a^*$ leads the structure observed in the V complex. Optimization of the $CpVP_6VCp$ complex at the theoretical methods used here (B3LYP/LANL2DZ, TZV, TZVP, and GGA/DZ, TZP) do not lead to a minimum for the structure having the observed distortion for the P_6 ring. However, the energy differences involved are very small. The 24 VE Ti complex has a distorted P_6 middle ring, similar to that of a chair conformation of cyclohexane, stemming from the stabilization of the +4 oxidation state of Ti. This leads to the distorted P_6^{-6} structure where the six axial lone pairs are donated to the two metals. The 22 VE complex involving Sc leads to different structures depending on the method used and the spin state. Though there is no

experimental structure to make comparisons, a related complex where three P atoms of the middle P_6 ring is replaced by CH and three C-H groups of the Cps are replaced by P is experimentally characterized. This is known to have four unpaired electrons. The experimental structure, modeled by $C_2P_3H_2ScC_3P_3H_3ScC_2P_3H_2$, is calculated to be a minimum in quintet state. However other structures with no unpaired electrons are not very different in energy. Better levels of calculations than employed here is required to obtain quantitative results for these molecules with several low lying excited states.

The 18 and 20 VEC complexes are modeled by $CpScP_3B_3H_3ScCp^{+,-}$ and $CpScC_3B_3H_6ScCp^{+,-}$. The 20 VEC complexes have two-long and four-short P-B (C-B) bonds for the middle ring as only one of the 4a, 4b pair (**Scheme 3.1**) will be filled. On the other hand 18 VE complexes, that have the minimum number stipulated by the *mno* Rule has a symmetrical middle ring. Triple-decker complexes with 18 and 20 VE are attractive synthetic targets that would expand the range from 34 to 18, the minimum expected according to the *mno* Rule.

3.6 References

1. (a) Grimes, R. N. *Chem. Rev.*, **1992**, 92, 251-268, (b) Plepgrass, K. W.; Meng. X.; Hölscher, M.; Sabat, M.; Grimes, R. N. *Inorg. Chem.*, **1992**, 31, 5202-5210. (c) Siebert, W. *Angew. Chem. Int. Ed. Engl.*, **1985**, 24, 943-958.
2. (a) Werner, H.; Saker, A. *Synth. Inorg. Met.-Org. Chem.*, **1972**, 2, 239-248. (b) Saker, A.; Werner, H. *Angew. Chem.*, **1972**, 84, 949-950.
3. (a) Ghosh, S.; Beatty, A. M.; Fehlner, T. P. *J. Am. Chem. Soc.*, **2001**, 123, 9188-9189. (b) Scherer, O. J.; Weigel, S.; Wolmershäuser, G. *Chem. Eur. J.*, **1998**, 4, 1910-1916. (c) Scherer, O. J.; Brück, T.; Wolmershäuser, G. *Chem. Ber.*, **1989**, 122, 2049-2054.

- (d) Scherer, O. J.; Brück, T.; Wolmershäuser, G. *Chem. Ber.*, **1988**, *121*, 935-938. (e) Hughes, A. K.; Murphy, V. J.; O' Hare, D. *Chem. Commun.*, **1994**, 163-164. (f) Kudinov, A. R.; Rybinskaya, M. I. *Russ. Chem. Bull.*, **1999**, *48*, 1615-1621. (g) Kudinov, A. R.; Loginov, D. A.; Starikova, Z. A.; Petrovskii, P. V.; Corsini, M.; Zanello, P. *Eur. J. Inorg. Chem.*, **2002**, 3018-3027.
4. (a) Scherer, O. J.; Sitzmann, H.; Wolmershäuser, G. *Angew. Chem. Int. Ed. Engl.*, **1989**, *28*, 212-213. (b) Scherer, O. J.; Wiedemann, W.; Wolmershäuser, G. *J. Organomet. Chem.*, **1989**, *361*, C11-C14.
5. (a) Rheingold, A. L.; Foley, M. J.; Sullivan, P. J. *J. Am. Chem. Soc.*, **1982**, *104*, 4727-4729. (b) Breunig, H. J.; Burford, N.; Rösler, R. *Angew. Chem. Int. Ed. Engl.*, **2000**, *39*, 4148-4150.
6. (a) Scherer, O. J.; Sitzmann, H.; Wolmershäuser, G. *Angew. Chem. Int. Ed. Engl.*, **1985**, *24*, 351-353. (b) Scherer, O. J.; Schwalb, J.; Swarowsky, H.; Wolmershäuser, G.; Kaim, W.; Gross, R. *Chem. Ber.*, **1988**, *121*, 443-449. (c) Scherer, O. J.; Vondung, J.; Wolmershäuser, G. *Angew. Chem. Int. Ed. Engl.*, **1989**, *28*, 1355-1357. (d) Scherer, O. J.; Swarowsky, H.; Wolmershäuser, G.; Kaim, W.; Kohlmann, S. *Angew. Chem. Int. Ed. Engl.*, **1987**, *26*, 1153-1155. (e) Arnold, P. L.; Cloke, F. G. N.; Hitchcock, P. B.; Nixon, J. F. *J. Am. Chem. Soc.*, **1996**, *118*, 7630-7631.
7. (a) Nagao, S.; Kata, A.; Nakajima, A. *J. Am. Chem. Soc.*, **2000**, *122*, 4221-4222. (b) Miyajima, K.; Yabushita, S.; Knickelbein, M. B.; Nakajima, A.; Kaya, K.; *J. Am. Chem. Soc.*, **2004**, *126*, 13202-13203. (c) Wang, J.; Acioli, P. H.; Jellinek, J. *J. Am. Chem. Soc.*, **2005**, *127*, 2812-2813. (d) Xiang, H.; Yang, J.; Hou, J. G.; Zhu, Q. *J. Am. Chem. Soc.*, **2006**, *128*, 2310-2314. (e) Maslyuk, V. V.; Bagrets, A.; Meded, V.;

- Arnold, A.; Evers, F.; Brandbyge, M.; Bredow, T.; Mertig, I. *Phy. Rev. Lett.*, **2006**, 97, 097201-4. (f) Miyajima, K.; Yabushita, S.; Knickelbein, M. B.; Nakajima, A. *J. Am. Chem. Soc.*, **2007**, 129, 8473-8480. (g) Wang, J.; Zhang, X.; Schleyer, P. v. R.; Chen, Z.; *J. Chem. Phys.*, **2008**, 128, 104706-6. (h) Zhou, L.; Yang, S-W.; Ng, M-F.; Sullivan, M. B.; Tan, V. B. C.; Shen, L. *J. Am. Chem. Soc.*, **2008**, 130, 4023-4027.
8. (a) Lauher, J. W.; Elian, M.; Summerville, R. H.; Hoffmann, R. *J. Am. Chem. Soc.*, **1976**, 98, 3219-3224. (b) Tremel, W.; Hoffmann, R.; Kertesz, M. *J. Am. Chem. Soc.*, **1989**, 111, 2030-2039. (c) Wadepohl, H. *Angew. Chem. Int. Ed. Engl.*, **2002**, 41, 4220-4223.
9. Chesky, P. T.; Hall, M. B. *J. Am. Chem. Soc.*, **1984**, 106, 5186-5188.
10. (a) Jemmis, E. D.; Reddy, A. C. *Organometallics*, **1988**, 7, 1561-1564. (b) Jemmis, E. D.; Reddy, A. C. *J. Am. Chem. Soc.*, **1990**, 112, 722-727.
11. Reddy, A. C.; Jemmis, E. D.; Scherer, O. J.; Winter, R.; Heckmann, G.; Wolmershäuser, G. *Organometallics*, **1992**, 11, 3894-3900.
12. Jemmis, E. D.; Balakrishnarajan, M. M.; Pancharatna, P. D. *J. Am. Chem. Soc.*, **2001**, 123, 4313-4323.
13. Jemmis, E. D.; Balakrishnarajan, M. M.; Pancharatna, P. D. *Chem. Rev.*, **2002**, 102, 93-144.
14. Jemmis, E. D.; Jayasree, E. G.; Parameswaran, P. *Chem. Soc. Rev.*, **2006**, 35, 157-168.
15. Dillon, K. B.; Mathey, F.; Nixon, J. F. *Phosphorus: The Carbon Copy*, John Wiley, Chichester, **1998**.

16. **Gaussian 03**, Revision C.02 Frisch, M. J.; Trucks, G. W.; Schlegel, H. B.; Scuseria, G. E.; Robb, M. A.; R. Cheeseman, J.; Montgomery, Jr, J. A.; Vreven, T.; Kudin, K. N.; Burant, J. C.; Millam, J. M.; Iyengar, S. S.; Tomasi, J.; Barone, V.; Mennucci, B.; Cossi, M.; Scalmani, G.; Rega, N.; Petersson, G. A.; Nakatsuji, H.; Hada, M.; Ehara, M.; Toyota, K.; Fukuda, R.; Hasegawa, J.; M. Ishida, M.; Nakajima, T.; Honda, Y.; Kitao, O.; Nakai, H.; Klene, M.; Li, X.; Knox, J. E.; Hratchian, H. P.; Cross, J. B.; Bakken, V.; Adamo, C.; Jaramillo, J.; Gomperts, R.; Stratmann, R. E.; Yazyev, O.; Austin, A. J.; Cammi, R.; Pomelli, C.; Ochterski, J. W.; Ayala, P. Y.; Morokuma, K.; Voth, G. A.; Salvador, P.; Dannenberg, J. J.; Zakrzewski, V. G.; Dapprich, S.; Daniels, A. D.; Strain, M. C.; Farkas, O.; Malick, D. K.; Rabuck, A. D.; Raghavachari, K. ; Foresman, J. B.; Ortiz, J. V.; Cui, Q.; Baboul, A. G.; Clifford, S.; Cioslowski, J.; Stefanov, B. B. ; Liu, G.; Liashenko, A.; Piskorz, P.; Komaromi, I.; Martin, R. L.; Fox, D. J.; Keith, T.; Al-Laham, M. A.; Peng, C. Y.; Nanayakkara, A.; Challacombe, M.; Gill, P. M. W.; Johnson, B.; Chen, W.; Wong, M. W.; Gonzalez, C.; Pople, J. A. Gaussian, Inc., Wallingford CT, **2004**.
17. Becke, A. D. *Phys. Rev. A.*, **1988**, 38, 3098-3100.
18. Perdew, J. P. *Phys. Rev. B.*, **1986**, 33, 8822-8824.
19. **ADF2003.01**, SCM, Theoretical Chemistry, Vrije Universiteit, Amsterdam, The Netherlands, Baerends, E. J.; Autschbach, J.; Bérces, A.; Bo, C.; Boerrigter, P. M.; Cavallo, L.; Chong, D. P.; Deng, L.; Dickson, R. M; Ellis, D. E.; VanFaassen, M.; Fan, L.; Fischer, T. H.; Fonseca C.; Guerra, Van Gisbergen, S. J. A.; Groeneveld, J. A.; Gritsenko, O. V.; Grüning, M.; Harris, F. E.; Vanden Hoek, P.; Jacobsen, H.; Jensen, L.; VanKessel, G.; Kootstra, F.; Van Lenthe, E.; McCormack, D. A.;

- Michalak, A.; Osinga, V. P.; Patchkovskii, S.; Philipsen, P. H. T.; Post, D.; Pye, C. C.; Ravenek, W.; Ros, P.; Schipper, P. R. T.; Schreckenbach, G.; Snijders, J. G.; Sola, M.; Swart, M.; Swerhone, D.; Te Velde, G.; Vernooijs, P.; Versluis, L.; Visser, O.; Wang, F.; Van Wezenbeek, E.; Wiesenekker, G. Wolff, S. K.; Woo, T. K.; Yakovlev, A. L.; Ziegler, T.
20. Dunning Jr, T. H.; Hay, P. J. *Modern Theoretical Chemistry*, Ed. H. F. Schaefer III, **1976**, 3, 1-28.
21. (a) Schaefer, A.; Horn, H.; Ahlrichs, R. *J. Chem. Phys.*, **1992**, 97, 2571-2577. (b) Schaefer, A.; Horn, H.; Ahlrichs, R. *J. Chem. Phys.*, **1994**, 100, 5829-5835.
22. Becke, A. D. *J. Chem. Phys.*, **1993**, 98, 5648-5652.
23. Lee, C.; Yang, W.; Parr, R. G. *Phys. Rev. B.*, **1988**, 37, 785-789.
24. Wade, K. *Chem. Commun.*, **1971**, 792-793.
25. Warren, D. S.; Gimarc, B. M. *J. Am. Chem. Soc.*, **1992**, 114, 5378-5385.
26. Mathey, F. *Angew. Chem. Int. Ed. Engl.*, **2003**, 42, 1578-1604.
27. Gleiter, R.; Lange, H.; Binger, P.; Stannek, J.; Krüger, C.; Bruckmann, J.; Zenneck, U.; Kummer, S. *Eur J Inorg Chem.*, **1998**, 1619-1621.
28. Clendenning, S. B.; Green, J. C.; Nixon, J. F. *J. Chem. Soc. Dalton. Trans.*, **2000**, 1507-1512.
29. Nguyen, M. T.; Hegarty, A. F. *Chem. Commun.*, **1986**, 383-385.
30. Thompson, M. E.; Bercaw, J. E. *Pure and Appl. Chem.*, **1984**, 56, 1-11.



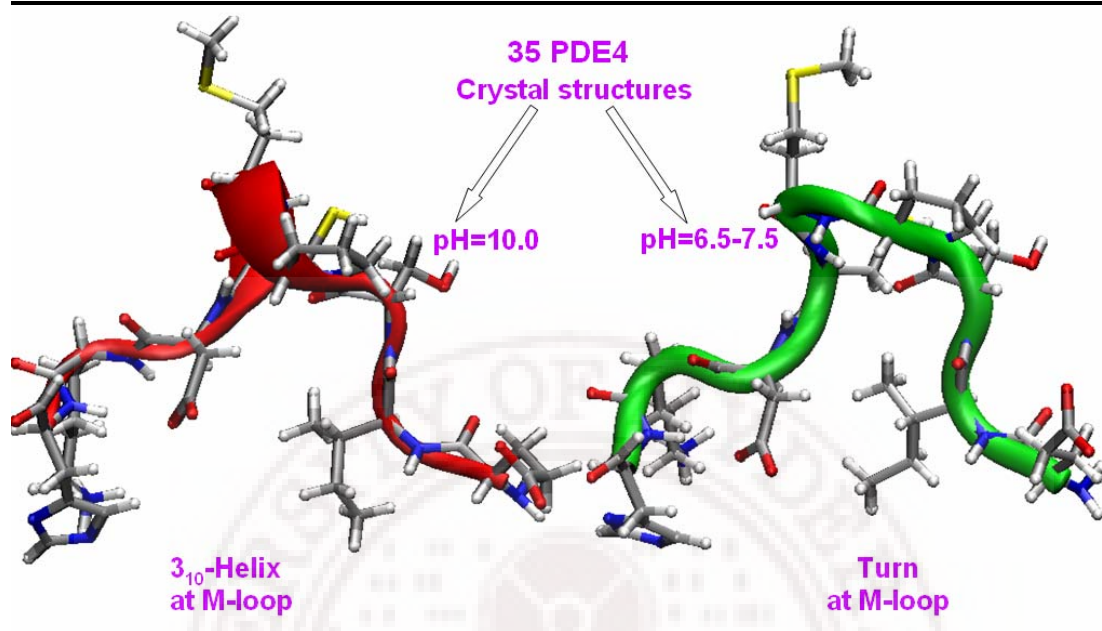
Chapter 4

A pH Dependence of 3_{10} -Helix versus Turn in M-loop Region of PDE4: Observations on PDB Entries and an Electronic Structure Study

Contents

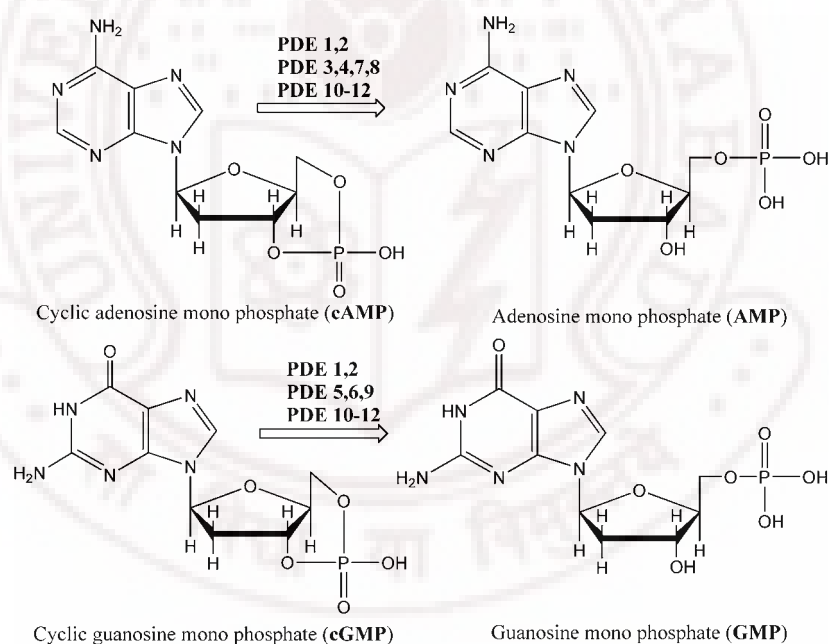
4.1	Abstract	137
4.2	Introduction	138
4.3	Details of Computational Methods	142
4.4	Results and Discussions	145
4.4.1	Crystal Structure Analysis	145
4.4.2	Root Mean Square Deviation	148
4.4.3	Importance of Secondary Structural Change and its Cause	150
4.4.4	Influence of pH on M-loop Region	153
4.4.5	Influence of M-loop Region on Subtype Selectivity	162
4.5	Conclusions	163
4.6	References	163

4.1 Abstract



4.2 Introduction

Cyclic nucleotide phosphodiesterases (PDEs) comprise a super family of metallophosphohydrolases. They specifically hydrolyze phosphodiesterase bond of cyclic adenosine 3',5'-monophosphate (cAMP) and guanosine 3',5'-monophosphate (cGMP) to produce the corresponding 5'-nucleotides (AMP and GMP) in various cells (**Scheme 4.1**).^{1,2} The second messengers (cAMP and cGMP) concentration affects the specific protein phosphorylation cascades. Hence, these isozymes play a vital role in the regulation of various physiological functions like smooth muscle relaxation, visual response, platelet aggregation, cardiac contractibility, immune response, etc.¹⁻³



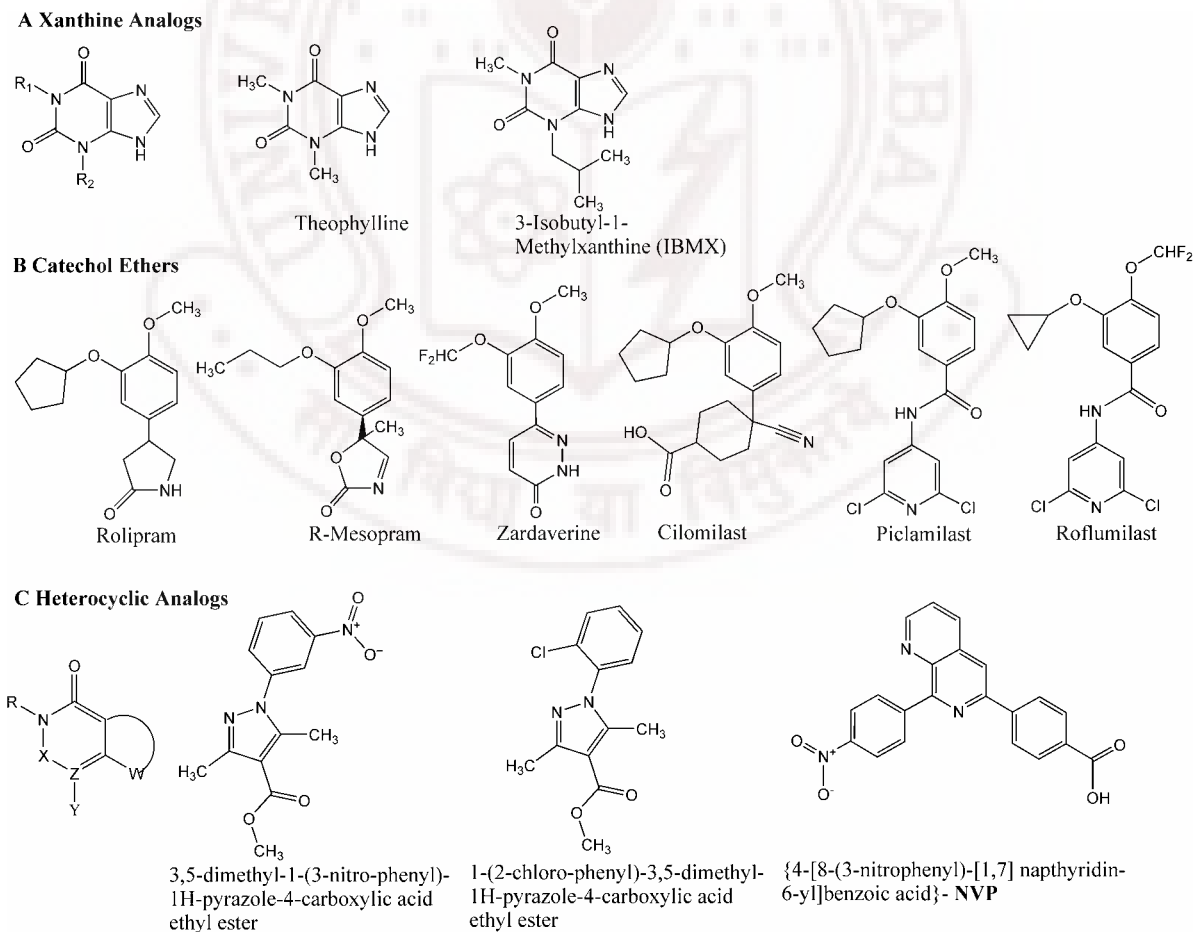
Scheme 4.1. Function of PDE enzymes

The human genome encodes 21 PDE genes that are grouped to 11 families. Alternative mRNA splicing of these genes generates over 200 splice variants or isoforms of PDE proteins.^{3b} The PDE isozymes differ substantially in their physicochemical properties, tissue distributions, substrate and inhibitor specificities and regulatory

mechanisms.² PDEs contain a conserved catalytic domain of about 250 amino acids and variations are observed in the regulatory domains (N- and C-terminal region).^{3a} They can be categorized into three groups based on substrate specificity: (a) cGMP specific (PDE5, 6 and 9), (b) cAMP specific (PDE4, 7 and 8), and (c) both cAMP and cGMP specific (PDE1, 2, 3, 10 and 11). PDEs are the therapeutic targets for cardiovascular, inflammatory, central nervous system (CNS) and erectile dysfunction diseases.⁴ Among the 11 PDE isozymes, PDE4 and PDE5 have received much attention in the recent years.⁵⁻⁷ cAMP specific PDE4 is abundant in various inflammatory cells such as eosinophils, T cells, B cells and neutrophils. Inhibition of PDE4 activity in these cells leads to higher cAMP levels and causes bronchodilation. Thus it is a keen target for the inflammatory diseases such as asthma, chronic obstructive pulmonary disease (COPD), rheumatoid arthritis, allergic rhinitis, and typeII diabetes.⁶

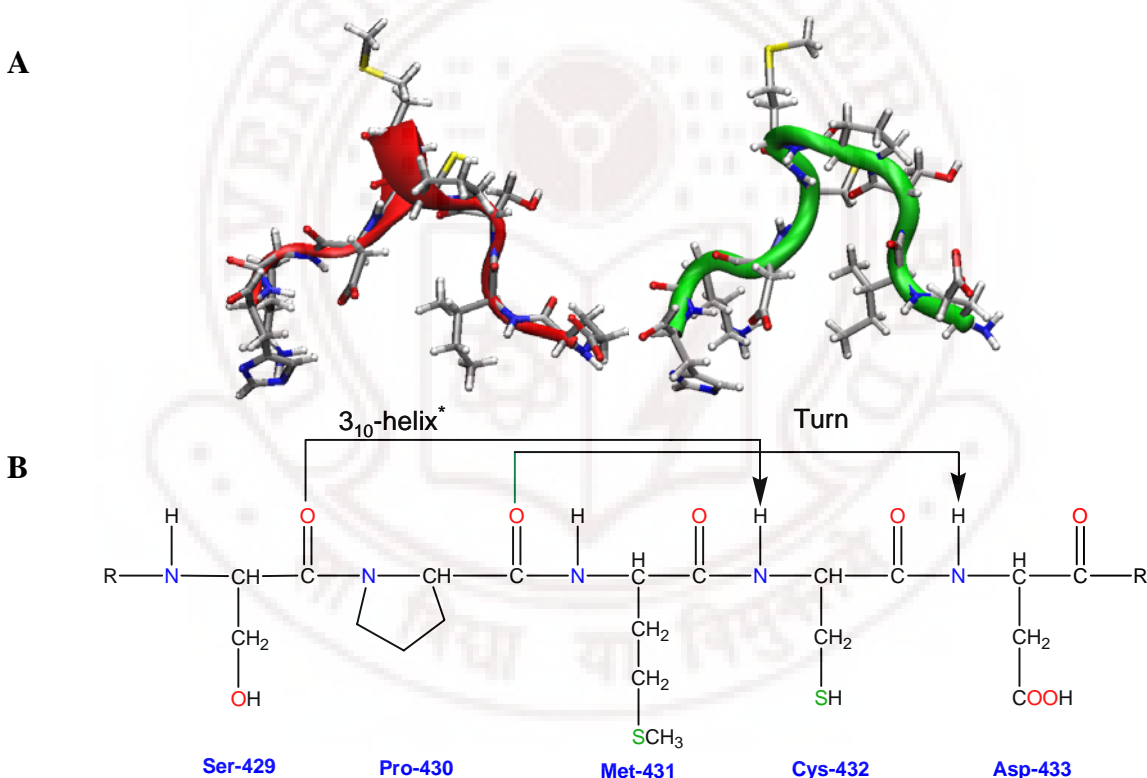
There are various classes of novel orally active PDE4 inhibitors discovered in this decade. Based on the structural motifs, PDE4 inhibitors can be broadly classified into three categories as xanthines, catechol ethers and hetrocyclics (nitraquanzone, benzofurans, indoles, isoquinoline, pyridopyrimidinones, pyrazolepyridines etc) (**Scheme 4.2**).⁸ Rolipram that belongs to catechol ether type has been reported as the first selective PDE4 inhibitor (**Scheme 4.2**). The first-generation PDE4 inhibitors rolipram, RO-20-1724 (mesopram) and zardaverine are discarded from clinical trials due to the side effects like nausea, vomiting, dyspepsia, headache and emesis.^{9a} The second-generation rolipram analogs (cilomilast, roflumilast and most potent piclamilast **Scheme 4.2 B**) that are now in clinical trials are also suffering from low therapeutic ratio.^{9b}

The reason for the side effects are (a) poor blood brain barrier (BBB) regions in the emetic centers of CNS allow absorption of the circulating drugs easily and lead to emesis,^{10a} (b) PDE4D subtype is over expressed in the emetic centers such as nucleus tractus solitarius and area postrema,^{10b} and (c) of the two conformation states of PDE, high-affinity rolipram binding form is stated to cause side effects.^{10c,d} The various strategies to overcome these side effects are (a) selectivity towards low affinity versus high affinity rolipram binding form, (b) low BBB permeable drugs, (c) disease activated drugs, (d) subtype selective PDE4 drugs, and (e) selectivity towards broader PDE family.⁶ Among these strategies subtype selectivity of PDE4 is a focus of present investigation.^{6c}



Scheme 4.2. Various classes of PDE4 inhibitors.

Lack of the 3-dimensional structure of a target protein is usually a bottleneck for rational drug design. In the last couple of years there has been a dramatic increase in the number of crystal structures of PDE4 class of enzymes in the protein data bank (PDB). Despite the availability of 39 X-ray structures along with co-crystals for PDE4, progress towards drugs without undesired side effects has been marginal. Our interest in the modeling of the subtype selective PDE4 drug candidates brought us to a close examination of these crystal structures. We found that there is a characteristic secondary structural conformation difference in the PDE4 crystal structures.¹¹⁻¹⁷



* 3₁₀-Helix is formed when the N-H group of an amino acid forms a hydrogen bond with the C = O group of the amino acid three residues earlier ($i + 3 \rightarrow i$ hydrogen bonding).¹³

Scheme 4.3. A) The secondary structure of PDE4 in the M-loop region existing as 3₁₀-helix (red color) and turn (green color) are shown along with the amino acids represented as capped stick model. B) Schematic 2-D representation of the 3₁₀-helix conformation where the hydrogen bonds are shown as lines and residue numbering is given for PDE4B.

Out of the 35 PDE4B and 4D crystal structures twelve of them have a 3_{10} -helix and the rest have a turn in the M-loop region (**Scheme 4.3A**)^{13b} which is near to the active site pocket. The four crystal structures, one for each PDE4 subtypes are deposited recently and are not included in this work.¹⁸ The distinct pattern of secondary structure in the highly flexible M-loop region is prominent in these crystal structures (**Scheme 4.3A**). According to the standard protein structural rules, three and half residues are required per turn of α -helix. The hydrogen of the amide group of first residue forms a hydrogen bond with the oxygen of amino-terminal peptide bond of the fourth residue in a α -helix where as in 3_{10} -helix it forms with the third residue (**Scheme 4.3 B**).^{19,20}

Here we would like to present the factor responsible for this secondary structural change in the M-loop region. The methionine of the M-loop region has a hydrophobic interaction with inhibitors such as rolipram analogs^{13a,15b} and exists in various conformations with NVP inhibitor.¹⁸ Is this structural change a determining factor for the subtype selectivity? We identify that an experimental variable pH seems to be controlling this structural variation rather than the sequential differences in the PDE4. The influence of pH is studied by calculating the various protonation states of side chains or amide bonds of these structures in the gas and explicit solvent phases.

4.3 Details of Computational Methods

4.3.1 Root Mean Square Deviation (RMSD): Residue-by-residue RMSD is calculated using a FORTRAN program.²¹ RMSDs were calculated for the backbone residues of all 4B and 4D crystal structures having similar ligands. Molecular operating environment (MOE) homology module²² is used for structural alignment of PDE4B and

4D structures. The RMSD values were calculated using the following equation where d_i is the distance between i th atoms and n is the number of such distances.

$$RMSD = \sqrt{\sum_i^n d_i^2 / n}$$

4.3.2 Electronic Structure Calculations: We have used *ab initio* calculations on the model structures, generated from the fragment SPMCD (Ser, Pro, Met, Cys, Asp) residue sequence of PDE4B and PDE4D PDB coordinates. The resulting dangling valencies were saturated by appropriately placing hydrogens. For uniformity and to average out the specific differences in the geometries arising from the process of formation of the crystals, only the hydrogen atom positions in each of the structures were optimized. The dihedral angles were kept constant during this process. The protonated and deprotonated states of aspartic acid, cysteine and amide bonds were calculated for seven sets of ligands. All electronic structure calculations were performed at the B3LYP/6-31+G* level of theory.²³

The gas phase optimized model structures 1TB5 having 3_{10} -helix and 1TB7 having turn were further taken and a layer of 5 angstrom thickness of water molecules is added using “soak” option in InsightII.²⁴ The total number of water molecules present around the pentapeptide protein structure is 119. The water molecules of the proteins were generally treated as low layer with molecular mechanics in QM/MM calculations to reduce the computational cost. The ONIOM^{25,26} calculation is implemented for this system to analyze the explicit solvent effect on the structures. A two layer ONIOM calculation is adopted for the system, where the pentapeptide sequence SPMCD is defined quantum mechanically (high layer) with B3LYP/6-31+G* level of theory and the

water molecules were defined as low layer molecular mechanics part with universal force field.²⁷ The ONIOM energy of the system is given as

$$E^{\text{ONIOM (QM:MM)}} = E_{\text{model}}^{\text{QM}} + E_{\text{real}}^{\text{MM}} - E_{\text{model}}^{\text{MM}} = E_{\text{model}}^{\text{high}} + E_{\text{real}}^{\text{low}} - E_{\text{model}}^{\text{low}}$$

All these calculations were done using Gaussian03 program package.²⁸

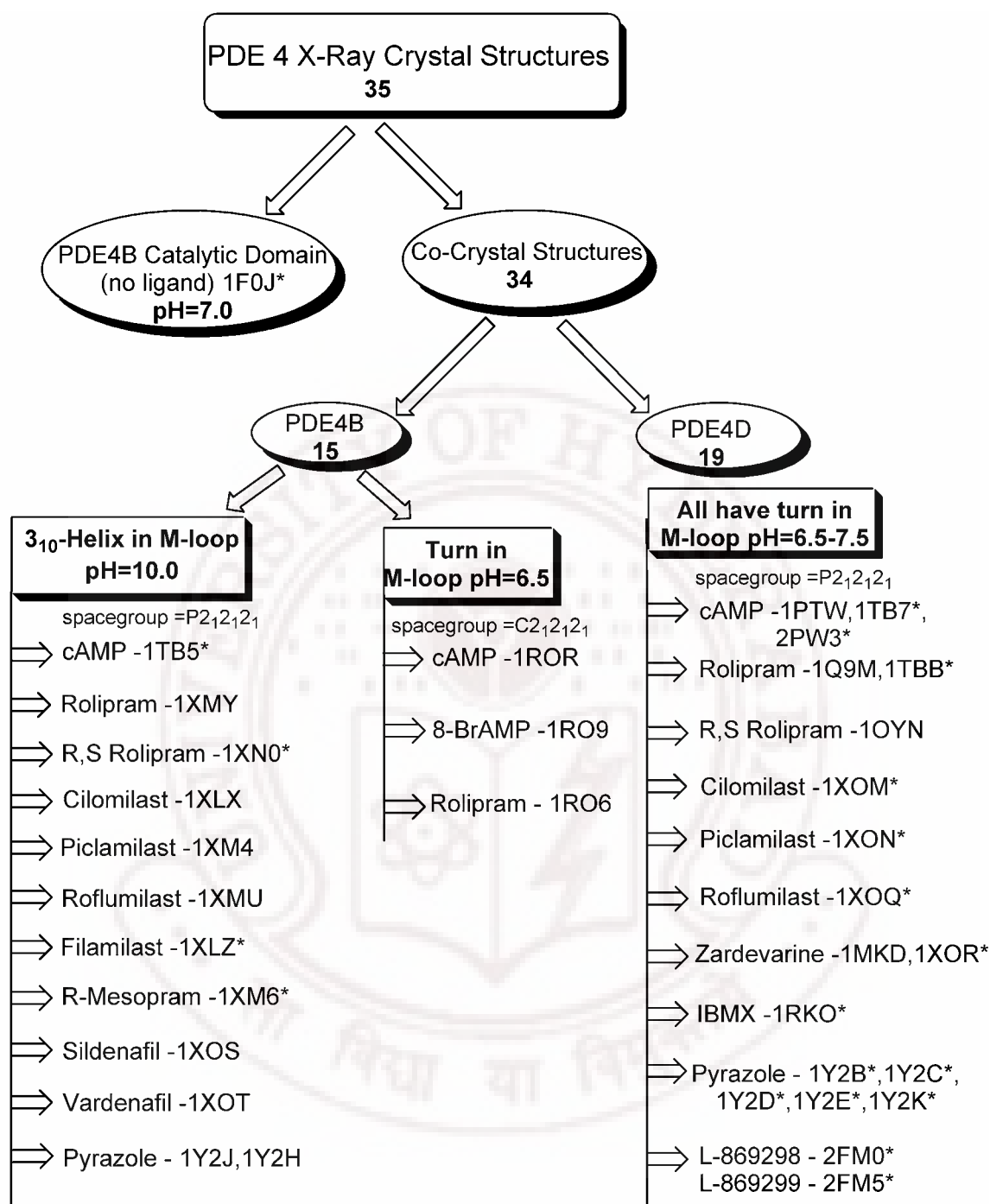
4.3.3 Molecular Dynamics Simulations: The simulations were performed using PMEMD module of AMBER9 version²⁹ in IBM BLUEGENE/L machine. The deposited PDB structures 1TB5 and 1TB7 were taken for the molecular simulations. The coordinates of M-loop region (423-440) of these protein structures were taken. The FF03 force field³⁰ was employed. The LEAP module was employed to construct a truncated octahedron solvate box (bcc) of cell length 56.46 Å with TIP3P water molecules around the protein. The solvation shell around the protein is 12Å. The total number of solute and solvent atoms present around the 1TB5 and TB7 were 12578 and 12932 respectively. The protein-solvent system was minimized with 1000 steps of steepest descent and 2000 steps of conjugate gradient method. The protein was fixed during minimization using a harmonic constraint with a force constant of 500kcal/mol/Å². This was done to remove any close contacts existing in the water shell with respect to protein. The whole system was also minimized after this for 200 steps steepest descent and 800 steps conjugate gradient method, so that the hydrogens of protein were optimized. The minimized structure obtained was then gradually heated up (over 40ps) from 0K to 300K with harmonic constraints on solute using SHAKE method. The dynamics was maintained under constant pressure-constant temperature (NPT) conditions using Berendsen (weak-coupling) temperature with a time step of 2fs.³¹ Finally, a production dynamics of 10ns with protein fixed under NPT conditions with time step of 1fs. The long range

interactions were calculated by particle mesh ewald (PME) method.³² The grid size of 60×60×60 with grid spacing of 1.0 Å with a direct sum tolerance of 0.00001 and 9.0 Å cutoff was used. The cubic B-spline of fourth order was interpolated in PME. The resulting trajectories of molecular simulations were analyzed using PTRAJ module of AMBER 8.0.

4.4 Results and Discussions

4.4.1 Crystal Structure Analysis

Out of the three domains of PDEs, catalytic domain and part of C-terminal containing amino acids are only crystallized. There are about 60 PDE crystal structures in the PDB and 35 of these belong to PDE4 class with various substrates such as (cAMP), AMP, 8-BrAMP and inhibitors such as rolipram analogs (rolipram, cilomilast, piclamilast, roflumilast, mesopram, and filamilast) and pyrazole analogs (**Scheme 4.2**).¹¹⁻¹⁷ PDE4 is coded by four genes named as A, B, C and D and are called as subtypes. These subtypes depending on m-RNA splicing are of 20 splice variants. The splice variants differ in the upstream conserved region (UCR)^{5a} that is UCR1 and UCR2 present in the regulatory domain (N-terminal) of the protein. Among the four genes coding for PDE4, about sixteen 4B and nineteen 4D structures are crystallized (**Figure 4.1**). There is one each for PDE4 subtype with NVP ({4-[8-(3-nitrophenyl)-[1,7] naphthyridin-6-yl] benzoic acid}) inhibitor containing structures which are deposited recently.¹⁸ The catalytic domain of the first crystal structure available for PDE4B contains 376 residues and explains the general architecture of PDE4.¹¹ The PDE4 has basically three sub domains comprising seventeen α helices and a β hairpin. The catalytic pocket contains two divalent metal ions (Zn and Mg) that are crucial in hydrolysis of the substrate.



* pertains to those PDB structures that have water or solvent molecules near to the M-loop region.

Figure 4.1. Details of the available X-ray crystallographic structures of PDE4 with various ligands deposited in the PDB.

Zn in the active site pocket has distorted trigonal bipyramid geometry, coordinating with Asp²⁷⁵, Asp³⁹², His²³³, His²⁷⁴ and a water molecule of the protein.¹¹ On the other hand Asp²⁷⁵ of the protein and five water molecules surround the Mg atom. Further the co-crystals of PDE4 with various ligands also have similar three subdomains comprising sixteen α helices and a β hairpin (**Figure 4.2**).¹²⁻¹⁷ Other than the conservation of helices and hairpin we noticed a surprising characteristic feature in these 35 structures: Twelve structures have a 3_{10} -helix in the M-loop region. The remaining 23 of them have a turn in the M-loop region,^{13b} nineteen of these twenty three belong to the PDE4D and four to PDE4B (**Figure 4.1**).

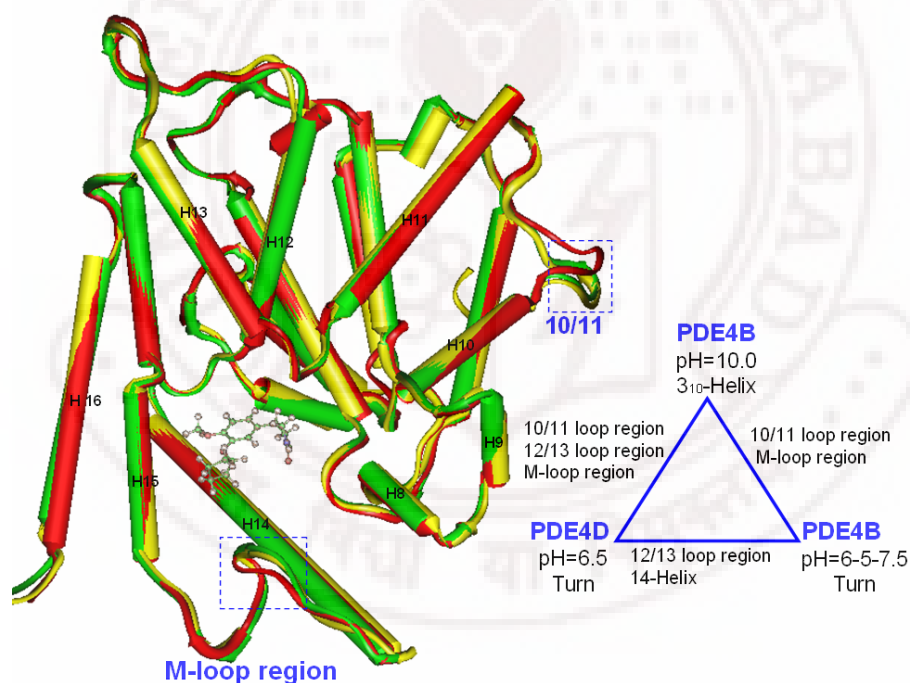
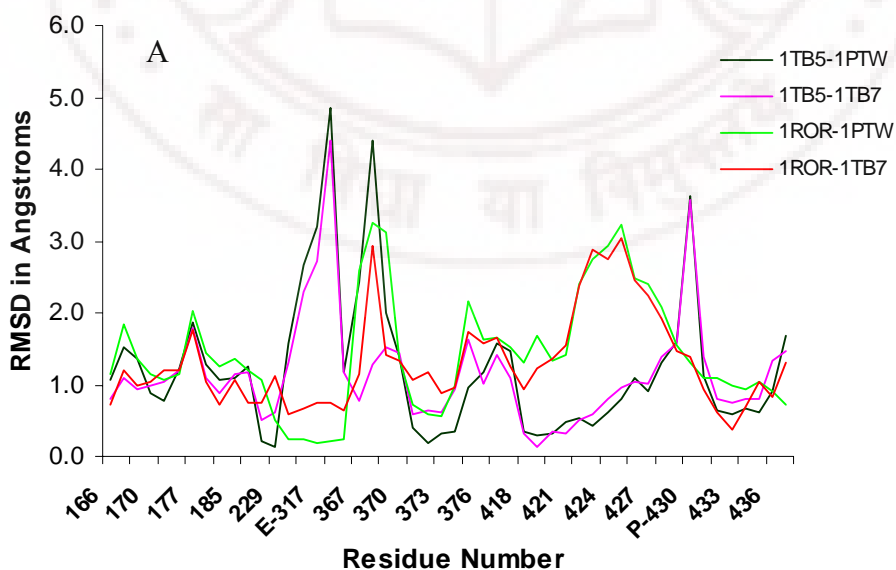


Figure 4.2. The superimposition of α -carbon of the turn having PDE4B and PDE4D and 3_{10} -helix having PDE4B structures with rolipram are shown with the yellow, green and red color secondary structure at pH= 6.5, 7.0 and 10.0 respectively (left side). The ball and stick model represents the rolipram ligand in the active site. A schematic representation of structural differences with all the other similar ligands is also shown (right side).

4.4.2 Root Mean Square Deviation (RMSD)

We superimposed all structures having the 3₁₀-helix and the turn with similar seven sets of ligands and the RMSD of residue by residue for the backbone is calculated.²¹ There are two structures each for PDE4B and 4D with cAMP, three each with rolipram and one each with cilomilast, piclamilast, roflumilast and pyrazole analogs (**Figure 4.1**). The superimposition of 4B containing 3₁₀-helix and 4D with similar ligand structures showed a major difference in three loop regions that is 10/11, 12/13 and in the M-loop region (**Figure 4.2**). The residues with varying RMSD are Glu³¹⁷ and Glu³¹⁸ of helix 10/11 (316-319) which interacts with UCR1 and UCR2 present in the regulatory domain (N-terminal) of the protein. The residues Ser³⁶⁸ and Ser³⁶⁹ of helix 12/13 (367-377) belong to extracellular signal-regulated kinases (ERK) docking site¹ that has protein-protein interactions is also altered. In case of the M-loop region^{13b} (424-437) Pro⁴³⁰ and Met⁴³¹ residues are altered in the backbone of protein structure (**Figure 4.3**). The extent of deviation in ERK docking site varies slightly with the ligands.



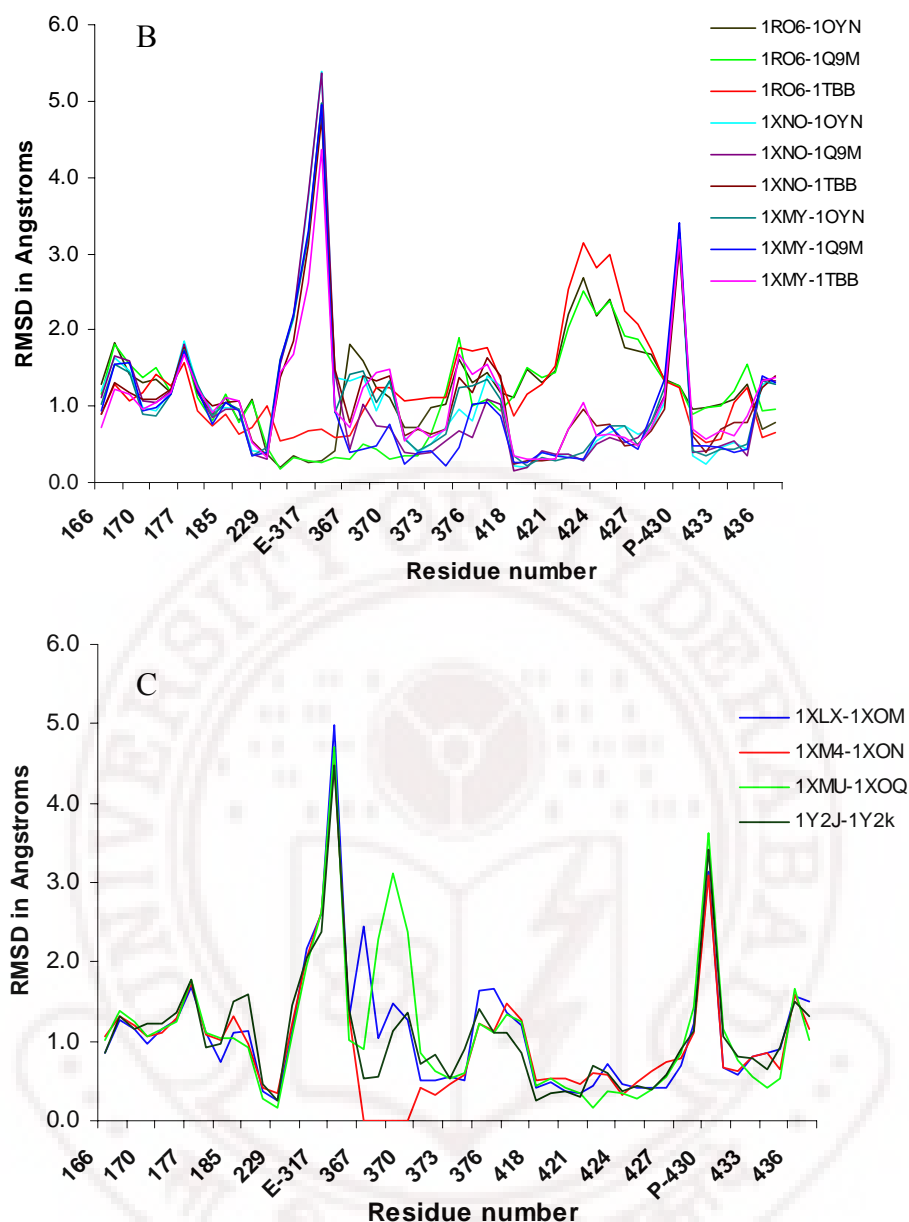


Figure 4.3. Comparison of RMSD values for backbone residues of PDE4B and 4D with A) cAMP B) Rolipram C) Cilomilast, Piclamilast, Roflumilast and Pyrazole analogs crystallized X-ray structures.

On the other hand the superimposition of the PDE4B and 4D structures containing turn with cAMP and rolipram shows a difference only in the 12/13 loop region (ERK docking site) and in helix 14, particularly from the residues Lys⁴²² to Glu⁴²⁷ that are oriented towards the solvent region (**Figure 4.3 A and B**). The superimposition of all the

4B with cAMP and rolipram structures has a difference in 10/11 and the M-loop region (**Figure 4.2**). In spite of the major homology sequence similarity between 4B and 4D subtypes^{6c} the common differences are found in 12/13-loop region and either at starting of the M-loop region or at Pro⁴³⁰ residue. Thus the PDE4 structures can be divided into the two groups: one with the 3₁₀-helix and the other with the turn varying at 10/11 and in the M-loop region (**Figure 4.2**).

4.4.3 Importance of Secondary Structural Change and its Cause

In view of the important role of the secondary structural alterations in specific enzymatic functions of PDE5,³³ the M-loop region in PDE4 is scrutinized because the methionine residue here has hydrophobic interactions with all rolipram analogs.^{13a,15b} The inhibitor selectivity of rolipram analogs to PDE4 is due to the hydrophobic interactions at the Q2 pocket, where methionine of the M-loop region is a constituent. The PDE4A, 4B, 4C and 4D with NVP, a subtype selective inhibitor also have shown large conformational changes of methionine having relatively high B-factors.¹⁸ The conformational changes of methionine thus can have impact on inhibitor binding. The analysis of these variations in PDE4 may help to understand the influence of the M-loop region in inhibitor selectivity.

The secondary structural difference of PDE4 crystals cannot be explained by the ligand binding or crystal packing or mutated residues. This is because there is a structural variation of 3₁₀- helix and turn in the M-loop region within PDE4B structures with the similar ligands and the same space group (**Figure 4.1**). The SPMCD residue sequence is conserved in all subtypes hence cannot account for this structural difference. After an extensive search, the only difference we could find between these two sets of structures is the pH maintained during crystallization. Without any exception it was found that all the

PDE4B structures having 3_{10} -helix are crystallized at pH=10.0 from the polar solvents such as aqueous LiSO_4 and NH_4SO_4 solution. In contrast, all the turn-containing PDE4B and 4D structures are obtained at pH=6.5-7.5 range with polyethylene glycol (PEG) conditions (**Table 4.1**). Though we do not know the reason for the use of different pH in these experiments, the results are surprising because in these examples the pH appears to dominate over the differences in sequences of PDE4B and 4D.

Table 4.1. The crystalline conditions, solvent water and ethane diol (EDO) molecules present in the various chains of 35 PDE4 crystal structures.

PDE4 Sub type	PDB ID	pH	Crystalline conditions	Secondary Structure	Chain	Solvent (H_2O) near NH	Solvent near CO
B	1F0J	7.0	PEG	II	a b	2 1	- -
B	1ROR	6.5	PEG 3000, sodium acetate,	II	a, b	-	-
B	1RO6	6.5	glycerol,	II	a, b	-	-
B	1RO9	6.5	sodium cacodylate,	II	a, b	-	-
B	1TB5	10.0	Ammonium sulfate, lithium sulfate	I	a b	1 -	- -
B	1XMY	10.0		I	a, b	-	-
B	1XN0	10.0		I	a b	- -	1 -
B	1XLX	10.0		I	a, b	-	-
B	1XM4	10.0		I	a, b	-	-
B	1XMU	10.0		I	a, b	-	-
B	1XLZ	10.0		I	a b	- -	1 -
B	1XM6	10.0		I	a, b	1	1
B	1XOS	10.0		I	a	-	-
B	1XOT	10.0		I	a, b	-	-
B	1Y2J	10.0		I	a, b	-	-
B	1Y2H	10.0		I	a, b	-	-
D	1PTW	7.50	50 mM Hepes, 15% PEG 3350, 25% Ethylene Glycol, 5% Methanol, 5% DMSO	II	a, b c, d	-	-
D	2PW3	7.50	0.1 M HEPES, 0.1M	II	a	1	1

			MgCl ₂ , 12% PEG3350, 30% Ethylene Glycol, 10% Isopropanol		b	2	1
D	1TB7	7.00	PEG 3000, ethylene glycol, isopropanol,	II	a	1	1 EDO
D	1TBB	7.00	glycerol, DTT	II	b	1	1 EDO
					a	2	1 EDO
D	1Q9M	7.50	0.1 M HEPES, 20% PEG3350, 30% Ethylene Glycol, 10% Isopropanol, 5% Glycerol	II	b	1	1 EDO
					a, b, c, d,	-	-
D	1OYN	7.50	50 MM HEPES, 20% PEG3350, 25%Ethylene glycol, 20% Isopropanol	II	a, b, c, d	-	-
D	1XOM	7.0		II	a	2	1
					b	2	1 EDO
D	1XON	7.0	PEG3350, Ethylene	II	a, b	1	1 EDO
D	1XOQ	7.0	Glycol, Isopropanol,	II	a, b	1	1 EDO
			Glycerol and DTT				
D	1XOR	7.0		II	a	1	1
					b	1	2
D	1MKD	6.5	PEG8000, Mg acetate, DTT,	II	a, b, c, d, e, f, g, h, i, j, k, l	-	-
					a, c, d	-	-
D	1RKO/ 1ZKN	7.50	0.1M HEPES, 20% PEG 3350, 30% Ethylene Glycol, 10% Isopropanol, 5% Glycerol	II	b	1	-
D	1Y2B	7.0	PEG3350, Ethylene	II	a, b	1	1 EDO
D	1Y2C	7.0	Glycol, Isopropanol,	II	a, b	2	1 EDO
D	1Y2D	7.0	Glycerol and DTT	II	a, b	2	1 EDO
D	1Y2E	7.0		II	a	2	1 EDO
					b	-	1 EDO
D	1Y2K	7.0		II	a	1	1 EDO
					b	2	1 EDO
D	2FM0	7.50	0.1 M HEPES, 15% PEG3350, 25% Ethylene Glycol, 5% Isopropanol, 5% Glycerol	II	a	-	2
					b	1	2
					c, d	-	1
D	2FM5	7.50	0.05 M HEPES, 15% PEG3350, 25% Ethylene Glycol, 5% Isopropanol, 5% Glycerol	II	a, b	-	2
					c, d	-	1

4.4.4 Influence of pH on M-loop Region

As a first approximation we assume that the pH dependence on the different conformations is caused by the loss or gain of a proton that leads to ionizations of carboxylates and amines.³⁴ The changes in the electrostatic environment of PDE4B and 4D may alter the conformations and finally affect the secondary structure of the protein. The influence of the pH on the structure is known for lysozymes, plastocyanin, γ -chymotrypsin, azurin and insulin.³⁵ Another example is of cubic insulin crystals that manifest alterations in the conformations of side chains of acidic residues as a function of the pH ranging from 7 to 11.³⁵ Such an alteration in the protonation states of acidic residues influencing the enzymatic role is well known for the cytochrome P-450s.³⁶ The difference in the conformation around the 10/11 loop region of PDE4 as a function of the pH might arise from the repulsion between the side chains of two glutamic acid residues that are adjacent to each other.

In the M-loop region the difference in the secondary structure is observed at the backbone of the SPMCD residue sequence that has conformation **I** in the 3_{10} -helix of PDE4B and **II** in all the turn containing PDE4B and 4D structures (**Figure 4.4**). The structures **I** and **II** have a conserved hydrogen bond between the CO of serine and the NH of cysteine. These two structures have a difference in the orientation of the carbonyl group of the proline in the amide bond. This difference of the carboxy group orientation of the proline helps to gain extra hydrogen bonding with NH group of the aspartic acid resulting in a twist and forming a 3_{10} -helix structure in **I** (**Figure 4.4**, **Scheme 4.3B**). Generally the constrained geometry of the proline initiates the turning of a protein strand, while here it brings a 3_{10} -helix structure of the conformation **I**.

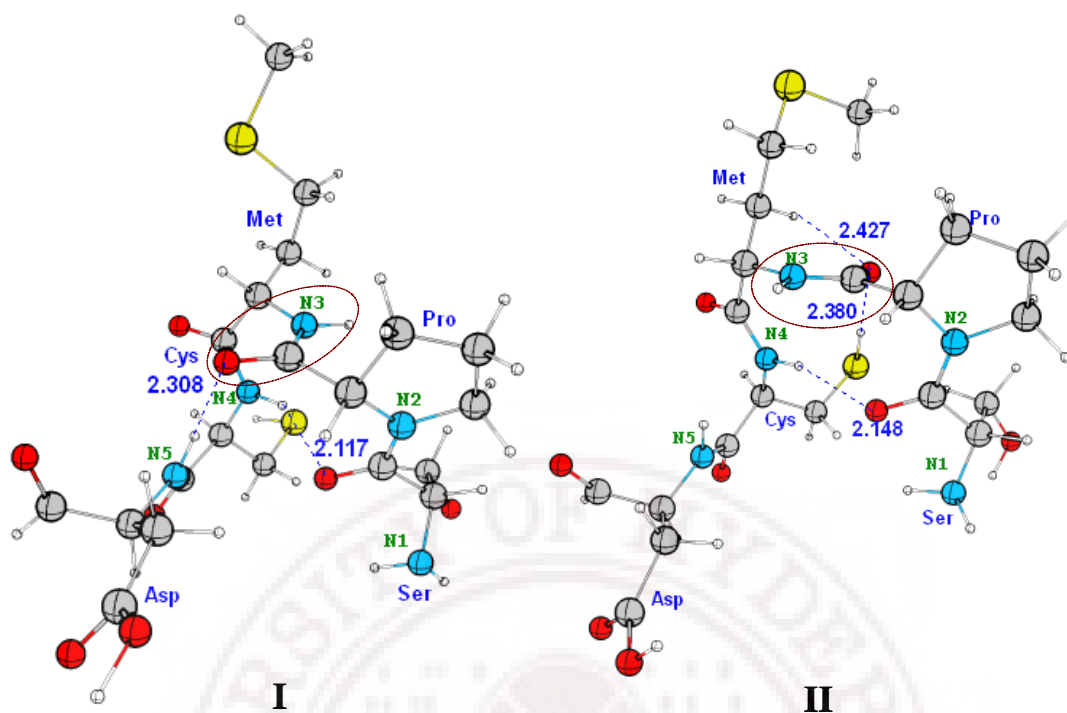


Figure 4.4. The optimized conformations, **I** (3_{10} -helix) and **II** (turn), of SPMCD residues at pH=10.0 and pH=6.5-7.5 respectively.

The influence of pH can lead to the existence of various protonation states of side chains or amide bonds in the structures **I** and **II**. The aspartic acid and cysteine side chains are generally known to be protonated in various protein structures.³⁵⁻³⁷ There are some examples of backbone amide bonds that undergo protonation when they are involved in interactions with a metal as in Belomycin.^{36c} So, we anticipate that in SPMCD residue sequence depending on pH, aspartic acid or cysteine side chains or amide bonds can be protonated. We simulate different pH conditions by adding or removing a proton of side chains or amide bonds. The energies of the protonated and deprotonated states of aspartic acid, cysteine and amide bonds in all seven sets of similar ligands having “ 3_{10} -helix” and “turn” containing structures are calculated. The protonation and deprotonation states of aspartic acid residue (isodesmic equation 4.1) do

not explain the existing structural variations (**Table 4.2**). The isodesmic equation 4.2 shows the energetics of the protonation and the deprotonation of the cysteine residue. Except in rolipram ligand containing structures, the formation of the protonation state of cysteine in structure **II** and the deprotonated state in structure **I** are exothermic in the gas phase (**Table 4.2**).

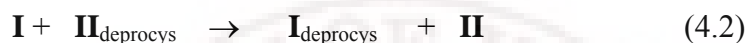


Table 4.2. The reaction energies in kcal/mol for equation (4.1 and 4.2)

Ligand	I	II	ΔH	
			(4.1)	(4.2)
cAMP	1TB5	1ROR	12.64	-4.00
	1TB5	1TB7	12.47	-8.75
Rolipram	1XMY	1RO6	-1.30	2.78
	1XMY	1TBB	3.56	-0.13
R,S Rolipram	1XN0	1OYN	8.77	-9.68
Cilomilast	1XLX	1XOM	-2.77	-10.78
Roflumilast	1XMU	1XOQ	10.17	-14.30
Piclamilast	1XM4	1XON	8.68	-9.82
Pyrazole	1Y2J	1Y2K	7.71	-4.48

The exothermicity of the reaction is due to the cysteine side chain (SH) in the protonated state gains a weak hydrogen bond with the CO group of the proline in structure **II** whereas in the deprotonated state it is missing (**Figure 4.4**). On the other hand in the structure **I**, the deprotonated state of the cysteine side chain can have weak electrostatic interactions with the NH group of methionine.³⁸ The protonated state of cysteine side chain in **II** and the deprotonated state in **I** have gained a non covalent interaction each justifying their thermodynamic stabilities.

The feasibility of protonation of backbone amide bonds is also studied. Even though the differences of pH by three units may not lead to the protonation and

deprotonation of amide bonds of PDE4 under experimental conditions, we anticipate that the protonation and deprotonation of N2 and N3 (**Figure 4.4**) of the structure **I** and **II** would be an indicator of the influence of the pH. The deprotonation and protonation are done at N3 (NH of methionine) and N2 (N of proline) of the amide bonds respectively where the change of conformation is observed (**Figure 4.4**). Reaction energies of the isodesmic equation (4.3) for seven sets of similar ligands in their protonated and deprotonated states indicate that **II** is more stable in the protonated form and **I** in the deprotonated form (**Table 4.3**). The isodesmic equation (4.4) shows that all turn containing PDE4 (**II**) on protonation at N2 are stable over 3_{10} -helix containing structures (**I**) and in isodesmic equation (4.5) the reverse is observed for deprotonation at N3 (**Table 4.3** column 6).

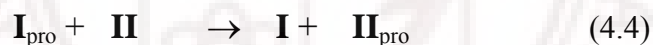
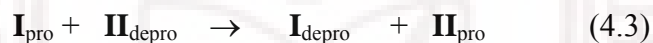


Table 4.3. The reaction energies in kcal/mol for equation (4.3, 4.4 and 4.5)

Ligand	I	II	ΔH		
			(4.3)	(4.4)	(4.5)
cAMP	1TB5	1ROR	-20.80	-15.89	-4.19
	1TB5	1TB7	-10.87	-3.87	-6.03
Rolipram	1XMY	1RO6	-39.32	-26.17	-13.15
	1XMY	1TBB	-24.68	-20.11	-4.57
R,S Rolipram	1XN0	1OYN	-23.36	-19.12	-4.24
Cilomilast	1XLX	1XOM	-19.79	-17.09	-2.70
Roflumilast	1XMU	1XOQ	-23.80	-15.36	-4.69
Piclamilast	1XM4	1XON	-15.21	-11.66	-3.55
Pyrazole	1Y2J	1Y2K	-16.72	-17.01	0.28

The order of stability of the protonated state in all **II** and deprotonated form in **I** is attributed to the increase in the number of hydrogen bonding interactions. In structure **II**,

the CO of the proline gains a 1,4 interaction with N2 on protonation and a weak interaction with the CH and SH of methionine and cysteine side chain residues.^{38,39} On the other hand the deprotonation of N3 leads to a weak C-H--N3 interaction⁴⁰ in **I** similar to the C-H--O interaction seen in **II** (**Figure 4.4**). The thermodynamic stability of the protonated and deprotonated states in structures **I** and **II** depends on the gain in non-covalent interactions such as hydrogen bonds and electrostatic interaction with the surrounding environment. The exothermicity of the backbone amide bond protonation is quite high than cysteine protonation.

The extent of non covalent interactions in the structures **I** and **II** can also differ with respect to the surrounding solvent molecules. The 35 crystal structures are thus thoroughly examined near the M-loop region to know the influence of the water molecules. In all the crystal structures with respect to the methionine of the M-loop region a sphere radius of 10.0Å is analyzed. There are 22 turn containing structures crystallized in PEG conditions. We found that the turn containing (**II**) PDE4D structures with resolution lower than 2.10Å have ethane diol (EDO) and water molecules in this region (**Table 4.1**). The carbonyl group of the proline of the structure **II** has a hydrogen bonding interaction with the EDO or water molecule. The amide group of the methionine of the structure **II** has a hydrogen bonding network with the NH of aspartic acid through two water molecules (**Figure 4.5**). These additional interactions with the solvent thus stabilize the structure **II**. The presence of EDO near to carbonyl group of proline in these structures may be due to PEG crystallization conditions. While such type of EDO or water molecules are not found at the carbonyl group of proline in the M-loop region of four PDE4B (1F0J, 1ROR, 1RO6 and 1RO9) and in high resolution PDE4D turn

containing structures, even though they have similar crystallization conditions (**Table 4.1**).

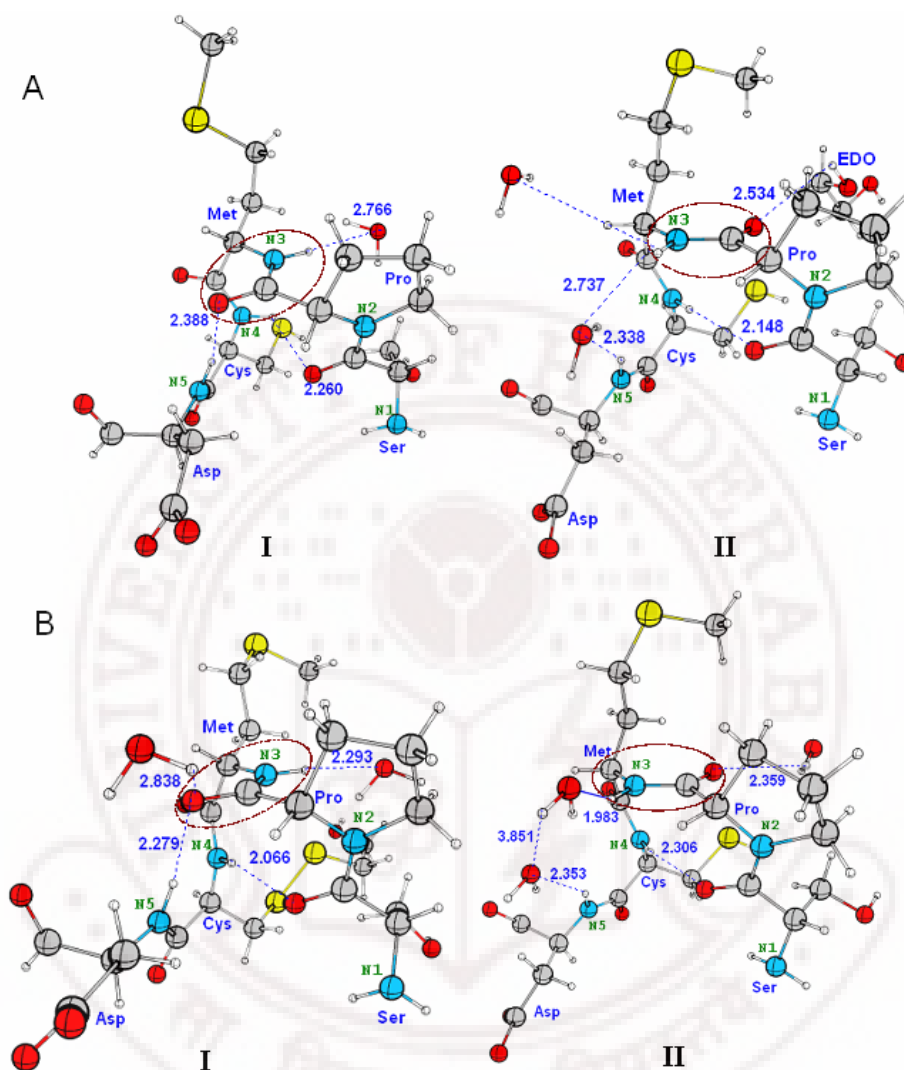
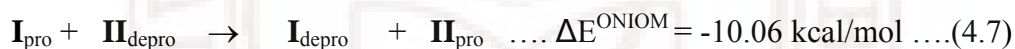
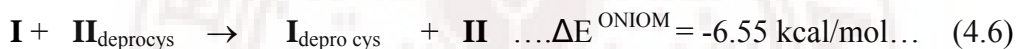


Figure 4.5. The X-ray crystal structural conformations of A) **I** (3₁₀- helix 1TB5) and **II** (turn 1TB7) B) **I** (3₁₀- helix 1XM6) and **II** (turn 2PW3) at pH=10.0 and pH=6.5-7.5 respectively. In the SPMCD residue sequence the hydrogen bonding interaction of the amide bond with solvent molecules such as water and EDO is also shown

Even the number of water molecules varies from 1-2 in the two chains (A and B) of the same crystal. This is also true in other crystals considered here (**Table 4.1**). It is possible to identify a water molecule even in the twelve low resolution structures with

3₁₀-helix showing hydrogen bonding interaction to the amide group of methionine and carbonyl group of proline (**Figure 4.5**). The number of solvent molecules present around the M-loop region in these crystal structures is varied (**Table 4.1**).

The irregularity in the number and position of the water and the EDO molecules in the crystal structures led us to study the influence of the solvent molecules on the structures. We model this by constructing a layer of 5Å thickness of water molecules around the pentapeptide SPMCD residue sequence of structures **I** and **II**. This model system with various protonation states of the cysteine and the amide bonds of 1TB5 and 1TB7 are studied using QM/MM ONIOM method. In this model the pentapeptide is defined as QM region and water molecules in the MM region (**Figure 4.6**).



(Where **I**= 1TB5 and **II**=1TB7)

The ONIOM energies of the protonated and the deprotonated states of the cysteine and amide bond (N2 and N3) in the structures **I** and **II** along with a water layer are given in isodesmic equation 4.6 and 4.7 respectively. The ONIOM calculation in explicit solvent shows the reaction is exothermic and similar as in the gas phase reaction (isodesmic eq 4.2 and 4.3). The water molecules forms a hydrogen bond with the NH group of methionine and the CO group of proline in the structures **I** and **II**. The gain in the hydrogen bonding interaction of amide bond in the structure **II** makes it more stable than **I**. The hydrogen bonding network of water with the residues in the crystal structures is reproduced by ONIOM calculations (**Figure 4.5** and **4.7**).

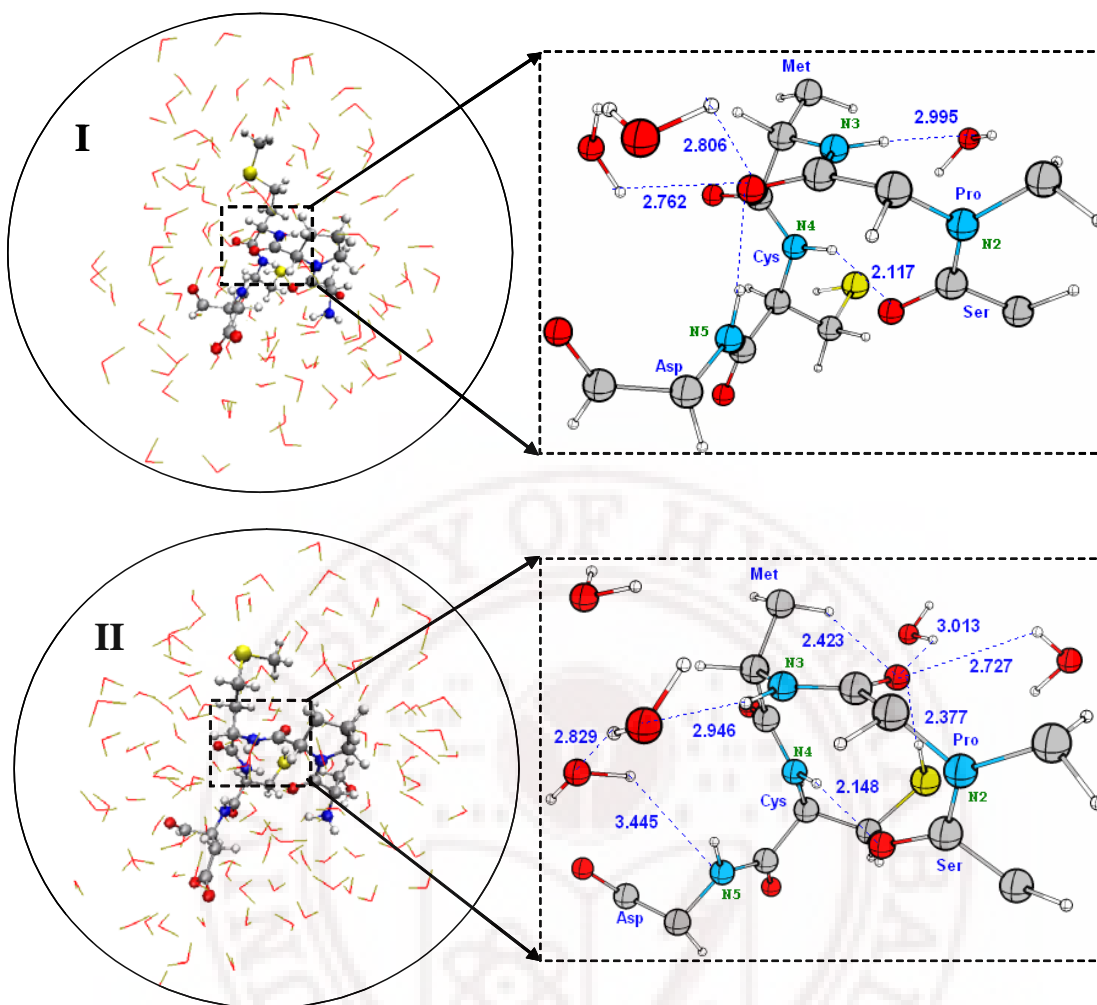


Figure 4.6. The ball and stick model represents the pentapeptide (SPMCD) that is considered high layer QM region and shell with of water molecules (lines) are considered as low layer MM region. The optimized geometry of **I** and **II** and their hydrogen bonding network with the solvent water molecules are also shown.

To reinvestigate the average number of water molecules that can exist near to the amide bond, CO group of the proline and NH group of the methionine, MD simulation on M-loop region of a 3_{10} -helix (1TB5) and turn (1TB7) containing structures are performed for 10ns in explicit solvent under NPT conditions. The simulation result also shows a similar hydrogen bonding interactions of water molecules around the CO group of the proline and the NH group of the methionine. The number of water molecules present

around the NH group of the methionine and the CO group of the proline are retained as in ONIOM model systems (**Figure 4.7**, **Table 4.4**). The gas phase, ONIOM and MD calculations of the model systems have shown non covalent interactions with adjacent residues and solvent molecules in the structures **I** and **II** are different.

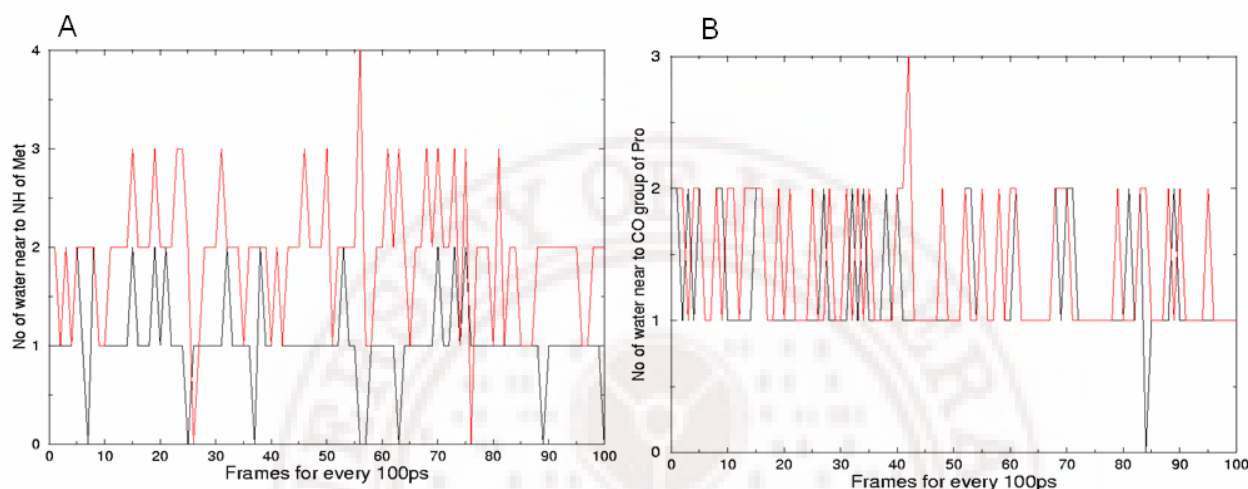


Figure 4.7. The number of water molecules A) around the NH group B) around the CO group of methionine in the M-loop region of 3_{10} -helix (**1TB5**, black color) and turn (**1TB7**, red color) containing structures for 10ns simulation is shown.

Table 4.4. The summary of number of water molecules present around in PDE4B (**1TB5**) and PDE4D (**1TB7**) structures.

Structure	No of water molecules near to CO group of Proline			No of water molecules near to NH group of Methionine		
	Crystal	ONIOM	MD(10ns)	Crystal	ONIOM	MD(10ns)
1TB5 (PDE4B)	0	2	1-2	1	2	0-2
1TB7 (PDE4D)	1 EDO	2	1-2	2	2-3	2-4

Electronic structure calculations thus explain the structural anomaly that at pH=10.0 conformation **I** is seen in all 3_{10} -helix PDE4B structures and at pH=6.5-7.5

prefer conformation **II** as observed in all turn containing crystal structures. The pH variation thus can have different protonation states of cysteine side chain or backbone amide bonds. The different protonated states are stabilized by the non covalent interactions of the amide bond with the surrounding environment such as adjacent residues and solvent molecules. Thus the orientation of the amide bond between proline and methionine is the deciding factor for the secondary structural change in the **II** or **I**. The pH dependence of the structures shows that there will be potential differences in the interaction at different parts of the cells in body at different pH for the same enzyme substrate combination.

4.4.5 Influence of M-loop Region on Subtype Selectivity

The secondary structural difference presented here had similar sequences and at physiological pH both subtypes PDE4B and 4D could have a turn structure. However, the variation in the sequence of residues in the M-loop region may change the interactions with the inhibitor that can help in subtype selectivity.^{6c} A Thr⁴³⁶ residue in PDE4B near to this secondary structural change is altered to Asn³⁶² in PDE4D. This variation of the residue does not account for secondary structural changes but influences the molecular properties of adjacent residues. The examination of molecular properties such as hydrophobicity and MOLCAD surfaces for the residues in the M-loop region were done. They show that a larger hydrophobic group containing ligands can be accommodated in the Q2 pocket of PDE4B.^{6c} This being a collaborative project is not discussed in detail in this chapter. The essence of that analysis shows exploration of PDE4 inhibitor that can accommodate M-loop region apart from the metal^{15b,16} and the solvent pocket⁴¹ of active site can lead to better subtype selectivity.

4.5 Conclusions

The 35 X-ray crystal structures of the two subtypes of PDE4 show an influence of pH of the crystallization medium as an experimental variable on the secondary structural change in the M-loop region. The pattern of secondary structural change in the highly flexible M-loop region as a function of pH is striking in these crystal structures. Electronic structure calculations on the model sequence of the SPMCD residue of PDE4 explain the thermodynamic preferences for the secondary structure in the pattern of 3_{10} -helix versus turn in the M-loop region. The protonated states of the cysteine side chain and amide bond of turn containing structures are exothermic according to the isodesmic equations. It is due to the increase in the number of hydrogen bonding interactions with surrounding environment such as adjacent residues and solvent molecules. The Thr⁴³⁶/Asn³⁶² mutation in the M-loop region influenced the hydrophobic nature in Q2 pocket of active site of PDE4B and 4D subtypes. Thus the variations in local (physiological) pH at the point of interaction and hydrophobic groups of Q2 pocket can be added parameters in optimizing the specificity of PDE4 inhibitors.

4.6 References

1. (a) Sutherland, E. W.; Rall, T. W. *J. Biol. Chem.*, **1958**, 232, 1077-1091. (b) Jonathan, B.; Sucha, S.; Subha, S. *Biochem. Biophys. Res. Commun.*, **2006**, 350, 25-32.
2. (a) Beavo, J. A.; Hardman, G.; Sutherland, E. W. *J. Biol. Chem.*, **1970**, 245, 5649-5655. (b) Bender, A. T.; Baevo, A. J. *Pharmacol Rev.*, **2006**, 58, 488-520.
3. (a) Sharron, H. F.; Illarion, V. T.; Jackie, D. C. *Prog. Nucleic Acid Res. Mol. Biol.*, **2001**, 65, 1-52. (b) Soderling, S. H.; Beavo, J. A. *Curr. Opin. Cell. Biol.*, **2000**, 12, 174-179.

4. (a) Chung, K. F. *Eur. J. Pharm.*, **2006**, 533, 110-117. (b) Boswell-Smith, B.; Spina, D.; Page, C. P. *British J. Pharm.*, **2006**, 147, S252-S257. (c) Menniti, F. S.; Faraci, W. S.; Christopher, S. J. *Nat. Rev. Drug Disc.*, **2006**, 5, 660-670.
5. (a) Houslay, M. D. *Prog. Nucleic. Acid. Res. Mol. Biol.*, **2001**, 69, 249-315. (b) Castro, A.; Jerez, M. J.; Martinez, A.; Gil, C. *Med. Res. Rev.*, **2005**, 25, 229-244.
6. (a) Zhang, K. Y. J.; Ibrahim, P. N.; Gillette, S.; Bollag, G. *Exp. Opin. Ther. Drugs*, **2005**, 9, 1283-1304. (b) Houslay, M. D.; Schafer, P.; Zhang, K. Y. J. *Drug Disc. Today*, **2005**, 10, 1503-1519. (c) Srivani, P.; Usharani, D.; Jemmis, E. D.; Sastry, G. N. *Curr. Pharm. Design*, **2008**, 14, 3854-3872.
7. (a) Jeon, J. H.; Heo, Y.-S.; Kim, C. M.; Hyun, Y. -L.; Lee, T. G.; Ro, S.; Cho, J. M. *Cell. Mol. Life. Sci.*, **2005**, 62, 1198-1220. (b) Srivani, P.; Srinivas, E.; Raghu, R.; Sastry, G. N. *J. Mol. Grap. Mod.*, **2007**, 26, 378-390.
8. (a) Spina, D.; *Drugs*, **2003**; 63, 1-20. (b) Montana, J. G.; Dyke, H. J. *Ann. Rep. Med. Chem.*, **2001**, 36, 41-56. (c) Burnouf, C.; Pruniaux, M. P. *Curr. Pharm. Design*, **2002**, 8, 1255-1296.
9. (a) Teixeira, M. M.; Gristwood, R. W.; Cooper, N.; Hellewell, P. G. *Trends Pharmacol. Sci.*, **1997**, 18, 164-71. (b) Giembycz, M. A. *Monaldi. Arch. Chest. Dis.*, **2002**, 57, 48-64.
10. (a) Spina, D. *Curr. Drug. Targ. Inflamm. Allergy*, **2004**, 3, 231-46. (b) Lamontagne, S.; Meadows, E.; Luk, P.; Normandin, D.; Muise, E.; Boulet, L.; Pon, D. J.; Robichaud, A.; Robertson, G. S.; Metters, K. M.; Nantel, F. *Brain Res.*, **2001**, 920, 84-96. (b) Souness, J. E.; Rao, S. *Cell Signal*, **1997**, 9, 227-236. (c) Zhang, H. T.;

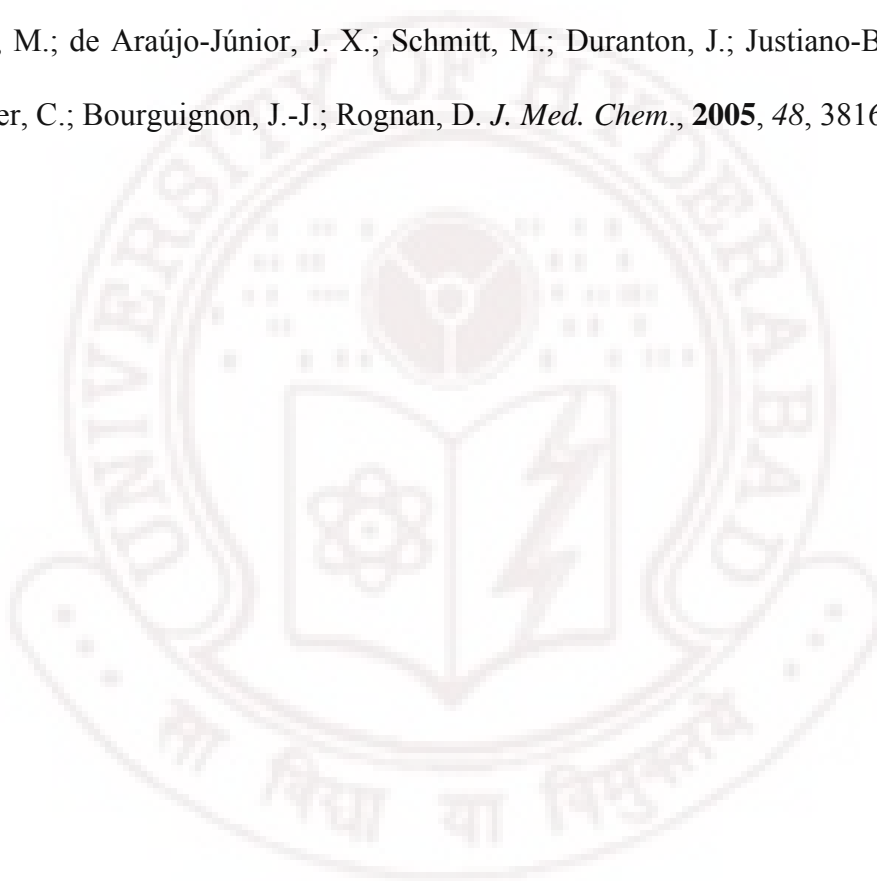
- Zhao, Y.; Huang, Y.; Deng, C.; Hopper A. T.; Vivo, M. D.; Rose, G. M.; O'Donnell, J. M. *Psychopharmacology*, **2006**, *186*, 209-217.
- 11 Xu, R. X.; Hassell, A. M.; Vanderwall, D.; Lambert, M. H.; Holmes, W. D.; Luthe, M. A.; Rocque, W. J.; Milburn, M. V.; Zhao, Y.; Ke, H.; Nolte, R. T. *Science*, **2000**, *288*, 1822-1825.
- 12 Lee, M. E.; Markowitz, J.; Lee, J-O.; Lee, H. *FEBS Letters*, **2002**, *530*, 53-58.
- 13 (a) Huai, Q.; Wang, H.; Sun, Y.; Kim, H-Y.; Liu, Y.; Ke, H. *Structure*, **2003**, *11*, 865-873. (b) Huai, Q.; Liu, Y.; Francis, S. H.; Corbin, J. D.; Ke, H. *J. Biol. Chem.*, **2004**, *279*, 13095-13101.
- 14 (a) Huai, Q.; Colicelli, J.; Ke, H. *Biochemistry*, **2003**, *42*, 13220-13226. (b) Xu, R. X.; Rocque, W. J.; Lambert, M. H.; Vanderwall, D. E.; Luther, M. A.; Nolte, R. T. *J. Mol. Biol.*, **2004**, *337*, 355-365.
- 15 (a) Zhang, K. Y. J.; Card, G. L.; Suzuki, Y.; Artis, D. R.; Fong, D.; Gillette, S.; Hsieh, D.; Neiman, J.; West, B. L.; Zhang, C.; Milburn, M. V.; Kim, S-H.; Schlessinger, J.; Bollag, G. A. *Mol. Cell.*, **2004**, *15*, 279-286. (b) Card, G. L.; England, B. P.; Suzuki, Y.; Fong, D.; Powell, B.; Lee, B.; Luu, C.; Tabrizizad, M.; Gillette, S.; Ibrahim, P. N.; Artis, D. R.; Bollag, G.; Milburn, M. V.; Kim, S-H.; Schlessinger, J.; Zhang, K. Y. J. *Structure*, **2004**, *12*, 2233-2247.
- 16 Card, G. L.; Blasdel, L.; England, B. P.; Zhang, C.; Suzuki, Y.; Gillette, S.; Fong, D.; Ibrahim, P. N.; Artis, D. R.; Bollag, G.; Milburn, M. V.; Kim, S-H.; Schlessinger, J.; Zhang, K. Y. J. *Nat. Biotechnol.*, **2005**, *23*, 201-207.
- 17 Huai, Q.; Sun, Y.; Wang, H.; Macdonald, D.; Aspiotis, R.; Robinson, H.; Huang, Z.; Ke, H. *J. Med. Chem.*, **2006**, *49*, 1867-1873.

- 18 Wang, H.; Peng, M.; Chen, Y.; Geng, J.; Robinson, H.; Houslay, M. D.; Cai, J.; Ke, H. *Biochem. J.*, **2007**, *408*, 193-201.
- 19 Nelson, D. L.; Cox, M. M. *Lehninger Principles of Biochemistry*, 4th ed.; W. H Freeman and company: 41 Madison avenue, NewYork, **2006**.
- 20 (a) Millhauser G. L. *Biochemistry*, **1995**, *34*, 3873-77. (b) Wu, Y-D.; Zhao, Y-L. A. *J. Am. Chem. Soc.*, **2001**, *123*, 5313-19. (c) Chin, W.; Piuzzi, F.; Dognon, J-P.; Dimicoli, I.; Tardivel, B.; Mons, M. *J. Am. Chem. Soc.*, **2005**, *127*, 11900-01.
- 21 Bindu, P. H.; Sastry, G. M.; Murty, U. S. N.; Sastry, G. N. *Biochem. Biophys. Res. Commun.*, **2004**, *319*, 312-320.
- 22 MOE version **2006** Chemical Computing Group, 954, First Floor, 16th Main, BTM Layout 2nd Stage, Bangalore, India 560 076.
- 23 (a) Becke, A. D. *J. Chem. Phys.*, **1993**, *98*, 5648-5652. (b) Becke, A. D. *Phys. Rev. A.*, **1988**, *38*, 3098-3100.
- 24 Insight **II** Version **2000** Molecular Modelling System 2000 Molecular Simulations. 9685 Scratan Road, San Deigo, CA.
- 25 Dapprich, S.; Komáromi, I.; Suzie Byun, K.; Morokuma K.; Frisch, M. J. *J. Mol. Struct. (THEOCHEM)*, **1999**, *462*, 1-21.
- 26 Vreven, T.; Morokuma, K.; Farkas, Ö.; Schlegel, H. B.; Frisch M. J. *J. Comput. Chem.*, **2003**, *24*, 760-769.
- 27 Rappé, A. K.; Casewit, C. J.; Colwell, K. S.; Goddard III, W. A.; Skiff, W. M. *J. Am. Chem. Soc.*, **1992**, *114*, 10024-10035.
- 28 **Gaussian 03**, Revision B.03, Frisch, M. J.; Trucks, G. W.; Schlegel, H. B.; Scuseria, G. E.; Robb, M. A.; Cheeseman, J. R.; Montgomery, Jr., J. A.; Vreven, T.; Kudin, K.

- N.; Burant, J. C.; Millam, J. M.; Iyengar, S. S.; Tomasi, J.; Barone, V.; Mennucci, B.; Cossi, M.; Scalmani, G.; Rega, N.; Petersson, G. A.; Nakatsuji, H.; Hada, M.; Ehara, M.; Toyota, K.; Fukuda, R.; Hasegawa, J.; Ishida, M.; Nakajima, T.; Honda, Y.; Kitao, O.; Nakai, H.; Klene, M.; Li, X.; Knox, J. E.; Hratchian, H. P.; Cross, J. B.; Bakken, V.; Adamo, C.; Jaramillo, J.; Gomperts, R.; Stratmann, R. E.; Yazyev, O.; Austin, A. J.; Cammi, R.; Pomelli, C.; Ochterski, J. W.; Ayala, P. Y.; Morokuma, K.; Voth, G. A.; Salvador, P.; Dannenberg, J. J.; Zakrzewski, V. G.; Dapprich, S.; Daniels, A. D.; Strain, M. C.; Farkas, O.; Malick, D. K.; Rabuck, A. D.; Raghavachari, K.; Foresman, J. B.; Ortiz, J. V.; Cui, Q.; Baboul, A. G.; Clifford, S.; Cioslowski, J.; Stefanov, B. B.; Liu, G.; Liashenko, A.; Piskorz, P.; Komaromi, I.; Martin, R. L.; Fox, D. J.; Keith, T.; Al-Laham, M. A.; Peng, C. Y.; Nanayakkara, A.; Challacombe, M.; Gill, P. M. W.; Johnson, B.; Chen, W.; Wong, M. W.; Gonzalez, C.; and Pople, J. A.; Gaussian, Inc., Wallingford CT, **2003**.
- 29 Case, D. A.; Darden, T. A.; Cheatham, III, T. E.; Simmerling, C.; Wang, J.; Duke, R. E.; Luo, R.; Merz, K. M.; Pearlman, D. A.; Crowley, M.; Walker, R. C.; Zhang, W.; Wang, B.; Hayik, S.; Roitberg, A.; Seabra, G.; Wong, K. F.; Paesani, F.; Wu, X.; Brozell, S.; Tsui, V.; Gohlke, H.; Yang, L.; Tan, C.; Mongan, J.; Hornak, V.; Cui, G.; Beroza, P.; Mathews, D. H.; Schafmeister, C.; Ross, W. S.; Kollman, P. A. AMBER9, 9th ed.; University of California: San Francisco, CA.
- 30 Duan, Y.; Wu, C.; Chowdhury, S.; Le, M. C.; Xiong, G.; Zhang, W.; Yang, R.; Cieplak, P.; Luo, R.; Lee, T. Caldwell, J.; Wang, J.; Kollman, P. J. *Comput. Chem.*, **2003**, 24, 1999-2012.

- 31 Berendsen, H. J. C.; Postma, J. P. M.; van Gunsteren, W. F.; DiNola, A.; Haak J. R. *J. Chem. Phys.*, **1984**, *81*, 3684-3690.
- 32 Darden, T.; York, D.; Pedersen, L. *J. Chem. Phys.*, **1993**, *98*, 10089-10092.
- 33 Wang, H.; Liu, Y.; Huai, Q.; Cai, J.; Zoraghi, R.; Francis, S. H.; Corbin, J. D.; Robinson, H.; Xin, Z.; Lin, G.; Ke, H. *J. Bio. Chem.*, **2006**, *281*, 21469-21479.
- 34 (a) Alexov, E. *Eur. J. Biochem.*, **2004**, *271*, 173-185. (b) Schaefer. M.; Sommer, M.; Karplus, M. *J. Phys. Chem.*, **1997**, *101*, 1663-1683. (c) Antosiewicz, J.; McCammon, J. A.; Gilson, M. K. *J. Mol. Biol.*, **1994**, *238*, 415-436. (d) Pujato, M.; Navarro, A.; Versace, R.; Mancusso, R.; Ghose, R.; Tasayco, M. L. *Biochimica. Biophysica. Acta.*, **2006**, *1764*, 1227-1233. (e) Thomas, P. G.; Russell, A. J.; Fersht, A. R. *Nature*, **1985**, *318*, 375-376.
- 35 Gursky, O.; Badger, J.; Li, Y.; Caspar, D. L. *Biophys. J.*, **1992**, *63*, 1210-1220.
- 36 (a) Murthy, J. N.; Nagaraju, M.; Sastry, G. M.; Rao, A. R.; Sastry, G. N.; *J. Comp. Aided Mol. Design.*, **2005**, *19*, 857-870. (b) Altun, A.; Guallar, V.; Friesner, R. A.; Shaik, S.; Thiel, W. *J. Am. Chem. Soc.*, **2006**, *128*, 3924-3925. (c) Kumar, D.; Hirao, H.; Shaik, S.; Kozlowski, P. M. *J. Am. Chem. Soc.*, **2006**, *128*, 16148-16158.
- 37 (a) Lide, D. R. *Handbook of Chemistry and Physics*; 84th ed.; CRC press: Boca Raton, FL, **2003**. (b) Thurlkill, R. L.; Grimsley, G. R.; Scholtz. J. M.; Pace, C. N. *Protein Science*, **2006**, *15*, 1214–1218. (c) Dawson, R. M. C.; Elliot, D. C.; Elliot, W. H.; Jones, K. M. *Data for Biochemical Research*, 3rd ed.; Clarendon Press: Oxford, **1995**. (d) Bombarda, E.; Morellet, N.; Cherradi, H.; Spiess, B.; Bouaziz, S.; Grell, E.; Roques, B. P.; Mély, Y. *J. Mol. Biol.*, **2001**, *310*, 659-672. (e) Dudev, T.; Lim, C. *J. Am. Chem. Soc.*, **2002**, *124*, 6759-6766.

- 38 Noar, M. M.; Jenson, J. H. *Proteins: Structure, Function, and Bioinformatics*, **2004**, 57, 799-803.
- 39 (a) Marino, T.; Russo, N.; Tocci, E.; Toscano, M.; *J. Mass. Spectrom.*, **2001**, 36, 301-305. (b) Sapse, A-M. *Molecular Orbital Calculations For Amino Acids And Peptides*, Birkhäuser, Boston, **2000**.
- 40 Joseph, J.; Jemmis, E. D. *J. Am. Chem. Soc.*, **2007**, 129, 4620-4632.
- 41 Krier, M.; de Araújo-Júnior, J. X.; Schmitt, M.; Duranton, J.; Justiano-Basaran, H.; Lugnier, C.; Bourguignon, J.-J.; Rognan, D. *J. Med. Chem.*, **2005**, 48, 3816-3822.





Chapter 5

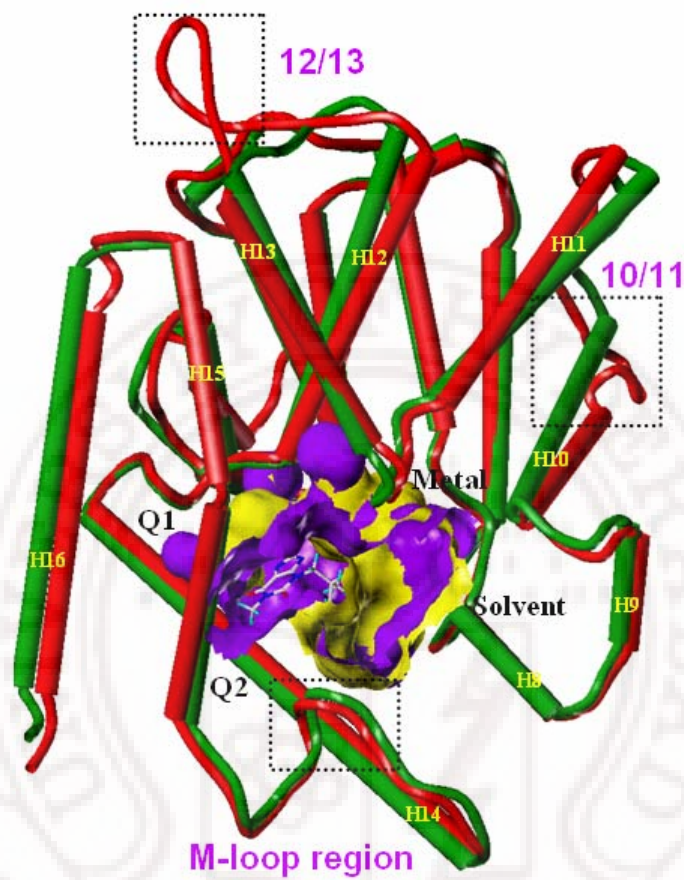
Molecular Insights for the Inhibitor Selectivity between
PDE4 and PDE7: Docking Study

Contents

5.1	Abstract	173
5.2	Introduction	174
5.3	Details of Computational Methods	178
5.4	Results and Discussions	179
5.4.1	Structural Comparison of PDE4 and PDE7	179
5.4.2	Docking	182
5.4.2.1	Substrate (cAMP)	182
5.4.2.2	Nonselective Inhibitor (IBMX)	183
5.4.2.3	PDE4 Inhibitors	184
5.4.2.4	PDE7 Inhibitors	188
5.4.2.5	Dual-Selective PDE4 and PDE7 Inhibitors	189
5.5	Conclusions	192
5.6	References	193

5.1 Abstract

PDE4D and PDE7A Structures



5.2 Introduction

Phosphodiesterase4 (PDE4) are ubiquitously distributed in mammalian inflammatory tissues and play a major role in cellular signaling by regulating 3',5'-cyclic adenosine monophosphate (cAMP) concentrations.¹⁻³ Although PDE4 is a focal target for inflammatory related diseases⁴ the dose limiting side effects of the PDE4 inhibitors hampered its development.⁵⁻⁶ As discussed in the earlier chapter for improving the therapeutic ratio and safety of the PDE4 inhibitors several strategies are proposed. They include (a) selectivity towards low affinity versus high affinity rolipram binding form, (b) low BBB permeable drugs, (c) disease activated drugs, (d) subtype selective PDE4 drugs, and (e) selectivity towards broader PDE family.⁶

Among them targeting the broader PDE family is the new hope of direction to overcome the side effects.⁷ This is rather a novel approach as it can enhance efficacy and eliminate off-target effects. Of the 11 PDE enzymes that have been unequivocally identified, dual-selective compounds that inhibit PDE4 as well as PDE1, PDE3, PDE5 or PDE7 could offer potential opportunities to enhance clinical efficacy.^{1a,9} Dual-selective inhibitors of PDE1C and PDE4 may target proliferating airways smooth muscle cells (that arrest remodeling process) and arrest inflammation (via PDE4 inhibition).^{1a,9} PDE3 and PDE4 dual-selective inhibitors may provide more bronchodilator and anti-inflammatory activity.^{1a,9} Inhibitors that block both PDE4 and PDE5 may possibly have beneficial effects on hypoxic pulmonary hypertension and vascular remodeling.^{1a,9} While dual-selective inhibitors of PDE4 and PDE7 were superior over others because of PDE7's isolation, characterization and tissue distribution in T-cells and inflammatory cells of asthma and COPD patients.¹⁰ The highly specific nature towards cAMP and its

distribution in proinflammatory and T-cells provoked PDE7 as new potential target for inflammatory and immunological diseases.^{11,12} While a cAMP-specific PDE8 is excluded due to its differential cellular distribution (**Table 5.1**).

PDE7 is coded by two genes (A and B) and have six isoforms so far.¹³ PDE7A is abundantly expressed in the lung and immune system where as PDE7B is enriched in pancreas, brain, heart, thyroid and skeletal muscle (**Table 5.1**). The catalytic activity of these subtypes PDE7A and PDE7B can be distinguished by sensitivity to the non selective PDE inhibitor isobutyl methyl xanthine (IBMX) and resistance to the PDE4 selective inhibitor rolipram.^{1a} On the other hand PDE4 subtypes (4B and 4D) almost have similar activity towards inhibitors (chapter 4).

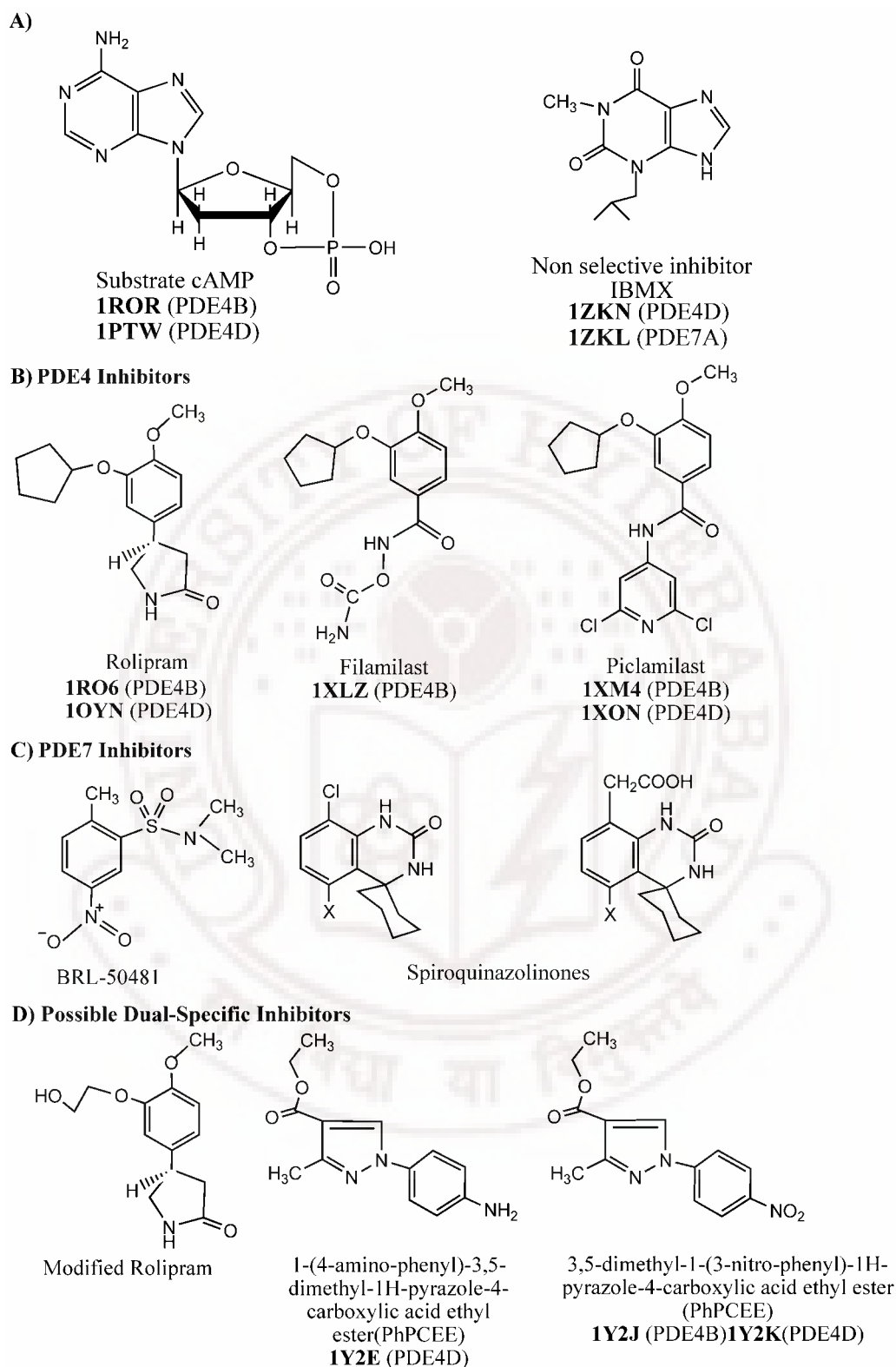
Table 5.1. The subtypes, isoforms, cellular distribution, regulatory function, inhibitors and available number of structures in PDB along with theoretical models (PDB ID labeled in italics) are mentioned for the cAMP specific phosphodiesterases PDE4, PDE7 and PDE8.

PDE	Subtypes	Iso-forms	Tissue expression	Regulatory function	Inhibitors	Number of Structures
4	4 (A, B, C, D)	20	Inflammatory cells	Asthma	Rolipramanalogs, Xanthine and Pyrazole analogs etc	39
7	2 (A, B)	4	Muscle, heart, brain, T-cells	Muscle, cell transduction	Etazolate, pyrimidines, thiadiazoles, Purine analogs, BRL-50481	1 (1ZKL) (<i>1LHQ</i>)
8	2 (A, B)	10	Endocrinal, neural	Alzhmeirs disease	Dipyrimidole	3 (3ECM, 3ECN) (<i>1LHW</i>)

There were about 60 X-ray crystal structures compromising nine PDE families (1-5, 7, 8, 9 and 10) deposited in protein data bank (PDB) in last ten years. These PDEs have

a common core catalytic domain with 300 amino acids and a compact α -helical structure consisting of 16 helices that can be divide into three subdomains.¹⁴ The crystal structures explain the mechanism of cAMP catalysis¹⁵ and substrate specificity (Glutamine switch mechanism),¹⁶ for each class of PDE family. For example PDE7A co-crystal structure explains nonselectivity towards rolipram is likely due to the steric interactions of cyclopentoxo group with Ile⁴¹² in the Q2 pocket¹⁷ and loss of crucial hydrogen bond between Gln⁴¹³ and Ser³⁷³ residues.¹⁸ Further site directed mutagenesis studies showed that the single mutations of S373Y, S377T and I412S in PDE7 or Y329S in PDE4 produce a several fold gain or loss of sensitivity to rolipram and mesopram.¹⁷ Although, inhibitor selectivity of PDE7 is explored there are some more questions puzzling such as (a) How does cAMP substrate bind to PDE7? (b) Why is PDE7A sensitive¹⁹ towards other rolipram analogs such as piclimilast cilomilast and flaminast? and (c) What are the crucial elements that control the inhibitor selectivity towards PDE4 and PDE7?

In view of the above questions and progress towards achieving the dual-specific PDE4-7 inhibitors,^{7,20} a molecular docking of the PDE4B, PDE4D and PDE7A X-ray crystal structures with substrate (cAMP),^{15,21} a nonselective inhibitor isobutyl methyl xanthine (IBMX),^{16,22} PDE4 inhibitors such as rolipram,^{17,21} piclimilast, cilomilast and PDE7 inhibitors such as BRL-50481,²³ spiroquinazolinones²⁴ are studied (**Scheme 5.1**). Autodock²⁵ is used for docking and the docked energies obtained are well correlated to specificity of the inhibitors. Based on the docking and active site exploration the modified rolipram and pyrazole analogs (**Scheme 5.1**) are further docked to understand the inhibitor selectivity for PDE4 and PDE7.



Scheme 5.1. Ligand structures that are docked to PDE4B, 4D and PDE7 proteins.

5.3 Details of Computational Methods

5.3.1 Preparation of Protein and Ligand for Docking: The X-ray crystal structures like catalytic domain 1F0J,^{26a} cAMP co-crystal structures 1ROR,^{26b} 1PTW,^{26c} Rolipram co-crystal structures 1RO6,^{26b} 1OYN^{26d} and IBMX co-crystal structures 1ZKN^{27a} and 1ZKL,¹⁷ pyrazole analogs 1Y2E, 1Y2J and 1Y2K respectively are downloaded from PDB.^{27b} The water molecules are excluded and ligands are extracted. The atom types of ligand are checked before adding all hydrogens and further assigned with Gasteiger-Huckel charges. These structures are minimized with conjugate gradient method with 0.01 derivative using Tripos force field and others settings are default as in SYBYL7.0.²⁸ BRL-50481, spiroquinazolinone ligands are drawn using SYBYL7.0 and minimized similarly to other ligands. The proteins have charged termini with only polar hydrogens been added. The proteins are assigned with Kollman-Uni charges and metals with Gasteiger-Huckel charges and are minimized with Powell method (0.05 gradient) using Tripos force field.

5.3.2 Preparation of GPF and DPF in AUTODOCK: ADT tools of Autodock 3.05 version is used for the ligand and protein input preparation as PDBQ file. A grid of 60x60x60 with grid center as the center of the ligand for the X-ray co-crystal structures is considered. The grid centers in the PDE4B (1F0J) protein structure is -0.414, 4.407, -10.849. The Zn atom is assigned as M parameter type with R_{ij} as 0.87 and ϵ_{ij} as 0.35 values. Lamarckian genetic algorithm is used for search of conformations as it is superior over simulated annealing procedure in reproducing various experimental structures.²⁹ 150 runs are carried out (ga_run =150) with population size of 100 in each run and with 50,000 energy evaluations. The GA run was for utmost 27000 generations

(ga_num_generations 27000) by preserving one as best in each generation (ga_elitism =1), mutation rate as 0.02, crossover rate as 0.8 and the GA's selection window to 10 generations are considered. The local search method of Solis and Wets algorithm was performed at 300 iterations.

5.4 Results and Discussions

5.4.1 Structural Comparison of PDE4 and PDE7

The catalytic domain of PDE7 has ~32% sequence identity with PDE4 and ~72% sequence identity with respect to the active site.^{1a} The secondary structural comparison of PDE4D and PDE7A show missing of only two 3_{10} -helices.¹⁷ The superimposition of Ca atoms of PDE4D and PDE7 X-ray structures have a 1.79 Å root mean square deviation. The most significant difference is the N-terminal portion of helix H11 has a positional displacement of 2.8 Å. While amongst the three loop regions (10/11, 12/13 and M-loop region) of PDE4, the ERK docking site (a β -turn, 12/13 region) is absent in PDE7. This suggests that there may be lack of protein–protein interactions in PDE7 (**Figure 5.1**).

The active site of PDE4 can be divided into three pockets²⁶ (a) a metal-binding pocket (M-pocket), (b) a solvent-filled side pocket (S-pocket), and (c) a pocket containing the purine-selective glutamine (Q-pocket). The M-pocket contains the two metal ions (Zn, Mg) and has highly conserved hydrophobic and polar residues which coordinate to the metal ions. The S-pocket consists mainly of hydrophilic amino acids and is filled with a network of water molecules. The Q-pocket consist of an glutamine that have hydrogen bond interactions with the ligand and is flanked by two asymmetrical hydrophobic sub pockets as Q1 and Q2 (**Figure 5.1**).

Out of the 31 active site residues that are lining the three pockets of PDE4 only eleven residues are different in PDE7 (**Table 5.2**).¹⁹ Most of these varying residues are seen in Q2 pocket and belong to helix 14 (**Figure 5.1**). All the metal interacting histidines and aspartic acids are conserved. Thus mechanism¹⁵ for the catalytic function may remain similar in PDE4 and PDE7. There is only one residue different (Asn²⁶⁰/Ser²⁰⁸) in solvent binding pocket and its significance is reported recently.³⁰

Table 5.2. The active site residues of PDE4B, PDE4D and PDE7A are tabulated.

Pocket Type	PDE4B	PDE4D	PDE7A
Metal binding	His ²³⁴ , His ²³⁸ , His ²⁷⁴ , Asp ²⁷⁵ , His ²⁷⁸ , Asn ²⁸³ , Leu ³⁰³ , Glu ³⁰⁴ , Asp ³⁴⁶ , Met ³⁴⁷ , Asp ³⁹²	His ¹⁶⁰ , His ¹⁶⁴ , His ²⁰⁰ , Asp ²⁰¹ , His ²⁰⁴ , Asn ²⁰⁹ , Leu ²²⁹ , Glu ²³⁰ , Asp ²⁷² , Met ²⁷³ , Asp ³¹⁸	His ²¹² , His ²¹⁶ , His ²⁵² , Asp ²⁵³ , His ²⁵⁶ , Gln²⁶¹ , Leu ²⁸¹ , Glu ²⁸² , Asp ³²² , Leu³²³ , Asp ³⁶²
Solvent binding	Gly ²⁸⁰ , Ser ²⁸² , Glu ⁴¹³ , Gln ⁴¹⁷ , Ser ⁴²⁹ , Cys ⁴³²	Gly ²⁰⁶ , Ser ²⁰⁸ , Glu ³³⁹ , Gln ³⁴³ , Ser ³⁵⁵ , Cys ³⁵⁸	Gly ²⁵⁸ , Asn²⁶⁰ , Glu ³⁸³ , Gln ³⁸⁸ , Ser ³⁹⁹ , Cys ⁴⁰²
Gln residue (as Q), Q1 and Q2 pocket	Tyr ²³³ , Leu ³⁹³ , Asn ³⁹⁵ , Pro ³⁹⁶ , Tyr ⁴⁰³ , Trp ⁴⁰⁶ , Thr ⁴⁰⁷ , Ile ⁴¹⁰ , Met ⁴¹¹ , Phe ⁴¹⁴ , Met ⁴³¹ , Val ⁴³⁹ , Ser ⁴⁴² , Gln ⁴⁴³ , Phe ⁴⁴⁶	Tyr ¹⁵⁹ , Leu ³¹⁹ , Asn ³²¹ , Pro ³²² , Tyr ³²⁹ , Trp ³³² , Thr ³³³ , Ile ³³⁶ , Met ³³⁷ , Phe ³⁴⁰ , Met ³⁵⁷ , Val ³⁶⁵ , Ser ³⁶⁸ , Gln ³⁶⁹ , Phe ³⁷²	Tyr ²¹¹ , Ileu³⁶³ , Asn ³⁶⁵ , Pro ³⁶⁶ , Ser³⁷³ , Trp ³⁷⁶ , Ser³⁷⁷ , Val³⁸⁰ , Thr³⁸¹ , Phe ³⁸⁴ , Leu⁴⁰¹ , Ile⁴⁰⁹ , Ile⁴¹² , Gln ⁴¹³ , Phe ⁴¹⁶

The replacement of Tyr³²⁹ in PDE4D to Ser³⁷³ residue has increased the size of the Q1 pocket (lined by Phe⁴¹⁶, Ser³⁷³, Pro³⁶⁶ and Ile³⁶³) in PDE7 (**Figure 5.1**) and has changed the hydrogen bonding interactions of glutamine residue in Q-pocket. In PDE7A the CO group of Gln residue is forming hydrogen bond with Ser³⁷⁷ residue¹⁷ and in PDE4D it is forming with Tyr³²⁹. The replacement of Ile³³⁶, Met³³⁷ and Ser³⁶⁸ residues in PDE4D to Val³⁸⁰, Thr³⁸¹ and Ile⁴¹² respectively in the PDE7 has decreased the size of the

Q2 pocket. It may also reduce hydrophobic interactions with the inhibitors or create a hydrophilic environment due to Thr³⁸¹ residue in PDE7 (**Figure 5.1**). Further Met³⁵⁷ and Val³⁶⁵ residues that are present on the surface of Q2 pocket (in the M-loop region) are also varied to Leu⁴⁰¹ and Ile⁴⁰⁹ residues in PDE7 and can also alter the shape of the Q2 pocket (**Table 5.2**).

In summary, the structural comparison of PDE4 and PDE7 shows a major change in the Q1 and Q2 pocket architectures but have a conserved metal and solvent binding pocket (**Figure 5.1**). To further characterize about the active site, docking studies of the substrate (cAMP) and inhibitors (IBMX, Rolipram and BRL-50481) are performed.

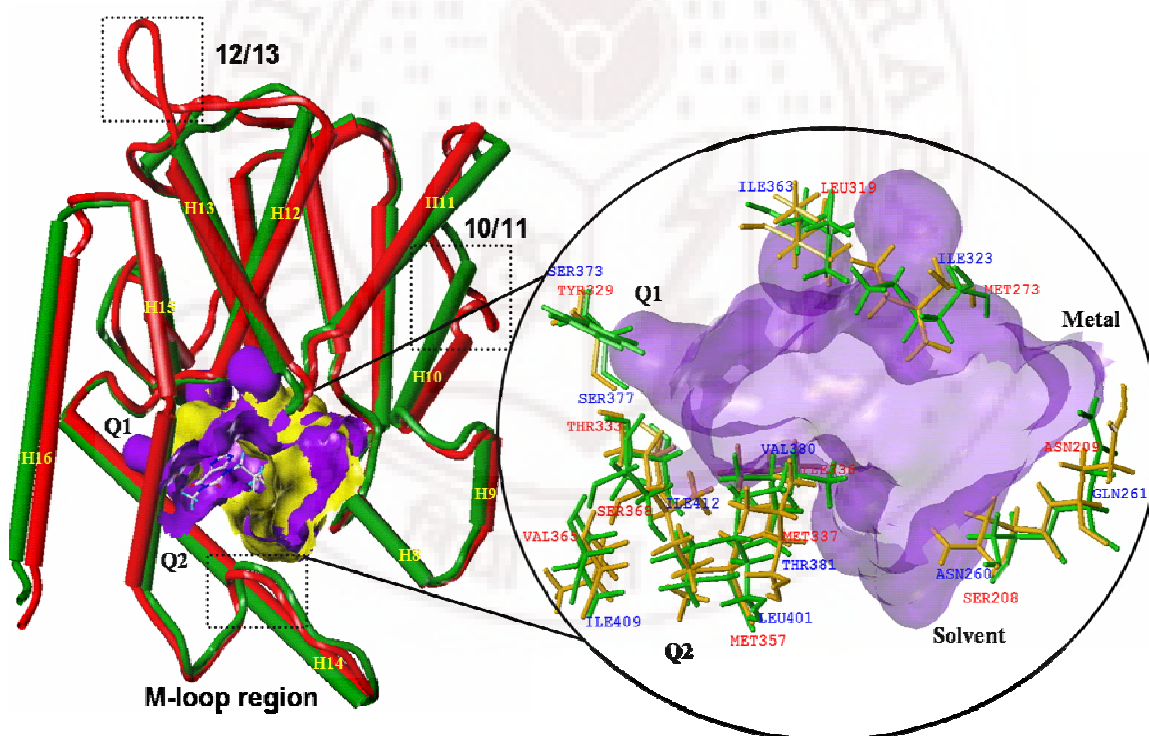


Figure 5.1. The protein structure of PDE4D is displayed in red color and PDE7A is in green color. The yellow and purple colors represent fast Connolly channel surface for PDE4D and PDE7A structures respectively. The IBMX ligand in the active site is shown in ball and stick.

5.4.2 Docking

The docking studies are promising tools in rational drug design as it helps in enlightening the type of interactions existing between the enzyme and ligands. The docking results with substrate specific cAMP, nonselective inhibitor IBMX, PDE4 specific inhibitor rolipram and PDE7 specific inhibitors such as BRL-50481 and spiroquinazolinones are discussed. Later modified rolipram and pyrazole analogs that have shown comparable binding affinity towards PDE4 and PDE7 are presented.

5.4.2.1 Substrate (cAMP)

The adenine moiety of the cAMP adopts an *anti* conformation and orients to the hydrophobic pocket made up of residues Tyr¹⁵⁹, Leu³¹⁹, Asn³²¹, Thr³³³, Ile³³⁶, Gln³⁶⁹ and Phe³⁷². In all X-ray crystal structures, adenine moiety forms two hydrogen bonds with each side chains of Gln³⁶⁹ and Asn³²¹ and one with Tyr¹⁵⁹ residue.^{15,21} The bicyclic (adenine) ring also has stacking interactions with Ile³³⁶ and Phe³⁷² residues. While ribose sugar stacks with Tyr¹⁵⁹ residue and has van der Waal's contacts with residues His¹⁶⁰, Met²⁷³, Ile³³⁶ and Phe³⁴⁰. The phosphate group of cAMP coordinates with both metal ions and forms hydrogen bonds with His¹⁶⁰ and Asp²⁰¹ residues. Similar types of interactions are found when the cAMP is docked to PDE4B, 4D and 7A (1F0J, 1ROR, 1PTW and 1ZKN) structures (**Figure 5.2**). The docked conformation in 4B (1ROR) and 4D (1PTW) are similar to its X-ray crystal conformation with a RMS deviation of 1.38 and 0.98 Å and shows high clustering among various sampled (**Table 5.3**). In spite of variations such as Ser³⁶² to Ile⁴¹² and Tyr³²⁹ to Ser³⁷³ residues in the Q1 and Q2 pocket of PDE7 the Gln⁴¹³ conformation is maintained because CO group of Gln forms hydrogen bond with OH group of Ser³⁷⁷ and Thr³⁸¹. So the variation of Tyr³²⁹/Ser³⁷³ residue does not

influence the binding mode of cAMP. The similar interactions of phosphate group in metal-pocket as PDE4 indicate possibility of similar mechanism for cAMP catalysis (Figure 5.2).

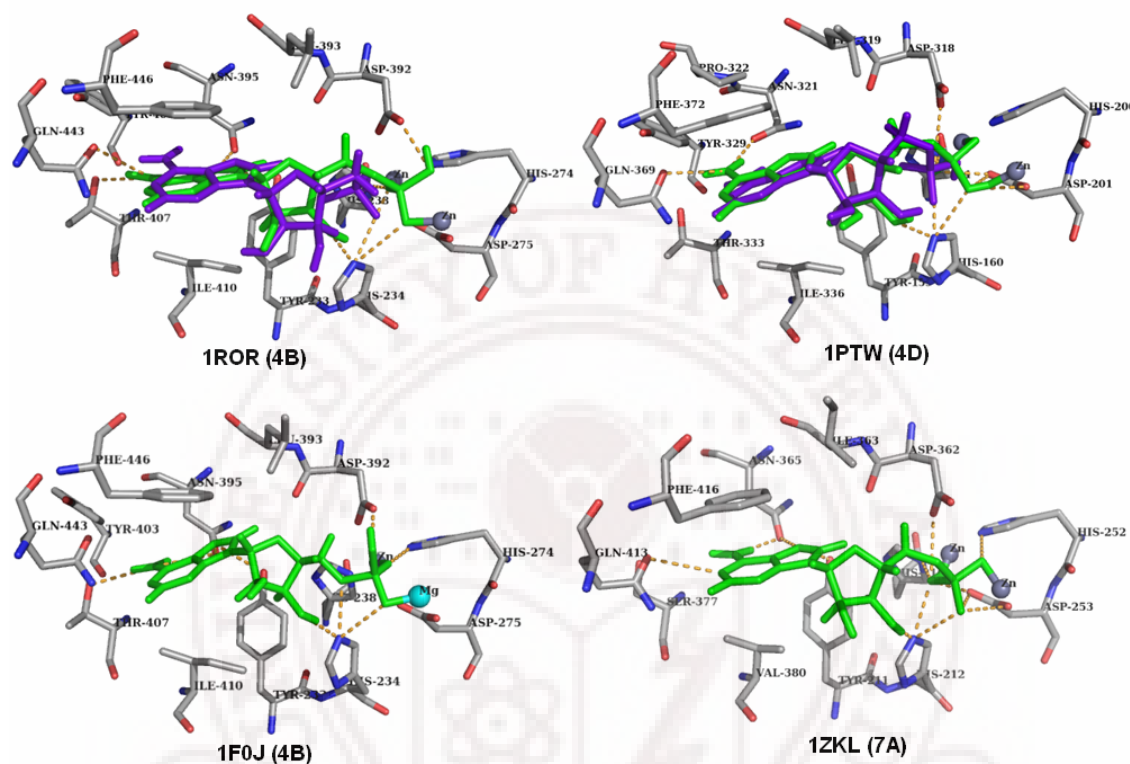


Figure 5.2. The active site residues of 1ROR, 1PTW, 1F0J and 1ZKL with cAMP are shown. The crystal and docked conformations of the ligand are in violet and green color capped sticks. The hydrogen bonding interactions with protein residues are shown in orange color.

5.4.2.2 Nonselective Inhibitor IBMX (Isobutyl Methyl Xanthine)

IBMX is a purine analog (**Scheme 5.1**) and is a weak nonselective inhibitor of the PDE4 and the PDE7A. IBMX is nonselective because it binds at common core of active site pocket and interacts with highly conserved residues of all PDEs. The six membered ring of this ligand has hydrogen bond donors and acceptors similar that of cGMP. The purine analog shows hydrogen-bonding interactions with Gln³⁶⁹, Asn³²¹ and Tyr¹⁵⁹

residues and stacking interactions with Phe³⁷² residue. The isopropyl group of IBMX has hydrophobic interactions with Tyr¹⁵⁹, His¹⁶⁰ and Ile³³⁶ residues in the PD4D crystal structure.^{17,22} The docking of IBMX to PDE4B, 4D and 7A (1F0J, 1ZKN and 1ZKL) have shown slight difference in similar hydrogen bond, stacking interactions and different orientation of isopropyl group (**Figure 5.3**). In the docked conformation bicyclic ring is displaced to deep into pocket and isopropyl group orients towards Ile³³⁶/Val³⁸⁰ in the PDE7 and towards the Met³⁴⁷ in PDE4B for hydrophobic interactions. The change in positions of hydrogen bonding acceptors and donors of the IBMX with respect to cAMP results in lesser number of interactions and lower docked energies. Thus indicate its weak binding similar to cGMP for these proteins.

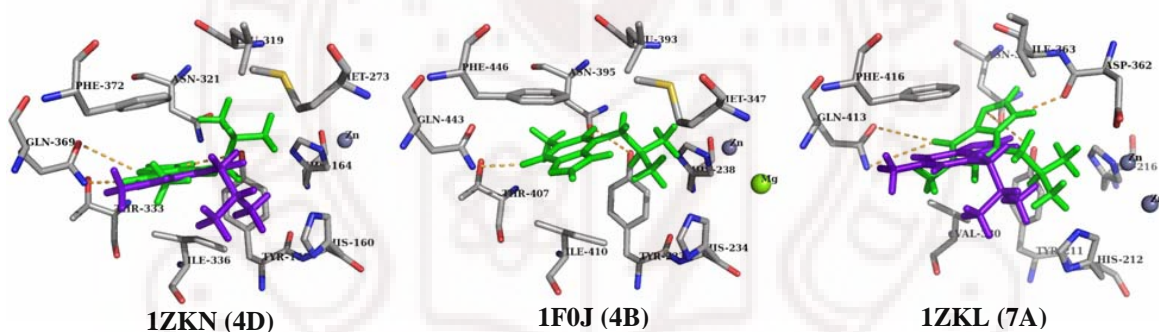


Figure 5.3. The active site residues of 1F0J, 1ZKN and 1ZKL are shown with IBMX ligand. The crystal and docked conformations of the ligand are in violet and green color capped sticks. The hydrogen bonding interactions with protein residues are shown in orange color

5.4.2.2 PDE4 Inhibitors

Rolipram is the first PDE4 specific inhibitor. The keen interactions in binding mode of rolipram are hydrogen-bonding interactions of the alkoxy oxygen atoms with Gln³⁶⁹ residue, stacking interactions of benzene with Phe³⁷² residue and pyrrolidine with Tyr¹⁵⁹ residue,^{17,21} and the hydrophobic interactions of cyclopentoxy group with Ile³³⁶,

Met³³⁷, Phe³⁴⁰ and Met³⁵⁷ residues in the Q2 pocket¹⁷ and methoxy group with Tyr⁴⁰³, Pro³⁹⁶ residues in the Q1 pocket. Rolipram does not interact with the divalent metals.

Table 5.3. The docked and intermolecular energies are mentioned in kcal/mole. The estimated inhibitors binding constant (Ki) and number of conformations in the cluster are tabulated for the PDE4B, PDE4D and PDE7A crystal structures that are docked with ligands cAMP, IBMX, rolipram, filaminast, piclimilast, BRL-50481, spiroquinazolinones, modified rolipram and pyrazole analogs respectively.

PDB ID	PDE type	Ligand	Docked energy	Inter-molecular Energy	K _i	Cluster Size
1F0J	4B	cAMP	-14.45	-14.55	1.76x10 ⁻¹⁰	29
1ROR	4B		-12.31	-10.81	5.79x10 ⁻⁸	75
1PTW	4D		-12.34	-12.20	9.36x10 ⁻⁹	102
1ZKL	7A		-12.83	-12.62	4.59x10 ⁻⁹	81
1F0J	4B	IBMX	-6.39	-6.24	7.59x10 ⁻⁵	20
1ZKN	4D		-7.70	-7.64	7.21x10 ⁻⁶	54
1ZKL	7A		-7.64	-7.45	9.93x10 ⁻⁶	100
1F0J	4B	Rolipram	-8.42	-9.48	9.17x10 ⁻⁷	70
1RO6	4B		-9.31	-10.08	3.37x10 ⁻⁷	127
1OYN	4D		-9.02	-10.10	3.16x10 ⁻⁷	88
1ZKL	7A		-4.26	-9.4	1.06x10 ⁻⁶	11
1XLZ	4B	Filaminast	-11.37	-11.52	8.46x10 ⁻⁸	33
1ZKL	7A		-10.09	-9.9	1.30 x10 ⁻⁶	69
1XM4	4B	Piclimilast	-10.89	-11.06	7.83x10 ⁻⁹	138
1XON	4D		-10.58	-10.75	1.33x10 ⁻⁸	34
1ZKL	7A		-10.32	-10.18	8.13x10 ⁻⁷	34
1F0J	4B	BRL-50481	-6.91	-7.01	3.54 x10 ⁻⁵	31
1ZKL	7A		-8.15	-8.18	4.91 x10 ⁻⁶	39
1F0J	4B	Spiroquinazolinones	-11.10	-11.14	3.29x10 ⁻⁸	54
1ZKL	7A		-10.87	-11.07	3.73x10 ⁻⁸	140
1F0J	4B	Modified rolipram	-7.72	-8.54	7.56x10 ⁻⁶	52
1OYN	4D		-7.98	-8.85	4.47 x10 ⁻⁶	43
1ZKL	7A		-7.89	-8.84	4.57 x10 ⁻⁶	132
1Y2E	4D	Para-aminoPhPCEE	-9.13	-9.08	1.79x10 ⁻⁶	57
1ZKL	7A		-9.45	-9.66	6.84 x10 ⁻⁷	105
1Y2K	4D	Meta-nitro PhPCEE	-9.26	-9.28	1.29 x10 ⁻⁶	70
1Y2J	4B		-9.06	-9.18	2.57 x10 ⁻⁶	27
1ZKL	7A		-7.87	-9.80	9.06 x10 ⁻⁷	66

The docking of this ligand to the PDE4B, 4D and 7A (1F0J, 1RO6 and 1OYN) has similar binding mode as X-ray structures with RMS deviation of 1.03 and 0.75 Å (**Figure 5.4**). In the case of PDE4B catalytic domain (1F0J) the docking pose has close resemblance to binding mode of 4B (1RO6). While the lowest docked conformation of PDE7 has pushed cyclopentoxy group away from the Q2 pocket. This is likely due to (a) unfavorable steric interaction of Ile⁴¹² and (b) less hydrophobic nature of Val³⁸⁰ and Thr³⁸¹ residues in the Q2 pocket.¹⁷ This also results in loss of hydrogen bond between dialkoxy atoms of rolipram to Gln⁴¹³ residue. These variations of Q2 pocket explain its reduced interactions, low docked energy (-4.26 kcal/mole) and insensitivity towards rolipram (**Table 5.3**). As the variation of residues alter the size, shape and nature of Q2 pocket may be less hydrophobic group such as CH₃, or hydrophilic groups such as CF₃, CH₂CH₂OH could increase binding affinity towards the PDE7 protein.

On the other hand the second generation rolipram analogs like flaminast, piclimilast and cilomilast also have 3,4-dialkoxyphenyl (catechol) pharmacophore but with variation of substituents (**Scheme 5.1**). All these ligands have similar interactions and cyclopentoxy group is present in Q2 pocket. The improved affinity of them over rolipram is because they reach deep into M-pocket and have electrostatic interactions with metal ions and mediated hydrogen bonds through water molecules to the residues.¹⁹ Docking of flaminast and piclimilast have shown similar binding mode but slight variation in placing substituents of catechol in PDE4. In PDE7 these ligands conformation indicate again a shift of cyclopentoxy group from Q2 pocket and loss of crucial hydrogen bond with Gln⁴¹³ residue but there is gain in electrostatic interactions with metal ions. Unlike rolipram, these ligands still have comparable docked energies

5.4.2.4 PDE7 inhibitors

There are various classes of the PDE7 specific inhibitors developed in the recent times. They are BRL-50481, benzothiadiazines,³² purine analogs,³³ thiadiazoles,³⁴ spiroquinazolinones²⁴ etc. BRL-50481 (Benzene sulphanamide, **Scheme 5.1**) has a secondary amine with methyl substitutions, which can have hydrophobic interactions. The oxygen atoms of the SO₂ and NO₂ groups of the ligand can act as hydrogen bond acceptors and benzene ring can have stacking interactions with the residues of protein. Docking of this inhibitor revealed absolutely different docking conformations for PDE4B and PDE7 where it is placed in Q pocket for PDE4B and in M-pocket for PDE7. In PDE4B, there are two hydrogen bonding interactions (oxygen atom of SO₂ group has hydrogen bond with NH group of Gln⁴⁴³ residue, NO₂ group of the ligand is placed in the solvent pocket), a hydrophobic interactions of secondary amine alkyl groups with residues of the Q1 pocket and stacking interactions of benzene ring with Phe³⁷² residue. In contrast PDE7 has the NO₂ group facing towards Asn³⁶⁵, and SO₂ group and its secondary amine are in metal binding pocket surrounded by His²¹², His²¹⁶ residues and Zn metal (**Figure 5.5**). The difference in docked energies of PDE4B and PDE7A is due to strong electrostatic interactions of ligand in PDE7 which explain its selectivity to PDE7 (**Table 5.3**).

Spiroquinazolinones also have bicyclic ring similar to IBMX (**Scheme 5.1**). Docking of this ligand to the PDE4B (1F0J) and PDE7A crystal structures indicated similar binding mode and interactions. The docked conformation has a hydrogen bonding interaction with Cl atom and NH group of ligand with Asn³²¹ and Asp³¹⁸ residues in the active site of the PDE4 and PDE7 protein. The replacement of Cl atom with CH₂COOH

has preserved its placement in the Q2 pocket. This supports that the shape of Q2 pocket is governing factor for the selectivity of PDE4 and PDE7 inhibitors. There is no significant change in docked energies between PDE4 (-11.10) and PDE7 (-10.87) (**Table 5.3**). Further to gain insight of inhibitor selectivity to PDE7 may be water molecules inside the protein should be considered.

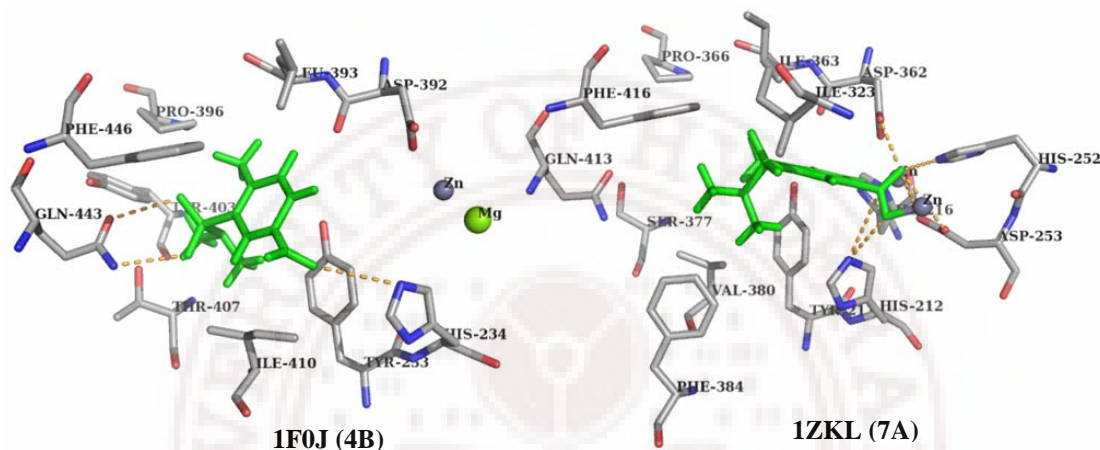


Figure 5.5. The active sites of 1F0J and 1ZKL with BR1-50481 ligand are shown. The docked conformation of the ligand is in green color capped sticks. The hydrogen bonding interactions with protein residues are shown in orange color.

5.4.2.5 Dual-Selective PDE4 and PDE7 Inhibitors

There are several dual-specific PDE4 and PDE7 inhibitors reported in the recent years.³⁵ But the main difference that we observed in the PDE4 and the PDE7 active sites from structural comparison (MOLCAD surfaces) and docking studies is the shapes of the Q1 and Q2 pocket. PDE4 has smaller Q1 and bigger Q2 pockets and PDE7 due to variations of residues (Tyr³²⁹/Ser³⁷³, Ser³⁶⁸/Ile⁴¹², Ile³³⁶/Val³⁸⁰ and Met³⁷⁷/Thr³⁸¹) has slightly bigger Q1 and smaller Q2 pockets. These variations also affected the size, shape and nature of pockets. In order to understand the influences of Q1 and Q2 pockets less

hydrophobic substituents of ligands are been docked such as modified rolipram and pyrazole analogs.

Modified Rolipram structure: It has replacement of cyclopentoxo group with the $\text{CH}_2\text{CH}_2\text{OH}$ (**Scheme 5.1**). Unlike rolipram, docking of this ligand to the PDE4B, 4D and 7A (1F0J, 1OYN and 1ZKN) protein structures indicated smaller differences in docking energies (**Table 5.3**). The docked conformations of PDE4B and 4D have similar catechol scaffold interactions, but $\text{CH}_2\text{CH}_2\text{OH}$ is placed in the Q2 pocket and Q1 pocket for PDE4D and PDE4B respectively. The $\text{CH}_2\text{CH}_2\text{OH}$ group of ligand in 4D gains only hydrophobic interactions and PDE4B has gained two more hydrogen bonds (CO group of Gln⁴⁴³ residue and with OH group of Thr⁴⁰⁷ residue). The docked conformation of PDE7 has $\text{CH}_2\text{CH}_2\text{OH}$ group in the Q1 pocket and gains hydrogen bond with Gln⁴¹³ residue and improved the binding affinity. This is expected due to alteration in size of the pockets (**Figure 5.6**).

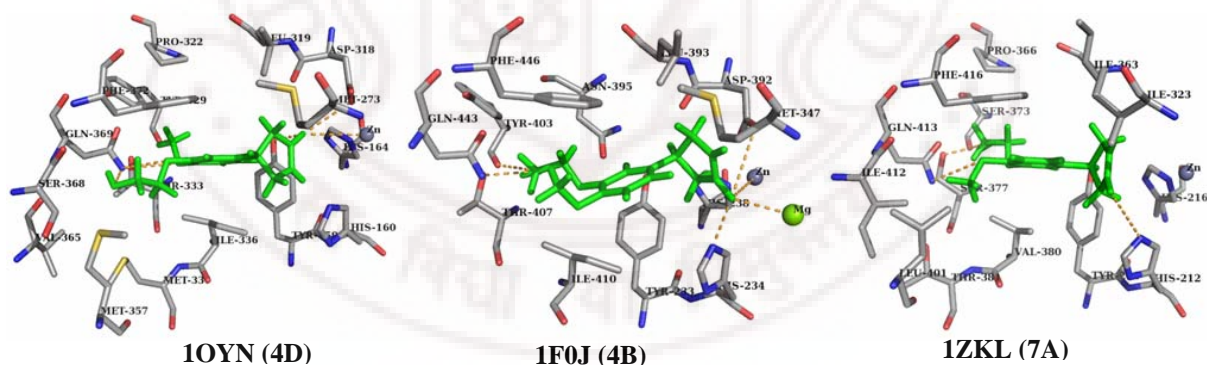


Figure 5.6. The active site residues of 1F0J, 1OYN and 1ZKL are shown with modified rolipram ligand. The docked conformation of the rolipram ligand is in green color capped sticks. The hydrogen bonding interactions with protein residues are shown in orange color.

Pyrazole analogs: The pyrazole analogs PhPCEE (3,5-dimethyl-1-phenyl-1H-pyrazole-4-carboxylic acid ethyl ester) are the new class of PDE4 inhibitors that are designed

based on scaffold based drug design (**Scheme 5.1**).^{27b} The carboxy group of the ligand form hydrogen bonds with Gln³⁶⁹ residue and pyrazole and the phenyl ring have stacking interactions with Phe³⁷² and Tyr¹⁵⁹ residues similar to rolipram. The difference in the substitution of phenyl group at para and meta position of pyrazole analog has influenced the binding affinity³⁶ to PDE4B and PDE4D. This is because the nitro group in M-pocket gains electrostatic interactions and para-amino group is instead in solvent pocket.¹⁷

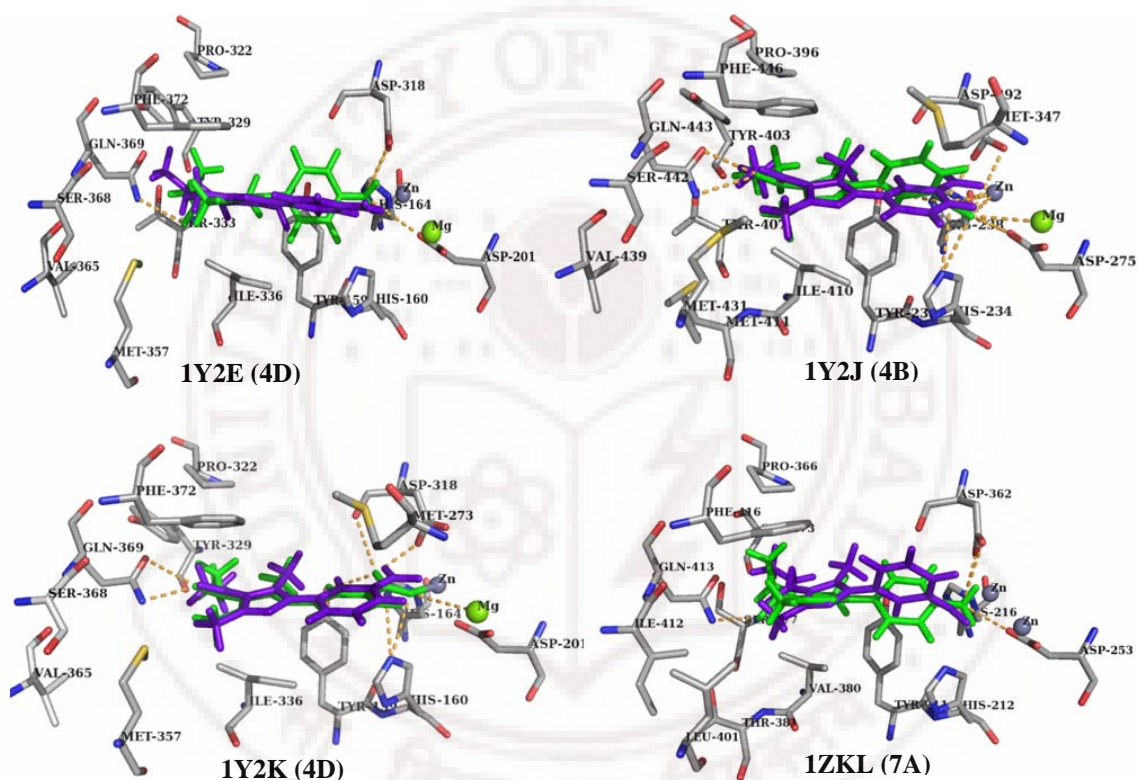


Figure 5.7. The active site residue of 1Y2E is with para amino PHCEE ligand, 1Y2J and 1Y2K are with meta-nitro PHCEE ligand and 1ZKL with both ligands are shown. The crystal and docked conformations of the ligand are in violet and green color capped sticks rendering. The hydrogen bonding interactions with protein residues are shown in orange color.

In contrast to rolipram, hydrophobic interactions are only due to ethoxy group with residues in the Q1 pocket and CH₃ group with residues of Q2 pocket. CH₃ group has reducing hydrophobic interactions in the Q2 pocket as compared to rolipram analogs.

Thus, these are docked to test its affinity towards the PDE7A. The PDE4B and 4D (1Y2J, 1Y2E and 1Y2K) crystallized with these ligands and the PDE7A are docked with these two PhPCEE analogs. The docked conformation has similar binding mode as in crystal structures of the PDE4B and 4D (1Y2J, 1Y2E and 1Y2K) with RMSD of 1.96, 1.39 and 1.43Å respectively. The docked energies of the PDE7 are comparable to the PDE4 structures. The docked conformation also shows that ethoxy group is placed in the Q1 pocket and CH₃ in the Q2 pocket (**Figure 5.7**).

5.5 Conclusions

A molecular docking of the PDE4 and PDE7 structures with the cAMP, IBMX, rolipram and BRL-50481 ligands were studied using AUTODOCK. The crystal structures deposited with cAMP, rolipram, piclamilast and fluminast were reproducible. The docked energy values are also well correlated to its specificity. The factors influencing the cAMP binding in PDE7 was due to the maintenance of Gln^{443/413} conformation similar to that in PDE4 and conservation of the metal binding residues. The small difference in docking energies of rolipram analogs and spiroquinazolinones cannot explain the selectivity as external conditions, water and peripheral residues can also influence binding. While the inhibitor selectivity of rolipram was due to the change in size and nature of the Q1 and Q2 pocket due to Tyr³²⁹/Ser³⁷³ and Ser³⁶⁸/Ile⁴¹² and Ile³³⁶/Val³⁸⁰, Met³³⁷/Thr³⁸¹ residues. In view of these changes in pocket a modified rolipram structure where cyclopentoxo group is replaced by CH₂CH₂OH and pyrazole ligand has been docked and it indicate increase in the binding affinity of the PDE7 and reduction in the affinity for PDE4. The docked energies of these ligands have very small difference between PDE4 and PDE7. This supports the hypothesis that an optimized hydrophobic

group in the Q2 pocket is parameter to obtain a PDE4, PDE7 or dual specific PDE4-7 inhibitors.

5.6 References

1. (a) Beavo, J. A.; Francis, S. H.; Houslay, M. D. *Cyclic Nucleotide Phosphodiesterases in Health and Disease*, **2007**, 195-203. (b) Sharron, H. F.; Illarion, V.T.; Jackie, D. C. *Prog. Nucleic Acid Res Mol Biol.*, **2001**, 65, 1-52.
2. (a) Houslay, M. D.; Milligan, G. *Trends. Biochem. Sci.*, **1997**, 22, 217-224. (b) Houslay, M. D.; Sullivan, M.; Bolger, G. B. *Adv. Pharmacol.*, **1998**, 44, 225-343.
3. (a) Soderling, S. H.; Beavo, J. A. *Curr. Opin. Cell. Biol.*, **2000**, 12, 174-179. (b) Beavo, J. A. *Physiol. Rev.*, **1995**, 75, 725-748.
4. (a) Teixeira, M. M.; Gristwood, R. W.; Cooper N.; Hellewell. P. G. *Trends Pharmacol. Sci.*, **1997**, 18, 164-171. (b) Spina, D.; Landells, L. J.; Page, C. P, *Adv. Pharmacol.*, **1998**, 44, 33-89. (c) Trophy, T. J. *Am. J. Respir. Crit. Care. Med.*, **1998**, 157, 351-370. (d) Zheng, H.; Joseph, A. M. *Curr. Med. Chem.*, **2006**, 10, 3253-3262. (e) Jeffery, P. *Pul. Pharma. Therap.*, **2005**, 18, 9-17.
5. (a) Trophy, T. J.; Page, C. P. *Trends. Pharmacol. Sci.*, **2000**, 21, 158-159. (b) Lipworth, B. J. *Lancet*, **2005**, 365, 167-175. (c) Spina, D.; *Curr. Drug. Targ. Inflamm. Allergy*, **2004**, 3, 231-246.
6. (a) Zhang, K. Y. J.; Ibrahim, P. N.; Gillette, S.; Bollag, G. *Exp. Opin. Ther. Drugs*, **2005**, 9, 1283-1304. (b) Houslay, M. D.; Schafer, P.; Zhang, K. Y. J. *Drug Disc. Today*, **2005**, 10, 1503-1519. (c) Srivani, P.; Usharani, D.; Jemmis, E. D.; Sastry, G. N. *Curr. Pharm. Design*, **2008**, 14, 3854-3872.
7. Giembycz, M. A. *Curr. Opin. Pharm.*, **2005**, 5, 238-244.
8. Chung, K. F. *Eur. J. Pharm.*, **2006**, 533, 110-117.

9. (a) Jones, N. A.; Leport, M.; Holand, T.; Vos, T.; Morgan, M.; Fink, M.; Pruniaux, M-P.; Berthelie, C.; O'Connor, B. J.; Bertrand, C.; Page, C. P. *Pulm. Pharma. Therap.*, **2007**, *20*, 60-68. (b) Giembycz, M. A.; Smith, S. J, *Curr. Pharma. Design*, **2006**, *12*, 3207-3220. (c) Castro, A.; Jerez, M. J.; Gil, C.; Martinez, A. *Med. Res. Rev.*, **2005**, *25*, 229-244.
10. Li, L.; Yee, C.; Beavo, J. A. *Science*, **1999**, *283*, 848-850.
11. (a) Smith, S. J.; Brookes-Fazakerley, S.; Donnelly, L. E.; Barnes, P. J.; Barnette, M. S.; Giembycz, M. A; *Am. J. Physiol. Lung. Cell. Mol. Physiol.*, **2003**, *284*, L279-L289. (b) Lee, R.; Wolda, S.; Moon, E.; Esselstyn, J.; Hertel, C.; Lerner, A. *Cell. Sig.*, **2002**, *14*, 277-284. (c) Giembycz, M. A.; Smith, S. J. *Drugs for Future*, **2006**, *31*, 207-229. (d) Jones, N. A.; Leport, M.; Holand, T.; Vos, T.; Morgan, M.; Fink, M.; Pruniaux, M.-P.; Berthelie, C.; O'Connor, B. J.; Bertrand, C.; Page, C. P. *Pharma. Therap.*, **2007**, *20*, 60-68.
12. (a) Perez-Torres, S.; Cortes, R.; Tolnay, M.; Probst, A.; Palacios, J. M.; Mengod, G. *Exp. Neurol.*, **2003**, *182*, 322-334. (b) Miro, X.; Perez-Torres, S.; Palacios, J. M.; Puigdomenech, P.; Mengod, G. *Synapse*, **2001**, *40*, 201-214. (c) Sasaki, T.; Kotera, J.; Omori, K. *Biochem J.*, **2002**, *361*, 211-220.
13. (a) Sasaki, T.; Kotera, J.; Yuasa, K.; Omori, K. *Biochem. Biophys. Res. Comm.*, **2000**, *271*, 575-583. (b) Barnette, M. S.; Giembycz, M. A.; Smith, S. J.; Fazakerley, S. B.; Donnelly, L. E.; Barnes, P. J. *Am. J. Physiol. Lung. Cell. Mol. Physiol.*, **2006**, *284*, 279-289. (c) Nakata, A.; Ogawa, T.; Sasaki, T.; Koyama, N.; Wada, K.; Kotera, J.; Kikkawa, H.; Omori, K.; Kaminuma, O. *Clin. Exp. Immunol.*, **2002**, *128*, 460-466.

14. (a) Jeon, Y. H.; Heo, Y. S.; Kim, C. M.; Hyun, Y. L.; Lee, T. G., Ro, S.; Cho, J. *M. Cell. Mol. Life Sci.*, **2005**, 62, 1198-1220. (b) Ke, H.; Wang, H.; *Curr. Top. Med. Chem.*, **2007**, 7, 391-403.
15. Huai, Q.; Colicelli, J.; Ke, H. *Biochemistry*, **2003**, 42, 13220-13226.
16. Zhang, K. Y. J.; Card, G. L.; Suzuki, Y.; Artis, D. R.; Fong, D.; Gillette. S.; Hsieh. D.; Neiman, J.; West, B. L.; Zhang, C.; Milburn, M. V.; Kim, S. H., Schlessinger. J.; Bollag, G. A. *Mol. Cell.*, **2004**, 15, 279-286.
17. Wang. H.; Liu. Y.; Chen. Y.; Robinson. H.; Ke. H. *J. Biol. Chem.*, **2005**, 280, 30949-30955.
18. Huai, Q.; Wang, H.; Sun, Y.; Kim, H. Y.; Liu, Y.; Ke, H. *Structure*, **2003**, 11, 865-873.
19. Card. G. L.; England. B. P.; Suzuki. Y.; Fong, D.; Powell, B.; Lee, B.; Lu, C.; Tabrizizad, M.; Gillette, S.; Ibrahim, P. N.; Artis, D. R.; Bollag, G.; Milburn, M. V.; Kim, S. H.; Schlessinger, J.; Zhang, K. Y. J. *Structure*, **2004**, 12, 2233-2247.
20. (a) Giembycz, M. A.; Smith, S. J. *Drugs of the Future*, **2006**, 31, 207-229. (b) Yamamoto, S.; Sugahara, S.; Naito, R.; Ichikaw. A.; Ikeda, K.; Yamada, T.; Shimizu, Y. *Euro. J. Pharm.*, **2006**, 541, 106-114. (c) Satoshi, Y.; Shingo, S.; Ryo, N.; Atsushi I.; Ken I.; Yasuaki, S.; *Euro. J. Pharm.*, **2006**, 550, 166-17. (d) Lalitha, V.; Sonali, R.; Mathew, E. S.; Sunanda, D.; Abhijit, R, *Exp. Opin. Invest. Drugs*, **2007**, 16, 1585-1599. (e) Vergne, F.; Bernardelli, P.; Chevalier, E. *Ann. Rep. Med. Chem.*, **2005**, 40, 227-241.
21. Xu. R. X.; Rocque. W. J.; Lambert. M. H.; Vanderwall. D. E.; Luther. M. A.; Nolte. R. T. *J. Mol. Biol.*, **2004**, 337, 355-365.

22. Huai, Q.; Liu, Y.; Francis, S. H.; Corbin, J. D.; Ke, H. *J. Biol. Chem.*, **2004**, 279, 13095-13101.
23. Smith, S. J.; Cieslinski, L. B.; Newton, R.; Donnelly, L. E.; Fenwick, P. S.; Nicholson, A. G.; Barnes, P. J.; Barnette, M. S.; Gienbycz, M. A. *Mol. Pharmacol.*, **2004**, 66, 1679-1689.
24. (a) Lorthiosis, E. *et al. Bio. Med. Chem. Lett.*, **2004**, 14, 4623-4626. (b) Bernardelli, P.; *Bio. Med. Chem. Lett.*, **2004**, 14, 4627-4631.
25. **AUTODOCK**, 10550, North Torrey Pines Road, La Jolla, CA 92037-1000, USA.
26. (a) Xu, R. X.; Hassell, A. M.; Vanderwall, D.; Lambert, M. H.; Holmes, W. D.; Luther, M. A.; Rocque, W. J.; Milburn, M. V.; Zhao, Y.; Ke, H.; Nolte, R. T. *Science*, **2000**, 288, 1822-1825. (b) Xu, R. X.; Rocque, W. J.; Lambert, M. H.; Vanderwall, D. E.; Luther, M. A.; Nolte, R. T. *J. Mol. Biol.*, **2004**, 337, 355-365. (c) Huai, Q.; Colicelli, J.; Ke, H. *Biochemistry*, **2003**, 42, 13220-13226. (d) Huai, Q.; Wang, H.; Sun, Y.; Kim, H-Y.; Liu, Y.; Ke, H. *Structure*, **2003**, 11, 865-873.
27. (a) Huai, Q.; Liu, Y.; Francis, S. H.; Corbin, J. D.; Ke, H. *J. Biol. Chem.*, **2004**, 279, 13095-13101. (b) Card, G. L.; Blasdel, L.; England, B. P.; Zhang, C.; Suzuki, Y.; Gillette, S.; Fong, D.; Ibrahim, P. N.; Artis, D. R.; Bollag, G.; Milburn, M. V.; Kim, S. H.; Schlessinger, J.; Zhang, K. Y. *J. Nat. Biotechnol.*, **2005**, 23, 201-207.
28. **SYBYL 7.0**, Tripos Inc., 1699 South Hanley Rd., St. Louis, Missouri, 63144, U. S. A.
29. (a) Morris, G. M.; Goodsell, D. S.; Halliday, R. S.; Huey, R.; Hart, W. E.; Belew, R. K.; Olson, A. J. *J. Comput. Chem.*, **1998**, 19, 1639-1662. (b) Hu, X.; Balaz, S.; Shelver, W. H. *J. Mol. Graph. Model.*, **2004**, 22, 293-307.

30. N. S. Kang, N. S.; Jhon, D. J.; Song, J. H.; Yoo, S-E. *Mol. Sim.*, **2007**, *33*, 1109-1117.
31. Lin, J.; Pahlke, G.; Conti, M. *J Biol Chem.*, **1999**, *274*, 19677-19685.
32. (a) Martinez, A., *et al. Bio. Med. Chem. Lett.*, **2000**, *43*, 683-689. (b) Castro, A., *et al. Eur. J. Med. Chem.*, **2001**, *36*, 333-338.
33. Kempson, J. *et al. Bio. Med. Chem. Lett.*, **2005**, *15*, 1829-1833.
34. (a) Vergne, F. *et al. Bio. Med. Chem. Lett.*, **2004**, *14*, 4607-4613. (b) Vergne, F. *et al. Bio. Med. Chem. Lett.*, **2004**, *14*, 4615-4621.
35. (a) Satoshi, Y.; Shingo, S.; Ryo, N.; Atsushi, I.; Ken, I.; Yasuaki, S.; *Euro. J. Pharm.*, **2007**, *559*, 219-226. (b) Pitts, W. J.; Watson, A. J.; Dodd, J. H.; *PCT Int. Appl.*, **2002**, 81. (c) Hatzelmann, A.; Marx, D.; Steinhilber, W.; Sterk, G. J. *PCT Int. Appl.*, **2002**, 42.